Capping of ZnS nanostructures: Optical and morphological Studies

A

Thesis

Submitted for the award of degree of

DOCTOR OF PHILOSOPHY

BY

MANOJ SHARMA

School of Physics and Materials Science

THAPAR UNIVERSITY

PATIALA (PUNJAB)-147004

INDIA

August 2011

CERTIFICATE

This is to certify that the thesis entitled **"Capping of ZnS nanostructures: Optical and morphological Studies"** which is being submitted by Manoj Sharma in fulfillment of the requirements for the award of the degree of Doctor of Philosophy in the School of Physics and Materials Science, Thapar University, Patiala, Punjab, India is an exclusive record of candidate's own research work under my supervision. The thesis in part or in full has not been submitted in any other university or institute for the award of any degree. The thesis is fit to be considered for the award of degree of Doctor of Philosophy.

O.P. Pandey 24/8/11

Dr. O.P. Pandey
Professor
School of Physics and Materials Science
Thapar University
Patiala-147 004 (INDIA)

i

ACKNOWLEDGEMENT

At this momentous occasion of binding my thesis I would like to acknowledge the contribution of all those benevolent people who helped me during my PhD work. In the first place I would like to record my gratitude to **Dr. Om Prakash Pandey** for his supervision, advice, and guidance from the very early stage of this research as well as giving me advice through out the work. Above all and the most needed, he provided me unflinching encouragement and support in various ways. His truly scientist intuition has made him a constant oasis of ideas and passions in science, which has inspired me for my growth as a student. The most important thing which I have enjoyed working under him is his kind gesture and commitment towards work which have encouraged me to perform well even in tough times.

Besides my supervisor, I would like to thank the rest of my thesis committee members: **Prof. N. K Verma** and **Dr. Bonamali Pal** for their encouragement, insightful comments and useful criticism.

I am profoundly obliged to **Prof. K.K. Raina**, Deputy Director, Thapar University, Patiala for his constant encouragement and needful help during various stages of the work.

I am thankful to **Dr. Kulvir Singh**, Head, School of Physics and Materials Science for constant encouragement and support.

I am very thankful all faculty of School of Physics and Materials Science, **Dr. Manoj Sharma, Dr. Suneel Kumar, Dr. Puneet Sharma, Dr. Bhupendra Chudasama** for their valuable suggestions during my PhD work.

Dr Sunil Kumar, Department of Physics, M. M. University, Mullana (Ambala) is specially acknowledged for his whole hearted support during initial years of my PhD.

My special thanks to **Mr. Tarun Jain and Ms. Jagdeep Kaur** for their help during synthesis of samples.

I am also thankful to **Dr. Sukhvir Singh**, **Dr. S.S Sekhon and Dr. R Thangaraj** for their whole hearted support.

My special thanks to **Mr. P.K. Singh** for his help and valuable suggestions for the characterization of materials.

Words are inadequate in expressing my sincere thanks to my friends and labmates **Mr. Akshay Kumar, Dr. Vishal Kumar, Mr. Manish Mittal, Mr. Deepak Kumar, Ms. Bhupinder Kaur, Ms. Gurbinder Kaur, Ms. Kamalpreet Kaur, Ms. Jasmeet Kaur, Mr. Ranvir Singh, Mr. Suresh Kumar, Mr. Mohit** for their support in every moment of difficulty.

I am also indebted to **Dr Pankaj Kumar, Dr Anu Arora, Ms. Neeraj Sharma, Ms. Shamita Thakur, Ms. Chandini Khurana, Mr. Paramjot Jha, Mr. Kapil Sood, Mr. Harjinder Singh, Mr. Paramjyot Jha and Mr. Vipin Sharma** for their kind help and valuable suggestions.

I also thankful to **Mr. Dinesh kumar** and **Mr. Ravi Sukhla** for their help and precious time which they devoted for my cause.

My special thanks to Mr**. Vijay Kumar, Mr. S. P. Yadav, Ms. Praveen, Mr. Indermani and Mr. Jant Singh** for providing all kinds of help. All the staff of School of Physics and Materials Science is acknowledged who never turned me down whenever I approached for any help.

My family especially my wife **Mrs. Ashma Sharma** deserve the special thanks and great appreciation for her patience, persistent moral support and capability to revitalize me during the course of the PhD work at each step. Special thanks to my sisters **Ms. Simmi Sharma, Mrs**. **Rimpy Joshi and her husband Mr. Jogesh Joshi** who stood by me all the times.

Last but not least my father **Mr. Bharat Bhushan Narad** and my mother **Mrs. Usha Devi** are the two guiding pillars of my success. The constant motivation of my

parents has been the sole source of inspiration and strength to carry out my work. Finally, I would like to thank everybody who was important to the successful realization of thesis as well as expressing my apology that I could not mention personally one by one.

Above all, hidden force by **Almighty God** steered me in the right direction to achieve the goal.

Manoj Sharma.

(Manoj Sharma)

iv

Index

LIST OF PUBLICATIONS

Journal Publications

1.**Manoj Sharma**, Sunil Kumar, O.P.Pandey, Photo-Physical and Morphological Studies of Organically Passivated Core-Shell ZnS Nanoparticles, **Digest Journal of Nanomaterials and Biostructures** Vol. 3, No.4, 2008, p. 189 – 197.

2. **Manoj Sharma**, Sunil Kumar, O.P.Pandey, Studies of 2 - mercaptoethanol passivated ZnS core-shell nanoparticles, **Optoelectronics and Advanced Materials- Rapid Communications,** Vol. 2, No. 12, December 2008, p. 881 – 885.

3. **Manoj Sharma**, Sunil Kumar, O.P.Pandey, Study of energy transfer from capping agents to intrinsic defects in passivated ZnS nanoparticles**, Journal of Nanoparticle Research:** Volume 12, Issue 7 (2010), Page 2655.

4. **Manoj Sharma,** Sukhvir Singh, O.P.Pandey, Excitation induced tunable emission in biocompatible chitosan capped ZnS nanophosphors, **Journal of Applied Physics**, 107, 104319 (2010); doi:10.1063/1.3374472 , **American Institute of Physics(AIP),** (Published online 26- 05-2010).

5.**Manoj Sharma**, O.P.Pandey, Excitation modulated blue-white-orange tunable emission in single PVP capped Mn doped ZnS nanocrystals (under review) **Journal of Applied Physics)**.

6.**Manoj Sharma**, Tarun Jain, Sukhvir Singh and O.P. Pandey, Photocatalytic degradation of organic dyes under UV-Visible light using capped ZnS nanoparticles. (accepted) **Solar Energy**.

7. **Manoj Sharma,** Tarun jain, O.P.Pandey, Tunable emission in chitosan capped Mn ZnS nanophosphors and its application for Glucose sensing (under review) **(AIP Advances).**

8.**Manoj Sharma,** O.P.Pandey, **Excitation** Modulated Tunable Emission in Chitosan Capped ZnS:Mn Nanophosphors Synthesized at Different pH, Journal of Luminescence(Manuscript under preparation).

Papers in conference proceedings

1.**Manoj Sharma,** Tarun jain, O.P.Pandey, Enzyme detection using DNA capped ZnS nanoparticles, Biomedical applications of nanostructured materials, Nano (2010) Macmillan Advanced research series (ISBN-023-033-201-3).

2. **Manoj Sharma**, Sunil Kumar, Sukhvir Singh and O.P. Pandey, Comparison of optical and morphological properties of uncapped and glutathione capped ZnS nanostructures, Proceedings of ICOP 2009-International Conference on Optics and Photonics CSIO, Chandigarh, India, 30 Oct.-1 Nov. 2009. (PS3.A.6).

Selected Papers in conference (National and International)

1. **Manoj Sharma**, O.P.Pandey, Sensing applications of capped ZnS nanomaterials, (2010) AGM of MRSI held in Bhopal, 2011 (**Best poster**).
2. **Manoj Sharma** and O.P.Pandey, Optical Studies of PVP capped ZnS nanoparticles, International Symposium on Nanostructured Materials: Structure, Properties And Applications, KMV, Jalandhar, Oct 28-29, 2009(**Selected as Best Poster**).
3. **Manoj Sharma**, G.S.Sekhon, O.P.Pandey, Effect of capping agents on stability of nanostructures of ZnS – An Overview, International conference on Metals and Alloys: Past, Present and Future (METALLO 2007), 07-10 Dec, 2007.

4. **Manoj Sharma**, Sunil Kumar, O.P.Pandey, Effect of different capping agent on optical properties of ZnS nanoparticles, UGC Sponsored National Seminar, Smart Materials: A Future Prospective (SMFP-08), September 19-20, 2008.
5. **Manoj Sharma**, Sunil Kumar, O.P.Pandey, Enhanced luminescence behavior of semiconducting core-shell nanostructures - An Overview,11th Punjab Science Congress held at Thapar University, Patiala,7-9 Feb. 2008.
6. **Manoj Sharma**, G.S.Sekhon, O.P.Pandey, Effect of PVP on stability of ZnS Quantum dots, National Seminar on Radiation and Materials held at Deptt. of Physics, Punjabi University, Patiala, March, 10-11, 2008.
7. **Manoj Sharma**, Tarun jain, Sukhvir Singh, O.P.Pandey, Photocatalytic degradation of organic dyes under UV-Visible light using capped ZnS nanoparticles, International conference on Renewable Energy, 17-21 Jan 2011, Jaipur Rajasthan.
8. **Manoj Sharma**, O.P.Pandey, Excitation Modulated Tunable Emission in Chitosan Capped ZnS:Mn Nanophosphors Synthesized at Different pH, International Conference on Luminescence, June 27 to July 1, 2011, Ann Arbor, Michigan, USA. **(Oral presentation).**

LIST OF FIGURES

LIST OF TABLES

PREFACE

The present thesis deals with the synthesis and characterization of capped ZnS nanostructures and their optical and morphological studies. The entire work is presented in **seven chapters**. In the **first chapter** general introduction of the present work is given.

Chapter 2 gives a detailed account of the literature survey in context of the capped ZnS NPs. The work done on the capped NPs for optical, morphological and sensing applications has been presented in this chapter. After reviewing all segment of literature the need to select these series was felt and accordingly the reason for it is given. In the last section of this chapter gaps in the study along with aims and objectives of the work of the thesis is presented.

Chapters 3 describe about experimental procedure followed in this present work. On the basis of literature, uncapped, capped and capped and doped ZnS NPs were synthesized by chemical precipitation technique. The as prepared semiconductor NPs were characterized by X-ray diffraction (XRD) studies, transmission electron microscopy (TEM), Energy Dispersive Analysis of X-rays (EDAX), Fourier transform infra-red spectroscopy (FTIR), UV-Visible absorption and photoluminescence (PL) spectroscopy. The details of NP preparation with characterization techniques are described in this chapter.

The results and discussions are given in **chapters 4, 5 and 6** separately.

Chapter 4 deals with optical (UV-Visible absorption and photoluminescence spectroscopy) and morphological (XRD, TEM, SAED, EDX etc.) studies of synthesized ZnS NPs.

Chapter 5 deals with optical (UV-Visible absorption and photoluminescence spectroscopy) and morphological(XRD, TEM, SAED, EDX etc.) studies of synthesized capped ZnS NPs with various capping agents (PVP, Chitosan, Mercaptoethanol, Thioglycerol, SHMP etc.) having different concentrations (0.1, 0.5, 1.0, 1.5 and 2.0 at. wt. %). All data collected from above mentioned series have been compared with each other. Energy transfer mechanisms have been proposed to explain PL results where needed.

In **Chapter 6** some selected samples from above mentioned series have been studied for various sensing and tunable emission applications. For the same polymer functionalized and Mn doped ZnS NPs have also been synthesized and their results have been compared for sensing applications. This tunable emission observed with proper selection of capping

polymer and dopant is compared with previously observed tunable emission in literature. In our case single sample is needed for this tunable emission whereas earlier many samples were needed for achieving same property. Possible energy transfer mechanism has been developed for organic- inorganic hybrid doped NPs. Some introductory results of capping ZnS NPs with DNA and their enzyme sensing studies has been presented in the last part of this chapter.

Chapter 7 gives the conclusions and future scope for all the work. The important conclusions are summarized below:

1. Capped ZnS NPs shows better stability, uniform size distribution, decrease in particle size, blue shift of absorption edge and enhanced PL intensities than corresponding uncapped ZnS NPs synthesized under same conditions.
2. With increase in capping concentration of particular capping agent we find blue shift of absorption edge, increase in PL intensity and better passivation property but it is found that after some specified concentration of particular capping polymer all properties start to degrade. It is observed that this particular capping concentration is different for different polymers.
3. Out of all selected seven series PVP (0.1-2.0%) capped ZnS and chitosan (0.1-2.0%) capped ZnS NPs shows a new kind of tunable emission which is excitation induced. Earlier for tunable emission samples of different particle sizes or samples with different dopants were required. But in our case single sample is observed to emit two or three colors. The reason for this new type of tunable emission is explained by FRET mechanism.
4. These biocompatible and tunable emitter samples were used for tagging bacteria (staphylococcus auerus). Tunable emission property helps to detect these bacteria.
5. At last these tunable chitosan capped ZnS Mn NPs have been used for glucose sensing applications. Also some initial experiments related to DNA capped ZnS NPs have been presented and used them further for enzyme detection.

CHAPTER 1

INTRODUCTION

Overview

In this chapter general introduction of the present work is given. First part of this chapter gives background of nanomaterials and discusses their unique properties. In the second section properties of semiconductor nanoparticles have been discussed along with quantum confinement effect. A brief idea of synthesis techniques of these nanoparticles is also presented here. Role of organic and inorganic capping is described in order to control the size and to passivate defects on nanoparticles surface. In this segment steric and electrostatic stabilization of nanoparticles has been described. In the last section of this chapter the recent applications of these capped nanoparticles as tunable light emitters, biosensors etc. have been described.

1.1 Background

Nanotechnology is the application of nanoscience for making useful devices. In turn, nanoscience is the science that relates to objects with at least one dimension between one and one hundred nanometres in length [1]. After more than twenty years of basic and applied research, nanotechnology is gaining its application for commercial use [2-6]. Nanoscale materials are used in electronic, cosmetics, automotive and medical products [7]. But it is difficult to find out how many "nano" consumer products are in the market and which merchandise could be called "nano." As of April 2011, there are already over 1300+ nanotech products existing in the world [7]. Basic objective of nanotechnology is to control the size in such a way where sharp transitions in properties as compared to bulk are observed. Nanoscale materials frequently show behavior which is intermediate between that of a macroscopic solid and an atomic or molecular system. Due to their reduced dimension and increased surface area, these materials possess new physical and chemical properties which are distinctively different from their bulk counterparts. Nanoparticles, in general, are supposed to have nearly half of their atoms contained in top two monolayers, which make optical properties highly sensitive to surface morphology. Control over movement of electrons and holes and structure of surface has been of special importance for technology development related to very low dimensional optonics and electronics. In semiconductor nanomaterials, the absorption edge is blue-shifted from the bulk bandgap when the dimension of the material is comparable or smaller than the Bohr radius of bulk exciton. In noble metal particles, as their particle size are reduced to tens of nanometers, a strong absorption known as surface plasmon absorption arises from the collective oscillation of electrons in their conduction band. In transition metal nanoparticles, the increase in the surface-to-volume ratio sometimes makes them useful as catalyst with high surface reactivity and selectivity. In metal nanowires, a reduced

electrical conductivity is observed as a result of increased electronic energy level spacing. In addition to that, ferromagnetism of bulk materials is transformed to superparamagnetism in the nanometer scale since the large surface energy can provide sufficient energy for domains to spontaneously switch polarization directions. Among many important physical properties, optical properties of nanomaterials have always been given special attention. The unique absorption and emission properties of nanomaterials result from their discrete electronic energy levels and make these nanomaterials useful in applications such as display devices, light emitting diodes, photocatalyst, solar cells and biological labels [1,3]. However, such usefulness relies strongly on the ability that one can control or tune the properties of these materials. For it the major three parameters are commonly modified to tailor the optical properties of nanomaterials, *i.e.* the size, shape and composition.

1.2 Semiconductor quantum dots

Quantum dots are semiconductor nanocrystals with a typical size of 1-20 nm, containing as few as 100 to 100,000 atoms in each particle. With confinement in all three spatial dimensions, quantum dots exhibit properties that are between those of bulk semiconductors and those of discrete molecules. For semiconductor nanoparticles Brus [8-9] was one of the first that reported changes in band gap with change in particle size. Related to this shift, the color of the QD solution has been observed to vary in visible spectrum. The shift of the absorption edge as a function of particle size is due to quantum size effects.

1.2.1 Quantum size effects

The electron and the hole as charged particles do interact via the Coulomb potential and form a third quasiparticle which is called exciton. It corresponds to a

hydrogen-like bound state of an electron-hole pair and is therefore characterized by the exciton bohr radius a_B [10]:

$$a_B = \frac{4\pi\varepsilon_0\varepsilon_r h^2}{e^2}.\left(\frac{1}{m_e^*} + \frac{1}{m_h^*}\right) \quad (1)$$

Typical values for a_B for common semiconductors range in the interval from 1-10 nm. When the radius of a particle approaches a_B, the exciton in the particles experience a spatial confinement and can only exist in the particle when it is in a state of higher energy which leads to an increase in the energy gap of the semiconductor. As a result of such a quantum confinement an exciton in a nanocrystal has to be considered as a particle in a box, so its kinetic energy becomes quantized and the energy bands split into discrete levels. This is the origin of the name quantum dots for such particles [10].

The most common QDs are the binary semiconductor compounds consisting of II-VI elements, i.e., cadmium sulfide (CdS), cadmium selenide (CdSe), cadmium telluride (CdTe), zinc selenide (ZnSe), lead sulfide (PbS), zinc sulphide (ZnS) and mercury sulfide (HgS), etc. There are also some QDs comprising III-V elements, i.e., indium phosphide (InP), gallium nitride (GaN), indium arsenide (InAs), etc. Moreover, some QDs composed of single element (such as silicon), or of ternary elements with two of them in either cation or anion site (such as CdZnS, CdSSe, InNP, etc.) have also been reported. All these QDs compositions are semiconductors with the bulk band gap energy of less than 4.0 eV usually.

1.3 Synthesis

There has been an explosive growth of nanoscience and technology in the last decade, primarily because of the availability of new methods of synthesizing nanomaterials, as well as tools for characterization and manipulation [3]. Controlling the size, shape and structure of nanoparticles is technologically important because there exist

strong correlation between these parameters and optical, electrical, magnetic and catalytic properties [11, 12]. The conventional approach for the synthesis of nanoparticles involves chemical or physical attrition from bulk into objects of desired sizes and shapes (e.g. mechanical milling, ion implantation, etc.), and is referred as the 'top-down' approach. Inverse to the 'top-down' approach is a process universal in nature, involving the assembly of materials from molecular levels to form micro or macro-sized shapes and structures, often referred as 'bottom-up' approach or 'self-assembly' [12]. Wet chemical synthesis involving colloids is the most energy efficient 'bottom up' technique for the synthesis of nanoparticles. The chemical synthesis has the advantages of producing size-controlled, un-agglomerated nanoparticles. Most of the physical or chemical properties exhibited by these nanoparticles are due to their crystallites. Further growth in their size is due to agglomeration of these crystallites to form primary particles. In order to control the size and size-distribution of colloidal nanomaterials, one must understand the nucleation and growth process of particles (Figure 1.1).

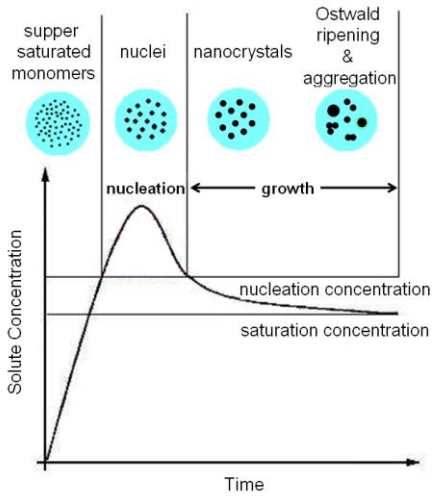

Figure 1.1 Nucleation and growth during the preparation of nanoparticles [13].

Classic studies by Lamer and Dinegar show that the production of monodisperse colloids requires fast nucleation followed by slower controlled growth of the existing

nuclei [13]. During the growth stage, the particles continue to grow by molecular addition. Size-focusing can occur when the nanocrystals present in the solution are all slightly larger than the critical size (*i.e.* the particle size at which atomic attachment and detachment are at equilibrium). Smaller particles grow faster than the larger ones. Desired size and narrow size distribution can be achieved by stopping the reaction at suitable time during the size-focusing process [14]. If this growth of particles is not controlled, then due to Ostwald ripening and Vander-Waals interactions between particles, they may agglomerate and settle down [8, 13-16]. This agglomeration can be arrested by either stabilizing them electrostatically or by inducing steric hindrance at appropriate stage(s) to achieve size selective synthesis during precipitation reaction. In order to control such a secondary growth, suitable surface protecting reagents must be used, *e.g.* organic ligands, inorganic capping materials, inorganic matrix or polymers [16]. The surface protecting reagents can provide a steric barrier to counteract the van der waals or magnetic attractions between nanoparticles, so as to prevent nanoparticle aggregation. They can also affect the reactivity and stability of the seeds as well as the nanoparticles produced. In order to control the growth one can use different organic and inorganic capping agents to passivate the free QDs. To control the growth of nanoparticles organic stabilizers (polymers) e.g. polyethylene oxide (PEO), poly (N-vinyl-2pyrroledone) (PVP), polyvinyl caracole (PVK), mercaptoethanol, thiophenol, thiourea, SHMP, sodium polyphosphate, chitosan etc. can be added during the wet chemical synthesis for capping [17-27]. Such materials have applications in luminescent devices, light emitters, phosphors optical sensors etc. [17-19]. Recently due to advancement in luminescent nanocrystals by successful capping results in fluorescent labeling by semiconductor QDs for biological detection. Capping causes noticeable change in properties of nanoparticles.

1.4 Capping molecules

In section 1.3 the key role of capping molecules in the synthesis of highly luminescent and stable QDs was mentioned. In this section the role of the capping molecules is considered in more detail. Capping molecules play vital role in three important aspects of QD synthesis:

1.4.1 Control the growth of QDs

Capping molecules have a chemical group with an affinity for either cation (e.g. TOPO, thiols and amines coordinate with Cd^{2+}) or the anion (e.g. TOP, capable of forming a TOP-Se complex). Under the growth conditions of the semiconductor nanocrystals the complexing properties of the coordinating molecules play an important role. The nanocrystal grows within a shell of capping molecules. The final particle size is determined by the growth kinetics. If bonding with the surface atoms of the QD is too weak there will be uncontrolled growth of the semiconductor beyond the quantum size regime. If the bonding is too strong the particle growth is inhibited. To obtain QDs of the desired nm size the growth conditions have to chosen such that the binding of the capping molecules is neither too strong nor too weak. The growth rate, and thus the particle size, is determined by the nature and concentration of the capping molecules, the growth temperature and precursor concentrations.

1.4.2 Prevent aggregation of QDs

Semiconductor QDs are not a thermodynamically stable phase. There will be a thermodynamically driven tendency for aggregation of QDs. Capping molecules play a key role in preventing aggregation. In order to discuss capping effects in detail both steric hinderance and electrostatic double layer formation are discussed in detail below:

1.4.2.1 Steric Stabilization

Colloidal dispersions can also be stabilized by the addition of a surfactant that is in most cases a polymer. The surfactant forms a protecting layer around the particle and so prevents flocculation. The adsorbed layers can influence the vander waals attractions or induce repulsion of the particles. This is called steric stabilization. It can be further divided into three cases:

(i) Anchored polymers:

Suppose 'a' is the radius of nanoparticles and 't' is the thickness of capping polymer. The polymer chains will extend into the dispersing medium in a degree that depends on the interaction between polymer and dispersing medium. The more the surfactant resembles the dispersing medium the more the polymer chains will be directed outward into the solvent. When two particles collide the surfactant or polymer chains will penetrate one another. This has two consequences: First, the local density of the polymer will be increased so that the osmotic effect will cause a diffusion of solvent molecules between the two surfaces to diminish the surfactant concentration. This will push apart the particles. This type of capping mechanism is shown in Figure 1.2(a). Second, the higher surfactant concentration between the particles will lead to a reduced number of possible arrangements of the chains. So the entropy decreases by a value ΔS causing increase in free repulsive energy by $T\Delta S$. This is called entropic repulsion. In this case the polymer chains of one layer penetrate in the layer of another particle, so the center-center distance of the particles can be smaller than $2(a + t)$, but the repulsive potential increases strongly. This type of mechanism is shown in Figure 2(b). In order to achieve a good steric stabilization the surfactant should be different from the nature of the particle but similar to the one of the dispersing agent. The longer the chain length the better the

stabilization, because the repulsive strength depends strongly on the thickness of the surfactant layer around the particle. The surfactant can be attached to the surface by chemical bonding or by a strong and specific binding [28, 29].

(ii) Non adsorbing polymers

Dissolved, non-adsorbing polymer molecules must alter their configuration if their centre of mass is to approach a particle surface. This leads to the formation of a so called depletion layer around each particle. That means a layer from which the polymer is excluded. A particle immersed in a polymer solution experiences an osmotic pressure acting normal to its surface. For an isolated particle, the integral of the pressure over the entire surface exhibits zero force. But when the depletion layers of two particles overlap, polymer will be excluded from a portion of the gap between the particles. Consequently, the pressure due to the polymer becomes unbalanced. The polymer concentration between the particles is lower than in the volume, so the dispersing agent diffuses in the volume leading to an attractive force and particle flocculation. This is called *depletion flocculation* [28, 29].

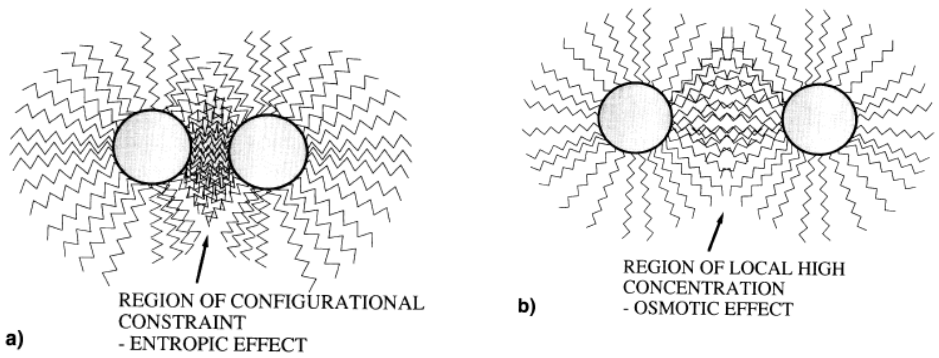

Figure1.2 Steric stabilization of colloidal particles with anchored polymers: **a)** in the interparticle space the configurational freedom of the polymer chains of two approaching particles is restricted causing a lowering of entropy; **b)** the local concentration of polymer chains between the approaching particles is raised and the resulting higher local activity is osmotically counteracted by solvation [30].

(iii) Adsorbing polymers

So far, we have considered only the extremes of irreversibly anchored and non adsorbing polymers. More commonly, though, polymers adsorb at random points along their backbone to a degree that depends on the nature of the polymer, the solvent and the surface. The interactions between surfaces are more complicated with adsorbed polymer layers than with terminally anchored chains for two reasons:

1. Chains originally attached to one surface can adsorb at the same time to the surface of a second particle to create a bridging between two particles.
2. Given enough time, chains can desorb from the surface and migrate out of the gap between two particles.

1.4.2.2 Electrostatic Stabilization

Electrostatic stabilization involves the creation of an electrical double layer arising from ions adsorbed on the surface and associated counter ions that surround the particle in the dispersing media [31]. Thus, if the electric potential associated with the double layer is sufficiently high, columbic repulsion between the particles will prevent their agglomeration. Particles in aqueous dispersion normally show a surface charge that can be due to the ionization of surface groups or to the adsorption of charged molecules or simply ions. Following coulomb's law every charge creates an electric potential that will be compensated by charges of opposite sign in its proximity. That means that around every negatively charged ion an excess of positive charges will be present and vice versa. This cloud of counter ions is called electric double layer. This double layer results in a coulombic repulsion between two particles which decays approximately exponentially with the interparticle distance z as given below:

$$\psi = \psi^0 e^{\frac{-k}{z}}$$

The net result is shown schematically in Figure 1.3. The weak minimum in the potential energy at moderate interparticle distances defines a stable arrangement for the colloidal particles which is easily disrupted by medium effects, and at room temperature, by the thermal motion of the particles. Thus, if the electric potential associated with the double layer is sufficiently high, then electrostatic repulsion will prevent particle agglomeration.

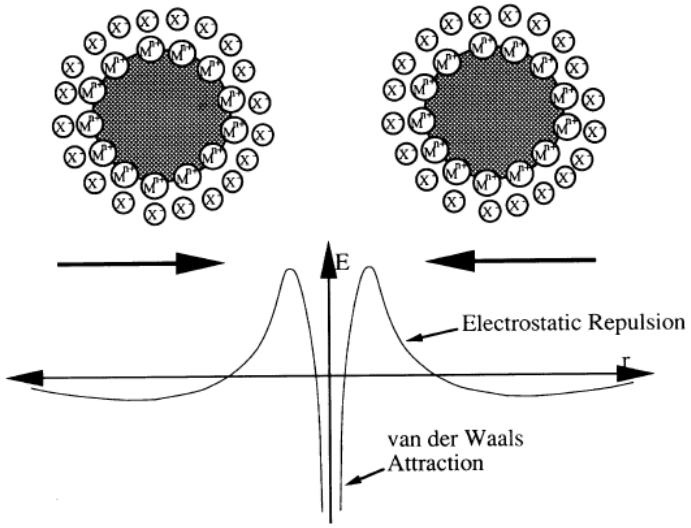

Figure 1.3: Electrostatic stabilization of colloidal particles. Attractive van der Waals forces are outweighed by repulsive electrostatic forces between adsorbed ions and associated counterions at moderate interparticle separation [30].

1.4.3. Passivate dangling bonds at the QD surface

Since QDs are extremely small crystallites, the surface to volume ratio is large. At the crystal surface the periodicity of the crystal breaks down which may result in states within the bandgap (i.e. a state between the bottom of the conduction band and the top of the valence band). These surface states act as recombination centers for the excitons by first trapping one of the charge carriers followed by radiative or non-recombination with the other charge carrier. In the case of radiative recombination an emission band is observed on the long wavelength side of the excitonic emission band. This emission is referred as defect emission or trap emission. Due to the large lattice relaxation involved in

the trapping and recombination process, often the presence of surface states leads to non-radiative recombination. The nonradiative losses lower the luminescence quantum efficiency (QE) and are undesirable in applications which rely on efficiently luminescing QDs. In Figure 1.4 the different recombination processes for an exciton are depicted schematically. Capping molecules by forming different bonds with surface present dangling bonds are capable of passivating surface states. Perfectly capped QDs can have a very high luminescence QE with values close unity.

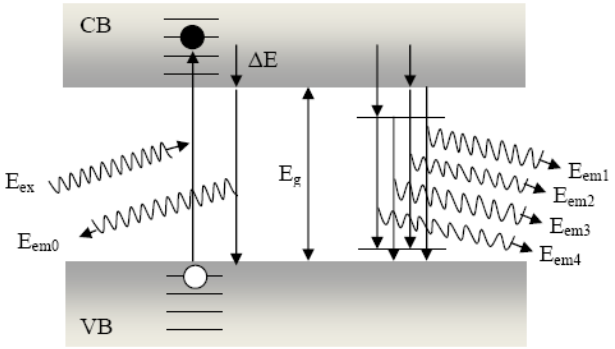

Figure 1.4 Schematic representations of different relaxation pathways of the exciton. From left to right excitation, radiative exciton recombination, defect related emission and non-radiative relaxation are depicted.

A different approach to reduce non-radiative losses at the surface is to grow a shell of higher bandgap material around the semiconductor core. The higher bandgap material confines the charge carriers, resulting in quantum size effects in the semiconductor core and prevents the formation of surface states. These so called core-shell QDs can have high quantum efficiencies and a higher stability against (photo-) oxidation. Core-shell type composite quantum dots exhibit novel properties making them attractive from both experimental and technological point of view [17].

1.5 Applications of QDs

Quantum dots displayed great potentials in numerous applications in the field of optoelectronic materials and biosensing. Wurtzite ZnS is a direct wide band gap (3.91 eV)

semiconductor that is one of the most important materials in photonics. This is because of its high transmittance in the visible range and its high index of refraction (about 2.2). ZnS is also an important phosphor host lattice material used in electroluminescent devices (ELD), because the band gap is large enough to emit visible light without absorption and the efficient transport of high energy electrons. Apart from this with suitable doping it can emit nearly all colors in visible spectrum. One of the most fascinating capabilities of many biological molecules is that of molecular recognition. Certain biological molecules can bind to other molecules with extremely high selectivity and specificity. This is similar to a lock-and-key system, but on a molecular level. This principle is used to visualize e.g. structural units in cells that due to a lack of contrast or resolution cannot be distinguished by just recording an image. In these cases fluorescence labels are attached specifically to a compartment in a cell. The idea is to chemically link a fluorescent dye to receptor molecules that specifically and selectively bind to the desired compartment in the cell. For using nanoparticles as biosensors they have to compete with organic dyes that have quantum yields of sometimes even 100 %. This cannot be achieved with nanoparticles. But they have other advantages. The most prominent is the large stokes shift between excitation and emission. Since the luminescence excitation takes place over the band gap, but the emission comes from electronic states within the d-orbitals of the dopant. So excitation and emission are well separated which facilitates the detection. It is often difficult to measure the fluorescence emission of organic dyes without measuring the excitation peak, since the excitation and emission spectra are normally very close. Secondly organic dyes suffer from photo bleaching. To use nanoparticles as fluorescent markers they have to be biofunctionalized. Several strategies for the conjugation of water-soluble semiconductor nanocrystals with biological molecules have been reported. In the

biomedical field, the QD-based fluorescent imaging approach was used as a sensitive and convenient tool for quantitative assessment of cancer cell behavior [31] and for sentinel lymph node mapping [32]. Labeled by QDs with different emission colors, the microbeads injected in a mouse body were imaged and differentiated under a single UV light source, as shown in Figure 1.5.

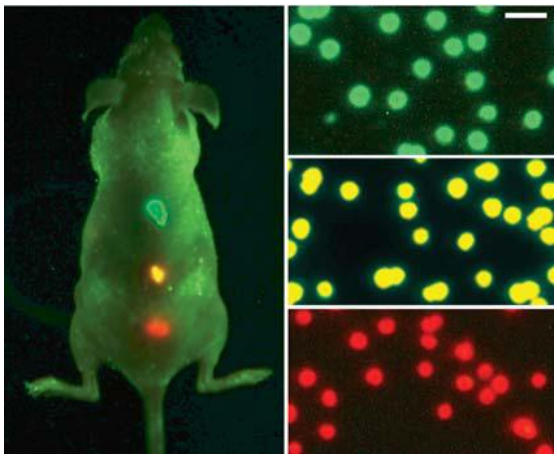

Figure 1.5. Simultaneous *in vivo* imaging of multicolor QD-encoded microbeads in a live animal (left) and the QD-encoded microbeads emitting green, yellow or red light (right). The scale bar is 1 μm.[33]

The QD-tagged microbeads are emerging as a new class of fluorescent labels with enhanced photostability and brightness, which are expected to open new opportunities in nanotechnology and biology [33]. In the last 20 years semiconductor nanoparticles have shown that they can be an alternative to common organic dyes used in biological and medical analytics, and as tags for biomolecules. ZnS also plays an important role in quantum dot based nanosensors. CdSe is typically an ideal quantum dot material. However, under certain conditions quantum dots with a CdSe core have been found to be acutely toxic to biological cells. In *in vitro* applications, quantum dots used for labeling have been found to be toxic. This is due to cadmium release into the system. Capping the CdSe quantum dots with a ZnS shell seems to help the toxicity [34, 35]. This coating eliminates all cytotoxicity following exposure of the core-shell quantum dots to air, but

UV light still induces some toxicity [35]. Recently doped ZnS NPs have shown tunablility in emission color without change in particle size [24]. These doped ZnS NPs capping with biocompatible polymer can be used as biosensors. So the objective of reviewing literature in the next chapter is studying the previously existing reported work on optical and morphological properties of different capped ZnS and doped ZnS NPs.

1.6 References

[1] G. Cao, *Nanostructures & Nanomaterials: Synthesis, Properties & Applications*; Imperial College Press, (2004).

[2] L. E. Brus, *J. Chem. Phys.,* **79**, 5566 (1983).

[3] C. N. Rao, A. Muller, A. K. Cheetham, *The Chemistry of Nanomaterials : Synthesis, Properties and Applications,* **1,** Wiley-VCH, Weinheim, (2004).

[4] A.P. Alivisatos, T.D. Harris, P.J. Carroll, M.L. Stiegerwald, L.E. Brus, *J Chem. Phys.*, **90,** 3463 (1989).

[5] T. J. Bukowski, and J. H. Simmons, *Solid state and Materials Sciences,* **27**, 119 (2002).

[6] J.H. Yao, K.R. Elder, H. Guo, M. Grant, *Phys. Rev. B,* **47,** 14110 (1993).

[7] Dr. Daniel J. Fiorino, *Voluntary Initiatives, Regulation, and Nanotechnology Oversight***, 2011.**

[8] R. Rosseti, S. Nakahara, L.E. Brus, *J. Chem. Phys.*, **79**, 1086 (1983).

[9] R. Rosseti, J.L. Ellision, J.M. Gibson, L.E. Brus, *J. Chem. Phys.*, **80**, 4464 (1984).

[10] S.V. Gaponenko, P L Knight, A Miller, *Optical Properties of Semiconductor Nanocrystals*, Cambridge University Press (2005).

[11] J. Dutta, H. Hofmann, *Self-organization of colloidal nanoparticles, Encyclopedia of Nanoscience and Nanotechnology,* American Scientific Publishers, California **617** (2004).

[12] H.C. Warad, S.C. Ghosh, A. Sugunan, C. Thanachayanont, J. Dutta., *Advances in Technology of Materials and materials processing Journal* (ISSN 1440-0731).

[13] V. K. LaMer, R. H. Dinegar, *Journal of the American Chemical Society* **72,** 4847 (1950).

[14] X. G. Peng, J. Wickham, A. P. Alivisatos, *Journal of the American Chemical Society* **120,** 5343 (1998).

[15] C. B. Murray, C. R. Kagan, M. G. Bawendi, *Annual Review of Materials Science.* ***30,*** 545 (2000).

[16] C. Burda, X. B. Chen, R. Narayanan, M. A. El. Sayed, *Chemical Reviews* **105,** 1025 (2005).

[17] S. W. Suchita Kalele, Gosavi, J. Urban and S. K. Kulkarni, Current Science, **91,** 8 (2006).

[18] E Matijevic. Monodispersed colloids: Art and Science. *Langmuir*, **2**, 12 (1986).

[19] D. H. Everett, *Basic principles of Colloid Science*, Royal Society of Chemistry, 213 (1988).

[20] Kumbhojkar, V.V. Nikesh, A. Kshirsagar, *Journal of Applied Physics*, **88,** 11 (2000).

[21] Chung Jaehun, LEE Sunbae, Jang Du-Jeon, Korea- Japan Forum, Seoul, Coree, Republiquede, **377**, 85 (2002).

[22] T. Kubo, T. Isobe, M. Senna, *Journal of Luminescence,* **99,** 39 (2002).

[23] Karar, Singh, and Mehta, *Journal of Applied Physics,* **95,** 656 (2004).

[24] K. Manzoor, S. R. Vadera, N. Kumar and T. R. N. Kutty, *Solid State Communications,* **129,** 469 (2004).

[25] Gopa Ghosh, Milan Kanti, Naskar, Amitava Patra, Minati Chatterjee, *Journal of Optical Materials,* **28,** 1047 (2006).

[26] Benjamin Gilbert, Feng Huang, Zhang Lin, Carmen Goodell, Hengzhong Zhang, Jillian F. Banfield, *Nano Lett.*, **6(4)**, 605 (2006).

[27] H.C. Warad, S.C. Ghosh, B. Hemtanon, C. Thanachayanont, J. Dutta, *Science and Technology of Advanced Materials,* **6**, 296 **(**2005).

[28] D.H. Everett, *Grundzge der Kolloidwissenschaft, Steinkopff Verlag Darmstadt,* **32,** (1992).

[29] W.B. Russel, D.A. Saville, W.R. Schowalter, *Colloidal Dispersions*, Cambridge University Press, Cambridge, (1989).

[30] G. Schmid, *Clusters and colloids*, Wiley VCH, New York, (1994).

[31] C. R. Estrada, M. Salanga, D. R. Bielenberg, W. B. Harrell, D. Zurakowski, X. P. Zhu, Palmer, N. R.; Freeman, M. R.; R. M. Adam, *Cancer Res.* **66(6)**, 3078 (2006).

[32] S. Kim, Y. T. Lim, E. G. Soltesz, A. M. De Grand, J. Lee, A. Nakayama, J. A. Parker, T. Mihaljevic, R. G. Laurence, D. M. Dor, L. H. Cohn, M. G. Bawendi, J. V. Frangioni, *Nat. Biotechnol.* **22(1)**, 93 (2004).

[33] Q. Ma, C. Wang, X. G. *J.* Su, *Nanosci. Nanotechnol.* **8,** 1138 (2008).

[34] S. Ravindran, Sunran Kim, Rebecca Martin, Elizabeth M Lord and Cengiz S Ozkan, *Quantum dots as bio-labels for the localization of a small plant adhesion protein.* Nanotechnology, **16(1),** 1 (2005).

[35] A.M. Derfus, W.C.W. Chan, and S.N. Bhatia, *Probing the Cytotoxicity of Semiconductor Quantum Dots.* Nano Letters, **4(1),** 11 (2004).

CHAPTER 2

LITERATURE REVIEW

Overview

In this chapter the earlier reported work on synthesis, properties and applications of nano sized zinc sulphide (ZnS) is reviewed. The literature review is divided in three parts; the first part summarizes the need of studying ZnS nanoparticles (NPs) among existing well studied semiconductors NPs. The second part deals with synthesis of ZnS NPs with chemical precipitation route. It also describes effect of different capping agents used during synthesis. Third part explains effect of different dopants on tunable color properties of ZnS NPs. It also describes other approaches to tune optical properties. At last gaps existing in literature and objectives have been presented.

2.1 History of existing semiconductor nanocrystals

The synthesis of nanocrystals is not trivial and it is for this reason that in the field of QD research there is fruitful interaction between chemists and physicists. Already in the middle ages semiconductor nanocrystals were present in colored glass panes. It took however, until 1982 for the field of semiconductor nanocrystals to emerge as a rapidly expanding new area of research. In this year the groups of Henglein, Brus and Gratzel [1-3] reported on the synthesis of colloidal CdS nanoparticles to study photochemical and catalytic processes as a possible alternative for TiO_2 nanocrystals. Soon it was observed by both Brus (for CdS) and Ekimov (for CuCl) that optical properties of these semiconductor nanocrystals were size dependent and the term quantum size effects was introduced [4,5]. With the increased control over the size and size dispersion Brus was able to show that the absorption spectrum of small colloidal CdS crystallites shifts towards red as the particles were growing. The first colloidal solutions of QDs were prepared by the reaction of Cd^{2+} (from a dissolved Cd salt) and S^{2-} (from H_2S) in the presence of a polymer or SiO_2 nanoparticles. This marks the beginning of the research on highly luminescent QDs. It took about 5 years after the first papers on quantum size effects in CdS before the first report on colloidal CdSe nanocrystals appeared [6] and, again some 5 years later, the next element in group VI of the periodic table (Te) was used in combination with Cd to study quantum size effects in CdTe semiconductor nanocrystals [7]. In spite of all this research the success of the QD synthesis still depends strongly on the skills and experience of the individual chemist involved in the synthesis. First report on nano ZnS was by Bhargava et al [8] in 1994 where they have shown visible luminescence from ZnS NPs by doping it with Mn. Later on different groups have studied UV Visible luminescence from undoped and doped ZnS NPs. Their synthesis by

chemical precipitation method has been intense topic of research in last two decades where numbers of papers have reported size, precursor, capping polymer dependent, optical properties of ZnS nanoparticles. Later on it has been observed that for biomedical applications with tunable color emitting QDs, ZnS doped with transition metal ions, CdSe capped with ZnS has been useful. Moreover, CdSe, CdS, CdTe etc. nanoparticles due to their toxic nature in comparison to ZnS cannot be used for biosensing applications. So detailed review for capped ZnS nanoparticles synthesised by chemical precipitation method has been done and is presented below:

2.2 Capped ZnS nanoparticles

The first observation of luminescence of ZnS was reported in 1866, where a young French chemist, TheoboreSidot observed that ZnS creatures grown by a sublimation method exhibit phosphorescence [9]. In 1920 it was established that a small amount of Cu in ZnS produces green luminescence. During the period from 1940 to 1970 the research on luminescence properties of bulk ZnS expanded. In 1945 Randal et al. [10] had studied phosphorescence and electron traps of various inorganic phosphors such as ZnS, CaS, SrS: Bi. In 1950 Bube et al. [11] had studied luminescence and trapping states of undoped and Cu doped ZnS phosphors. This material turned out to be a good cathode ray tube (CRT) phosphor and was applied in oscilloscopes. This shows luminescence in bulk solids with wide band gaps that has been investigated for a long time. However, nanocrystals of such materials became of interest just recently. Among the previous studies, luminescence and absorption in colloidal ZnS have been performed for pure ZnS samples [12-14]. The reported luminescence spectra show a broad ultraviolet peak at around 420 nm. Among the most studied particles in colloidal form are the II-VI semiconductor compounds CdS and ZnS [11-12].

Vacassy et al. [15] have synthesized ZnS nanoparticles in the powder form by precipitation method from homogeneous solutions of various zinc compounds, with S^{2-} as precipitating anion, formed by decomposition of thioacetamide. They have observed that nucleation is accelerated by the use of acetic acid but limited particle growth occurs because of the formation of complexes with zinc cations that lowers the concentration of free cations in the solution. Also, the complexing-attachment phenomena of the ZnS particles with acetate and acetylacetonate anions lead to the arrest of particle growth processes. The presence of complexed Zn^{2+}species in the acidic solution is demonstrated both theoretically (using a model based on the calculations of the solubility isotherms of the soluble species) and experimentally by Fourier-transform infrared techniques.

Denzler et al. [16] have synthesised ZnS nanoparticles by chemical precipitation method. They observed doublet pattern in the long wavelength region which they attribute to the coexistence of the two crystalline forms in ZnS particles. The important finding in their paper is explanation of four transitions at short wavelengths which exhibits a quadruple fine structure with peaks located at 416.1, 423.9, 430.1, and 437.8 nm. They identified these optical transitions arising from vacancy and interstitial sites for both Zn and S atoms.

Kumbhojkar et al. [17] have synthesized ZnS (QDs) using wet chemical routes with 1- thioglycerol, thiophenol and mercaptoethanol to passivate the nanoclustors. Thiophenol and mercaptoethanol were used to synthesize the QDs at room temperature. They have used size selective precipitation to obtain remarkably narrow size distribution of QDs. Optical absorption spectra of ZnS nanoclusters passivated with above mentioned organic ligands and uncapped ZnS QDs was also studied. They have calculated size of nanoparticles from optical absorption data with EPM and EMA studies. They have shown

the comparison of theoretical results with the experimental results of other workers. They found in their results that excitonic energies calculated for cubic shaped quantum dots show appreciable deviation from the earlier reported experimental values. But reasonable agreement was found for spherical QDs. It signifies that crystallites prefer to be spherical in shape. They have shown that mercaptoethanol is best capping agent among other mentioned above which was not reported earlier.

Kanemeto et al. [18] have observed the photo-physical and photocatalytic properties of ZnS nanoparticles and indicated that the defect levels play a crucial role in determining the luminescence characteristics of quantum particles.

In PL studies they observed a peak at 325 nm (3.82eV) which according to them is due to transition of trapped electrons to valence levels. From above observation they have concluded that capping agents are important in removing Zn dangling orbitals (electron traps) from the gap. Appearance of broad red shifted luminescence and absence of band edge luminescence is due to unsaturated sp^3 hybridized orbitals of surface S atoms. In this paper they have measured PL emission for various excitation wavelengths. They observed a broad peak at about 363nm (3.41eV) for all samples in the PL spectra for all organic passivating agents at 220nm excitation wavelength.

Chem et al. [19] have studied nature and properties of surface states of ZnS nanoparticles using optical techniques. Yanagida et al. [20] have reported for synthesis and spectroscopic studies of cubic and hexagonal ZnS NPs. It has been observed that there is high emission quantum efficiency and very short luminescence decay times in doped ZnS nanoclusters. They have reported a long wavelength peak having energy less than that of the band gap in the optical absorption spectrum of ZnS QDs. According to them it is due to presence of surface states but Kumbhojkar et al. [17] have not observed

any such red shifted peak in the absorption spectra recorded for ZnS QDs. Uclida et al. [21] studied bulk ZnS with varying stoichiometries of excess Zn^{2+} and S^{-2}. Emission at about 350nm is for excess Zn in ZnS which is responsible for an additional peak at 395nm whereas Samelson [22] have got PL peak at 340nm (3.64eV) and attribute it to sulfur vacancy in bulk cubic ZnS. Murase et al. [23] reported that blue emission band at 470nm is due to Zn^{2+} vacancy acting as acceptor site. Later on Bard et al. [24] have explained the origin of blue emission band of 428nm due to S^{2-} vacancies.

Jaehun et al. [25] have found that the luminescence, shape, and stability of ZnS nanoparticles in ethanol are enhanced by capping the surface with (3-mercaptopropyl trimethoxy silane) (MPS) or by treating the surface with SiO_2. While MPS forms an exterior network to encapsulate the ZnS surface SiO_2 surrounds ZnS NPs to smoothen the surface.

Wageh et al. [26] have synthesized ZnS NPs with mercaptoacetic acid as capping agent and obtained NPs of different sizes. The optical properties of ZnS nanoclusters were studied by optical absorption and photoluminescence. High sample quality is reflected in sharp absorption features and strong band edge emission, which is tunable with particle size. The selectively excited luminescence properties and the coupling between electronic and vibrational excitation in ZnS nanoparticles have been discussed.

Khiew et al. [27] have synthesized ZnS nanostructured materials in micellar solution system, containing chitosan laurate as the surfactant. They have adopted self-assembling of the surfactant molecules in water solution as the reaction template for the formation of nanomaterials. The spectroscopic results showed that the synthesized NPs exhibited strong quantum confinement effect. The optical band gap increased significantly as compared to the bulk materials. In addition to this the size of the resulting

nanoparticles is greatly affected by the surfactant concentration that resulted the particle size in the range from 2 to 10 nm. It was found that the nanomaterials have face-centered cubic structure and exhibited the characteristic line broadening feature in the XRD patterns.

Wang et al. [28] have synthesised in situ ZnS semiconductor nanoparticles in chitosan films with average size of 3.4nm. TEM, UV–vis spectra and PL spectra show the ZnS nanoparticles in chitosan template were monodispersed and well passivated. The two-photon absorption coefficient (β) of the chitosan–ZnS quantum dots (QDs) nanocomposite films was observed. Their results show the novel biomacromolecule/QDs nanocomposite film that has large third order optical nonlinear absorption.

Ghosh et al. [29] have synthesized polyvinyl pyrrolidone (PVP) encapsulated ZnS nanoparticles. They added calculated quantity of zinc acetate, thiourea and PVP and dissolved it in N, N- dimethyl form amide (DMF) medium with constant stirring of 150 rpm. Their observed TEM image of ZnS NPs suggests the effect of capping on size separation. It shows that PVP capped ZnS nanoparticles are mono dispersed in nature. Their size is 2-3 nm which matches with XRD results. While uncapped nanoparticles on the other hand are agglomerated and are larger than capped one's. This illustrates the use of PVP as capping agent. Blue shift of absorption edge compared to bulk ZnS clearly explained quantum confinement effect of ZnS nanoparticles.

Gilbert et al. [30] have combined real space pair distribution function (PDF) analysis of nanoparticle structure with particle size analysis and FTIR to reveal that the nature of surface solvent or ligand interactions can affect the interior crystallinity of nanoparticles. The availability of particles with a range of crystallinity provides a model system in which it is possible to determine the interior disorder effects of nanoparticle,

where properties such as mechanical stiffness and fluorescent quantum yield are affected. PDF analysis showed that samples of ZnS nanoparticle with similar mean diameters (3.2 – 3.6 nm) but synthesized and treated differently possess a dramatic range of interior disorder.

Warad et al. [31] have synthesized quantum dots of manganese doped ZnS by a simple precipitation reaction using aqueous route resulting in primary particle sizes of 60–80 nm. The nanoparticles were sterically stabilized using polyphosphates of sodium namely sodium tripolyphosphate (STTP) and sodium hexametaphosphate (SHMP). It was established that SHMP was a superior capping agent than STTP. It was observed that the particle sizes are dependent on the amounts of stabilizing agents (SHMP) used during synthesis, thus making it possible to alter the particle sizes by changing the concentrations of stabilizing agents used during synthesis.

Kim et al. [32] have studied optical properties of ZnS: Cu nanocrystals using sodium polyphosphate (SPP) as a capping agent. ZnS nanoparticles had the cubic structure (β-ZnS), and the crystal structure was not changed with the input of SPP. The particle morphology was spherical with decreased grain size and particle agglomeration was reduced with an increase of SPP input amount. The position of UV absorption edge was found to depend upon the SPP input amount and it was decreased from 340 to 280 nm with the increase of SPP from 0.0 to 1.89 g, clearly showing the remarkable blue-shift phenomenon. Photoluminescence (PL) intensities were also dependent upon the amount of capping agent, and the highest PL intensity was obtained for the sample capped with SPP (1.13 g). PL emission wavelength was also blue-shifted, and it was decreased from 518 to 462 nm with the increase in SPP from 0.0 to 1.89g .

2.3 Capped and doped ZnS nanoparticles

A most effective method to alter the optical properties of semiconductors is by impurity doping. It is well known that the incorporation of impurities into semiconductor lattices can affect the electrical conductivity, as well as the magnetic and optical properties of the semiconductor. For example, pure stoichiometric ZnO is an insulator, while the conductivity of ZnO can be greatly improved with the addition of non-native defects such as Group III and V elements [33, 34]. Doping magnetic ions into semiconductor results in a new family of materials known as "dilute magnetic semiconductors (DMS)". The giant Zeeman splitting of such materials leads to applications in spin-based electronics devices [35, 36]. In terms of optical properties, luminescence activators such as Mn^{2+} or Eu^{2+} make semiconductor nanocrystals interesting candidates for optical imaging applications due to their narrow emission line shapes and broadband excitation profiles [37, 38].

Many approaches have been taken to prepare colloidal doped semiconductor nanocrystals covering most transition metal and rare-earth metal doped II-VI, III-V and IV-VI semiconductors. However, successful doping with desired amount of dopant is often hindered by the self-purification property of nanomaterials. In the first place, it is difficult for doped crystals to nucleate if the dopant-host lattice compatibility is low. Moreover, even in the case of very high dopant-host compatibility such as Co^{2+} doped ZnO, the nucleation reaction is very sensitive to the perturbation as the dopants replace the host ions [39]. Absorption spectra of the reaction solution of Co^{2+} doped ZnO nanocrystals indicate that the dopant ions are excluded from the critical nuclei formed at the early stage of the reaction, probably because of the large influence of the dopants (even at very small number) on the stability of the extremely small nuclei. Another study

on the synthesis of Co^{2+} doped CdS nanocrystals in reverse micelles shows that dopant incorporation is kinetically uncompetitive with host nanocrystal growth at the early stage [40]. The host nanocrystals grow without incorporating the dopant ions at this stage. As the reaction progresses, however, the dopant binding eventually becomes competitive and the addition of dopant ions to the nanocrystals surfaces exceeds the deposition of the host precursor.

In capped NPs size has been controlled by capping agent during precipitation. Nowadays lot of research is focused for doped and capped ZnS NPs. The first report on doped nanocrystals also abbreviated as DNCs showed all features such as increased band gap, shift of excitation and emission spectra of nanosized semiconductor by Bhargava et al. [8] in 1994. They synthesized manganese doped nanocrystals of zinc sulfide. The nanomaterials had external photoluminescence quantum efficiency of 18% and it ushered the era of nanophosphors. The synthesis involved reaction of diethyl zinc with hydrogen sulfide in toluene. The dopant manganese is added as ethyl manganese in tetrahydrofuran solvent to the parent solution of zinc salt before precipitation reaction. Capping agent methacrylic acid was used to maintain separation between the particles formed. Thus formed DNC are separated by centrifugation, washed and vacuum dried. The UV curing effect was established by their further work on dependence of luminescence efficiency on time of curing. The enhancement of efficiency has been explained on the basis of surface passivation of the nanocrystals due to photopolymerization of the surfactant. The photoluminescent (PL) and photoluminescence excitation (PLE) spectra of the nanophosphor has been compared with bulk ZnS:Mn. The PL is slightly shifted and there is a larger line width in the nanophosphor as compared to bulk. It is due to combination of inhomogeneous broadening and phonon assisted transitions. The large shift in PLE

spectrum is attributed to an increase in value of s–p electron band gap in the ZnS nanocrystals as a result of quantum confinement. Further luminescent decay has been reported to be faster by five orders of magnitude. The presence of an impurity within a nanocrystal and localization of electron and hole wave function due to quantum confinement leads to faster energy transfer to impurity in smaller particles as compared to transfer rate for band to band transition or surface recombination. Hence, luminescence efficiency increases with decrease of particle size. Following the encouraging results of Bhargava et al. [8, 40] on Mn doped ZnS nanophosphor Khosravi et al. [41] reported synthesis of manganese doped ZnS nanoparticles by aqueous method. They followed process similar to the one, used by Nosaka et al. [42] for ZnS quantum dots. In this method, aqueous solution of zinc chloride with required amount of dopant manganese chloride is mixed slowly with mercaptoethanol under constant agitation and then reacted dropwise with sodium sulfide solution. The reaction was carried out under inert atmosphere of nitrogen gas to avoid oxidation of freshly formed highly reactive nanoparticles. Then usual washing, centrifugation and drying are followed to obtain the freestanding nanophosphors. They observed PLE and PL peaks at 312 and 600 nm, respectively. Mn concentration of 12 at wt.% was found to be optimum. About the same time, Khosravi et al. [43] with slightly different team reported synthesis of copper doped zinc sulfide quantum particles. Method used by Weller et al [44] for synthesis of CdS was employed for the purpose. The basic idea had been the formation of polymeric chains by phosphate groups and their attachment to metal ions. Copper doped zinc sulfide nanocrystals were synthesized by first preparing a solution of zinc chloride, copper chloride and sodium acetate of pH 8–9. Solution of sodium hexametaphosphate was added before precipitation reaction with sodium sulfide solution. As the sulfide solution is

added, sulfur reacts with excess metal ions forming sulfide clusters. Clusters grow by the coalescence of smaller clusters or on metal ion seeds present in the solution. On a growing metal sulfide cluster, phosphate chains get attached through metal ions. These chains separate the clusters due to their length and avoid coalescence. The reaction is once again carried out in nitrogen atmosphere. Diameter of the particles determined from XRD is reported to be 2.1nm. Excitation was at 300 nm which corresponds to 4.1 eV and emission has been at 480 nm. Luminescence of undoped ZnS prepared by same process has been compared and found to be 326 and 424 nm for excitation and emission, respectively. Luminescence decay times were determined for both Cu doped and undoped ZnS. Two exponential decay times of 2.9, 54.2 and 1.62, 22.12 ns were observed. Undoped sample obviously had shorter decay times. There is no mention of curing or annealing of any type in the two methods given by Kosaravi teams. Yu et al. [45] prepared zinc sulfide nanoparticles with homogeneous Mn distribution and studied optical properties along with other characteristics. Procedure followed was of reaction between methanolic solution of zinc acetate with manganese acetate and aqueous solution of sodium sulfide. Dispersion of precipitates was achieved with methacrylic acid. They reported variation of crystallite sizes from 2.3 to 2.7 nm using different amount of methacrylic acid. Homogeneous distribution of Mn^{2+} ions in the ZnS formed was established by the workers with well-resolved ESR spectra of the samples with use of methacrylic acid. ESR spectra of the sample without the addition of methacrylic acid had broad lines with unresolved structure. From the shape of hyperfine lines, these spectra can be interpreted as the superposition of these corresponding to isolated Mn^{2+} ions and to Mn^{2+} pairs caused by inhomogeneous distribution of manganese. TEM and XRD studies confirmed the nanocrystalline structure of the phosphor prepared and size ranged from

2.3 to 2.7 nm. The effect of addition of methacrylic acid on particle size, UV absorption and PL has been highlighted in their research article. Bhargava [46] after two years from his previous paper elucidated in detail the effect of UV curing that was mentioned in his first paper of 1994. He has shown increase in PLE and PL intensity with increasing time of curing. UV curing is conducive to surface passivation which greatly improves the efficiency. Yang et al. [47] studied optical properties of manganese doped ZnS nanocrystals. Synthesis process adopted was chemical precipitation route in presence of a capping agent. They studied and compared the behaviour of the nanophosphor in sol form and the dried powder obtained after centrifugation, washing, drying and calcining at 200–700° C for 2 h. Particle size of nanocrystals in sol was reported to be around 5 nm and that of powder after calcining at 400 °C was 12 nm. PLE and PL spectra of nanophosphor sol and powder were presented without and with capping agent. These were found to be similar and there was slight shift in peaks in both cases towards shorter wavelength for sol and powder, with and without capping agent. Stanic et al. [48] have reported sol–gel synthesis of nanosize ZnS, which is a key material to a large number of phosphors. Zinc tert-butoxide in butanol and water free toluene was taken and high purity hydrogen sulfide gas was bubbled through the solution till complete gelation occurred. Gel was allowed to age for 24 h and dried in vacuum. Formation of ZnS was confirmed by X-ray diffraction (XRD) and IR absorption spectra.

Senna et al. [49] synthesized and studied nanocrystalline ZnS: Mn phosphor from solutions containing carboxylic acids. Methanolic solutions of zinc acetate and manganese acetate were mixed under continuous stirring and Na_2S solution in methanol was then added to the above solution. Acrylic acid or methacrylic acid was added after precipitation while stirring was continued. The phosphor was obtained after washing,

centrifugation and drying at 50 °C for 24 h. Different properties were studied with varying amounts of acrylic acid from 0 to 1.0 mol with respect to 20 mol. of ZnS. PL intensity increased up to 0.72 mol acrylic acid and then it started decreasing with increase of acrylic acid. The excitation peak shifts towards shorter wavelength as the amount of acrylic acid was increased. Xu et al. [50] synthesized impurities-activated ZnS nanocrystals in micro emulsion with hydrothermal treatment. They used petroleum ether as oil phase and mixture of poly (oxyethylene) 5- nonyl phenol ether (NP-5) and poly(oxyethylene)nonyl phenol ether as surfactant phase. Two reverse micro emulsions of the system with aqueous solutions of $ZnCl_2$ along with dopant and sodium sulfide were prepared separately and mixed with continuous stirring. The micro emulsion system was also treated under hydrothermal conditions for surface passivation. ZnS:Cu, ZnS:Eu and ZnS:Mn nanocrystals were prepared and particle size was found to vary from 3 to 18 nm. Emission intensity enhancement of 60 times as compared to Mn doped ZnS nanocrystals synthesized by conventional aqueous reaction method has been reported. Another significant observation of the workers is increase of integrated PL intensity with increasing atomic number of dopants. Bol and Meijerink [51] synthesised nanocrystalline ZnS:Mn^{2+} by two methods and made lifetime measurements and conducted time-resolved spectroscopy. Synthesis involved solutions of diethyl zinc, manganesecyclohexabutyrate and methacrylic acid in toluene. Precipitation was achieved with saturated solution of hydrogen sulfide gas in toluene. In the second method, they used aqueous solutions of zinc acetate, manganese acetate and $Na(PO_3)n$ and Na_2S solution as precipitant. The methods have been nearly similar to the one described earlier. They reported some contradiction to earlier work of Bhargava [8,46] in regard to shorter decay times explained on the basis that the spin forbidden $^4T_1$-$^6A_1$ transition of Mn^{2+} impurity

becomes less spin forbidden due to hybridization of s–p states of ZnS host and the d states of Mn^{2+} impurity. They measured decay times at emission of 400 and 600 nm by exciting the samples at 308 nm with excimer laser. They also recorded time-resolved emission spectra for time delay of 0 ms, 3 ms and 0.5 ms with gate width of 2 ms, 200 ms and 1 ms, respectively. Emission peaked at 420, 420 and 590 nm (two peaks), 590 nm, respectively, for the three delay times. From the data, it can be said that short decay time is ascribed to defect related emission of ZnS and not to decay from transition of Mn^{2+} impurity. Xu and Ji [52] gave an interesting new route for preparation of nanoparticles of ZnS. The new route is via synthesis of Zn nanoparticles by inert-gas evaporation with induction heating. These particles were made to react with sodium sulfide aqueous solution under ultrasonic radiation at 50 °C. XRD analysis showed highly crystalline phase of ZnS and TEM confirmed spherical particles with narrow size distribution averaging 40 nm. However, presence of some unreacted zinc was observed by XRD. Pingbo et al. [53] prepared nanocrystalline ZnS: Mn using capping agent dodecyl benzene sulfonic acid sodium salt (DBS). Chemical precipitation method has been used employing aqueous solutions of Zn $(NO_3)^2$, $MnCl_2$ and Na_2S. Different amount of Na_2S was taken to create Zn^{2+} vacancies. They studied PL properties varying Mn concentration and also compared the luminescence with and without surface-modification. In this work, fluorescence lifetime have also been analyzed for different emission wavelengths and observed that nanosecond decay is due to zinc vacancies and millisecond decay is attributed to Mn. Photo aging was also studied for these samples. Wang and Hong [54] reported, a new preparation procedure for nanosized zinc sulfide particles by solid-state method at low temperature. Zinc acetate and thioacetamide were milled separately, mixed and further milled for through and uniform dispersion of the components in the mass. The

mixture was heated in an oven at different temperatures up to 300 °C for 4 h. Formation of nanocrystalline zinc sulfide with size of 3.2 nm at 100 °C is confirmed. TEM and PL studies also establised nanocrystalline nature of the sample prepared.

Manzoor et al. [55] have studied multi-colour emitting doped ZnS nanocrystals capped with pyridine (P-ZnS) or polyvinyl pyrrolidone (PVP-ZnS) synthesized by wet chemical methods. The photoluminescence studies show that the dopant related emission from P-ZnS nanocrystals are caused by the energy transfer from band-to-band excitation of the host lattice. However, in the case of PVP capped ZnS, considerable enhancement in the emission intensity was observed and the corresponding excitation spectra appeared to be broadened due to the presence of multiple excitation bands with peak maxima at 235, 253, 260, 275, and 310 nm. The presence of PVP related energy bands in the excitation spectrum indicates the process of energy transfer from the surface adsorbed PVP molecules to dopant centers in ZnS nanocrystals. This study brings out a heterogeneous sensitizer-activator relation between organic surface adsorbate and doped semi conducting nanocrystals.

Kubo et al. [56] have reported the modification of ZnS:Mn nanocrystal suspension by a capping agent with a phosphate or carboxyl group. They have found increase in photoluminescence intensity and its quantum efficiency due to d–d transition of Mn^{2+} ions through two routes of energy transfer: (1) ZnS-Mn^{2+} and (2) ZnS-phosphate or carboxyl groups-Mn^{2+}.

Karar et al. [57] have prepared ZnS: Mn in nanocrystalline form by a chemical method using PVP as a capping agent. They have varied Mn concentration over entire solid solution limit in ZnS, i.e. from 0 to 40%.

Warad et al. [58] have reported the synthesis of redispersible zinc sulphide nanophosphor doped with manganese passivated with biocompatible chitosan molecules. The presence of biocompatible capping agent, chitosan, makes it suitable for bio-labels (markers). Further research articles on effect of doping and capping on ZnS NPs are discussed at relevant places in results and discussions (chapter 4-6).

From above studies it is clear that when ZnS transforms from bulk to nano all optical and morphological properties are changing. The properties such as excitonic binding energy, absorbtion edge, excitonic emission, particle size etc. changes with the slight variations in nature of the capping agents, molar concentration of capping agent/Zn/S/dopants, nature of the dopants. The particle morphology was spherical, and grain size was decreased and particle agglomeration was reduced with an increase in capping input amount. The position of UV absorption edge was found to depend upon the capping input amount, and it decreases with increase in capping input which clearly shows the remarkable blue-shift phenomenon. This change in properties is mainly due to the quantum confinement effects and use of capping agent which leads to observed variation in the band gap of the ZnS. So it is clear that nature of capping agent, their amount and charge affects optical and morphological properties of ZnS NPs. Further by doping various dopants in host ZnS the emission color varies from blue to nearly all colors in visible region depending upon polymer used.

2.4 Thesis layout

In this review the details of doped and undoped ZnS nanoparticles with variable capping agents have been studied. The studies include the effect of dopants, capping agent, ageing time, molar ratio and concentration of impurity on ZnS nanoparticles. These effects were seen on the absorption spectra, emission spectra and on the particle size of

the ZnS nano particles. The properties such as excitonic binding energy, absorption edge, excitonic emission, emission intensity and particle size changes with the slight variations in nature of the capping agents, molar concentration of capping agent/Zn/S/dopants, nature of the dopants. The particle morphology was spherical, and grain size was decreased and particle agglomeration was reduced with an increase of capping agent amount. Bulk ZnS has a wide bandgap of ~ 3.68 eV. Blue-shifted from its bulk bandgap, the band edge emission of ZnS nanocrystals can be tuned in the ultraviolet region via controlled synthesis that produces particles of different shapes and sizes. Also tunable emission characteristics are reported with variation in particle size, using core- shell, alloyed and doped nanostructures. But in all cases multi step synthesis, multiple samples and controlled synthesis parameters are required. Moreover, many samples with different concentrations of precursors give tunable emission color in whole visible region. As discussed above in literature review doped ZnS NPs have been synthesized in aqueous and organic medium by coprecipitation of the host and the dopant. They also emit different colors without change in particle size which can be very useful for tunable emitters. For this we concentrated on capped and doped ZnS nanocrystals. Also this system is less toxic as compared to CdSe, CdTe, and there are no size selective methods or control of kinetics necessary to exactly control the size for obtaining different emission colors, because this can be obtained with different doping metals independent of particle size. Another advantage of this system is the large stokes shift between excitation and emission. The overall goal of this research work is to study effect of different capping agents and their concentration on optical and morphological properties of ZnS NPs. Secondly to achieve tunable emission color in visible region with minimum number of samples along with good stability which is suitable for optoelectronic and biomedical

imaging applications. So this thesis sets out to synthesize and investigate several capped and doped nanomaterials with optical properties that can be tuned without changing the particle size, shape or composition.

2.5 References

[1] A. Henglein, *J. Phys. Chem.* **86**, 2291 (1982).

[2] R. Rossetti, L.E. Brus, *J. Phys. Chem.* **86,** 4470 (1982).

[3] D. Duonghong, J. Ramsden, M. Grätzel, *J Am. Chem. Soc.* **104,** 2977 (1982).

[4] R. Rossetti, J.L. Ellison, J.M. Gibson, L.E. Brus, *J. Chem. Phys.*, **80,** 4464 (1984).

[5] A.I. Ekimov, A. A. Onushchenko, *Fizika i Tekhnika Poluprovodnikov* **16,** 1215 (1982).

[6] N. M. Dimitrijevic, P.V. Kamat, *J. Phys. Chem.* **91**, 2096 (1987).

[7] T. Rajh, O. I. Micic, A. J. Nozik, *J. Phys. Chem.* 97, 11999 (1993).

[8] R.N. Bhargava, D. Gallagher, X. Hong, A. Nurmikko, *Phys. Rev. Lett.* **72** 416 (1994).

[9] Sidot. T, C. R., **62,** 999 (1866).

[10] J. T. Randall and H. F. Wilkins, *Proc. R. Soc. London, Ser.* A **184,** 366 (1945).

[11] R H Bube, F Herman, and H W Leverenz, *Annual Review of Physical Chemistry,* **5,** 199-214, (1954).

[12] C.B. Murray, D.B. Norris and M.G. Bawendi, *J. Am. Chem. Soc.* **115,** 8706 *(*1993).

[13] S. M. Stuczynski, J.G. Brennan, M. L. Steigerwald, *Inorg. Chem.* **28,** 4431 (1989).

[14] M. A. Hines, P. G. Sionnest, *J. Phys. Chem.* **100,** 468-471(1996).

[15] R. Vacassy, S.M. Scholz, J. Dutta, C.J.G. Plummer, R. Houriet, H. Hofmann, *J. Am. Ceram. Soc.* **81,** 2699–2705 (1998).

[16] D. Denzler, M. Olschewski, and K. Sattler, *J. Appl. Phys.*, **84,** 5, (1998).

[17] Kumbhojkar, V.V.Nikesh, A.Kshirsagar, *Journal of Applied Physics,* **88,** 11(2000).

[18] M. Kanemoto, T. Shiragami, C. Pac, and S. Yanagida, *J. Phys. Chem.* **96,** 3521, (1992).

[19] W. Chen, Z. G. Wang, Z. J. Lin, and L. Y. Lin, J. Appl. Phys. **82**, 3111 (1997).

[20] S.Yanagida , Y. Ishimaru, Y. Miyake, T. Shiragami, C. Pac, K. Hashimoto, T. Sakata, *J.Phys. Chem.*, **93**, 2576, (1989).

[21] I. Uchida, *J. Phys. Soc. Jpn.* **19,** 670, (1964).

[22] H. Samelson, A. Lempicki, *Phys. Rev.* **125** 901(1962).

[23] N. Murase, R. Jagannathan, Y. Kanematsu, M. Watanabe, A. Kurita, K. Hirata, T. Yazawa, , T. Kushida, *Journal of Physical Chemistry B.* ***103,*** 754 (1999).

[24] W.G. Becker, A.J. Bard, *J. Phys. Chem.* **78** 4888 (1983).

[25] C. Jaehun, L. Sunbae, J. Du-Jeon, Korea- Japan Forum, Seoul, Coree, Republiquede, **377,** 85-88 (2002).

[26] S. Wageh, Liu Shu-Man, Fang Tian You and Xu Xu-Rong, *Journal of Luminescence,* **102-103,** 768-773 (2003).

[27] P.S. Khiew, S. Radiman, N.M. Huang, Md. Soot Ahmad, K. Nadarajah, *Materials Letters* **59,** 989–993 (2005).

[28] X. Wang, Y. D. S. Ding, L. Fan, X. Shi, Q. Wang, G. Xiong, *Physica E* **30,** 96–100 (2005).

[29] G. Ghosh, M. Kanti, Naskar, A. Patra, M. Chatterjee, *Journal of Optical Materials,* **28,** 1047-1053 (2006).

[30] B. Gilbert, F. Huang, Z. Lin, C. Goodell, H. Zhang, J. F. Banfield, *Nano Lett.,***6(4),** 605-610 (2006).

[31] H.C.Warad, S.C.Ghosh, B. Hemtanon, C. Thanachayanont, J. Dutta, *Science and Technology of Advanced Materials,* **6,** 296–301, (2005).

[32] D Kim, K. D. Min, J. Lee, J. H. Park, J. H. Chun, *Materials Science and Engineering: B,* **131,** 13-17 (2006).

[33] A. Segura, J. A. Sans, D. Errandonea, D. M. Garcia, V. Fages, *Applied Physics Letters* **88,** 3 (2006).

[34] J. G. Lu, Q. N. Liang, Y. Z. Zhang, Z. H. Ye, S. Z. Fujita, *Journal of Physics D-Applied Physics* ***40,*** 3177 (2007).

[35] S. J. Pearton, W. H. Heo, M. Ivill, D. P. Norton, T. Steiner, *Semiconductor Science and Technology* ***19,*** R59 (2004).

[36] V. A. Ivanov, T. G. Aminov, V. M. Novotortsev, V. T. Kalinnikov, *Russian Chemical Bulletin* ***53,*** 2357 (2004).

[37] C. Song, K. W. Geng, F. Zeng, X. B.Wang, Y. X. Shen, F. Pan, Y. N. Xie, T. Liu, Zhou, H. T. Fan, Z. *Physical Review B* ***73,*** 6 *(*2006).

[38] F. H. Su, Z. L. Fang, B. S. Ma, K. Ding, G. H. Li, S. J. Xu, *Journal of Applied Physics* ***95,*** 3344 (2004).

[39] W. Chen, A. G. Joly, J. O. Malm, J. O. Bovin, *Journal of Applied Physics* ***95,*** 667 (**2004).**

[40] D. A. Schwartz, N. S. Norberg, Q. P. Nguyen, J. M. Parker, D. R. Gamelin, *Journal of the American Chemical Society* ***125,*** 13205 (2003).

[41] A.A. Khosravi, M. Kundu, B.A. Kuruvilla, G.S. Shekhawat, R.P. Gupta, A.K. Sharma, P.D. Vyas, S.K. Kulkarrni, *Appl. Phys. Lett.* **67 (17)** 2506 (1995).

[42] Y. Nosaka, K. Yamaguchi, H. Miyama, M. Hayashi, *Chem. Lett.* **17,** 605 (1988).

[43] A.A. Khosravi, M. Kundu, B.A. Kuruvilla, G.S. Shekhawat, R.P. Gupta, A.K. Sharma, P.D. Vyas, S.K. Kulkarrni, Appl. Phys. Lett. **67 (17)** 2506 (1995).

[44] D.V. Talapin, A. L. Rogach, A. Kornowski, M. Haase, H. Weller, *Nano Lett.* **1,** 207 (2001).

[45] W. W. Yu, X. Peng, *Angew. Chem. Int. Ed.* **41,** 23681 **(2002).**

[46] R.N. Bhargava, *J. Lumin.* **70,** 85 (1996).

[47] H. Yang, Z. Wang, L. Song, M. Zhao, Y. Chen, K. Dou, J. Yu, L. Wang, *Mater. Chem. Phys.* **47** 249 (1997).

[48] V. Stanic, T.H. Etsell, A.C. Pierre, R.J. Mikula, *Mater. Lett.* **31,** 35 (1997)..

[49] M. Senna, T. Igarashi, M. Konishi, T. Isobe, *Fourth International Display Workshop, Nogoya, Japan*, November **19–21,** pp. 613–616 (1997).

[50] S.J. Xu, S.J. Chua, B. Liu, L.M. Gan, C.H. Chew, G.Q. Xu, *Appl. Phys. Lett.* **73 (4)** 478 (1998).

[51] A.A. Bol, A. Meijerink, *Phys. Rev. B* **54 (24)** R15 997 (1998).

[52] J. Xu, W. Ji, J. Mater. *Sci. Lett.* **18,** 115 (1999).

[53] X. Pingbo, Z. Weiping, Y. Min, Z. Weiwei, L. Liren, X. Shangda, J. Colloid Surf. *Sci.* **229,** 534 (2000).

[54] L.P. Wang, G.Y. Hong, *Mater. Res. Bull.* **35** 695 (2000).

[55] K. Manzoor, S.R. Vadera, N. Kumar, T.R.N. Kutty, *Solid State Commun.* **129** 469 (2004).

[56] T. Kubo, T. Isobe, M. Senna, *Journal of Luminescence* **99,** 39–45 (2002).

[57] N. Karar, H. Chander, S.M. Shivaprasad, *Appl. Phys. Lett.* **85,** 5058 (2004).

CHAPTER 3

EXPERIMENTAL TECHNIQUES

Overview

This chapter describes the details of experimentation. The experimental procedures followed to prepare ZnS nanoparticles with different capping agents having different capping concentration are given. The characterization procedures along with instruments used to generate and analyze the data has been given. The details about each of the instruments, their model number, working and operating conditions have been given. The steps followed for different experiments have been discussed in detail. This chapter sums up the whole scheme of events leading to successful completion of experimental work.

3.1 Raw Materials

In the present study, raw materials used for preparing the samples were zinc acetate (Zn $(CH_3COO)_2$. $2H_2O$) (99.99%, Sigma Aldrich), sodium sulphide nonahydrate (99.99%, Sigma Aldrich), Poly Vinyl Pyrrolidone (PVP, 99.99%, Sigma Aldrich), 2-mercaptoethanol (ME, 99.99%, Sigma Aldrich), thioglycerol (TG, 99.99%, Sigma Aldrich), chitosan (CH, 99.99%, Sigma Aldrich), and sodium hexametaphosphate (SHMP, 99.99%, Sigma Aldrich), Deoxyribonucleic acid (apple DNA), Manganese acetate (Mn $(CH_3COO)_2$. $2H_2O$, 99.99%, Sigma Aldrich), ethanol (Merk), acetone (Merk), double distilled water. All these materials were used without any further purification.

3.1.1 Sample Preparation (Capped and uncapped ZnS nanoparticles)

Zinc sulphide (ZnS) nanoparticles were synthesized by chemical precipitation method [1, 2]. These NPs were prepared under similar conditions to compare their properties (same ratio of Zn^{2+}/S^{2-}) using seven different capping agents. In the first step 40mL homogenous solutions of 0.5M zinc acetate and 0.5M sodium sulphide were prepared in distilled water separately by stirring them for half an hour. Also (0.1, 0.5, 1.0, 1.5, 2.0 at. wt. %) solutions of all capping agents used in present investigation were prepared in 40mL distilled water separately. For the synthesis of uncapped ZnS NPs, 40mL of 0.5M sodium sulphide solution was added drop wise to 40mL solution of 0.5M zinc acetate (Zn $(CH_3COO)_2$. $2H_2O$) in aqueous medium. Solution containing ZnS NPs was stirred for half an hour using a magnetic stirrer. For the synthesis of capped ZnS NPs instead of direct addition of sodium sulphide to zinc acetate solution, 40mL solution of capping agents was added slowly in 40mL solution of 0.5M zinc acetate. The solution was stirred for half an hour at room temperature. Then to this reaction mixture 40mL

solution of 0.5 M sodium sulphide was added drop wise. Soon after the addition of sodium sulphide the precipitation phenomenon occurs and concentration of precipitates increases as addition was increased. The stirring was allowed for half an hour. The capping agents PVP, TG, ME, CH, SHMP were used for avoiding the particle agglomeration and passivating surface defects. The solution containing particles were then centrifuged at 4000 rpm for 5 minutes. The precipitated particles were filtered using Whatman 40 filter paper. To remove the last traces of adhered impurities, the particles were washed several times using double distilled water. The washed particles were dried in vacuum oven at 60ºC for 24 hours. For the entire study the concentration (0.1, 0.5, 1.0, 1.5, 2.0 at. wt. %) of capping agents were taken same for every series. Secondly by capping same amount (0.1-2.0%) of capping agents removal of defect states in the band gap of host ZnS was also compared.

3.1.2 Sample Preparation (Capped and doped ZnS nanoparticles)

High purity research grade chemicals as mentioned above were purchased from Sigma Aldrich. PVP and CH (a natural biopolymer) were also purchased from Sigma Aldrich. CH capped Mn doped and PVP capped Mn doped, ZnS NPs were synthesized by chemical precipitation method. Chitosan is hydrophilic, nontoxic, biocompatible and biodegradable. In the first step 40mL homogenous solutions of 0.5M zinc acetate, 0.5M sodium sulphide and 0.1 at. % manganese acetate was prepared separately in distilled water by stirring them for half an hour. Also solution of different concentration (0.01, 0.1, 1.0 at. wt. %) of capping agent chitosan used in present investigation were prepared in 40mL solution of 1% acetic acid in distilled water separately. Chitosan is insoluble in water and strong acids but is soluble in dilute acids, as amine group is protanated to NH_3^+. Here we have used 1% acetic acid solution in distilled water to dissolve chitosan. For

PVP capped ZnS: Mn^{2+} NPs, PVP (0.1, 1.5 at. %) solutions were prepared in 40mL distilled water. For the synthesis of capped ZnS: Mn^{2+} NPs 40mL solution of zinc acetate and manganese acetate were mixed in a beaker and stirred for 20 minutes. Then to this reaction mixture 40mL solution of capping agent (chitosan or PVP) was added slowly. The solution was stirred for half an hour at room temperature. Then 40mL solution of 0.5M sodium sulphide was added drop wise in this reaction mixture. Soon after the addition of sodium sulphide the precipitation phenomenon occurs and concentration of precipitates increases as addition was increased. The stirring was done for half an hour. The solution containing ZnS:Mn nanoparticles were then centrifuged at 4000 rpm for 5 minutes. The precipitated particles were filtered using Whatman 40 filter paper. To remove the last traces of adhered impurities and excess chitosan, PVP in capped ZnS: Mn^{2+}, the particles were washed several times using double distilled water and 0.1 % acetic acid (for CH capped NPs) solution for 48 hours. The washed particles were dried in vacuum oven at 60ºC for 24 hours.

In this study, chitosan and PVP were used as surfactant or capping agent to control the nanocrystal growth and to stabilize the nanocrystals against aggregation. In addition, these polymers were also used to render the nanocrystals water soluble and provide functional chemical groups for further attachment of glucose. For glucose sensing five sets of 0.2 gm of ZnS: Mn^{2+} @ chitosan particles dispersed in 5 mL of Mili-Q water were made. First one is labeled as control. In other four sets 2.5µL, 5µL, 7.5 µL and 10µL of 0.5M glucose-D solution was added and used for further studies.

3.1.3 Sample Preparation (DNA Capped ZnS nanoparticles)

For this study chemicals of analytical grade were purchased from Sigma Aldrich. Zinc sulphide (ZnS) NPs were synthesized by chemical precipitation. 0.01M (20 mL) zinc

acetate in ethanol solution (medium) was poured in reaction flask. Solution was stirred continuously for 2 h by magnetic stirrer. Now Plasmid DNA (Deoxyribonucleic Acid) having average size of 3550 base pair (bp) was added. This mixture was allowed to stir for another 1 h. Then to this reaction mixture sodium sulphide (0.01M) was added drop wise. Stirring was further continued for another 2 h. The crystal growth was further prevented by keeping the reaction flask in ultrasonic bath system. The ultasonication was continued for 10 h. The resulting white precipitate was centrifuged at 4000 rpm for 5 minutes and washed thrice with alcohol. This precipitate was subsequently washed continuously with hot Mili Q water (75^0C) for half hour to remove unbound polymer (DNA) and non reacted zinc and sulphide ions. White precipitate hence obtained was dried at 60^0C in vacuum oven for 8 hours. Hence DNA @ ZnS particles were synthesized. For further characterizations and studies particles were kept in cold (2-8^0C) to avoid further crystal growth.

3.2 Morphological and Optical Characterization

The ZnS nanoparticles were characterized by X-ray diffraction (XRD) technique using Rigaku, model D–max IIIC diffractometer and Panalytical Xpert Pro MPD with Cu (Kα) radiation. TEM studies were conducted using Transmission Electron Microscope, JEOL (JEM 2000FX) operating at 200 kV and Analytical Transmission electron microscope (FEI model Technai G2-F30) S-Twin having field emission gun with EDS attachment and also having accelerating voltage of 300KV. For TEM study the powder was ultrasonicated in ethanol. One drop of this solution was dropped on carbon coated Cu grid. Ethanol was allowed to evaporate allowing powder to remain on grid. Optical absorption spectra of the ZnS particles were recorded with a double beam UV-Visible spectrophotometer (Model: Perkin Elmer Lambda 3500) in the range 200–800 nm. PL

studies were done with spectrometer (Model: Perkin Elmer55). For PL (excitation and emission) studies ZnS nanoparticles in powder form were used in equal amount. Suitable filter was used to prevent the irradiation of light with doubled wavelength when the emission was detected. FTIR spectra have been recorded in range of 4000-400cm^{-1} with Perkin Elmer Spectrum BX (2). For the zeta potential measurement, Malvern Zetasizer 2000 (UK) with a He–Ne laser was used. Zeta potential measurement was done to see surface charge and hence stability of ZnS nanoparticles. Details about characterization techniques are given in detail in respective chapters of results and discussion.

3.2.2 References

[1] K Manzoor.,S.R. Vadera, N Kumar, T. R. N. Kutty, *Materials Chemistry and Physics*, **82,** 718, (2003).

[2] H.C. Warad, S.C. Ghosh, Hemtanon, C. Thanachayanont, J. Dutta, *Science and Technology of Advanced Materials*, **6,** 296, (2005) .

RESULTS AND DISCUSSION

CHAPTER 4

OPTICAL AND MORPHOLOGICAL STUDIES OF SYNTHESISED UNCAPPED ZnS NANOPARTICLES

Overview

In this chapter the experimental results of ZnS nanostructures synthesised by chemical precipitation route are presented. The entire work has been done to study emission properties with enhanced emission intensity. This chapter deals with optical (UV-Visible absorption and photoluminescence spectroscopy) and morphological (XRD, TEM, SAED etc.) studies of synthesized ZnS NPs.

4.1 Experimental Studies

For this study chemicals of analytical grade were purchased from Sigma Aldrich. Zinc sulphide (ZnS) nanoparticles (NPs) were synthesized by chemical precipitation method as described earlier in chapter 3 (experimental section). Briefly discussing in the first step 40mL homogenous solutions of 0.5M zinc acetate (Zn $(CH_3COO)_2$. $2H_2O$) and 0.5M sodium sulphide (Na_2S) were prepared in distilled water separately by stirring them for half an hour. For the synthesis of ZnS NPs, 40mL of 0.5M sodium sulphide solution was added drop wise to 40mL solution of 0.5M zinc acetate in aqueous medium. Soon after the addition of sodium sulphide the precipitation phenomenon occurs and concentration of precipitates increases as addition was increased. Solution containing ZnS NPs was stirred for half an hour using a magnetic stirrer. The solution containing particles were then centrifuged at 4000 rpm for 5 minutes. The precipitated particles were filtered using Whatman 40 filter paper. To remove the last traces of adhered impurities, the particles were washed several times using double distilled water. The washed particles were dried in vacuum oven at 60ºC for 24 hours.

4.2 XRD Studies

Figure 4.1 shows X-ray diffraction pattern of ZnS NPs. Intensities of the three most important peaks of ZnS namely <111>, <220> and <311> reflections corresponding to 2θ values 28.5º, 47.6º and 56.4º is observed in the XRD pattern which match well with those of the cubic zinc blende structure mentioned in ICDD card No. 05-0566. Broadening of the XRD peaks indicates the formation of ZnS nano crystallites (NC's). The nano crystals have lesser lattice planes compared to bulk which contributes to the broadening of peaks in the diffraction pattern. This broadening can also arise from micro straining of the crystal structure which arises from dislocation and twinning [1]. These

defects were believed to be associated with the chemically synthesized nanocrystals as they grow spontaneously during chemical reaction since chemical species get very little time to diffuse to an energetically favourable site.

Crystallite size of ZnS nanoparticles was calculated by following Scherer's equation [2],

$$D = k\lambda / \beta\cos\theta \qquad (1)$$

where k=0.9, D- crystallite size (Å), λ (Å) the wavelength of Cu (Kα) radiation and β(in radians) is full width at half maximum (FWHM). The average crystallite size estimated from three planes is 5.6 nm for ZnS NC's.

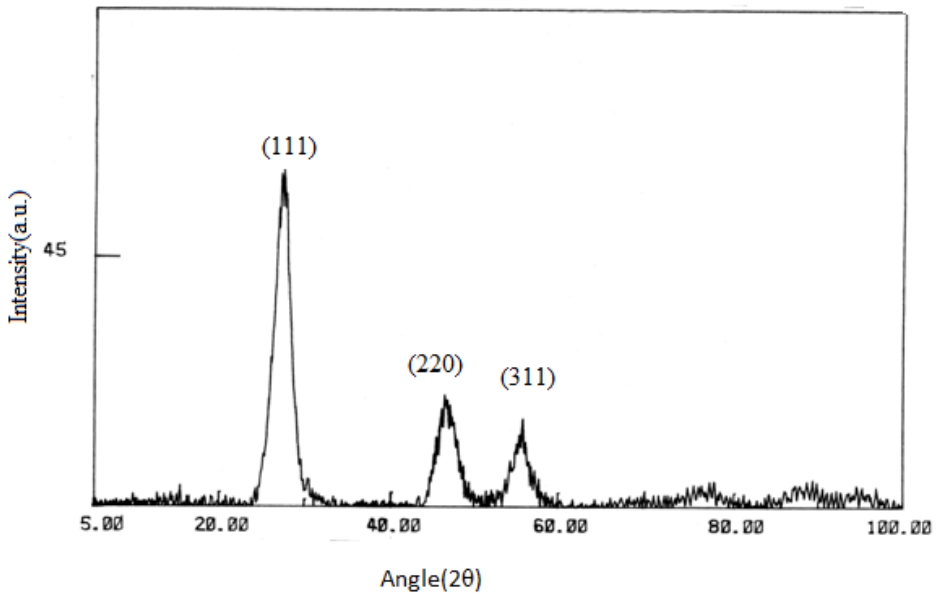

Figure 4.1 X-ray diffraction pattern of uncapped ZnS NPs.

4.3 TEM Studies

Figure 4.2(a) shows TEM micrograph of synthesised ZnS nanoparticles. Average size of NPs varies from 4-6nm. Along with NPs, formation of nanorods (NRs) is also observed in same micrograph. This could be due to uncontrolled agglomeration of ZnS nanostructures which minimizes its high surface energy. The diameter of nanorods is about 8-10nm and length is 80nm. Figure 4.2 (b) shows SAED pattern of synthesised

nanostructures. It shows crystalline nature of synthesised nanostructures showing (111), (220) and (311) plane which corrugates with XRD results. Formation of NRs in uncapped ZnS samples is also evident from bright field and high-angle annular dark-field (HAAD) images shown in Figure 4.2 (c, d).

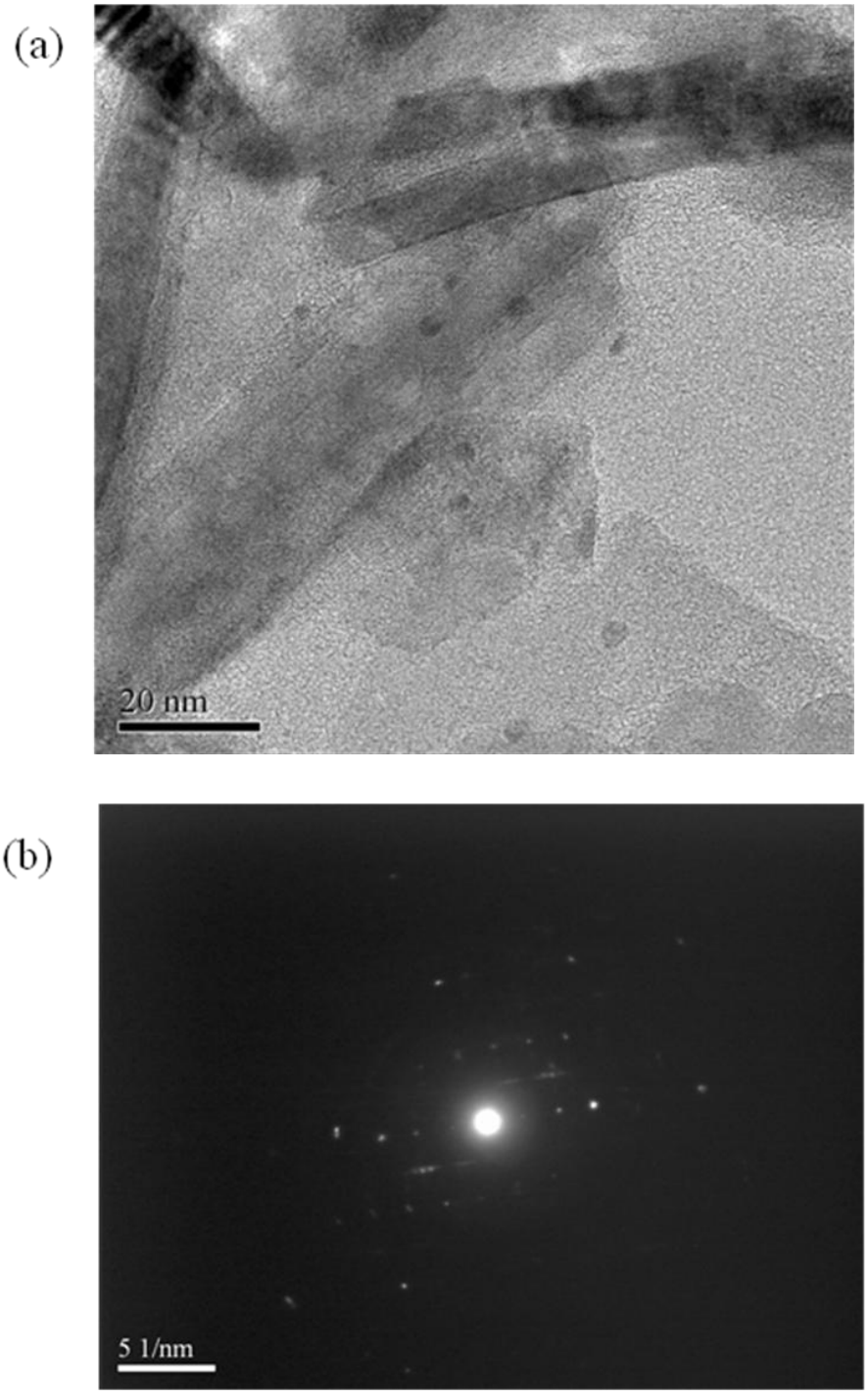

(c)

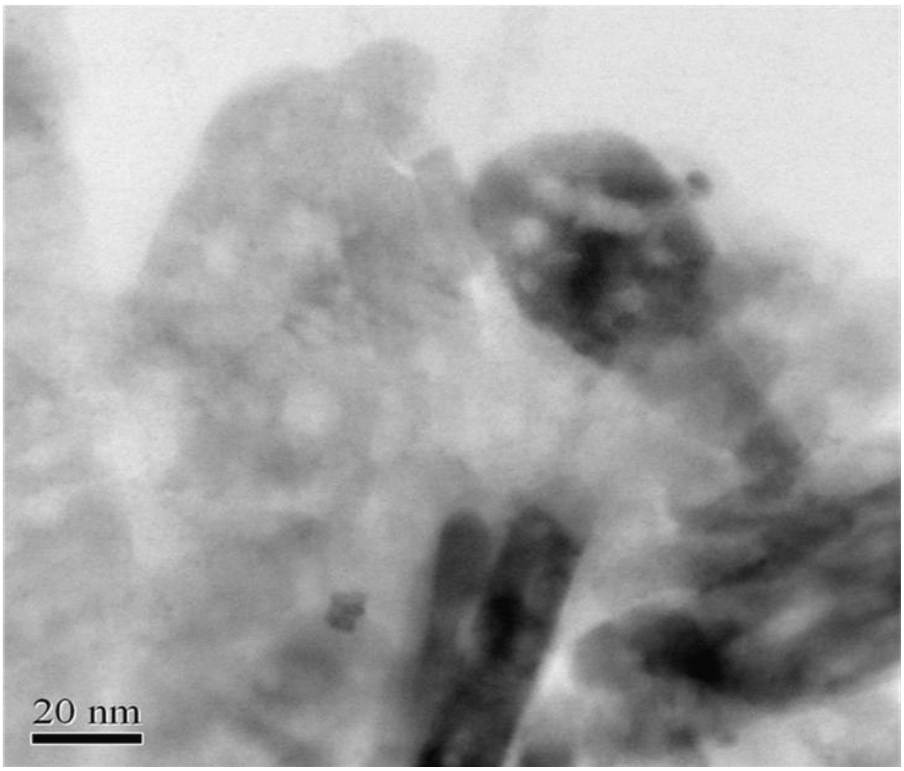

(d)

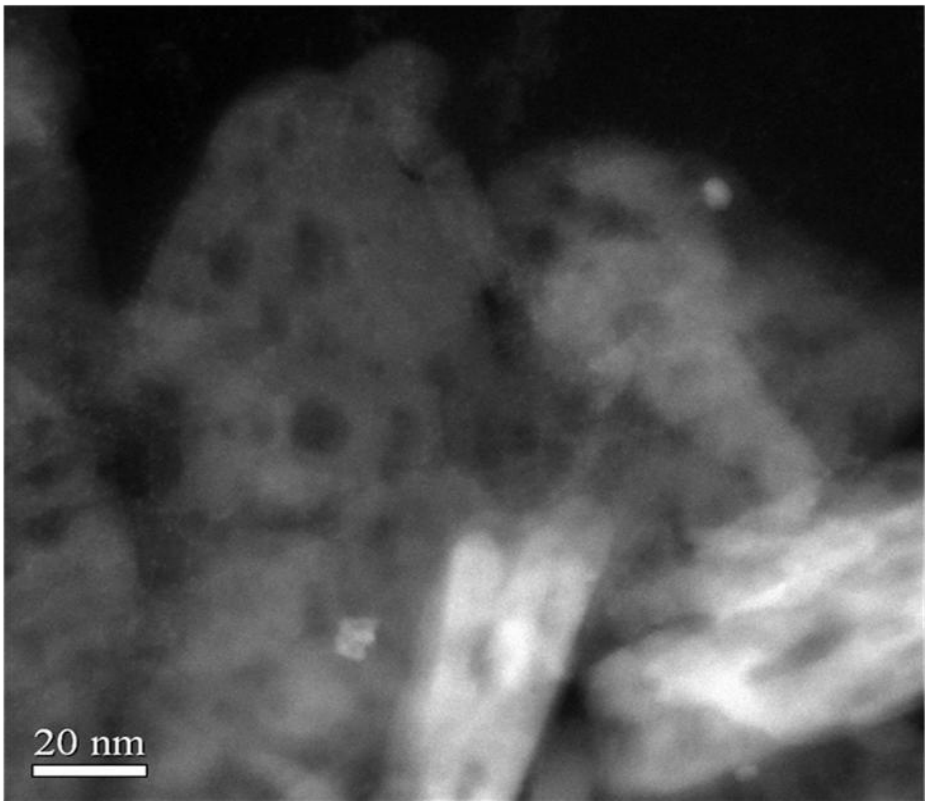

Figure 4.2(a) HRTEM micrograph, (b) SAED pattern of ZnS NPs, (c, d) shows bright field and high-angle annular dark-field (HAAD) images of ZnS NPs.

4.4 FTIR studies

Figure 4.3 represents FTIR spectra of uncapped ZnS NPs in the range of 4000-400cm^{-1}. The sharp peaks in all samples at 2358cm^{-1} is due to carbon which is an instrumental error which is verified one. The weak bands at 1408cm^{-1} and 1698 cm^{-1} in uncapped ZnS can be assigned to the symmetric and asymmetric stretching of COO^- respectively [1, 3]. O-H symmetric streching vibrations around 3216cm^{-1} appear in all samples. The weak peaks at 470 and 672cm^{-1} are assigned to the ZnS band (i.e., corresponding to sulphides). Bands around 1200 and 1100 cm^{-1} are due to the characteristic frequency of inorganic ions. These modes indicate the presence of resonance interaction between vibrational modes of sulphide ions in the crystal.

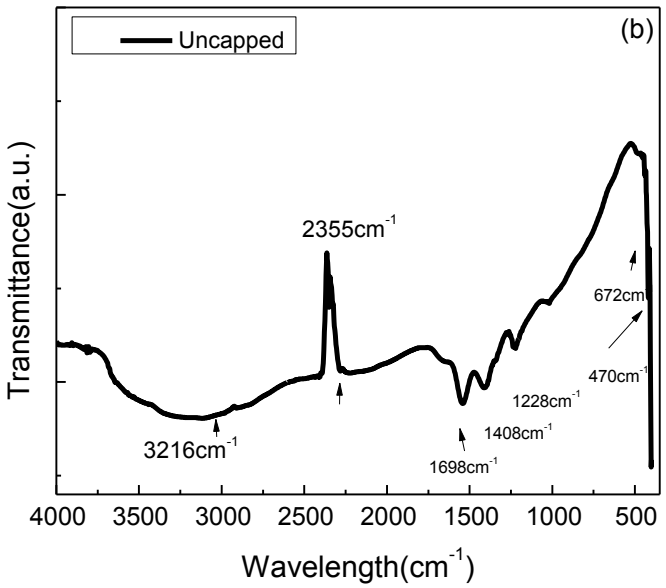

Figure 4.3 FTIR spectra of ZnS nanoparticles

4.5 UV- Visible studies

Figure 4.4(a) shows the absorbance versus wavelength (λ) traces of the ZnS NPs. The absorption spectrum of ZnS NPs show absorption shoulder edge at 326nm which is blue shifted in comparison to bulk ZnS (340nm). This blue shift in absorption shoulder is

due to quantum confinement effect. By calculating transmittance data using the Manifacier model [4], the absorption coefficients (α) were calculated in the region of strong absorption. To determine the band gap of synthesized ZnS NPs, the fundamental absorption, which corresponds to the transition from valence band to the conduction band was used. The relation between absorption coefficient *(α)* and incident photon energy *(hv)* can be written as [4]

$$\alpha = A\,(hv - E_g)^n/hv \qquad (1)$$

where A is a constant, E_g is the band gap of the material and the exponent n depends on the type of transition. n may have values 1/2, 2, 3/2 and 3 corresponding to the allowed direct, allowed indirect, forbidden direct and forbidden indirect transitions respectively [4]. The exact values of the band gap were determined by extrapolating the straight line portion of the $(\alpha hv)^{1/n}$ versus hv graphs to the hv axis as shown in Figure 4.4 (b). From the plots the values of band gap were obtained as 4.11eV for ZnS NPs respectively.

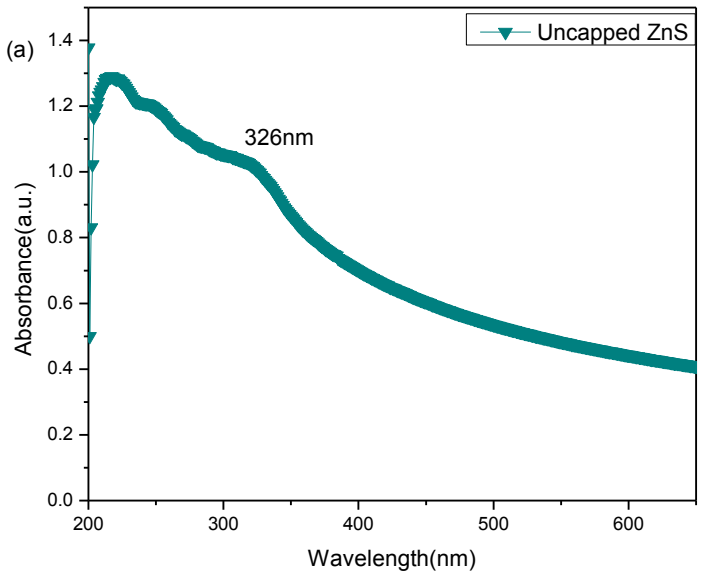

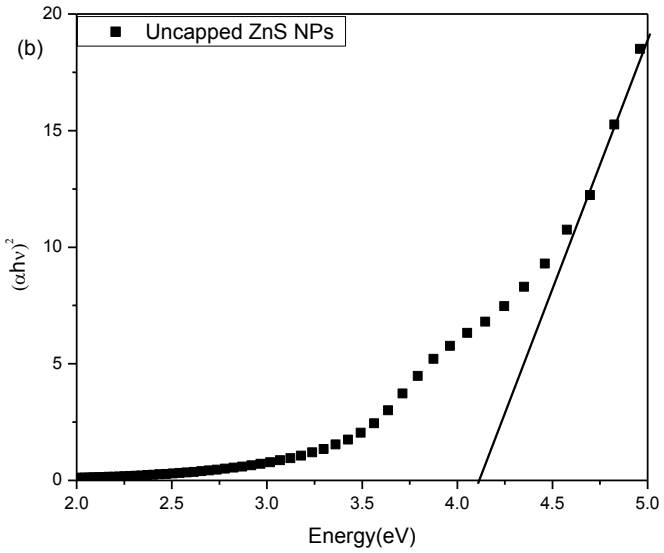

Figure 4.4. **(a)** UV-Visible absorption spectra of ZnS NPs, (b) $(\alpha h\nu)^2$ Vs. hν graph to find out band gap of ZnS NPs

4.6 Photoluminescence studies

Fig.4.5 (a) shows excitation spectra of ZnS NPs at fixed emission wavelength of 412nm. It shows excitonic peak centred around 356nm i.e. at larger wavelengths comparable with bulk (340nm). Since the diameters of the NPs and NRs for ZnS NC's are larger than the Bohr exciton diameter of the bulk ZnS (5 nm) [5], the optical behaviour of NPs and NRs should be similar to that of the bulk.

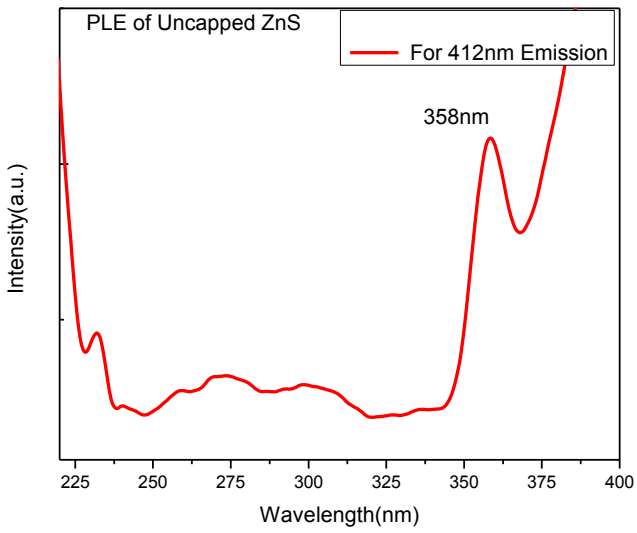

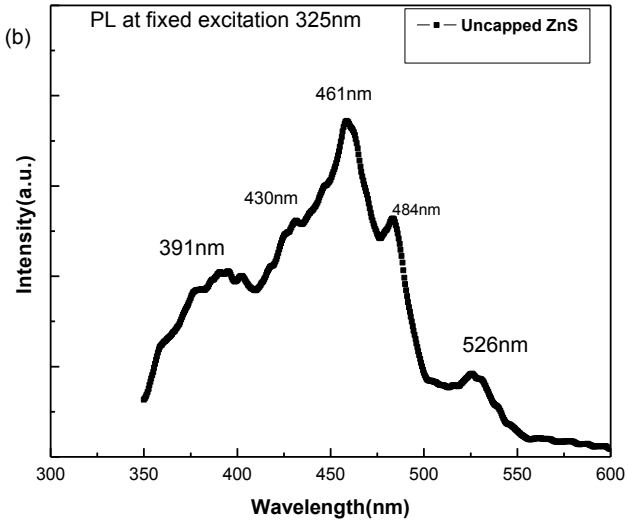

Figure.4.5 (a) Excitation spectra, (b) emission spectra of ZnS NPs.

Figure 4.5(b) shows steady state room temperature photoluminescence spectroscopy results of ZnS NPs. It shows PL emission spectra of ZnS NPs at 325nm excitation wavelength. The spectra were recorded using an emission filter of 350nm for corresponding excitation wavelength of 325nm. Emission peak is observed at 391, 430, 461 and 484nm. It can be seen in Figure 4.5 (b) that the spectral shapes are asymmetric and broad. The peaks are not very smooth but have closely separated multiple peaks. Major emission peaks are observed at 461nm and 430nm for ZnS NPs. At nano regime due to high surface energy there would be more defect states with dangling bonds. Due to these there are well resolved multiple emissions instead of band to band emission. Several research groups [6-9] studied the blue emission from ZnS nanoparticles under UV excitation. Yanagida et al. [6] have observed defect related longer wavelength luminescence at about 420 nm in addition to the band gap luminescence. Becker and Bard [9] have attributed the blue emission band at 428 nm to sulphur vacancies. Murase et al. [11] ascribed the blue emission band at 470 nm to zinc acceptors. Denzler et al. [12] identified four types of point defects, which can be present in pure ZnS generating four

trap levels inside the energy gap. Vacancies of zinc and sulphur could be treated as localized acceptor and donor states, whereas, the interstitial atoms of sulphur and zinc led to acceptor and donor states respectively. In the present work, the PL peaks appeared at energy levels substantially lower than the band gap. This suggests that the transitions from energy states inside the band gap are being favoured in comparison to band edge transitions for these nanocrystalline ZnS NPs. Based on literature reports mentioned above it is observed that 392 and 430nm emission peaks are due to sulphur interstitials and sulphur vacancies and 461 and 484nm emission peaks are due to zinc vacancies and zinc defects respectively. Furthermore, it is well reported that sulphur vacancies at surface gives rise to formation of zinc dangling bonds at shallow donor levels just below conduction band. In our case main emission peak around 430nm is due to recombination between these shallow donor levels acting as trap states and valence band. So ZnS NPs synthesised by chemical precipitation method gives broad emission spectra consisting of four well reported [12] emission multiples viz. 392, 430, 461 and 484nm respectively. In order to enhance and eliminate one emission out of all mentioned above different capping polymers with different concentrations are studied and discussed in detail in following chapters.

4.7 References

[1] H.C. Warad, S.C. Ghosh, B. Hemtanon, C. Thanachayanont, J. Dutta *Sci Technol Adv Mater*. **6,** 296 (2005).

[2] B.D. Cullity, Elements of X-Ray Diffraction, second ed., Addison-Wesley publishing, Massachusetts, **2003.**

[3] K Manzoor, S.R. Vadera, N. Kumar, T.R.N. Kutty Mater, *Chem Phys.* **82**, 718 (2003).

[4] J.I. Pankove, Optical Processes in Semiconductors (Prentice-Hall, Englewood Cliffs, NJ) (1971).

[5] W.C.W. Chan, S. Nie, *Science*, **281**, 2016 (1998).

[6] S. Yanagida, Y. Ishimaru, Y. Miyake, T. Shiragami, C. Pac, K. Hashimoto, T. Sakata, *J Phys Chem.* **93**, 2576 (1989).

[7] B. Bhattacharjee , C. Hsin Lu, *Thin Solid Films* **514,** 132 (2006)

[8] N. T.D. Chestnoy, R. Harris, L.E. Hull, J. Brus, *Phys. Chem.* **90,** 3393 (1986).

[9] R. Schmechel, M.. Kennedy, H. von Seggern, H. Winkler, M. Kolbe, R.A. J. Fischer, *Appl. Phys*. **89,** 1679 (2001).

[10] W.G. Becker, A.J. Bard, J. *Phys. Chem.* **87,** 4888 (1983).

[11] N. Murase, K. Hirata, T. Yazawa, T. J. Kushida, *Phys Chem B*. **103**, 754 (1999).

[12] D. Denzler, M. Olschewski, K. J. Sattlera, *J Appl Phys.* **84(5),** 2841 (1998).

CHAPTER 5

OPTICAL AND MORPHOLOGICAL STUDIES OF CAPPED ZnS NANOPARTICLES

Overview

In this chapter the experimental results of different series of capped nanostructures are presented. The entire work has been done to achieve tunable emission properties with enhanced emission intensity. Different capping agents with variation in concentrations have been used to control agglomeration and also to passivate defects present on the surface of nanostructures. This chapter deals with optical (UV-Visible absorption and photoluminescence spectroscopy) and morphological (XRD, TEM, SAED, EDX etc.) studies of synthesized capped ZnS NPs with various capping agents (PVP, Chitosan, Mercaptoethanol, Thioglycerol, SHMP) having different concentrations. All data collected from above mentioned series have been compared with each other.

5.1 Nanoparticles capping and their properties

Semiconductor nanoparticles exhibit unique optical properties which are strongly governed by their size [1, 2]. Photoluminescence can also be used effectively to determine the size dependent electronic structure. These quantum particles have demonstrated high luminescence efficiencies and remarkably short luminescence decay times [3-5]. The photoluminescence efficiency is however, adversely affected by the presence of intrinsic surface states. In addition to this, the nature of the chemical treatment can dramatically affect the emission and its kinetics without affecting the absorption spectrum. Most of the physical or chemical properties exhibited by these nanoparticles are due to their crystallites. Further growth in their size is due to agglomeration of these crystallites to form primary particles. If this growth of particles is not controlled, then due to Ostwald ripening and Vander-Waals interactions between particles, they agglomerate and settle down [6-8]. This agglomeration can be arrested by either stabilizing them electrostatically or by inducing steric hindrance at appropriate stage(s) to achieve size selective synthesis during precipitation reaction.

Electrostatic stabilization involves the creation of an electrical double layer arising from ions adsorbed on the surface and associated counter ions that surround the particle in the dispersing media. Thus, if the electric potential associated with the double layer is sufficiently high, columbic repulsion between the particles will prevent their agglomeration. Steric hindrance can be achieved by the adsorption of large molecules such as polymers on the surface of the particles. Capping agents are used for isolating nanoparticles from each other and nearly monodispersed nanoparticles appear as transparent colored solutions with no precipitate formation. Lyophobic (having no affinity for a solvent colloidal) particles are known to attract each other by vander Waals forces.

The attraction is strong due to the near additivity of forces between pairs of unit cells in different particles. Colloids remain stable with respect to aggregation only if there exists a repulsive force of sufficient strength within the range to counteract the van der Waals attraction [6, 9]. Therefore, an ideal capping molecule should form a strong bond with the nanoparticle surface to remain attached almost permanently without interfering in any of the processes occurring inside the nanoparticles. A proper capping passivates the surface (reduces its reactivity) and prevents the coalescence of nanoparticles.

Normally, the absorption onset and emission spectrum shifts to higher energy with decreasing size of nanoparticles. The excitation tracks the absorbance, resulting in a tunable fluorophor that can be excited efficiently at any wavelength shorter than the emission peak [10-14]. It will yet emit with the same characteristic of narrow, symmetric spectrum regardless of the excitation wavelength. Since there is a large stoke shift in case of quantum dots, their excitation wavelengths can be shifted to shorter wavelengths for the same emission wavelength. These characteristics make QD's ideal for multicolor experiments because a whole range of emission wavelengths that can be obtained with a single excitation wavelength [7, 8, 15]. Localized trap states inside the bandgap were studied in detail to recognize the sub-bandgap energy levels [10]. It was found that the defect levels play an important role in determining the luminescence characteristics of the ZnS nanoparticles and most of the nanoparticles exhibit broad and Stokes-shifted luminescence arising from the deep traps of the surface states [16, 18]. Only clusters with good surface passivation may show high band-edge luminescence [19]. Visible luminescence from ZnS was achieved mainly by adding appropriate dopants in it [20, 21]. Very few studies have reported visible red luminescence from undoped ZnS when capped

in some silica matrix [22, 23]. Therefore, more investigations are needed to explore the possibility of producing multicolor luminescence from undoped ZnS nanoparticles.

5.2 PVP capped ZnS nanoparticles

This series comprises of five categories of ZnS nanoparticle samples capped with 0.1, 0.5, 1.0, 1.5 and 2.0% PVP.

5.2.1 X-Ray Diffraction (XRD) Studies

Figure 5.1 shows XRD pattern of PVP (0.1-2.0%) capped ZnS NPs. Intensities of the three most important peaks of ZnS namely <111>, <220> and <311> reflections corresponding to 2θ values 28.5º, 47.6º and 56.4º are observed in the XRD pattern which match well with those of the β-ZnS (cubic) reported in the ICDD Powder Diffraction files (File. No.05-0566). Broadening of the XRD peaks indicates the formation of ZnS nano crystallites (NC's). The nano crystals have lesser lattice planes compared to bulk which contributes to the broadening of peaks in the diffraction pattern. This broadening can also arise from micro straining of the crystal structure which arises from dislocation and twinning [6]. These defects were believed to be associated with the chemically synthesized NC's as they grow spontaneously during chemical reaction since chemical species get very little time to diffuse to an energetically favorable site.

Crystallite size of ZnS nanoparticles was calculated by following Scherer's equation [24],

$$D = k\lambda / \beta\cos\theta \qquad (1)$$

where k=0.9, D- crystallite size (Å), λ(Å) the wavelength of Cu(Kα) radiation and β (in radians) is full width at half maximum (FWHM). The average crystallite size estimated from three planes is 3.93nm, 3.41nm, 3.35nm, 3.62nm and 3.51nm for PVP (0.1, 0.5, 1.0, 1.5, 2.0 at. %) capped ZnS NC's respectively.

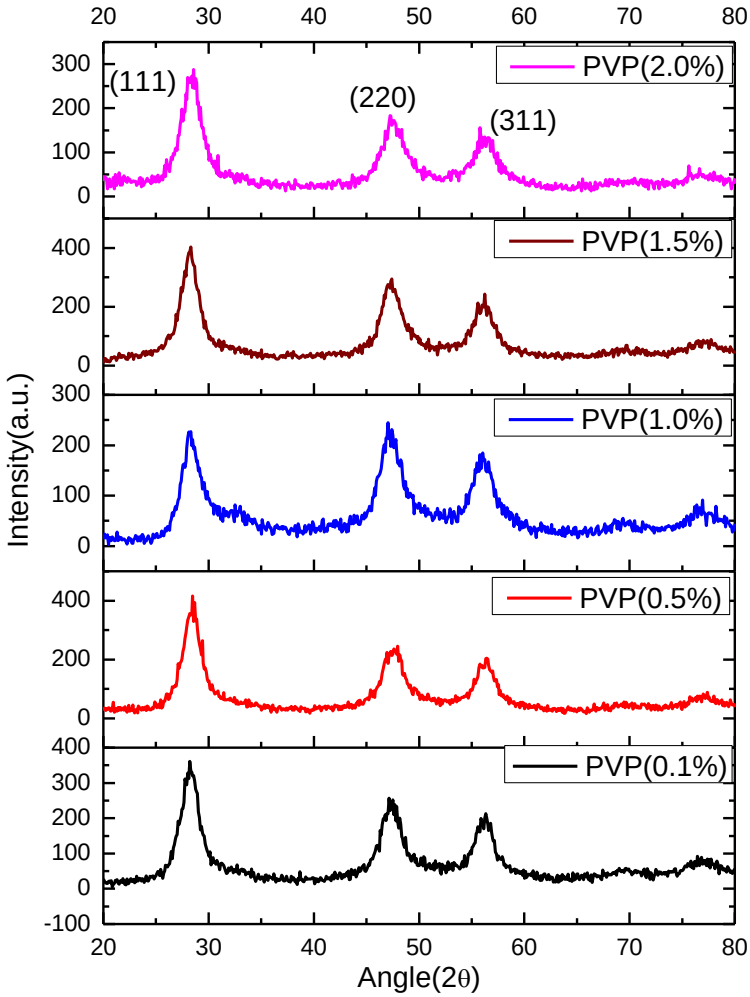

Figure 5.1 XRD pattern of PVP (0.1-2.0%) capped ZnS NPs

5.2.2 TEM Studies

Figure 5.2 shows the HRTEM images of PVP (1.5%) capped ZnS NC's. It shows particles of uniform size about 4.0-5.0nm. Figure 5.3 shows SAED pattern of same sample which shows a set of rings instead of spots due to random orientation of crystallites. The ED pattern shows three rings that correspond to (111), (220) and (311) planes of the cubic phase of ZnS and are in well agreement with the results obtained from XRD. Figure 5.4 (a, b) shows bright field and high-angle annular dark-field (HAAD) images of PVP (2.0%) capped ZnS NPs. It shows nanorod like assembly of particles at high concentration of PVP (2.0%). Inset of Figure 5.4(a) shows SAED pattern of 2.0%

PVP capped ZnS NPs. It shows points showing FCC cubic structure of ZnS instead of rings which suggests microcrystalline nature of nanorods.

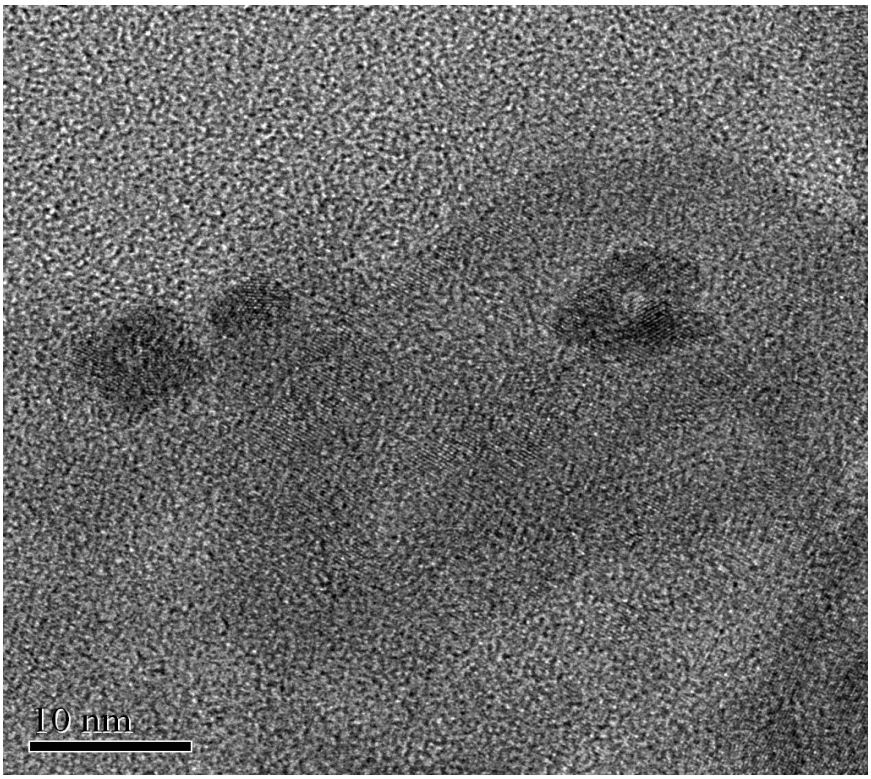

Figure 5.2 HRTEM of PVP(1.5%) capped ZnS NPs

Figure 5.3 SAED of PVP(1.5%) capped ZnS NPs

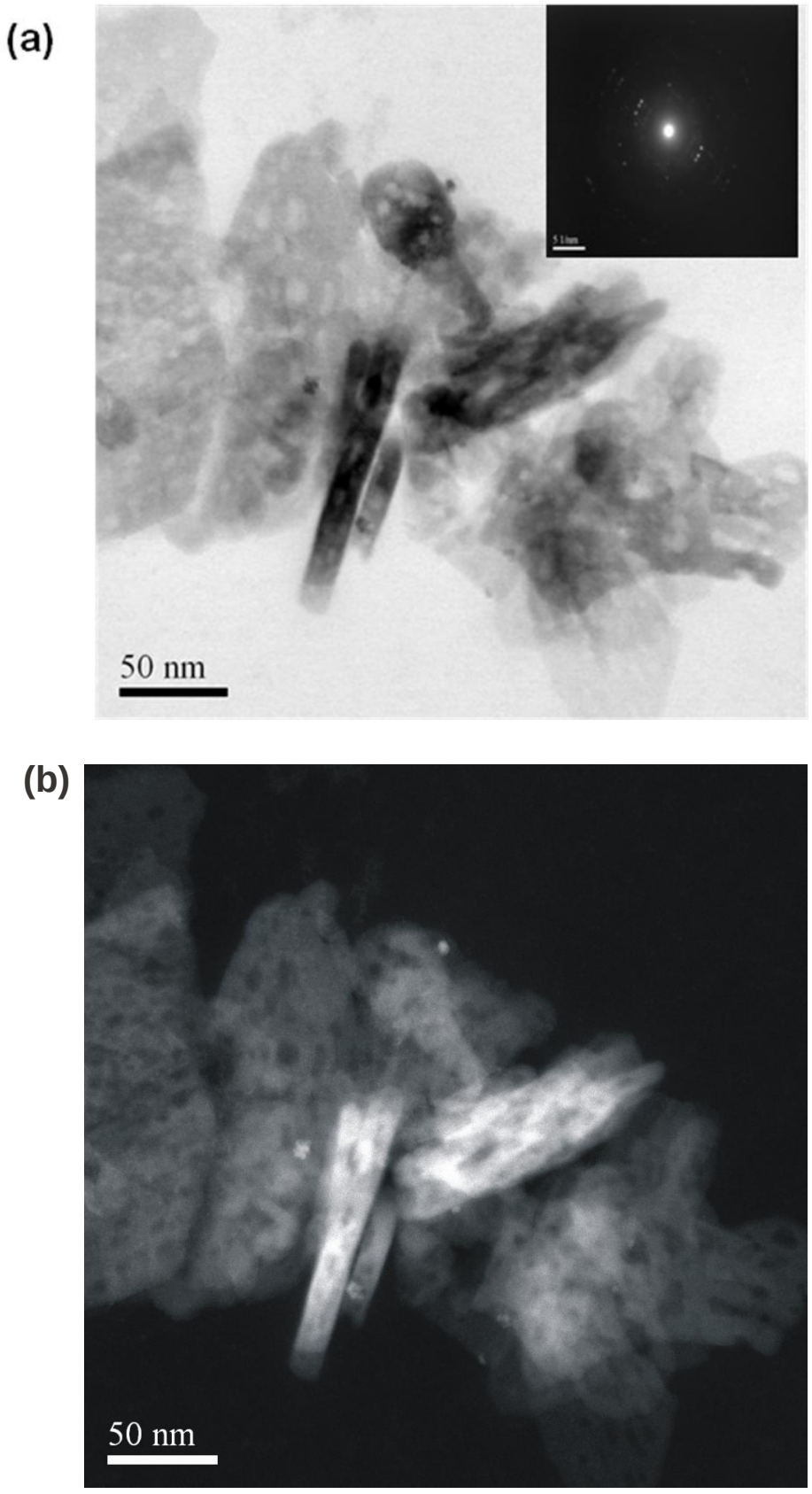

Figure 5.4(a, b) Bright field and High-angle annular dark-field (HAAD) images of PVP(2.0%) capped ZnS NPs (inset in Figure 5.4(a) shows SAED pattern of PVP(2.0%) capped nanorods).

5.2.3 FTIR Studies

Figure 5.5 shows FTIR spectra of PVP along with PVP (1.5%) capped ZnS NC's. It show peaks between 1540-1554cm^{-1}, 1222- 1262cm^{-1} present in pure PVP which gets slightly shifted in PVP capped ZnS nanoparticles. Table-5.1 shows peak assignment of various groups present in PVP and PVP capped ZnS NPs. From the spectra, it is clear that there is water of hydration in the samples because of the presence of a broad absorption band in the region from 3200 to 3500 cm^{-1}. The peaks at 1632 and 1234 cm^{-1} in both are assigned to the characteristic vibrations of C=O and C–O groups on the surface of NCs. Pyrrolidone moiety in PVP has both N as well as C=O groups. Studies on zinc-pyrrolidone-carboxylate complex systems [8] show that the oxygen in carboxylates makes coordinate bonding with the Zn atoms whereas the lone pair electron on nitrogen in pyrrolidone is conjugated with the adjacent carbonyl group. In PVP-ZnS samples, we expect a similar bonding at the surface of nanoparticles wherein C=O groups coordinate with the metal ions to form –C=O→ Zn^{2+} bonds which can give rise to overlapping of molecular orbitals of PVP with atomic orbitals of metal ions, particularly located at the surface regions. These interactions can cause both (i) alteration of the tautomeric form of surface adsorbed organic molecules due to change in effective charge on N and C=O and (ii) transfer the excited state energy from the molecular orbital of PVP to ZnS nanocrystals. From FTIR spectra of PVP(1.5%) capped ZnS nanoparticles, it is observed that there is decrease in intensity of absorption peaks followed by increase in broadness in the range 2959-2879cm^{-1}, 1374-1548 cm^{-1}. This also corresponds for coordinate bond between nitrogen of PVP with Zn^{2+} ions [8, 11].

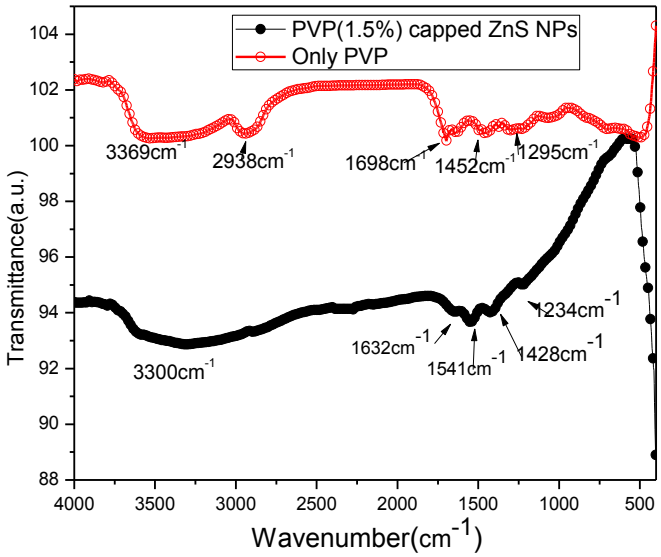

Figure 5.5 FTIR spectra of PVP and PVP capped ZnS NPs

Table 5.1 Peak assignment for pure PVP with PVP capped ZnS NPs

Peak assignment	**Peak position (cm^{-1})**	
	PVP	**PVP + ZnS NPs**
C-H bonding(a & s)	2959- 2879, 1494-1414, 1374	1428
C=O bonding	1698, 1295	1632, 1541, 1234
O-H stretch	3369	3300

5.2.4 UV-Visible Studies

Figure 5.6 shows the absorbance versus wavelength (λ) traces of the PVP (0.1-2.0%) capped ZnS NPs. The absorption spectrum of capped sample shows absorption shoulder edge at 318, 326, 318, 319 and 334 nm respectively for PVP (0.1, 0.5, 1.0, 1.5, and 2.0%) capped ZnS NPs. All samples show blue shift of absorption peak in comparison to bulk ZnS (340nm) which is due to quantum size effect.

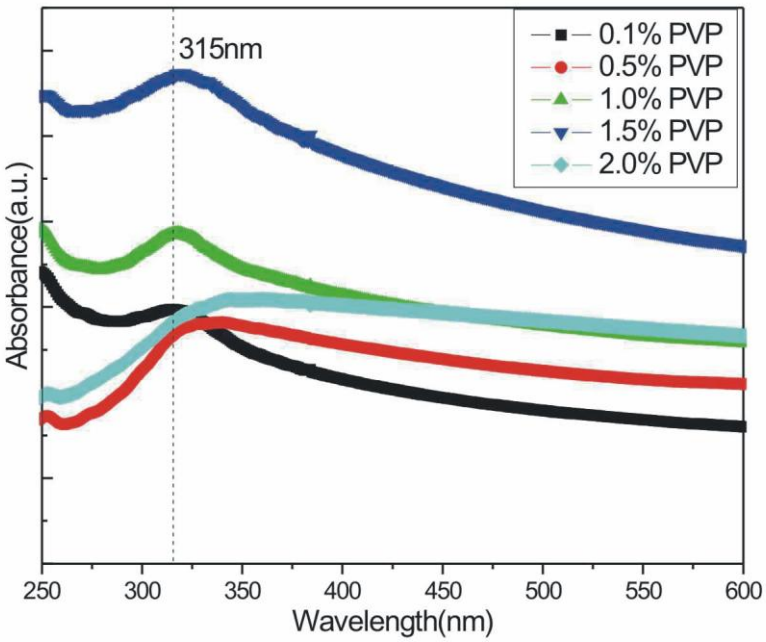

Figure 5.6 UV- Visible absorption spectra of PVP (0.1-2.0%) capped ZnS NPs

5.2.5 Photoluminescence studies

Figure 5.7 shows steady state room temperature photoluminescence spectroscopy results of all PVP (0.1-2.0%) capped samples. Figure 5.7a shows PL spectra of PVP (0.1-2.0%) capped ZnS NPs at 310nm excitation wavelength. It can be seen in Figure 5.7a that the spectral shapes are asymmetric and broad. The peaks are not very smooth but have closely separated doublet. Major emission peaks are observed at 428nm and 458nm for PVP (0.1-2.0 %) capped ZnS NPs. The integrated highest emission intensity for all peaks is for (1.5%) PVP capped ZnS NPs (Figure 5.7a). With further increase in PVP concentration from 1.5 - 2.0 % emission intensity is decreased and also emission peak at 428nm is nearly quenched. The NPs synthesized at lower concentration of PVP showed broader PL peak. Shift of these peaks from UV to blue color (392-461nm) emission was noted for NPs synthesized at higher concentration of PVP. Table 5.2 shows all emission wavelengths for different samples at different excitation wavelengths. Several research groups [25–27] studied the blue emission from ZnS nanoparticles under UV excitation.

Becker and Bard [24] have attributed the blue emission band at 428 nm to S^{2-} vacancies. Murase et al. [13] ascribed the blue emission band at 470 nm to Zn^{2+} acceptor.

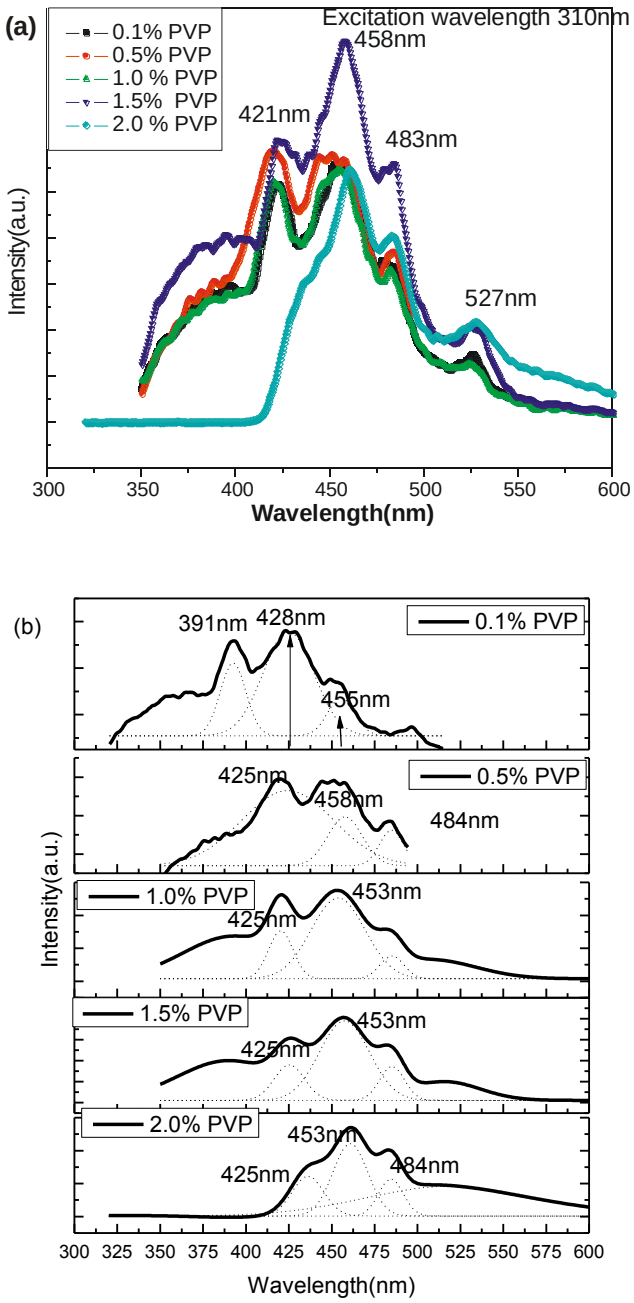

Figure 5.7 (a) Emission spectra of PVP (0.1-2.0%) capped ZnS NPs, (b) Photoluminescence spectra of PVP capped ZnS NPs along with Gaussian curve fit for possible emission sites.

Studies conducted by Kanemoto et al. [16] revealed a peak at around 325 nm and ascribed that for the trapped electrons transiting to valance levels. Yanagida et al. [25] have observed defect related longer wavelength luminescence at about 420 nm in addition

to the band gap luminescence. Denzler et al. [10] identified four types of point defects, which can be present in pure ZnS generating four trap levels inside the energy gap. Vacancies of zinc and sulphur could be treated as localized acceptor and donor states, whereas, the interstitial atoms of sulphur and zinc led to acceptor and donor states respectively. In the present work, the PL peaks appeared at energy levels substantially lower than the band gap. This suggests that the transitions from energy states inside the band gap are being favoured in comparison to band edge transitions for these nanocrystalline ZnS NPs. Based on literature reports mentioned above it is observed that 392 and 425nm emission peaks are due to sulphur interstials and sulphur vacancies and 453 and 484nm emission peaks are due to zinc vacancies and zinc defects respectively. Furthermore, it is well reported that sulphur vacancies at surface gives rise to formation of zinc dangling bonds that form shallow donor levels just below conduction band. In our case main emission peak around 425nm is due to recombination between these shallow donor levels acting as trap states and valence band. Chen et al. [18] assigned the surface states to the observed PL peak positioned at the energy levels lower than band gap energy and it was also supported by the thermoluminescence measurements made by them. The density of surface states in the QDs would increase with a decrease in the size of crystallites, due to the increased surface-to-volume ratio in NPs having smaller crystallites. This would reduce the probability of excitonic emission via non-radiative surface recombination [18]. The band-edge or excitonic emission will thus be effectively overlapped with the absorption of the surface states and as such would show photoluminescence at energy levels lower than the band gap. To resolve the doublet structure and to locate the exact peak positions, each spectrum was deconvoluted as shown in Figure 5.7b. The experimentally observed spectra could be regarded as the resultant of the contribution from these two peaks. The spectrum corresponding to the

NPs synthesized with 0.1% PVP was deconvoluted into three peaks at 392, 428 and 455 nm. It is discussed above that 428nm peak in ZnS is due to sulphur vacancies acting as trap states and 455nm emission is due to zinc vacancies respectively. Also emission peak at 392nm is assigned to sulphur interstitial sites [18, 26]. With increase in PVP concentration from 0.1 to 0.5% emission peak at 392nm is quenched suggesting passivation or absence of sulphur interstitials. Also peak intensity around 425nm is observed to decrease and at 453nm to increase with increase of PVP concentration from 0.1-2.0%. At 2.0% PVP 425nm emission peak is nearly absent and from intensity comparison from deconvoluted peaks it is clear that in emission spectrum red shift is observed with increasing concentration of capping agent PVP from 0.1 to 2.0%. The model proposed by Chen et al. [18] can explain the size-dependent blue shift in emission spectrum. In our case large shift in particle size with change in capping concentration is not observed (3.93-3.35nm). Here we observe red shift emission (from 392-461nm) with increase in capping concentration (0.1-2.0%) from almost similar size particles. So, in our case quenching of 428nm peak with increase in PVP concentration cannot be explained by Chen and Chenstnoy model [18, 27]. This can be explained by passivation of zinc dangling bonds (formed due to sulphur vacancies) responsible for 428nm emission, by increase in concentration (0.1-2.0%) of adsorbed PVP molecules. As the intensity of PL originating from a particular defect level is proportional to the population of that defect site present in the sample, the relative change in PL peak intensity between Zn^{2+} vacancy and S^{2-} vacancy levels with capping concentration can be explained qualitatively in terms of the change in population of those sites with increasing capping concentration. The peak intensity of the emission originated due to S^{2-} vacancy (zinc dangling bonds) was always lower than the emission due to Zn^{2+} vacancies because of the fact that zinc dangling bonds were more likely to become passivated by capping agent PVP by $C{=}O{\rightarrow}Zn^{2+}$

bonding and nitrogen of PVP with Zn^{2+} bonding as discussed previously in FTIR studies. The intensity ratio ($I_{423/453}$) decreased primarily due to increasing passivation of zinc dangling bonds formed due to S^{2-} vacancy sites by the same process (increase in PVP concentration from 0.1-2.0%), resulting in lowering PL intensity of the corresponding peak with increasing capping concentration. This resulted in an increase in the population of energy states due to Zn^{2+} vacancies and led to a corresponding increase in the PL intensity originating from these vacancy sites. The PL peak at 484nm is also observed to increase with increase in capping concentration. The PL spectra of all the ZnS NPs showed a weak shoulder around 550 nm. The origin of this shoulder structure at lower energy compared to the main peak can be attributed to the recombination of electron-hole pair at the surface traps, which arise for the high surface to volume ratio of the nanoparticles due to their small sizes. Emission in green region from undoped ZnS was observed by Hu et al. [28] and they assigned the emission to some self-activated centers, probably surface states, vacancy or interstitial states within the structure.

Figure 5.8(a) shows excitation spectra of PVP (1.5%) capped NPs for different possible emission sites observed in emission spectra. Table 5.2 shows excitation wavelengths of all samples at possible emission wavelengths. The reason for showing PLE spectra for only 1.5% PVP capped ZnS NC's is due to high integrated PL intensity for this sample in comparison to other synthesized samples. Based on this in excitation studies of synthesized capped NC's emission wavelength used is 461nm and 423nm respectively. In excitation spectra of PVP capped NC's, broad excitonic peak around 325nm is observed for 461nm emission. This suggests zinc vacancies related emission in capped NC's which is arising from excitation in host ZnS (as 325nm excitation is near 340nm for bulk ZnS). Also from UV-Visible absorption studies maximum absorption

peak comes out near 318nm. But for 423nm emission in same sample excitation spectra is broadened having multiple excitation peaks instead of single excitonic peak. Maximum intensity peak is at 235nm with small peaks at 275nm and 304nm respectively. Excitonic peak around 304nm corresponds for band to band excitation in host ZnS, but 235nm and 275nm excitonic peaks cannot be due to ZnS as has been reported earlier by Manzoor et al. [4] that these excitation are in PVP molecular states. Band-to-band excitation observed in maximum nanocrystalline semiconductor can be blue shifted or broadened due to (i) quantum confinement effects or (ii) high polydispersity [4]. However, in the frame of well accepted effective mass approximation theory, the maximum size dependant blue shift in band gap (Eg) that can occur for, 4.0 nm sized ZnS particles of zinc-blende structure is 0.6 eV [29]. Therefore, the larger shift in band gap (Eg) by, 1.60 eV (i.e., from 3.67 to 5.27 eV or $\lambda_{exc.}$ from 340nm to 235nm) observed in the case of PVP-ZnS cannot be attributed to the quantum size effects. Further, the TEM studies show low polydispersity for PVP-ZnS particles. Therefore, the broadening in the PLE due to PVP capping cannot be also accounted by polydispersity in particle size. In this context, we believe that, the high energy bands in the PLE of PVP-ZnS NC's are originated from the energy levels other than that host ZnS, probably from the surface adsorbed PVP molecules. Also absorption spectra shows absorption peak around 320nm for all samples, which suggests 235, 275nm excitation peaks have different origin, other than ZnS. After observing difference in excitation spectra for different emission sites in capped NC's we have also studied excitation spectra of only PVP for 423nm emission (Figure 5.8d). Interestingly it shows weak excitonic peaks at 258nm, 286nm and 321nm respectively. Also excitation spectra were deconvoluted for possible excitation peaks. This clearly suggests PVP has multiple energy levels having multiple absorptions at 235, 258, 286, 321 and 333nm

respectively. This shows introduction of new excitonic peaks (235, 275nm) in PVP (1.5%) capped ZnS NPs for 423nm emission is due to PVP molecular energy states. So, we observed variation in PLE peak from 325 to 235nm and 275nm for variation in emission site from 461 to 423nm respectively. Similar results were also reported by Manzoor et al. [4] where they have observed similar shift of excitation peak with change in PVP concentration for 590nm emission (dopant related). But here we have observed this change in excitation peak for different possible emission sites (423, 461nm) in single sample. As reported earlier by Manzoor et al [4] that 235nm and 275nm excitations is due to chemisorbed PVP molecular energy levels and 325nm excitation is due to band to band transitions of host ZnS (bulk ZnS excitation is 340nm) so, it can be proposed that 461nm emission can be due to 325nm excitation which is band to band excitation in ZnS. Furthermore, 423nm emission can be due to 235nm and 275nm excitations of surface adsorbed PVP. It is observed that 235 and 275nm excitations are due to excitation in PVP molecular energy states so there could be transfer of energy from adsorbed PVP to trap states (because 423nm emission is due to sulphur vacancy acting as trap states) of host ZnS for 423nm emission. This interaction causes alteration of tautomeric form of surface adsorbed organic molecules due to change in effective charge on N and C=O. The excitation peaks at 235, 258 nm arise from enol-tautomer of pyrrolidone whereas 275 and 286, 321 nm are from the keto form of pyrrolidone moiety [4]. As discussed in FTIR studies, electrostatic interaction of the adsorbed molecules, leading to hydrogen bonding with C=O as well as N groups, will change the charge distribution in the molecules, resulting in enhanced electronic delocalization which changes with the concentration, nature of solvent as well as the intermolecular interactions in the chemisorbed layers. This together with the vibrational relaxations account for the broad, multiple maxima in the

excitation spectra of the adsorbed PVP molecules. Also this interaction of PVP and surface defects facilitates excited energy transfer from PVP molecular energy levels to trap states of ZnS. Furthermore, Figure 5.8e shows that, PVP molecules are weakly emissive showing emission spectra having emission peaks around 411nm and 442nm at 275nm excitation. This shows either PVP's molecular energy levels overlaps with atomic orbitals of metal ions present at surface. Secondly emission spectra of PVP must have overlapped with trap state emission around 420nm in ZnS showing peak enhancement and shift in emission peak from 461nm to 423nm with shift in excitation energy (Figure 5.8e).

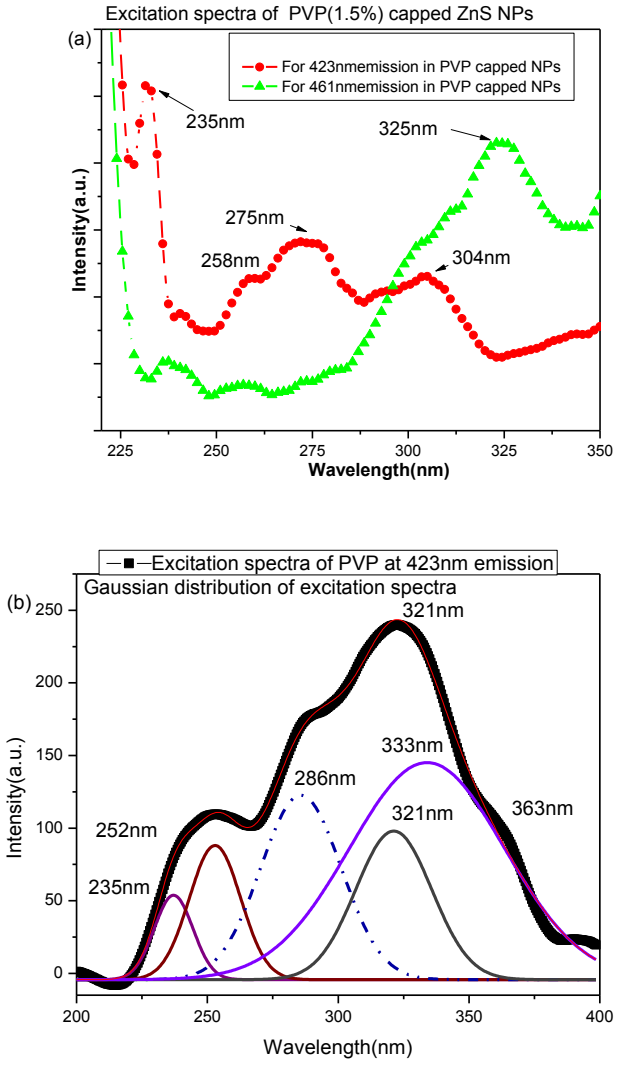

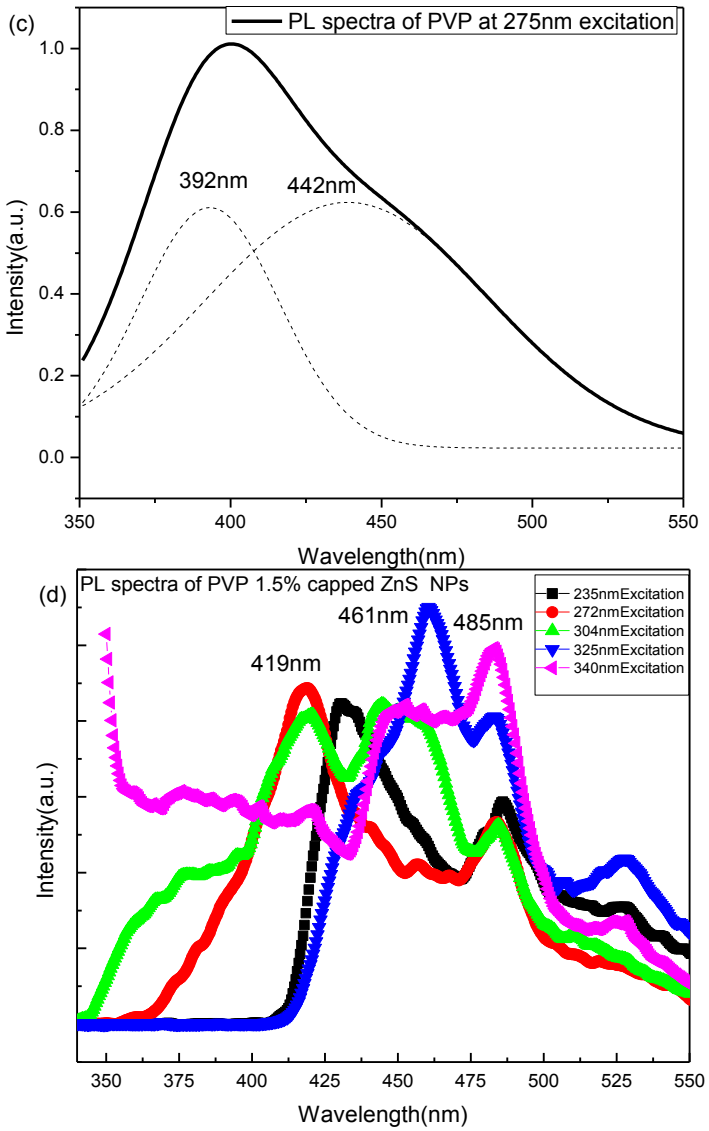

Figure 5.8 (a) Excitation spectra of PVP capped ZnS NPs, (b) excitation spectra of only PVP, (c) emission spectra of only PVP at 275nm excitation; (d) PL spectra of PVP (1.5%) capped ZnS NPs at variable excitation wavelengths.

Finally we noticed shift of PL peak positions from 392 to 461nm with increase in capping concentration from 0.1-2.0%. Also single sample (PVP 1.5%) is showing shift in PL peak positions (392-461nm) by changing excitation wavelength from 235 to 325nm. This shows single sample can emit different colors from UV to blue- green with change in excitation energy which according to earlier reports and as shown above for PVP(0.1-2.0%) capped ZnS NPs needs many samples with different concentrations of precursors,

experimental conditions etc. Detailed influence of PVP emission on PL properties of NPs is shown in next chapter with doped and capped ZnS NPs (Chapter 6.1).

Table- 5.2 Showing particle size variation of all samples with absorption and photoluminescence results.

Sample	Particle Size(nm		Absorption wavelength (nm)	Excitation wavelength (nm)		Band gap (eV)		Emission wavelength(nm) at fixed excitation(PLE)			
	XRD	TEM	UV-Vis. Spectra	At 423nm PL	At 461nm PL	UV-Vis	PLE	235nm PLE	272nm PLE	304nm PLE	320nm PLE
PVP(0.1% ZnS NPs	3.93	-	318	(233, 258, 281, 315)*	350*	3.89	4.42	-	-	-	392, 428
PVP(0.5% ZnS NPs	3.41	-	326	(240, 272, 339)*	340*	3.80	4.41	-	-	-	425, 458
PVP(1.0% ZnS NPs	3.35	-	318	(236, 270, 323)*	329*	3.89	4.36	-	-	-	425, 453
PVP(1.5%) ZnS NPs	3.62	3.0-4.0	319	(235, 272, 304)*	329	3.88	4.39	417	416	418, 442	425, 461, 484
PVP(2.0% ZnS NPs	3.51	nanorods 15nm dia.	334	(235, 258, 272, 310)*	328*	3.71	4.42	-	-	-	461, 484

* Not shown in figures.

5.3 Chitosan capped ZnS nanoparticles

5.3.1 XRD Studies

Figure 5.9 shows X-ray diffraction pattern of chitosan (CH) capped (0.1, 0.5, 1.0, 1.5, and 2.0%) ZnS NPs. It shows three broad peaks corresponding to the (111), (220) and (311) planes of FCC ZnS structure. It is to be noted that, the peaks observed in the XRD pattern match well with those of the β-ZnS (cubic) reported in the ICDD powder

diffraction file No. 80-0020. Broadening of the XRD peaks indicates the formation of ZnS NC's. Broadening of the XRD peaks for all samples indicates the formation of ZnS nanocrystals. Crystallite size of ZnS nanoparticles was calculated by following Scherer's equation [24],

$$D = k\lambda / \beta\cos\theta \qquad (1)$$

where k = 0.9, D- crystallite size (Å), λ(Å) the wavelength of Cu(Kα) radiation and β(in radians) is full width at half maximum (FWHM). The average crystallite size estimated from three plane s is 4.91, 3.49, 3.83, 4.54 and 4.49nm for CH (0.1, 0.5, 1.0, 1.5, 2.0 at. %) capped ZnS NPs.

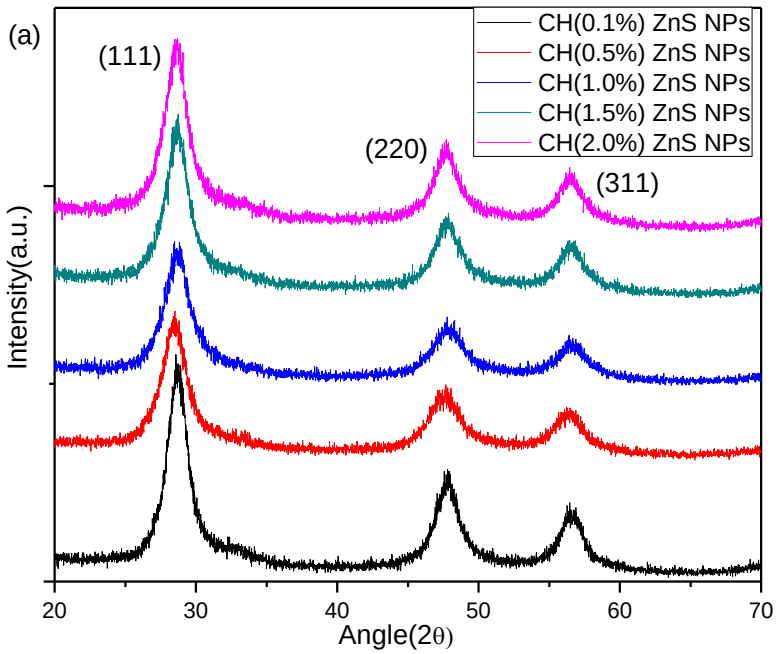

Figure 5.9 XRD pattern of CH (0.1-2.0%) capped ZnS NC's

5.3.2 TEM Studies

Figure 5.10 (a, b) shows TEM micrograph of CH (0.1% and 1.0%) capped NPs. Both micrographs show spherical crystallites having mean size ~3.0-5.0 nm.

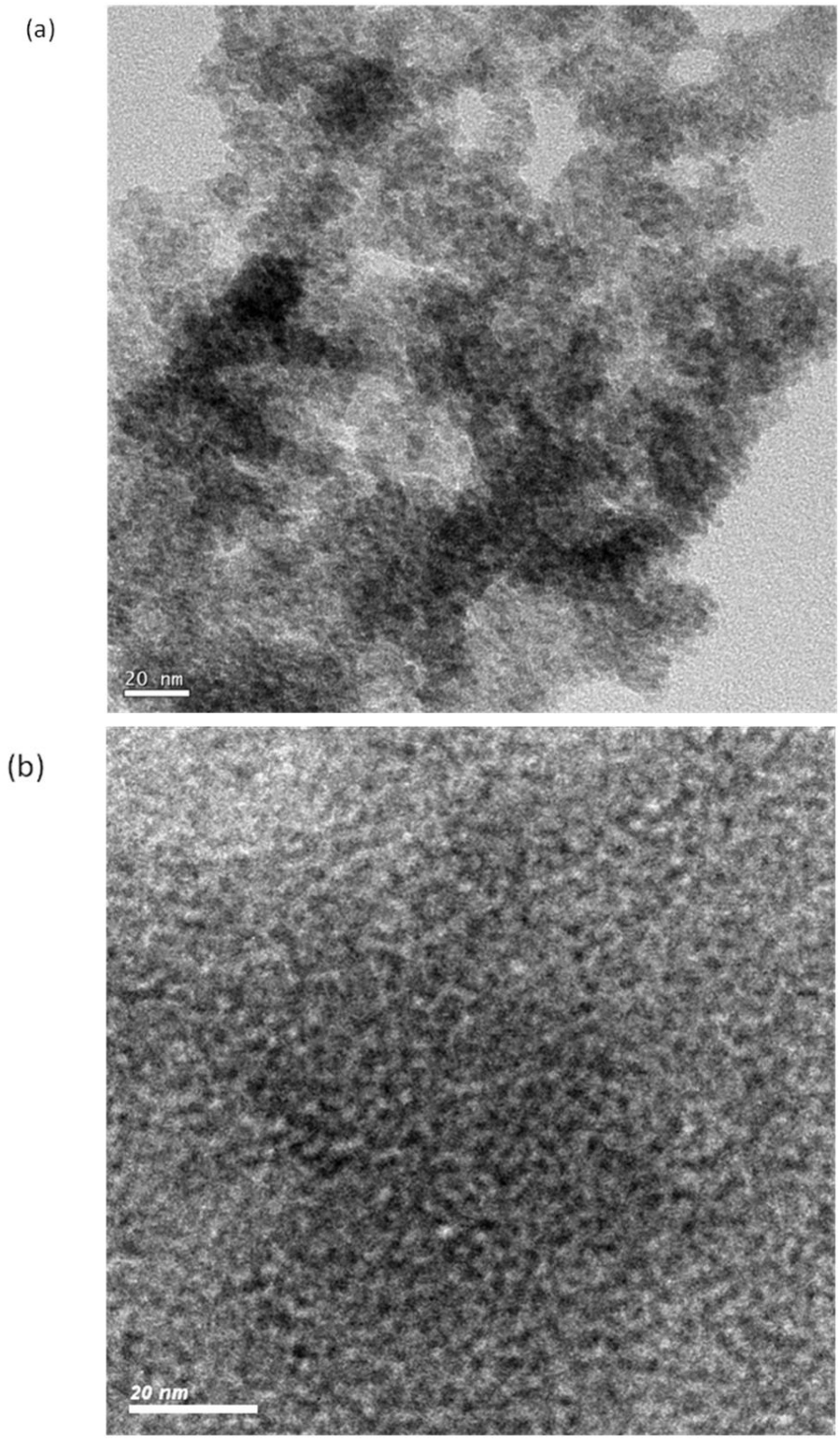

Figure 5.10 TEM micrograph of (a) CH (0.1%) capped, (b) CH (1.0%) capped ZnS NPs

5.3.3. UV-Visible Absorption Studies

Figure 5.11(a) shows the absorbance versus wavelength (λ) traces of the CH (0.1-2.0%) capped ZnS NPs. The absorption spectrum of capped samples show blue shifted

absorption shoulder edge in comparison to bulk ZnS (340nm) which is due to quantum size effect. By calculating transmittance data using the Manifacier model [30], the absorption coefficients (α) were calculated in the region of strong absorption. To determine the band gap of synthesized ZnS NPs, the fundamental absorption, which corresponds to the transition from valence band to the conduction band was used. The relation between absorption coefficient *(α)* and incident photon energy *(hv)* can be written as [30]

$$\alpha = A\,(h\nu - E_g)^n/h\nu \qquad (1)$$

where A is a constant, E_g is the band gap of the material and the exponent n depends on the type of transition. n may have values 1/2, 2, 3/2 and 3 corresponding to the allowed direct, allowed indirect, forbidden direct and forbidden indirect transitions respectively [30]. The exact values of the band gap were determined by extrapolating the straight line portion of the $(\alpha h\nu)^{1/n}$ versus $h\nu$ graphs to the $h\nu$ axis as shown in Figure 4.11(b) and Table 5.3. From the plots the values of band gap were obtained as 3.92, 4.32, 4.65, 4.42 and 4.42eV for CH (0.1, 0.5, 1.0, 1.5, 2.0 at. wt. %) capped ZnS NPs respectively. The results for 1.0% capped sample shows maximum band gap which accounts for high quantum confinement of electrons in this concentration of chitosan.

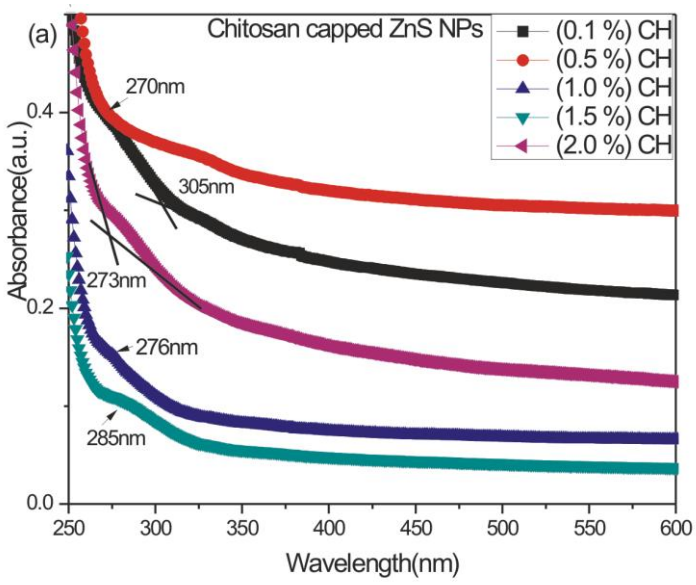

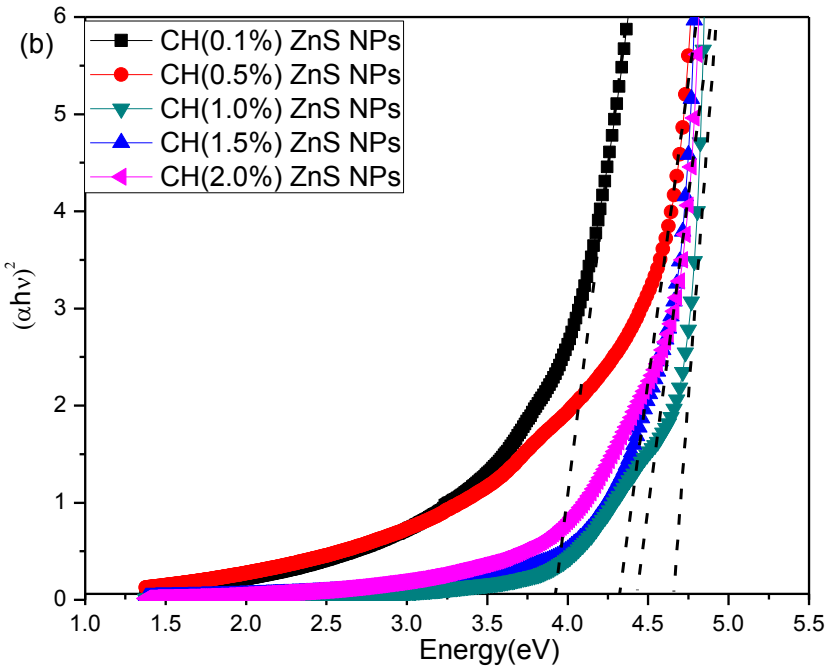

Figure 5.11 (a) Absorbance spectra, (b) estimated band gap by tauc's plot for CH (0.1-2.0%) capped ZnS NPs.

5.3.4. FTIR Studies

In order to further ascertain the presence of chitosan in chitosan capped ZnS NPs, FTIR spectra of pure chitosan and chitosan capped ZnS NPs were compared. Figure 5.12 represents FTIR spectra of chitosan capped NPs with pure chitosan in the range of 4000-400cm^{-1}. The weak bands at 1426cm^{-1} and 1570 cm^{-1} in CH (0.1%) capped ZnS NPs can be assigned to the symmetric and asymmetric stretching of COO^- respectively [31]. Also absorption bands at: 3569 cm^{-1} (O-H stretch overlapped with N-H stretch), 1650 cm^{-1} (amide I band), 1570 cm^{-1} (amide band, N-H stretch (*str.*)) and 1011 cm^{-1}, 1014 cm^{-1}, 1043 cm^{-1} (C-O *str.)* are present in capped ZnS NPs. These peaks correspond to presence of chitosan in sample as they are also present in pure chitosan. The peaks at 662 cm^{-1}, 692 cm^{-1} correspond to weak (N-H *str.)*, 418 cm^{-1} and 501 cm^{-1} correspond to weak –S-S- stretch or manganese–oxygen or sulfur–oxygen interaction [20]. So it is clear that capping forms bonds with unsaturated ions on nano sized ZnS, as surface to volume ratio is more in this case. The sharp peaks in all samples at 2358cm^{-1} is due to carbon which is an

instrumental error which is verified one. The weak bands at 1407cm^{-1} and 1551 cm^{-1} in uncapped ZnS can be assigned to the symmetric and asymmetric stretching of COO^- respectively [31]. Chitosan is a coordination polymer and can bind to transition metal ions through its amino groups to form a complex [32-23]. The absence of NH_2 peaks in FTIR spectra and presence of amide peak (NH_3^+) at 1570cm^{-1} suggests protonation of amine group to NH_3^+ which is adsorbed on the surface of host ZnS preventing agglomeration of particles [31]. For rare earth doped chitosan films it is reported that small portion of amine group participate for the coordination and remaining amine groups are unused. These unused groups can further bind nanocrystals with biomolecules [34]. Presence of amide peak clearly indicate that capping polymer is adsorbed on the surface of ZnS and can make bonds with unsaturated ions on nano sized ZnS. Due to high surface to volume ratio in nano ZnS, probability of defect states is more and probably because of this the interaction of adsorbed polymer layers with defect states is more than bulk ZnS. As seen from the UV-visible studies, band gap of capped ZnS NPs is 3.9-4.5 eV which is attributed to strong quantum confinement and very narrow distribution of particle sizes, which is confirmed from TEM and XRD studies also.

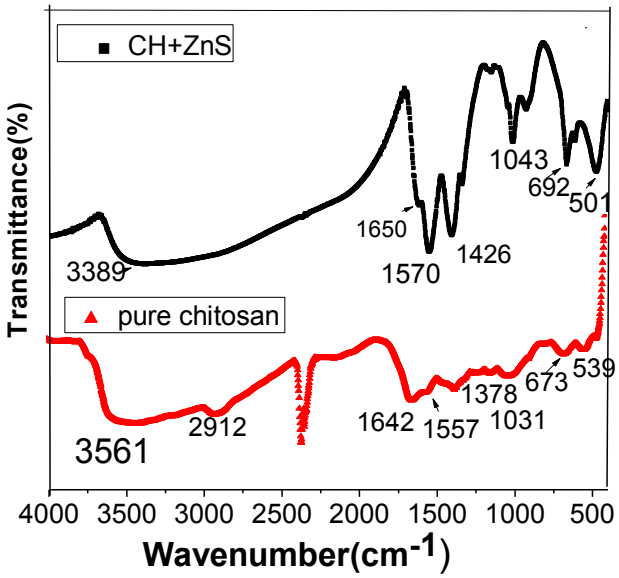

Figure 5.12 FTIR spectra of chitosan, chitosan capped ZnS nanoparticles

5.3.5 Photoluminescence Studies

Figure 5.13 (a) shows excitation spectra of CH (0.1-2.0%) capped ZnS NPs at fixed emission wavelength of 410nm. It shows excitonic peak centered around 280nm for all CH (0.1-2.0%) concentrations. With increase in concentration of capping agent CH from 0.1-1.0% intensity of excitonic peak increases and spectra becomes broadened. With further increase in CH from 1.0-1.5 and 2.0% intensity of excitonic peak decreases with slight reduction in broadening. Calculated band gap from excitation spectra are given in Table 5.3 for all samples which matches with those calculated with absorption spectroscopy.

Figure 5.13 (b) shows PL spectra of CH (0.1-2.0%) capped ZnS NPs at 284nm excitation wavelength. Emission peak is observed at 395nm for CH capped ZnS NPs. With increase in capping concentration from 0.1 to 0.5% and further to 1.0% there is increase in emission intensity along with increase in full-width at half maximum. From Table 5.3 it is clear that with increase in capping polymer from 0.1-1.0% there is increase in band gap and decrease in crystallite size. Hence this increase in PL intensity can be due to strong quantum confinement effect and decrease of surface defects with increase in capping agent as explained above in FTIR studies. But as this emission around 390-410nm results from defect states (sulphur vacancies acting as trap states), so with effective passivation this emission peak should decrease with increase in capping agent. So, this increase in PL intensity of defect states (for 0.1-1.0% CH) is surprising. With further increase in CH concentration from 1.0-1.5 and 2.0 % emission intensity is decreased. This decrease is probable because with increased capping concentration zinc dangling bonds may be partially passivated resulting decrease of their characteristic emission. Figure 5.13(c) shows the emission peak around 350-450 nm for pure chitosan

having maxima at 364nm. So with increase in chitosan concentration from 0.1-0.5 and 1.0% increase in PL intensity can be attributed to convolution of chitosan emission with defect related emission around 410nm. It is reported earlier that 410nm peak in ZnS is due to transfer of electrons from sulphur vacancies acting as trap states to valence band [7, 10, 18, 25]. It is possible that for 1.5% and 2.0% CH sample, zinc dangling bonds originated due to sulphur vacancies are passivated resulting in elimination of its corresponding peak at 410nm. This might have decreased the integrated emission around 395nm slightly in this case. The adsorbed polymer lies on surface of NP and due to high surface to volume ratio at nano regime more defects would lie on surface so sufficient amount of polymer can passivate defects causing decrease in emission intensity of 410nm peak for 1.5 and 2.0 % CH. Since we wish to achieve tunable emission color in single sample and 1.0% CH capped NC's show maximum PL intensity for 395nm emission so for further PL studies (discussed in section 6.2 of next chapter) with capping and doping both, this concentration of CH is selected.

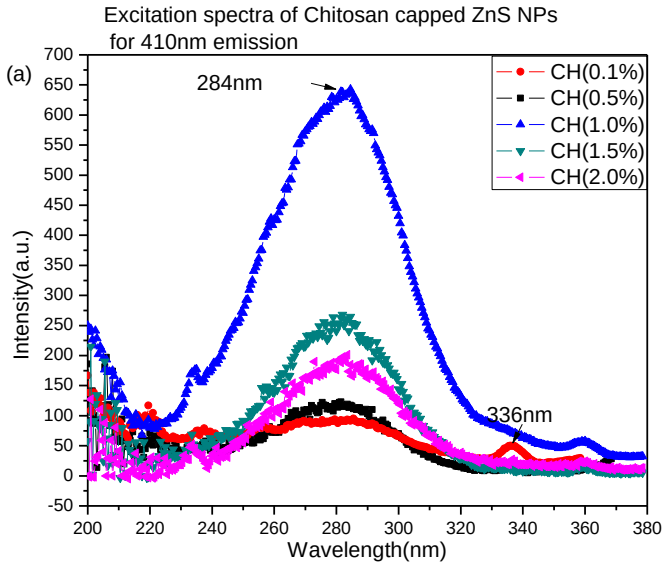

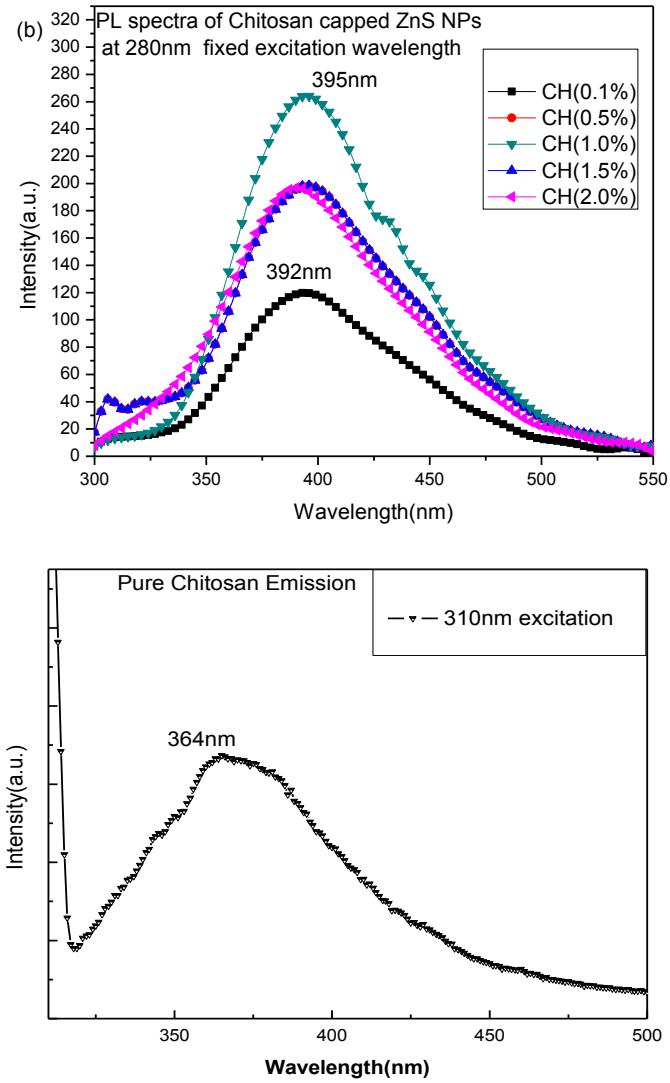

Figure 5.13 (a) Excitation spectra (b) Emission spectra of of CH (0.1-2.0%) capped ZnS NPs, (c) PL spectra of pure chitosan at fixed excitation wavelength.

Table-5.3 Showing particle size variation of all samples with absorption and photoluminescence results.

Sample	**Particle Size(nm)**		**Absorption wavelength(nm)**	**Excitation wavelength(nm)**	**Band gap(eV)**		**Emission wavelength(nm)**
	XRD	**TEM**	**UV-Vis. Spectra**	**410nm emission**	$(\alpha h\nu)^{1/n}$ **vs.** $h\nu$	**PLE**	**284nm PLE**
CH(0.1%)ZnS NPs	4.91	3.0-4.0	305	280	3.92	4.42	393
CH(0.5%)ZnS NPs	3.49	-	270	281	4.32	4.41	395
CH(1.0%)ZnS NPs	3.83	3.0-4.0	276	284	4.65	4.36	395
CH(1.5%)ZnS NPs	4.54	-	285	282	4.42	4.39	395
CH(2.0%)ZnS NPs	4.49	-	305	280	4.42	4.42	392

5.4 Thioglycerol capped ZnS nanoparticles

This series comprises of five samples named as (0.1, 0.5, 1.0, 1.5 and 2.0%) TG capped ZnS nanoparticles.

5.4.1. XRD Studies

Figure 5.14 shows X-ray diffraction pattern of TG (0.1, 0.5, 1.0, 1.5, and 2.0%) capped ZnS NPs. It shows three broad peaks corresponding to the (111), (220) and (311) planes of FCC ZnS structure. It is to be noted that, the peaks observed in the XRD pattern match well with those of the β-ZnS (cubic) reported in the ICDD Powder Diffraction files (File. No.03-0570). Broadening of the XRD peaks for capped samples indicates the formation of ZnS nanocrystals. The nano crystals have lesser lattice planes compared to bulk which contributes to the broadening of peaks in the diffraction pattern. This broadening can also arise from micro straining of the crystal structure which arises from dislocation and twinning [6]. These defects were believed to be associated with the chemically synthesized nanocrystals as they grow spontaneously during chemical reaction since chemical species get very little time to diffuse to an energetically favorable site.

Crystallite size of ZnS nanoparticles was calculated by following Scherer's equation [24],

$$D = k\lambda / \beta\cos\theta$$

where k=0.9, D- crystallite size (Å), λ(Å) the wavelength of Cu(Kα) radiation and β(in radians) is full width at half maximum (FWHM). Broadening of the XRD peaks indicates the formation of ZnS NC's. The average crystallite size using Scherer's formula is estimated from three planes is 2.56, 2.46, 2.73, 2.68, 2.38nm for TG (0.1-2.0%) capped ZnS NC's.

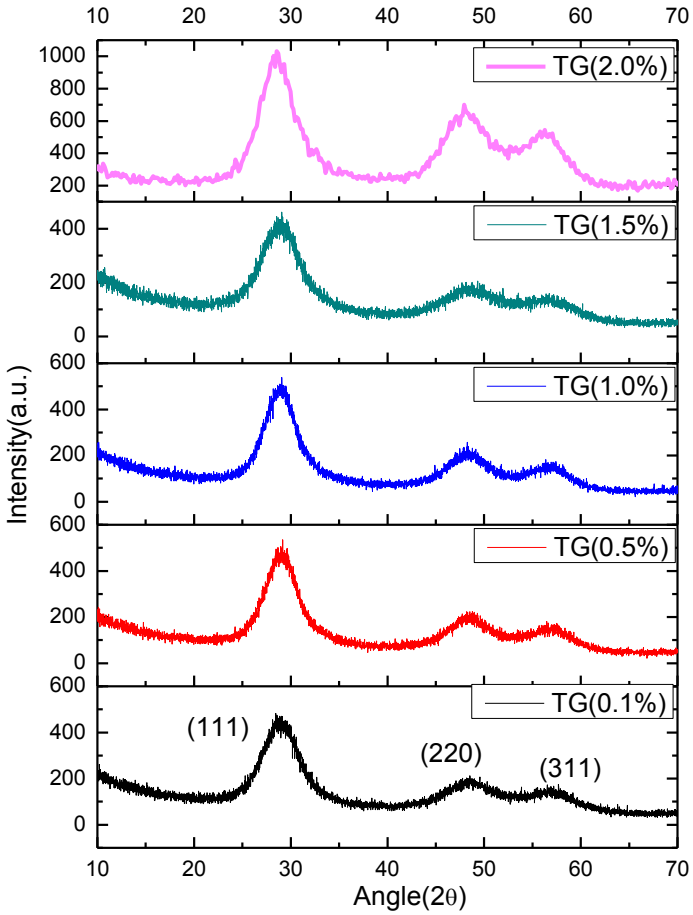

Figure 5.14 XRD pattern of TG (0.1-2.0%) capped ZnS NPs.

5.4.2 TEM Studies

HRTEM micrograph of TG (1.0%) capped NPs are shown in Figure 5.15 which shows spherical crystallites having particle size ~5.0-6.0 nm. This shows estimated particle size of TG capped ZnS NPs is somewhat larger than crystallite size measured from XRD measurements. Figure 5.16 shows SAED pattern of same sample which shows a set of rings instead of spots due to random orientation of crystallites. The ED pattern shows three rings that correspond to (111), (220) and (311) planes of the cubic phase of ZnS and are well agreed with the results obtained from XRD. Figure 5.17 shows high-angle annular dark-field (HAAD) images of TG (1.0%) capped ZnS NPs. It also shows uniformly dispersed particles of 5.0-6.0nm having spherical morphology.

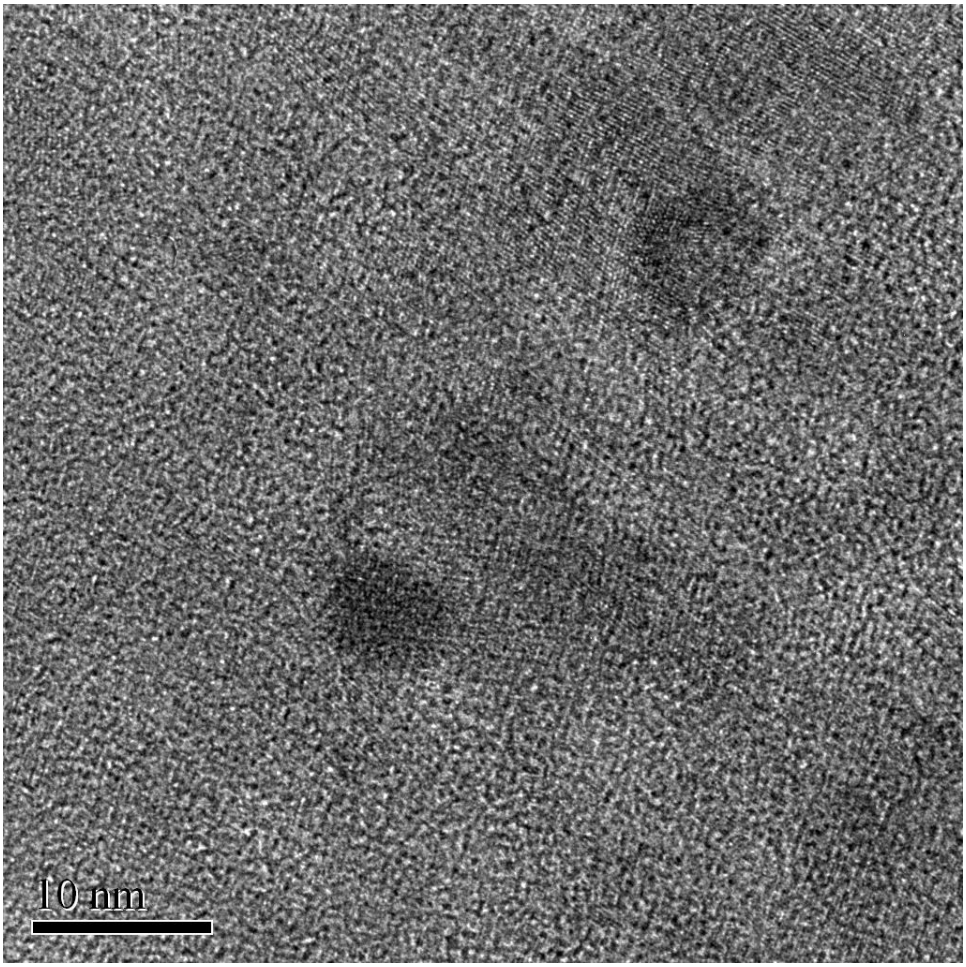

Figure 5.15 HRTEM of TG (1.0%) capped ZnS NPs

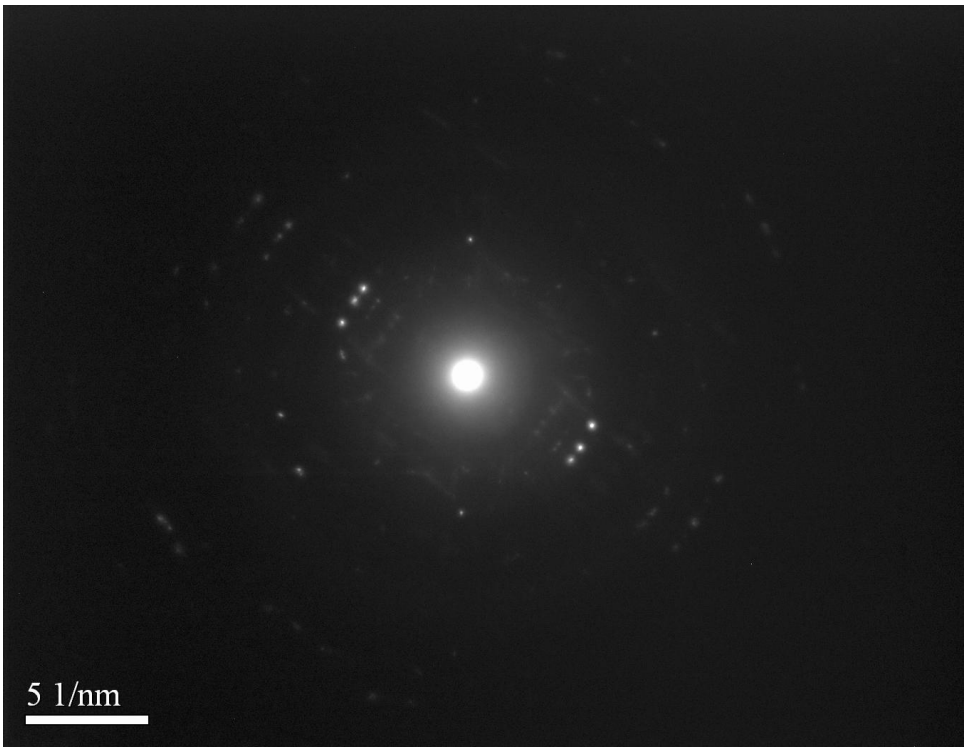

Figure 5.16 SAED pattern of TG 1.0% capped ZnS NPs

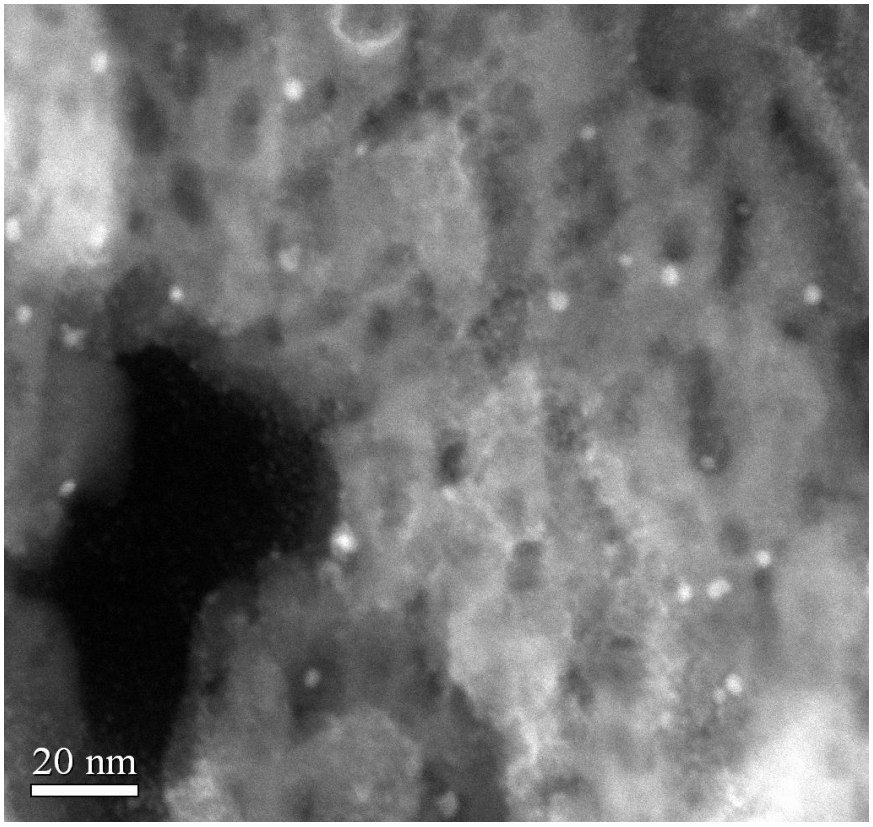

Figure 5.17 Dark field transmission electron micrograph of 1.0% TG capped ZnS NPs.

5.4.3. FTIR Studies

Figure 5.18(a) represents FTIR spectra of TG capped and uncapped ZnS nanoparticles in the range of 4000-400cm^{-1} whereas Figure 5.18(b) represents the proposed interaction mechanism of different capping agents with ZnS nanoparticles. Table-5.4 represents the FTIR spectra data showing the position of different groups of pure capping agents along with some observed position in our experiment for ZnS capped nanoparticles. The sharp peaks in all samples at 2358cm^{-1} is due to carbon which is instrumental error. For TG capped ZnS nanoparticles the breaking of S–H bond and formation of S–S bond in the region of 400–600 cm^{-1} shows interactions of ZnS NPs with thioglycerol. Since the S-H vibration observed at 2555 cm^{-1} of the free TG ligand, was not observed for any of the subsequent capped ZnS sample. So it is clearly indicates that the TG was de-protonated and coordinated to the surface of the ZnS nanoparticle through the

sulphur [30]. Passivation is furthered confirmed by the formation of the S–S bond (400-600cm^{-1}) as a consequence of the S–H bonds breaking. S–S bond arises between sulfur from thiol group existing in the capping agent and sulfur in the ZnS nanoparticles. Table 5.4 shows (CH_2-O [δs CH_2]) bonding range from 1470 to 1300 cm^{-1} as observed in pure sample. Intensity of it has decreased or disappeared in TG passivated ZnS samples [35]. Intensity of 1417.8 cm^{-1} peak assigned to –CH_2–S in pure thioglycerol decreases in ZnS passivated with thioglycerol sample. The doublet of C–C stretch seen in pure sample in the region of 1300–800 cm^{-1} was replaced by a sharp band near 1117 cm^{-1} corresponding to asymmetric stretching vibrational mode indicating a surface modification due to the passivation of ZnS nanoparticles. This phenomenon proves the fact that TG got assembled on the ZnS surface. The proposed mechanism of interaction of capping agents with ZnS NPs is shown in Figure 5.18(b). The bands at 2873 cm^{-1}and 2932 cm^{-1} of vibration of -CH_2- for TG clearly exists in capped ZnS. These facts prove further that the bond of S–Zn is strong and other groups in the TG molecule don't affect its assembling.

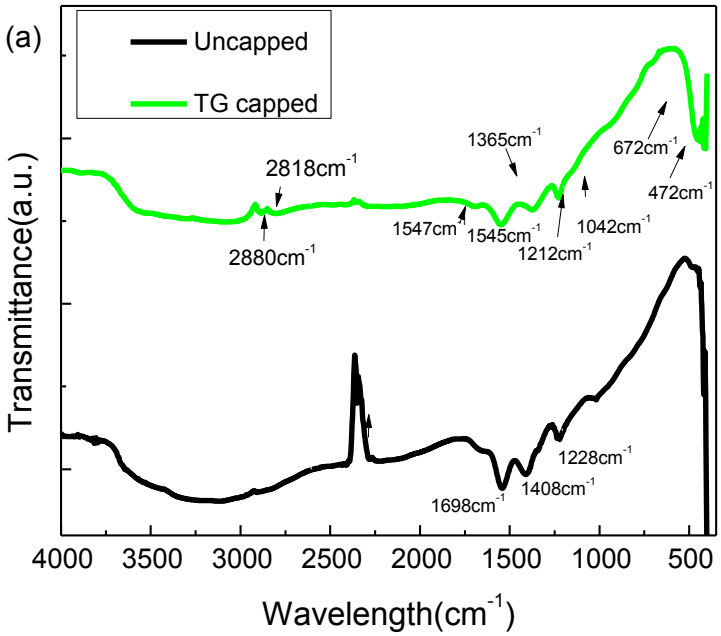

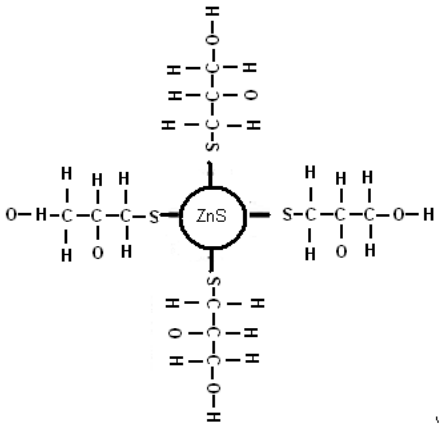

Figure 5.18(a) FTIR spectra of uncapped ZnS, TG capped ZnS, (b) Proposed capping interactions of TG capped ZnS NPs.

Table 5.4 Showing peak assignment of various bonds in TG and TG capped ZnS NPs in comparison to uncapped ZnS NPs

Peak assignment	**TG**	**TG + ZnS NPs**	**Uncapped ZnS NPs**
C-H bonding(a & s)	-	2918, 2852, 1362	1404
C-O bonding	-	-	
O-H stretch			3250
$CH_2O[\delta sCH_2]$ bonding	1470-1300*	1362	-
CH_2 a(stretch)	2930*	2918	-
S-H stretching bond	2555.5*	-	-
S-S bond	-	400-600	-

* Ref. [35].

5.4.4 UV Visible absorption Studies

Figure 5.19(a) shows the absorbance versus wavelength (λ) traces of the TG (0.1-2.0%) capped ZnS NPs. The absorption spectrum of capped samples show absorption shoulder edge blue shifted in comparison to bulk ZnS (340nm) which is due to quantum size effect. By calculating transmittance data using the Manifacier model [30], the

absorption coefficients (α) were calculated in the region of strong absorption. To determine the band gap of synthesized ZnS NPs, the fundamental absorption, which corresponds to the transition from valence band to the conduction band was used. The relation between absorption coefficient *(α)* and incident photon energy *($h\nu$)* can be written as [30]

$$\alpha = A\,(h\nu - E_g)^{n}/h\nu \qquad (1)$$

where A is a constant, E_g is the band gap of the material and the exponent n depends on the type of transition. n may have values 1/2, 2, 3/2 and 3 corresponding to the allowed direct, allowed indirect, forbidden direct and forbidden indirect transitions respectively [30]. The exact values of the band gap were determined by extrapolating the straight line portion of the $(\alpha h\nu)^{1/n}$ versus $h\nu$ graphs to the $h\nu$ axis as shown in Figure 5.19(b) and Table 5.5. From the plots the values of band gap were obtained as 3.68, 3.69, 4.33, 3.94 and 3.74eV for TG (0.1, 0.5, 1.0, 1.5, 2.0 at. wt. %) capped ZnS NPs respectively. The result indicates that 1.0% capped sample has maximum band gap which accounts for high quantum confinement of electrons at this concentration of thioglycerol.

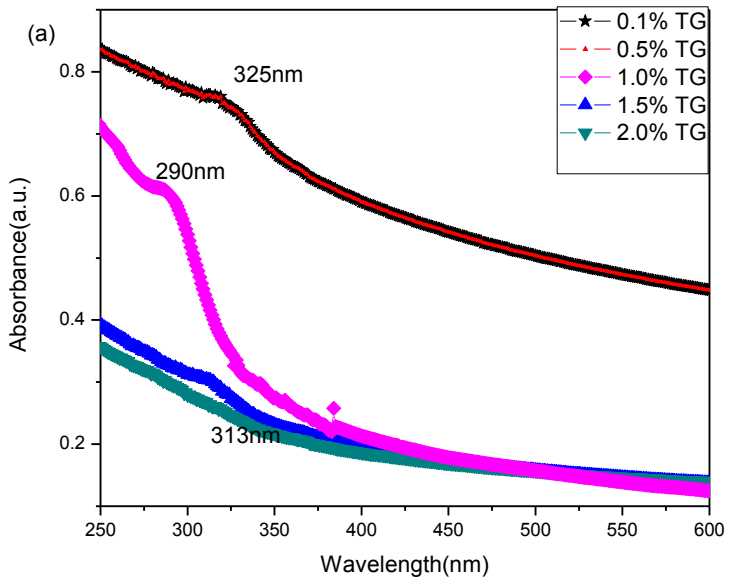

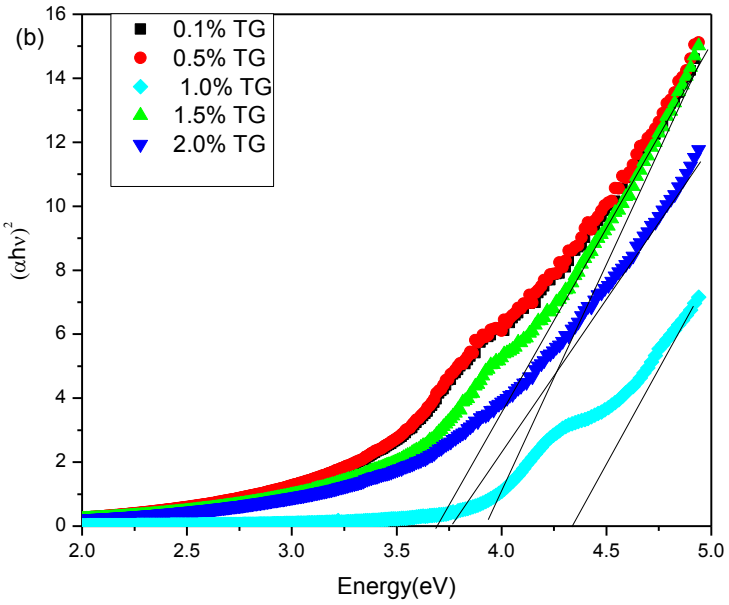

Figure 5.19(a) UV-Visible absorption spectra of TG (0.1-2.0%) capped ZnS NPs, (b) $(\alpha h\nu)^2$ Vs. hν graph to find out band gap of TG (0.1-2.0%) capped ZnS NPs.

5.4.5. Photoluminescence Studies

Figure 5.20 shows steady state room temperature photoluminescence spectroscopy results of all TG (0.1-2.0%) capped samples. Figure 5.20(a) shows PL spectra of TG (0.1-2.0%) capped ZnS NPs at 325nm excitation wavelength. It can be seen that the spectral shapes are asymmetric and broad. The peaks are not very smooth having fine structure with a closely separated doublet. To resolve the doublet structure and to locate the exact peak positions, each spectrum was deconvoluted as shown in Figure 5.20(b). The experimentally observed spectra could be regarded as the resultant of the contribution from these two deconvoluted peaks. Emission peaks are observed at 368nm (high) and 401nm (low) for TG (0.1%) capped ZnS NPs. With increase in capping concentration from 0.1 to 0.5%, there is slight increase in integrated PL intensity (Figure 5.20(a)) but as shown in deconvoluted gaussian curve fitting, intensity of peak around 368nm decreases and 401 start increasing. With further increase in capping concentration to 1.0%, emission

peaks around 400nm red shifts to 422-430nm and its intensity increases in comparison to 363nm. Also a new peak around 454 and 517nm starts increasing. With further increase in TG concentration to 1.5% and from 1.5 - 2.0 % emission intensity of 363nm peak is decreased. Secondly shift of these peaks from UV (363nm) to blue color (422-487nm) was noted for NPs synthesized at higher concentration of TG. With further increase in capping concentration to 2.0% total integrated emission intensity is observed to decrease as shown in Figure 5.20(a). But as shown in Figure 5.20(b), 2.0% TG capped ZnS NPs have broad emission spectra having multiple emission peaks from 363-517nm. The integrated highest emission intensity for all peaks is for (1.0%) TG capped ZnS NPs (Figure 5.20(a)). The origin of blue emission from ZnS nanoparticles under UV excitation has been discussed in detail earlier (section-5.1, 5.2). In the present work, the PL peaks appeared at energy levels substantially lower than the band gap, suggesting that the transitions from energy states inside the band gap (trap states) are being favoured for the luminescence process in these nanocrystalline ZnS NPs. It is mentioned in previous section that 422nm peak in ZnS is due to transfer of electrons from sulphur vacancies acting as trap states and 444-470nm emission is due to zinc vacancies respectively. Also emission peak at 363-392nm is assigned to sulphur interstitial sites or band edge luminescence [18]. With increase in TG concentration from 0.1 to 0.5% emission peak at 363nm is partially quenched suggesting passivation or absence of sulphur interstitials. Emission peak intensity around 423nm and 454nm is observed to increase with increase of TG concentration from 0.1-2.0%. At 2.0% TG 363nm peak is nearly absent and from intensity comparison of deconvoluted peaks the red shifts with increasing concentration of capping agent TG from 0.1 to 2.0% is observed. But in our case large shift in particle size with change in capping concentration is not observed (2.38-2.73nm). So, in our case

shifting of emission peak with increase in TG concentration cannot be explained by Chen and Chenstnoy model [3, 27]. This can be explained by passivation of interstitial sulphur and its vacancy by increase in concentration of adsorbed TG molecules. Since the intensity of PL originating from a particular defect level is proportional to the population of that defect site present in the sample, the relative change in PL peak intensity between zinc vacancy and sulphur vacancy levels with capping concentration can be explained qualitatively in terms of the change in population of those sites with increasing capping concentration. The peak intensity of the emission originated due to sulphur interstitials was always lower than the emission due to sulphur vacancies and zinc vacancy because of the fact that sulphur interstitial sites were more likely to become passivated by capping agent TG. Formation of S-S bonds between excess sulphur of ZnS and sulphur of TG, and breakage of S-H bond of pure TG is already discussed in FTIR studies of TG capped ZnS NPs. This suggests that decrease in excess sulphur related emission with increase in TG concentration from 0.1-2.0% is due to effective capping as described above. Also this explains shifting of PL spectra from UV to blue region with increase in capping. The intensity ratio decreased primarily due to increasing passivation of sulphur interstial sites by the same process (increase in TG concentration from 0.1-2.0%), resulting in lowering PL intensity of the corresponding peak with increasing capping concentration. This resulted in an increase in the population of zinc vacancies and led to a corresponding increase in the PL intensity originating from these vacancy sites. The PL peak at 484-516nm is also observed to increase with increase in capping concentration. The PL spectra of all the ZnS NPs showed a weak shoulder around 520 nm. The origin of this shoulder structure at lower energy compared to the main peak can be attributed to the recombination of electron-hole pair at the surface traps, which arise for the high surface

to volume ratio of the nanoparticles due to their small sizes. Emission in green region from undoped ZnS was observed by Hu et al. [28] and they assigned the emission to some self-activated centers, probably surface states, vacancy or interstitial states within the structure.

Figure 5.20(a) shows excitation spectra of TG (2.0%) capped NPs for different possible emission sites observed in emission spectra shown above. In excitation studies of synthesized capped NC's, emission wavelength used is 422nm and 363nm respectively. In excitation spectra of TG capped NC's, broad excitonic peak around 329nm is observed for both 363 and 422nm emission. It suggests that all defect or vacancies related emission in capped NC's is arising from band to band excitation in host ZnS (as 329nm excitation is near 340nm for bulk ZnS).

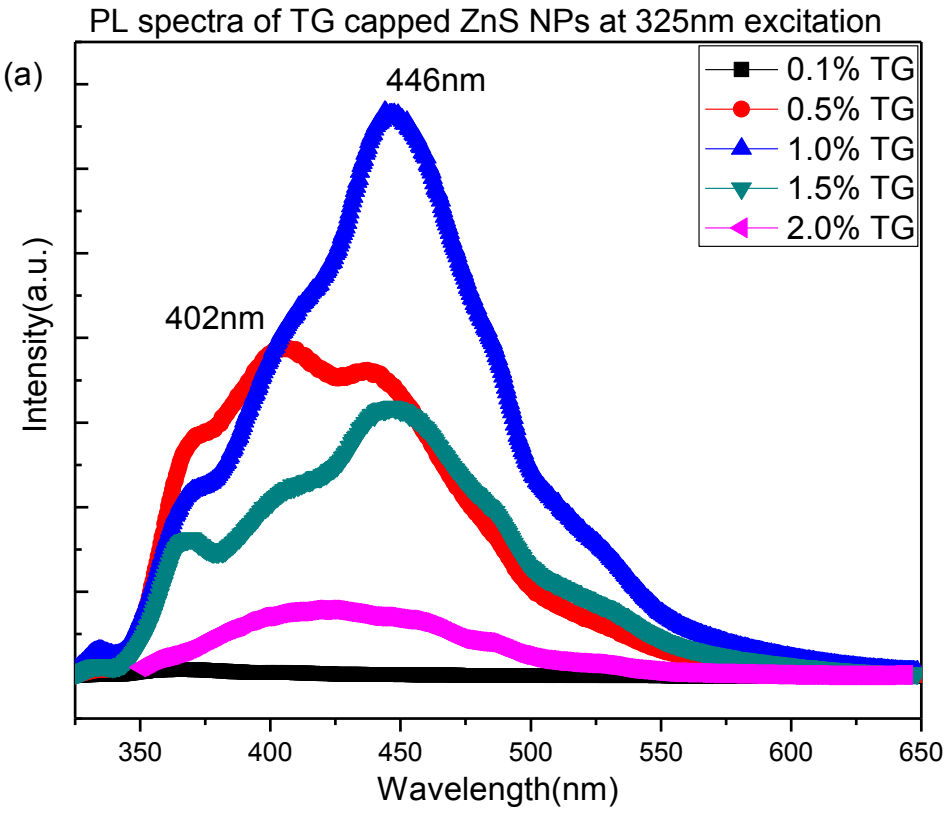

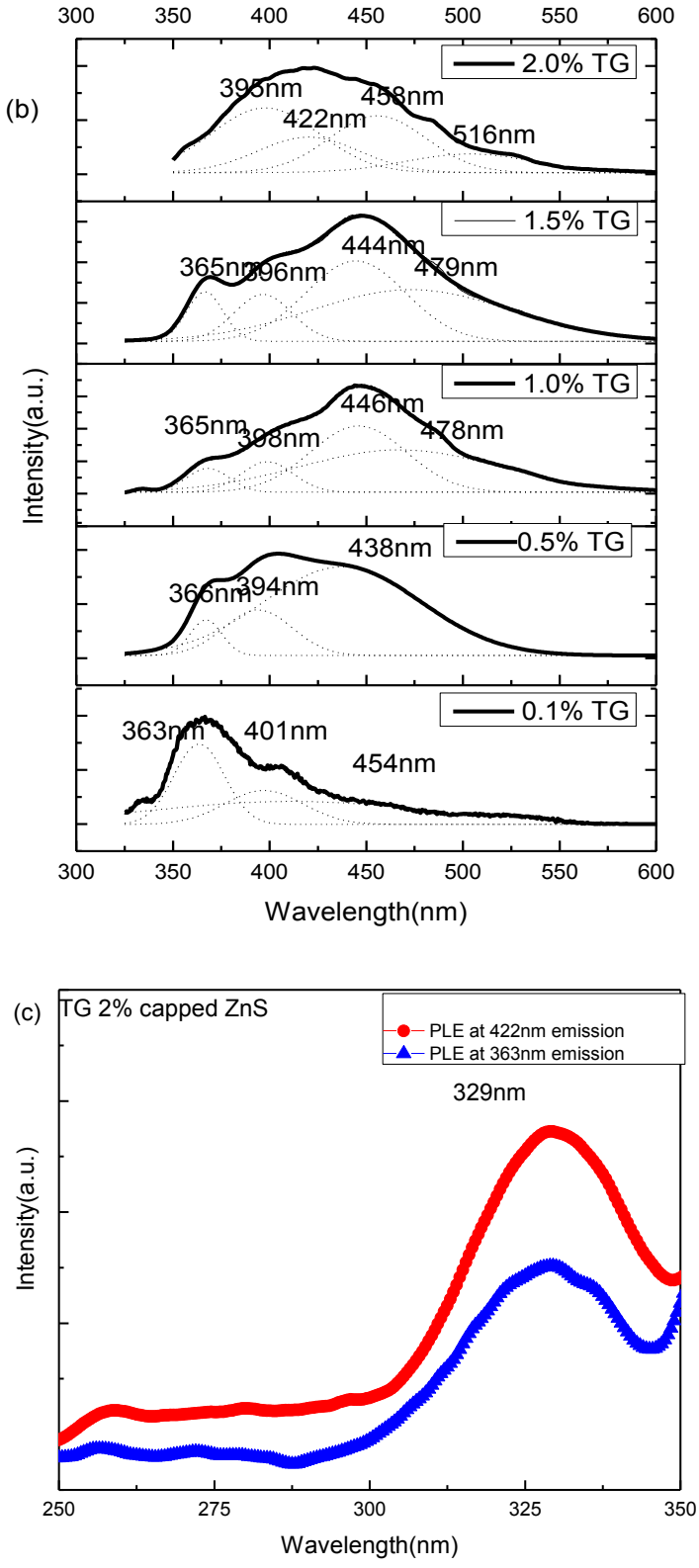

Figure 5.20 (a) PL spectra of TG(0.1-2.0%) capped ZnS NPs, (b) Gaussian distribution of most dominant peaks in emission spectra of TG(0.1-2.0%) capped ZnS NPs, (c) excitation spectra of TG(2.0%) capped ZnS NPs at possible emissions.

Table 5.5 Showing particle size variation of all samples with absorption and photoluminescence results.

Sample	Particle Size (nm)		Absorption wavelength (nm)	Excitation wavelength (nm)		Band gap (eV)		Emission wavelength(nm) at fixed excitation(PLE)			
	XRD	TEM	UV-Vis. Spectra	At 423nm emission	At 461nm emission	UV-Vis.	PLE	235nm PLE	272nm PLE	304nm PLE	329nm PLE
TG0.1%) ZnS NPs	2.56	-	325	-	-	3.68	-	-	-	-	{363}, (401)
TG(0.5%) ZnS NPs	2.46	-	326	-	-	3.69	-	-	-	-	365, {394, 438}
TG(1.0%) ZnS NPs	2.73	-	294	-	-	4.33	-	-	-	-	(365, 396), {446}, (478)
TG(1.5%) ZnS NPs	2.68	3.0-4.0	319	-	-	3.94	-	-	-	-	(365, 396), {444}, (479)
TG(2.0%) ZnS NPs	2.38	-	334	329	329	3.70	3.76	422	422	422	{398, 422}, (456, 516)

Note: Emission peaks in Table above with in { } shows high emission intensity and with ( ) shows low intensity.

5.5 Mercaptoethanol capped ZnS Nanoparticles

This series comprises of five samples named as (0.1, 0.5, 1.0, 1.5 and 2.0%) ME capped ZnS nanoparticles.

5.5.1. XRD Studies

Figure 5.21 shows X-ray diffraction pattern of ME (0.1, 0.5, 1.0, 1.5, and 2.0%) capped ZnS NPs. It shows three broad peaks corresponding to (111), (220) and (311) planes of FCC ZnS structure. It is to be noted that, the peaks observed in the XRD pattern match well with those of the β-ZnS (cubic) reported in the ICDD Powder Diffraction files (File. No.80-0020). Broadening of the XRD peaks for capped samples indicates the formation of ZnS nanocrystals. With increase in capping concentration increase of broadening is observed with reduction in crystalline nature.

Crystallite size of ZnS nanoparticles was calculated by following Scherer's equation [24]

$$D = k\lambda / \beta\cos\theta$$

where k=0.9, D- crystallite size (Å), λ(Å) the wavelength of Cu(Kα) radiation and β(in radians) is full width at half maximum (FWHM). Broadening of the XRD peaks indicates the formation of ZnS NC's. The average crystallite size using Scherer's formula is estimated from three planes is 4.27, 3.34, 1.78, 2.08, 2.41nm for ME (0.1-2.0%) capped ZnS NC's.

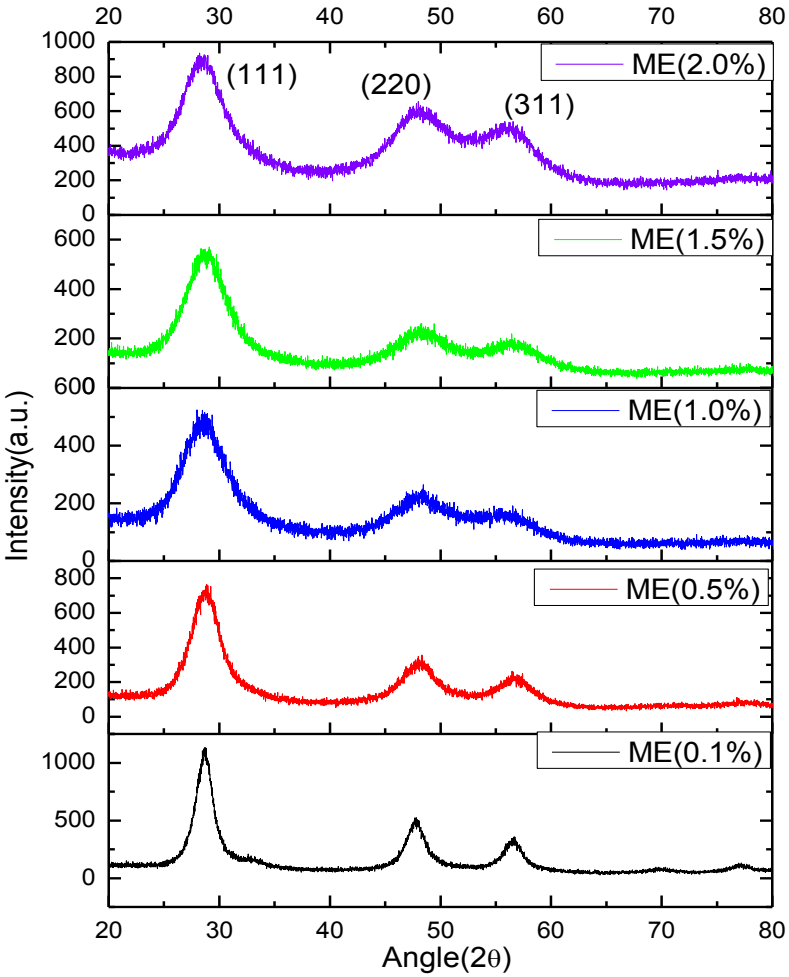

Figure 5.21 X-ray diffraction pattern of ME (0.1, 0.5, 1.0, 1.5, and 2.0%) capped ZnS NPs.

5.5.2 TEM Studies

Figure 5.22(a) shows bright field TEM micrograph of 1.0% ME capped ZnS NPs. It shows abundance of spherical nanoparticles having average size 3.0nm. TEM micrograph of ME (2.0%) capped NPs are shown in Figure 5.22 (b-d) which shows spherical crystallites having particle size in between 3.0-5.0 nm along with presence of some nanorods having average diameter 20nm. Figure 5.22(d, e) shows TEM and HRTEM images of selected region of whole TEM micrograph of 2.0% capped sample, showing formation of nanorods of ZnS. Lattice fringing is clearly seen in Figure 5.22(e)

showing random orientation of (111) plane as observed by broadening in XRD pattern for 2.0% sample. This can be due to start of agglomeration of spherical NPs of size 4nm to form nanorod as seen in HRTEM micrograph that (111) plane is not showing preferential growth in one direction. This suggests that with higher amount of ME, agglomeration phenomenon starts. As discussed earlier, the broadening in X- ray peaks also arises from micro straining of the crystal from dislocation and twinning [6]. These defects were believed to be associated with the chemically synthesized NC's as they grow spontaneously during chemical reaction since chemical species get very little time to diffuse to an energetically favorable site.

(a)

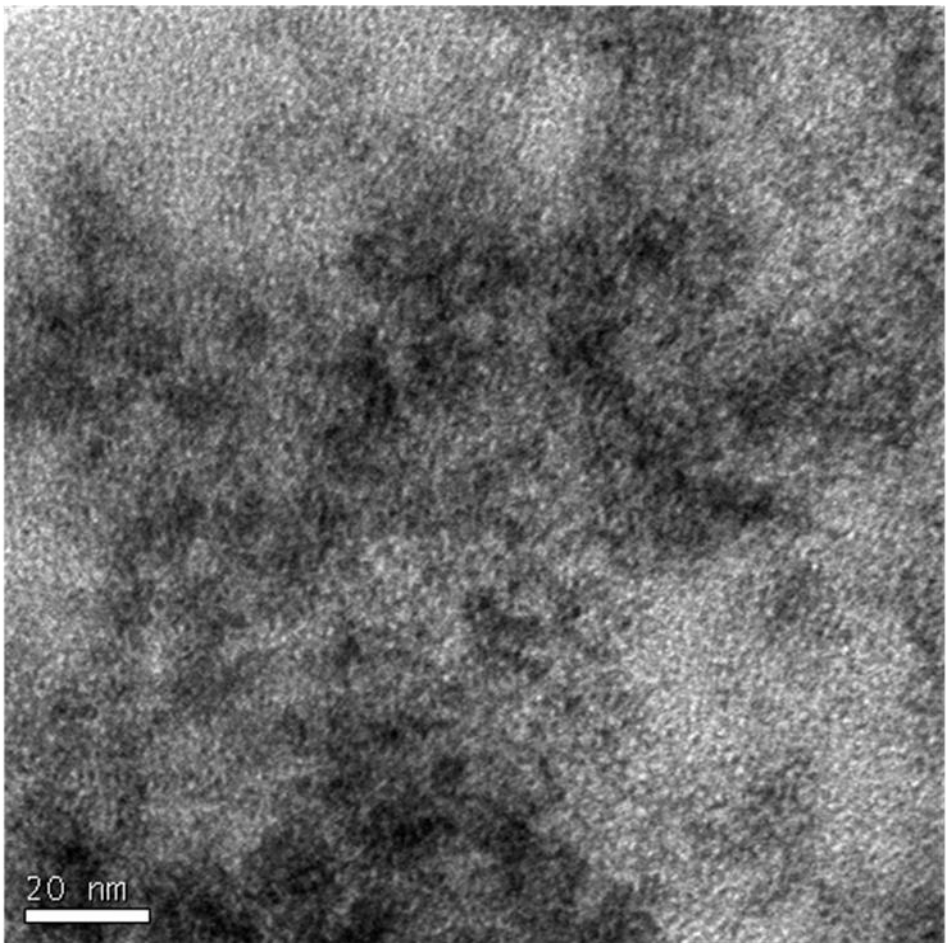

(b)

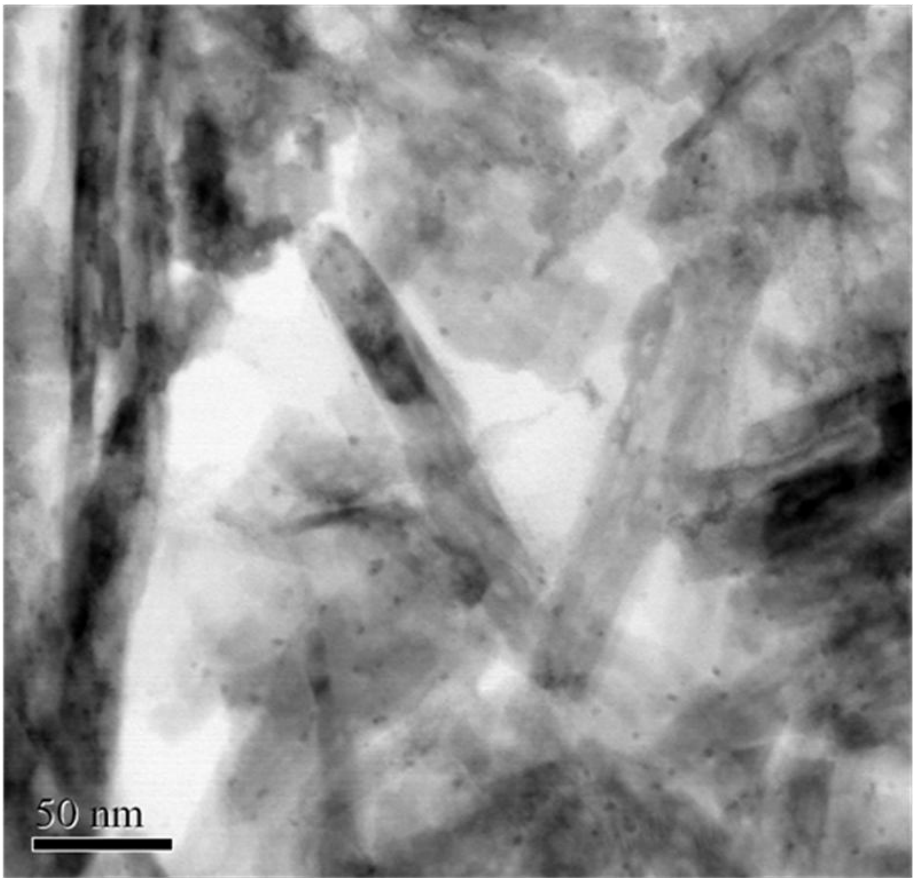

(c)

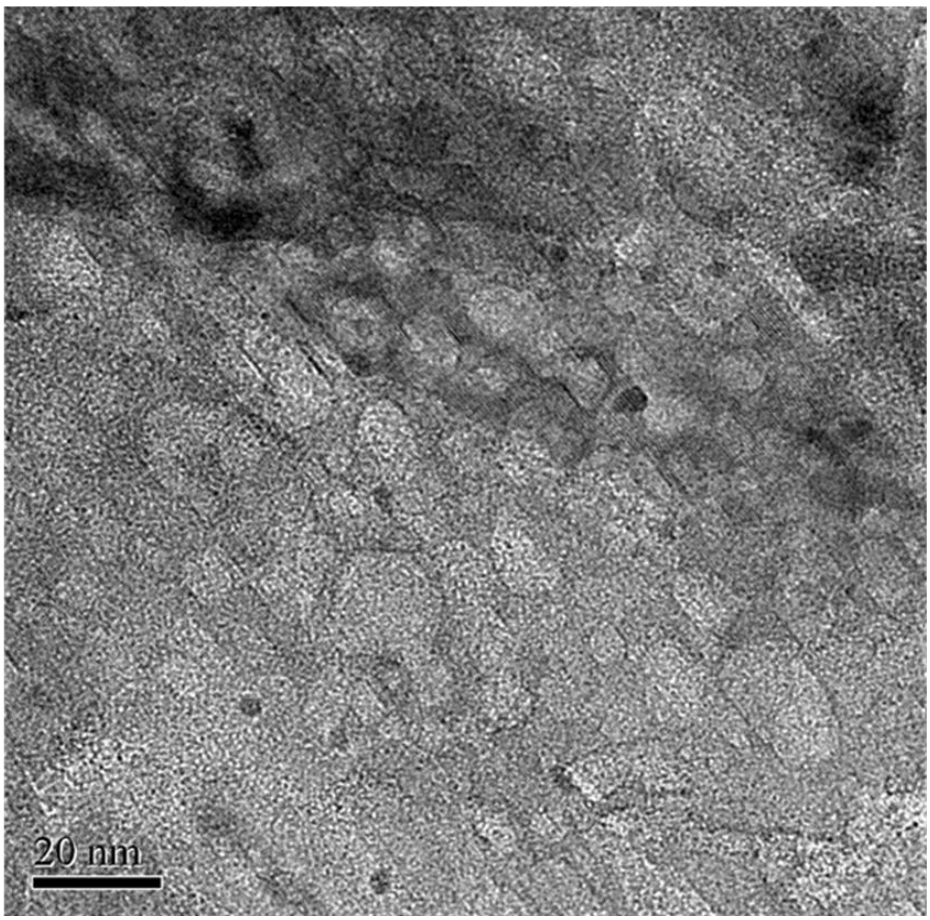

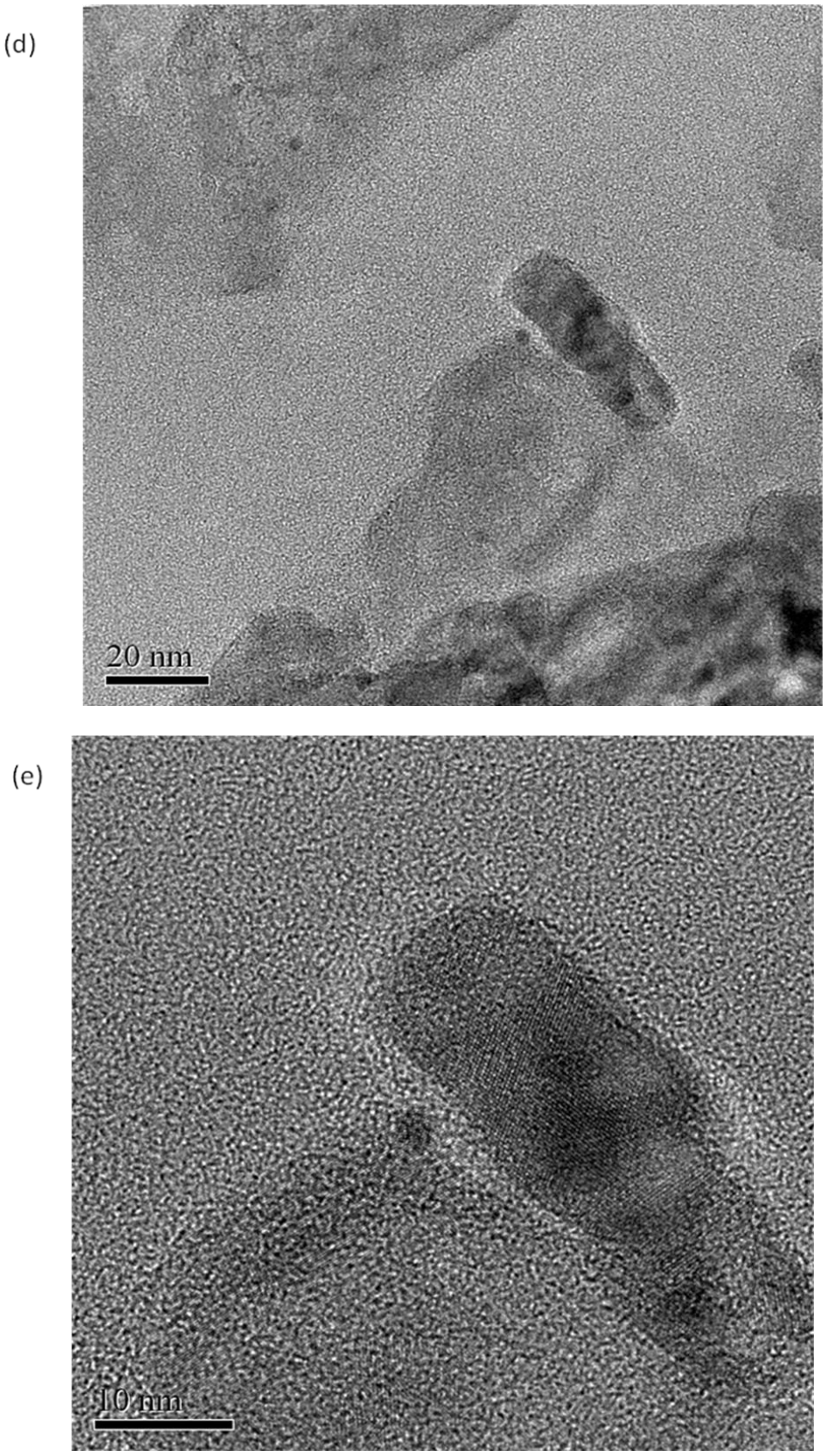

Figure 5.22. Bright field transmission electron micrograph of (a) 1.0% ME capped, (b, c, d, e) 2.0% ME capped ZnS NPs at different magnifications.

5.5.3. FTIR Studies

Figure 5.23 (a) represents FTIR spectra of ME capped and uncapped ZnS NC's in the range of 4000-400cm^{-1} whereas Figure 5.23(b) represents the proposed interaction mechanism of different capping agents with ZnS NC's. Table-5.6 represents the FTIR spectra data showing the position of different groups of pure capping agents along with some observed position in our experiment for ZnS capped NC's. The sharp peaks in all samples at 2358cm^{-1} is due to carbon which is instrumental error mentioned previously. For ME capped ZnS NC's the breaking of S–H bond and formation of S–S bond in the region of 400–600 cm^{-1} shows interactions of ZnS NC's with ME as the S-H vibration observed at 2555 cm^{-1} of the free ME ligand, was not observed for any of the subsequent capped ZnS sample. This is a clear indication that the ME was de-protonated and coordinated to the surface of the ZnS nanoparticle through the sulphur [35]. Passivation is confirmed by the formation of the S–S bond (400-600cm^{-1}) as a consequence of the S–H bonds breaking. S–S bond arises between sulfur from thiol group existing in the capping agent and sulfur in the ZnS nanoparticles. Table-5.6 shows (CH_2-O [δs CH_2]) bonding range from 1470 to 1300 cm^{-1} as observed in pure sample that got decreased in intensity or disappeared in ME passivated ZnS samples [35]. Intensity of 1417.8 cm^{-1} peak assigned to –CH_2–S in pure ME decreases in ZnS passivated with ME sample. The doublet of C–C stretch seen in pure sample in the region of 1300–800 cm^{-1} was replaced by a sharp band near 1117 cm^{-1} corresponding to asymmetric stretching vibrational mode indicating a surface modification due to the passivation of ZnS NPs. This phenomenon proves the fact that ME got assembled on the ZnS surface. The proposed mechanism of interaction of capping agents with ZnS NPs is shown in Figure 5.23(b). The bands at 2873 $cm^{-1}$and 2932 cm^{-1} of vibration of -CH_2- for ME clearly exists in capped ZnS. These facts prove further that the bond of S–Zn is strong and other groups in the ME

molecule don't affect its assembling. On comparing the above FTIR spectra with TG capped ZnS NPs discussed in previous section it is observed that the bonding of the substituted element differs; such as S–H and CH (OH) in TG, S–H in ME. It is interesting to note that though both TG and ME have S–H group at one end and OH group at the other end, ME has only two C atoms chain with one OH group, whereas TG has three C atoms with two OH groups [35]. As the nature of capping differs drastically, it alters the size distribution monodispersion or polydispersion of particles. The main difference in these organic capping agents (ME and TG) is the number of carbon atoms present in the molecule. In spite of these differences, when the synthesis conditions are same, all the passivating agents give rise to excitonic peak at almost the same position with 5 nm deviation.

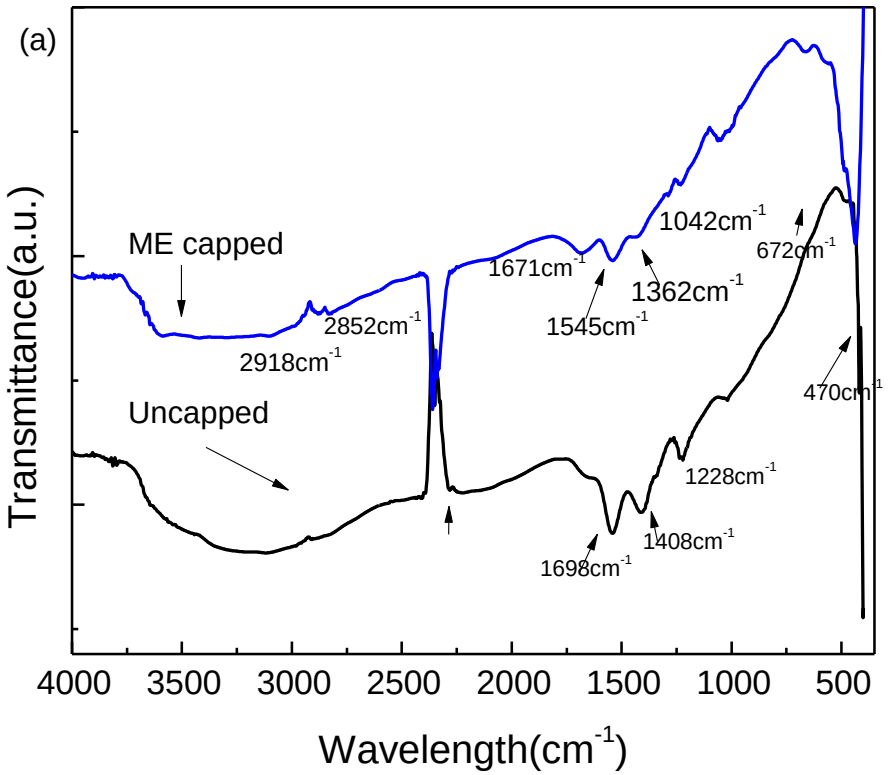

(b)

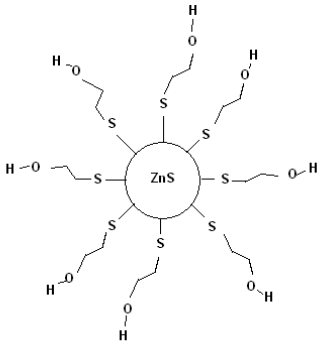

Figure 5.23(a) FTIR spectra of uncapped ZnS, ME capped ZnS; (b) Proposed capping interactions of ME capped ZnS NPs.

Table-5.6 Showing peak assignment of various bonds in ME and ME capped ZnS NPs in comparison to uncapped ZnS NPs

Peak assignment	**ME**	**ME + ZnS NPs**	**Uncapped ZnS NPs**
C-H bonding(a & s)	-	2918, 2852, 1362	1404
C-O bonding	-	-	
O-H stretch			3250
$CH_2O[\delta sCH_2]$ bonding	1470-1300	1362	-
CH_2 a(stretch)	2930	2918	-
S-H stretching bond	2555.5	-	-
S-S bond	-	400-600	-

*Ref. [30].

5.5.4. UV-Visible absorption studies

After confirming single phase for all ME capped ZnS NC's, optical studies were performed to observe absorption characteristics in synthesized nanomaterials. Figure 5.24 (a) shows the absorbance versus wavelength (λ) traces of the ME (0.1- 2.0%) capped ZnS NPs. All samples show blue shift of absorption peak in comparison to bulk ZnS (340nm) which is due to quantum size effect. The band gap for capped ZnS NPs were determined by extrapolating the straight line portion of the $(\alpha hv)^{1/n}$ versus hv graphs to the hv axis as

shown in Figure 5.24(b). From the plots we find band gap energies to be 4.39, 4.35, 3.95, 4.42eV for 0.1-1.5% capped ME capped NPs respectively. The data for finding band gap of 2.0% ME capped ZnS NPs comes out of range which gives no slope or extrapolation. Its band gap from absorption edge comes out to be 3.78eV.

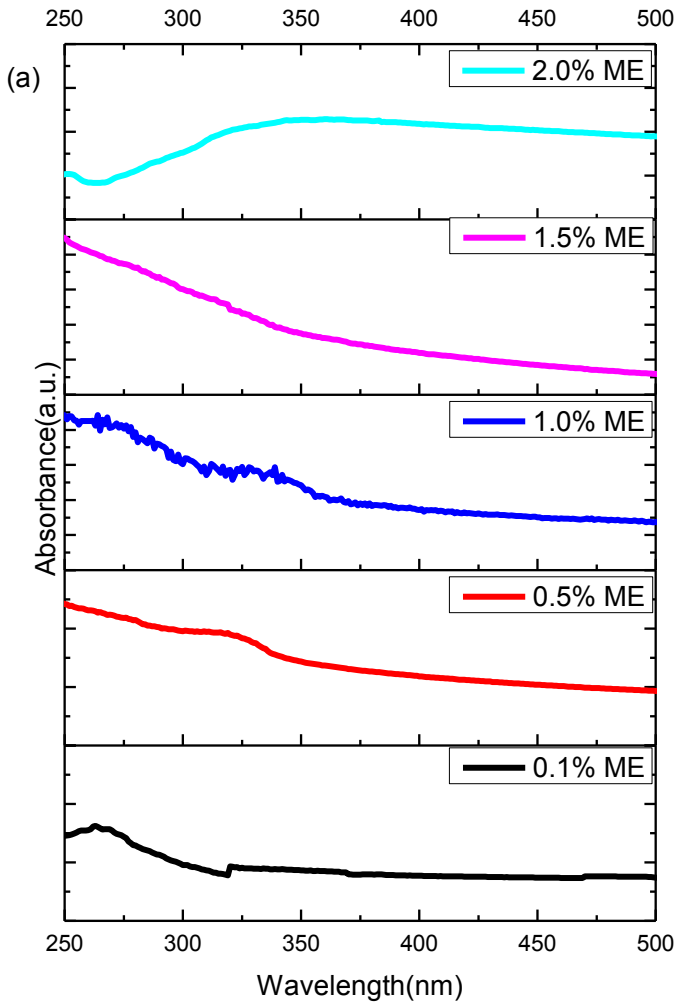

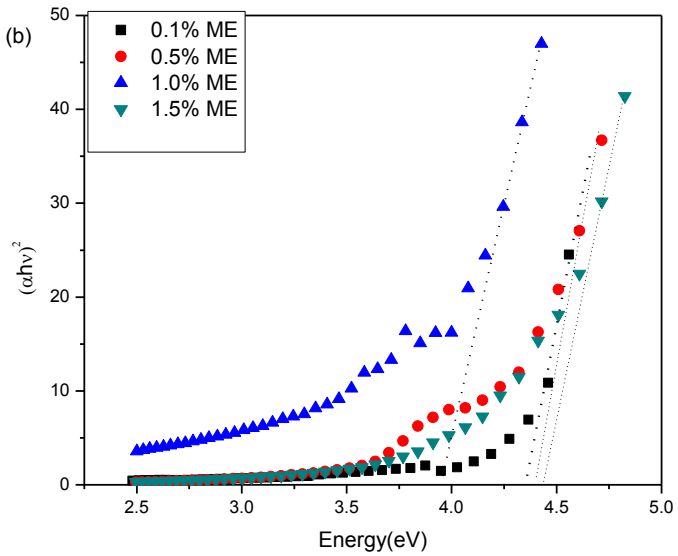

Figure 5.24. UV-Visible absorption spectra of ME (0.1-2.0%) capped ZnS NPs, (b) $(\alpha h\nu)^2$ Vs. hν graph to find out band gap of ME (0.1-2.0%) capped ZnS NPs

5.5.5. Photoluminescence Studies

Figure 5.25 shows steady state room temperature photoluminescence spectroscopy results of all ME (0.1-2.0%) capped samples. Figure 5.25(a) shows PL spectra of ME (0.1-2.0%) capped ZnS NPs at 325nm excitation wavelength. It can be seen that the spectral shapes are asymmetric and broad. The peaks are not very smooth having fine structure with a closely separated doublet. To resolve the doublet structure and to locate the exact peak positions, each spectrum was deconvoluted as shown in Figure 5.25(b). The experimentally observed spectra could be regarded as the resultant of the contribution from these two peaks. Emission peaks are observed at 360nm (high) and 401nm (low) for ME (0.1%) capped ZnS NPs. With increase in capping concentration from 0.1 to 0.5% there is decrease in integrated PL intensity (Figure 5.25(a)) but as shown in deconvoluted gaussian curve fitting intensity of peak around 360nm decreases and 408 and 443nm starts increasing. With further increase in capping concentration to 1.0%, emission peaks around 408 and 443nm converges into single broad peak aroung 433nm. With further

increase in ME concentration to 1.5% emission intensity of 363nm peak is decreased. But 408 and 443nm peaks which converge into 433nm peak for 1.0 % ME again separates into doublet. From its deconvoluted spectra in order to resolve its doublet, high emission peak at 411nm with considerable small peaks at 448 and 367nm is observed. With further increase in capping concentration to 2.0% total integrated emission intensity is observed to decrease as shown in Figure 5.25(a). But as shown in Figure 5.25(b), 2.0% ME capped ZnS NPs have broad emission spectra having multiple emission peaks from 363-517nm. The integrated highest emission intensity for all peaks is for (0.1%) ME capped ZnS NPs (Figure 5.25a). The origin of blue emission from ZnS nanoparticles under UV excitation has been discussed in detail in previous section of this chapter (5.1-5.3). In the present work, the PL peaks appeared at energy levels substantially lower than the band gap, suggesting that the transitions from energy states inside the band gap (trap states) are being favoured for the luminescence process in these nanocrystalline ZnS NPs. Here shifting of these peaks from UV (363nm) to blue color (408-448nm) was noted for NPs synthesized at higher concentration of ME. This can be explained by passivation of interstitial sulphur and its vacancy by increase in concentration of adsorbed ME molecules. As the intensity of PL originating from a particular defect level is proportional to the population of that defect site present in the sample, the relative change in PL peak intensity between zinc vacancy and sulphur vacancy levels with capping concentration can be explained qualitatively in terms of the change in population of those sites with increasing capping concentration. The peak intensity of the emission originated due to sulphur interstitials was always lower than the emission due to sulphur vacancies and zinc vacancy because of the fact that sulphur interstitial sites were more likely to become passivated by capping agent ME. Formation of S-S bonds between excess sulphur of ZnS and sulphur of ME, and breakage of S-H bond of pure ME is already discussed above in

FTIR studies of ME capped ZnS NPs. This suggests decrease of excess sulphur related emission with increase in ME concentration from 0.1-1.5% is due to effective capping as described above. Also this explains shifting of PL spectra from UV to blue region with increase in capping. Results of PL studies are somewhat similar to what observed in TG capped ZnS NPs which has been discussed in last section. The reason for this behavior can be similar nature of capping in TG and ME molecules.

Figure 5.25(c) shows excitation of ME (0.1, 2.0%) capped NPs for different possible emission sites observed in emission spectra shown above. It shows excitation peak at 290nm for emission at 360nm. In excitation spectra of 2.0% ME capped NC's, broad excitonic peak around 329nm is observed for both 363 and 422nm emission which suggests that all defect or vacancies related emission in capped NC's is arising from band to band excitation in host ZnS (as 329nm excitation is near 340nm for bulk ZnS). So shifting of excitonic peak from 290-329nm is observed for change in capping concentration of ME from 0.1% -2.0%. Calculated band gaps from excitation studies are 4.27, 3.76eV for ME (0.1, 2.0%) ME capped NPs and are comparable with those calculated from UV-Visible studies which are presented in Table-5.7.

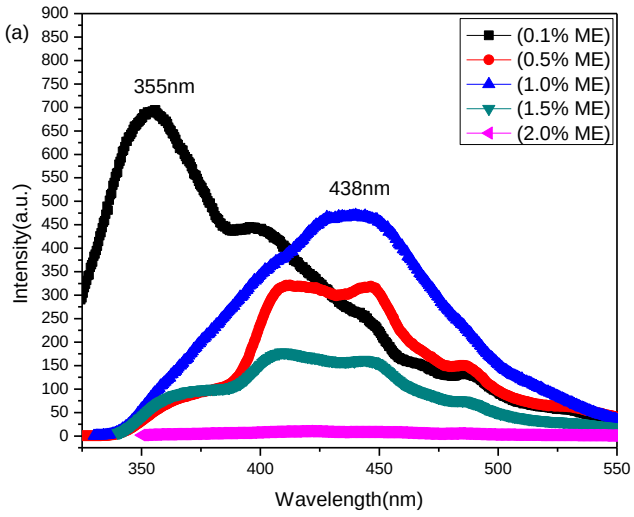

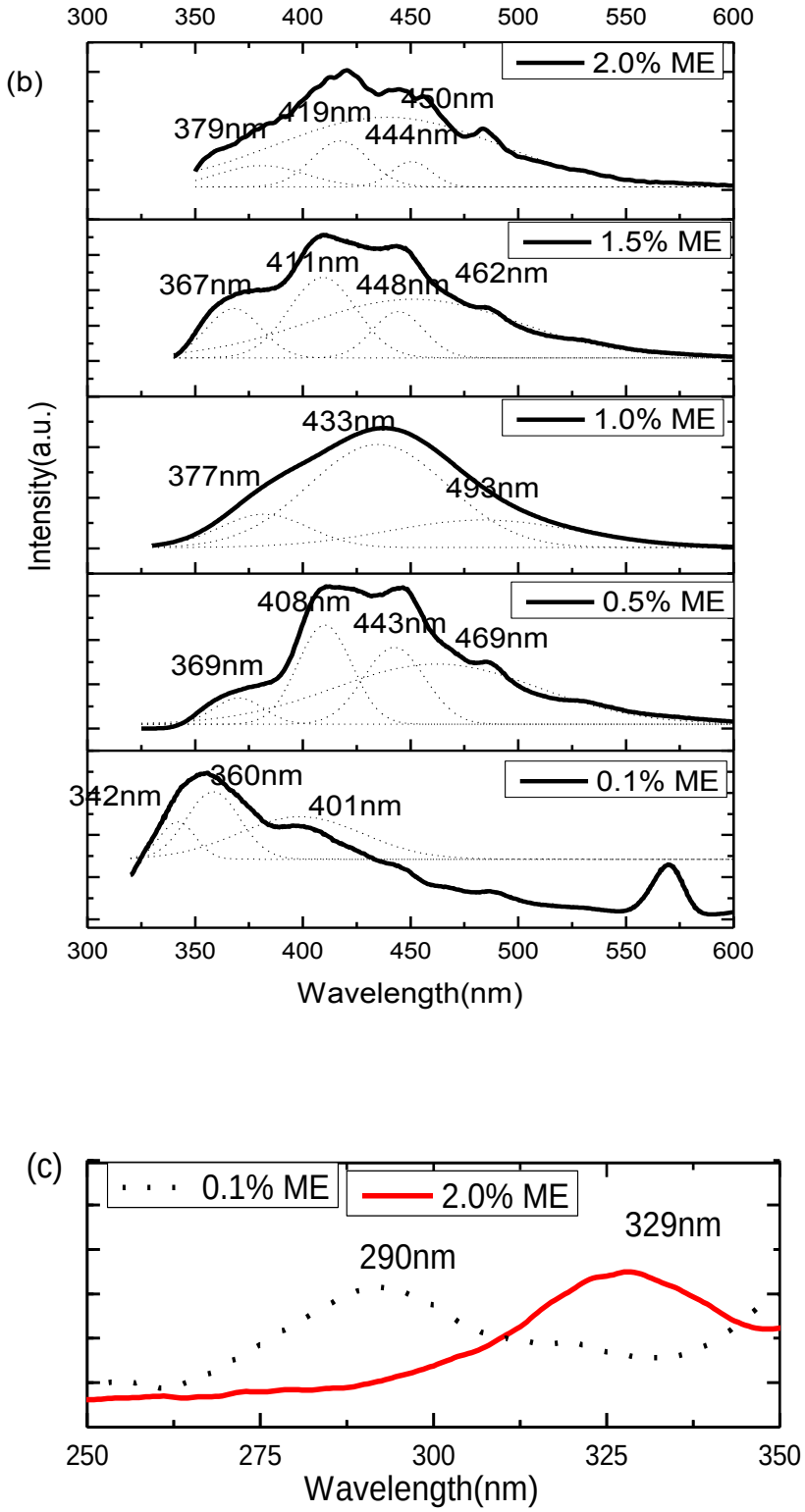

Figure 5.25 (a) PL spectra of ME(0.1-2.0%) capped ZnS NPs, (b) Gaussian distribution of most dominant peaks in emission spectra of ME (0.1-2.0%) capped ZnS NPs, (c) excitation spectra of 0.1% ME and 2.0% ME capped ZnS NPs at possible emissions.

Table-5.7 Showing particle size variation of ME capped ZnS NPs with absorption and photoluminescence results.

Sample	Particle Size (nm)		Absorption wavelength (nm)	Excitation wavelength(nm) (At fixed emission)		Band gap(eV)		Emission wavelength(nm) at fixed excitation (PLE) mentioned below:			
	XRD	TEM	UV-Vis. Spectra	360 nm	461 nm	UV-Vis.	PLE	235 nm	272 nm	304 nm	329 nm
ME(0.1%) ZnS NPs	4.27	-	325	-	-	4.39	4.27	-	-	-	{360}, (401)
ME(0.5%) ZnS NPs	3.34	-	326	-	-	4.35	-	-	-	-	(369), {408, 443}
ME(1.0%) ZnS NPs	1.78	3.0-4.0	294	-	-	3.95	-	-	-	-	(377), {433}
ME(1.5%) ZnS NPs	2.08		319	-	-	4.42	-	-	-	-	(367), {411}, 448}
ME(2.0%) ZnS NPs	2.41	NRs15 nm dia.	334	290	329	3.78	3.76	422	422	422	{419, 444}, (379)

Note: Emission peaks in Table above with in { } shows high emission intensity and with ( ) shows less intensity

5.6 SHMP capped ZnS nanoparticles

This series comprises of five samples named as (0.1, 0.5, 1.0, 1.5 and 2.0%) SHMP capped ZnS nanoparticles.

5.6.1 XRD Studies

Figure 5.26 shows X-ray diffraction pattern of SHMP (0.1-2.0%) capped ZnS NPs. X- ray pattern is similar to those reported in previous sections. The average crystallite size estimated from Scherer formula for (111), (220) and (311) planes is 3.36nm, 3.20nm, 3.05nm, 2.54nm and 2.45nm, for SHMP (0.1, 0.5, 1.0, 1.5, 2.0 at. %) capped ZnS NC's respectively. The peaks observed in the XRD pattern match well with those of the β-ZnS (cubic) reported in the ICDD Powder Diffraction files (File. No.03-0570).

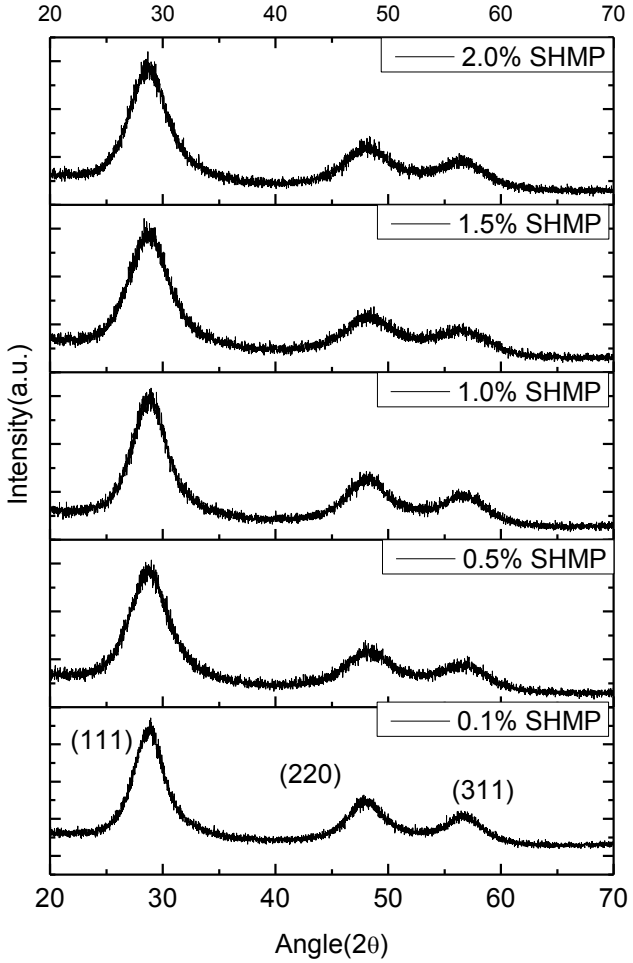

Figure 5.26 X-ray diffraction pattern of SHMP (0.1-2.0%) capped ZnS NPs.

5.6.2 TEM Studies

Figure 5.27 (a, b) shows TEM micrograph of 1.5 % SHMP capped ZnS NPs at lower and slightly higher magnifications. It shows abundance of spherical NPs having average size 12-15nm.

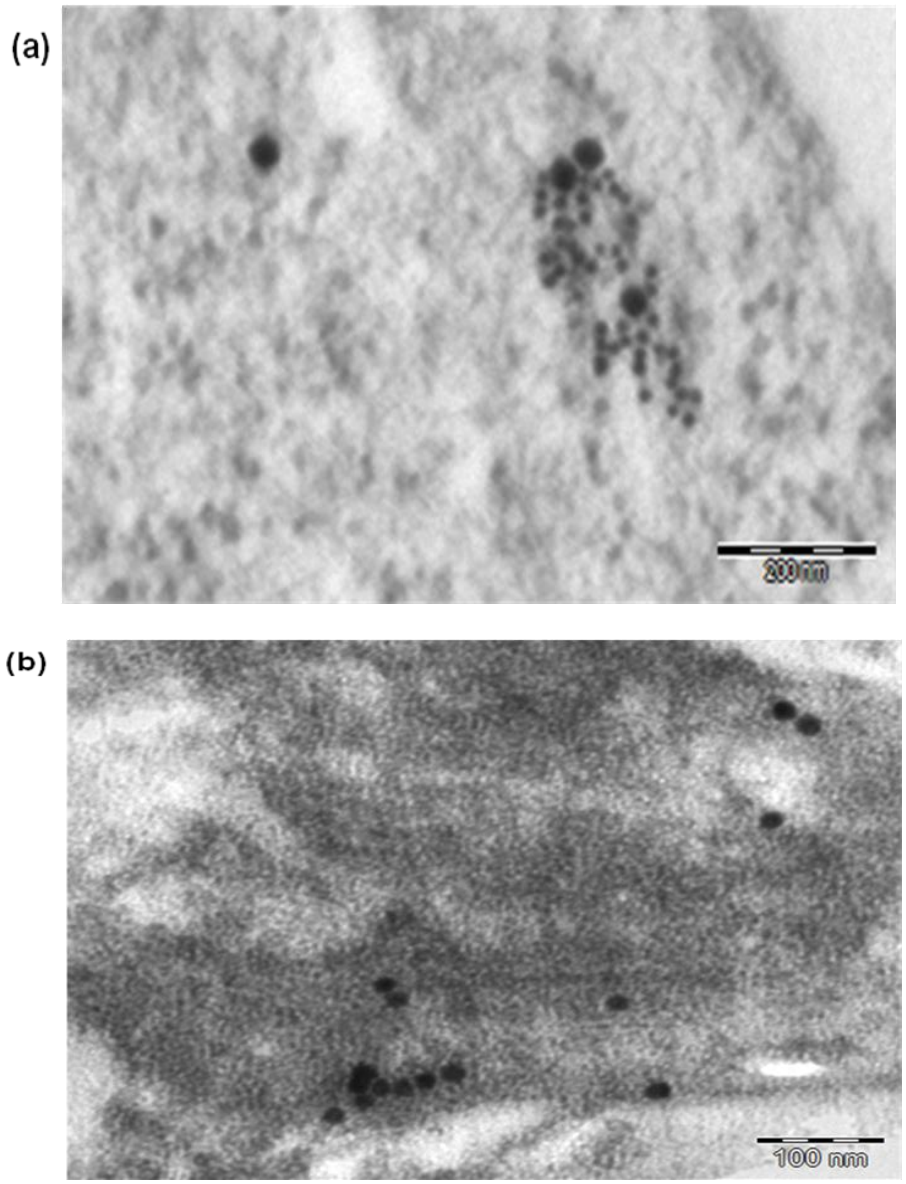

Figure 5.27 (a) TEM micrograph of 1.5 % SHMP capped ZnS NPs, (b) TEM micrograph of 1.5% SHMP capped ZnS NPs at slightly higher magnification.

5.6.3 FTIR Studies

Figure 5.28 shows FTIR spectra of SHMP capped ZnS NPs along with only SHMP in the same range. The FTIR spectra showed peak at 1593 cm^{-1}, representing the nitrogen–oxygen interaction. The distinct peaks at 1255 and 1045 cm^{-1} are due to phosphorus–oxygen interaction, establishing the presence of covalently bonded phosphates on ZnS nanoparticles. From FTIR spectroscopy, it can be inferred that the stabilizing agent passivates the surface of the particle. The presence of these covalently

bonded phosphate groups even after rigorous washing of the colloidal nanoparticles (to remove all unwanted impurities) suggests that SHMP inhibits the growth of particle by steric stabilization. The peak at 537 cm^{-1} represents sulfur–oxygen interaction. Passivation with polymers reduces the unsaturated bond density [25], thereby reducing the surface trap sites for non-radiative recombination processes. Thus, capping agents play an important role in the luminosity of the nanophosphors. The larger number of IR bending modes (<1000cm^{-1}) observed for SHMP capped ZnS nanoparticles indicate the formation of smaller particles. The broad absorption peak in the range of 3090 and 3141cm^{-1} corresponding to –OH group indicates the existence of water absorbed in the surface of nanocrystals. The presence of this band can be clearly attributed to the adsorption of same atmospheric water during FTIR measurements. The bands at 2342cm^{-1} are due to the C-O stretching modes arising from the absorption of atmospheric CO_2 on the surface of the nanoparticles [16].

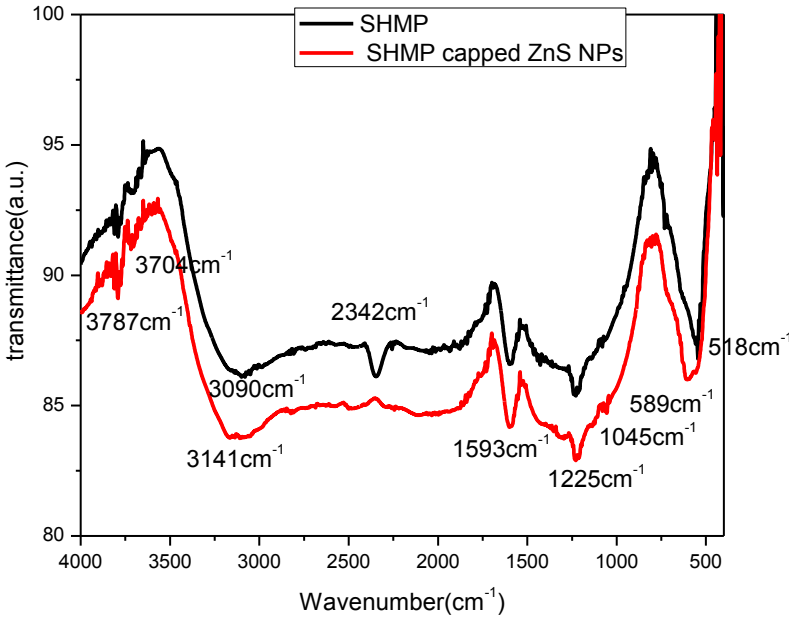

Figure 5.28 FTIR spectra of SHMP capped ZnS NPs along with only SHMP in the same range.

5.6.4 UV-Visible absorption studies

After confirming single phase for all samples and capping of SHMP on ZnS NC's, optical studies were performed to observe absorption characteristics in synthesized nanomaterials. Figure 5.29 (a) shows the absorbance versus wavelength (λ) traces of the SHMP (0.1- 2.0%) capped ZnS NPs. All samples show blue shift of absorption peak in comparison to bulk ZnS (340nm) which is due to quantum size effect. The band gap for capped ZnS NPs were determined by extrapolating the straight line portion of the $(\alpha hv)^{1/n}$ versus hv graphs to the hv axis as shown in Figure 5.29(b). From the plots we find band gap energies to be 4.72, 4.75, 4.93, 5.16, and 5.38eV for 0.1-2.0% capped SHMP capped NPs respectively.

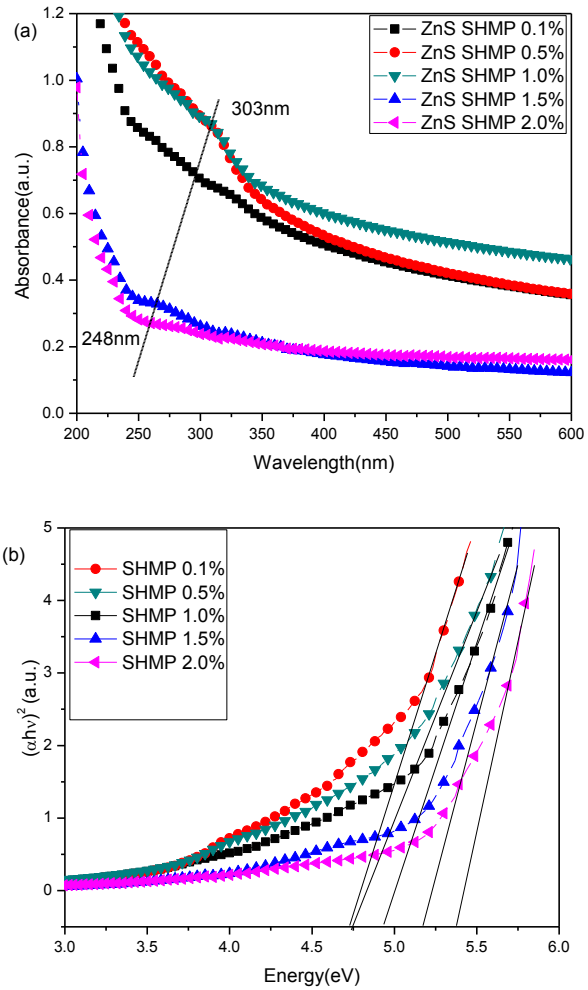

Figure 5.29 (a) Absorbance spectra, (b) estimated band gap $(\alpha h\nu)^2$ Vs hν plot for SHMP (0.1-2.0%) capped ZnS NPs.

5.6.5 Photoluminescence Studies

Figure 5.30 shows excitation spectra of SHMP (0.1-2.0%) capped ZnS NPs at fixed emission wavelength of 448nm. It shows strong excitonic peak centered at 325nm for all SHMP (0.1-2.0%) concentrations. Along with this a weak shoulder around 280nm is also observed whose intensity varies invariably with change in SHMP concentrations. The reason for having existence of more than one excitation states in SHMP capped ZnS NPs can be explained on the basis of poly dispersity of synthesized NPs as shown in TEM micrograph. This type of mechanism is discussed earlier in chapter 5.1 but there reason for shift of excitation energy is different from polydispersity. Here as shown in TEM micrographs of SHMP capped ZnS NPs all particles are in nano regime have spherical shape. But these NPs are not monodispersed which can be seen in TEM micrographs. So particles of different sizes existing in same sample have different band gap and different excitation wavelength. Calculated band gap from excitation spectra are given in Table 5.8 for all samples.

Figure 5.31 shows PL spectra of SHMP (0.1-2.0%) capped ZnS NPs at 325nm excitation wavelength. A broad peak centered around 448nm is observed for all samples. However, emission peak is observed at 367nm along with weak shoulder at 448nm for 0.1% SHMP capped ZnS NPs. As discussed in previous segments 367nm emission peak corresponds to band edge emission or emission from sulphur interstitials. Emission peak at 448nm emission is due to defect states created by zinc vacancies having energy between band gap of nanocrystalline ZnS. With increase in capping concentration from 0.1 to 0.5% and further to 1.0% there is no emission observed around 367nm. At the same time with increase in capping concentration considerable increase in 448nm emission peak is observed. Emission intensity is maximum for 2.0% capped ZnS NPs. This corresponds to better passivation at this concentration of SHMP. From Table 5.8, it is

clear that with increase in capping polymer from 0.1-2.0% there is increase in band gap and decrease in crystallite size. Hence this increase in emission intensity with decrease of particle size and increase of band gap is due to strong quantum confinement effect causing reduction of non-radiative decay. But this emission around 360-420nm results from sulphur interstitials and sulphur vacancies causing zinc dangling bonds. As earlier discussed in chapter 5.1 chen et al. [18] explained blue shifting of emission spectra due to decreased particle size and increase in band gap. But in our case red shift in emission color from 367nm to 448nm with considerable increase in emission intensity is observed. This is explained by effective passivation of zinc dangling bonds and sulphur interstitials with surface adsorbed polymer SHMP. As 325nm excitation represents 3.81eV excitation energy which is less than band gap of SHMP capped NPs which is shown by UV-Visible absorption spectroscopy to be around 4.72-5.38eV. Also excitation studies shows excitonic peak around 280nm with 325nm, so using 280nm as excitation wavelength emission spectra have been recorded and shown in Figure 5.32. Interestingly It shows unsymmetrical emission peak around 412nm for (0.1, 0.5, 1.0%) SHMP capped ZnS NPs. This emission peak as discussed in chapter 5.1 and above is due to sulphur vacancies which is responsible for creating zinc dangling bonds. These dangling bonds forms shallow donor states below conduction band of ZnS. With increase in capping concentration from 1.0-1.5% emission peak around 412nm is not observed but at the same time intense peak around 370nm is observed. This observed blue shift in emission spectrum with increase in capping concentration is explained by decrease in particle size as explained by Chen et al.[18] model discussed earlier. Further increase in SHMP concentration to 2.0% results shift of emission peak from 370 to 350nm which suggests further blue shift. This emission peak corresponds to band edge emission. The removal of 412nm peak at 1.5 and 2.0% SHMP is due to successful passivation of zinc dangling

bonds causing removal of their characteristic peak. It is described in FTIR studies that phosphates are present on surface of ZnS NPs. These negative group phosphates make covalent bonds with zinc dangling atoms on the surface on ZnS NPs. This bonding removes trap states due to dangling bonds and their charactersitic emission around 412nm is not observed at higher concentrations of SHMP. Secongly emission intensity is increased which is also due to decrease in nano radiative decays with passivation of dangling bonds.

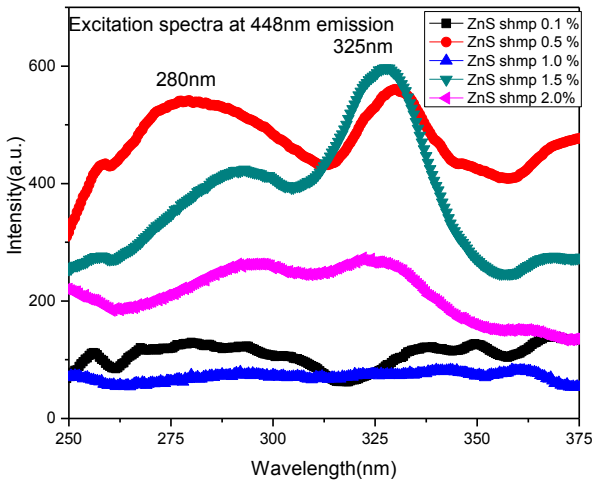

Figure 5.30 Excitation spectra of SHMP (0.1-2.0%) ZnS NPs for 448nm emission.

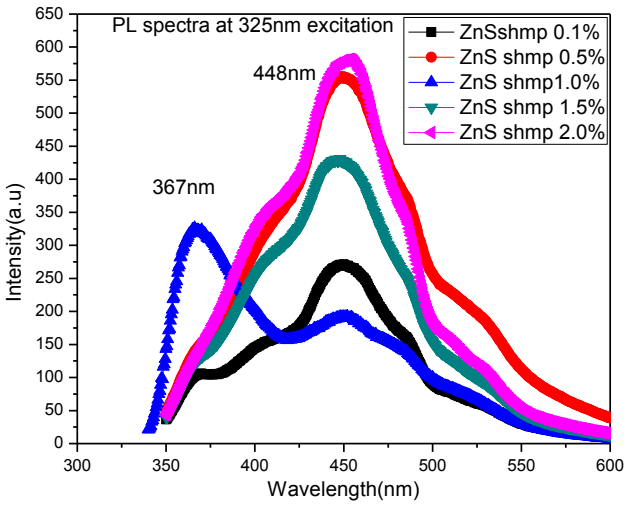

Figure 5.31 PL spectra of SHMP (0.1-2.0%) capped ZnS NPs at 325nm excitation wavelength

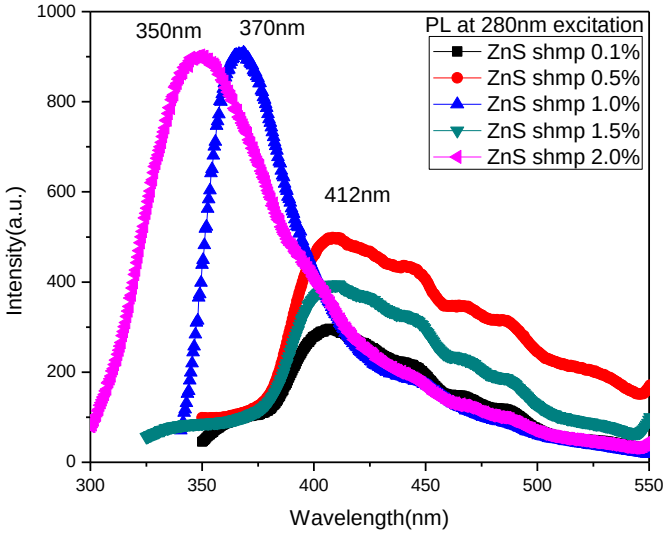

Figure 5.32 PL emission spectra of SHMP (0.1-2.0%) capped NPs at 280nm excitation wavelength.

Table-5.8 Showing particle size variation of all samples with absorption and photoluminescence results.

Sample	Particle Size(nm)		Absorption wavelength (nm)	Excitation wavelength (nm)	Excitation wavelength (nm)	Band gap(eV)		Emission wavelength (nm)	
	XRD	TEM	UV-Vis. Spectra	448nm emission	448nm emission	UV-Vis.(E=hν)	PLE	280nm PLE	325nm PLE
SHMP(0.1%) ZnS NPs	3.36	-	303	280, 336	280, 336	4.72	3.69, 4.41	412	367, 448
SHMP(0.5%) ZnS NPs	3.20	-	304	281, 330	281, 330	4.75	3.75, 4.42	412	448
SHMP(1.0%) ZnS NPs	3.05	-	283	288, 341	288, 341	4.93	3.63, 4.30	412	448
SHMP(1.5%) ZnS NPs	2.54	12-18nm	254	290, 325	290, 325	5.16	3.81, 4.27	370	448
SHMP(2.0%) ZnS NPs	2.45	-	248	292, 324	292, 324	5.38	3.82, 4.24	350	450

5.6.6 References

[1] A.P. Alivisatos, T.D. Harris, P.J. Carroll, M.L. Stiegerwald, L.E. Brus, *J Chem Phys*. **90**, 3463 (1989).

[2] S. Kalele, S.W. Gosavi, J. Urban, S.K Kulkarni, *Curr Sci*. **91(8),** 1038 (2006).

[3] R.N. Bhargava, *J Lumin*. **70**, 85 (1996).

[4] T. Kubo, T. Isobe, M. Senna, *J. Lumin*, **99**, 39 (2002).

[5] B. Gilbert, F. Huang, Z. Lin, C. Goodell, H. Zhang, J.F. Banfield, *Nano Lett*. **6(4)**, 605 (2006).

[6] H.C. Warad, S.C. Ghosh, B. Hemtanon, C. Thanachayanont, J. Dutta, *Sci Technol Adv Mater*. **6**, 296 (2005).

[7] K. Manzoor, S.R. Vadera, N. Kumar, T.R.N. Kutty, *Mater Chem Phys*. **82**, 718 (2003).

[8] K. Manzoor, S.R. Vadera, N. Kumar, T.R.N. Kutty, *Solid State Commun*. **129**, 469 (2004).

[9] K. Dongjin, K-D. Min, J. Lee, J.H. Park, J.H. Chun, *Mater Sci Eng B*. **131**,13 (2006).

[10] D. Denzler, M. Olschewski, K. Sattlera, *J Appl Phys*. **84(5),** 2841 (1998).

[11] G. Ghosh, M.K. Naskar, A. Patra, M. Chatterjee, *J Opt Mater*. **28,**1047 (2006).

[12] N. Kumbhojkar, V.V. Nikesh, A. Kshirsagar, *J Appl Phys*, **88(11)**, 6260 (2000).

[13] N. Murase, K. Hirata, T. Yazawa, T. Kushida, *J Phys Chem B*. **103,** 754 (1999).

[14] C.B. Murray, C.R. Kagan, *Annu Rev Mater Sci*. **30**, 545 (2000).

[15] J.F. Suyver, S.F. Wuister, J.J. Kelly, A. Meijerink, *Nano Lett*. **1**, 429 (2001).

[16] K. Kanemoto, H. Hosokawa, Y. Wada, K. Murakoshi, S. Yanagida, T. Sakata, H. Mori, M. Isikawa, H. Kobayashi, *J. Chem. Soc. Faraday Trans*. **92**, 2401 (1996).

[17] S.K. Mandal, S. Chaudhuri, A.K. Pal, *Thin Solid Films*. **30,** 209 (1992).

[18] W. Chen, Z. Wang, Z. Lin, L. Lin, *J. Appl. Phys*. **82**, 3111 (1997).

[19] C.B. Murray, D.J. Noris, M.G. Bawendi, *J. Am. Chem. Soc*. **115**, 8706 (1993).

[20] R.N. Bhargava, D. Ghallaghr, X. Hong, A. Nurmikko, *Phys. Rev. Lett*. **72,** 416 (1994).

[21] R. Menner, B. Dimmler, R.H. Mauch, H.W. Schock, *J. Cryst. Growth*. **86**, 906 (1998).

[22] Y. Zhu, C.L. Yuan, P.P. Ong, *J. Appl. Phys*. **92**, 6828 (2002).

[23] K.W. Cheah, L. Xu, X. Huang, *Nanotechnology*. **13**, 238 (2002).

[24] B.D. Cullity, Elements of X-Ray Diffraction, second ed., Addison-Wesley publishing, Massachusetts, **2003.**

[25] S. Yanagida, Y. Ishimaru, Y. Miyake, T. Shiragami, C. Pac, K. Hashimoto, T. Sakata, *J. Phys Chem*. **93**, 2576 (1989).

[26] Baibaswata Bhattacharjee, Chung-Hsin Lu, *Thin Solid Films*. **514**, 132 (2006).

[27] N. Chestnoy, T.D. Harris, R. Hull, L.E. Brus, *J. Phys. Chem*. **90**, 3393 (1986).

[28] J. Hu, Y. Bando, J. Zhan, D. Golberg, *Adv. Funct. Mater*. **15**, 757 (2005).

[29] L.E. Brus, *J. Chem. Phys*. **80**, 4403 (1984).

[30] J.I. Pankove, Optical Processes in Semiconductors (Prentice-Hall, Englewood Cliffs, NJ) (1971).

[31] H. C. Warad, C Thanachayanont, G Tumcharern and J. Dutta, Proceedings of the 2nd IEEE International Conference on Nano/Micro Engineered and Molecular Systems January 16 - 19 Bangkok Thailand (2007).

[32] N. Kubota, *J. Appl. Polym. Sci*. **64**, 819 (1997).

[33] F. Wang, Y. Zhang, X. Fan and M. Wang, *Nanotechnology* 17, 1527 (2006).

[34] H. Jiang, J Liang, J. T. Grant, W. Su, T. J. Bunning, T. M. Cooper, W. W. Adams. *Macromol. Chem.Phys*. **198**, 1561 (1997).

[35] N.V. Hullavarada, S.S. Hullavarad, *J Vac Sci Technol A*. 26, 1050 (2008).

CHAPTER 6

TUNABLE EMISSION OF CAPPED AND DOPED ZnS NANOSTRUCTURES

Overview

In this part of chapter we have selected two series of capping agents from the five which have been studied earlier and described in chapter 5. The selection of these two series is done on the basis of achieving tunable emission color property. In these two series with change in excitation energy shift of emission energy and hence emission color have been observed. This excitation modulated emission color is further studied with capped and doped combinations to get two or three colors in single sample when excited in different regions. Earlier it is reported that tunable emission color is achieved by synthesizing different sizes of nanoparticles or by doping suitable transition metal in host semiconductor QDs. In all cases multiple samples are needed. In order to address this problem and give viable solution PVP, chitosan capped and Mn doped ZnS NPs have been synthesized and tunable emission color in visible region is achieved in a single sample which according to earlier reports needed many samples. Apart from this biocompatibility of synthesized samples has been confirmed with staphylococcus (SAU) bacteria along with multicolor tunable emission in blue white orange color in a single sample. Fluorescent microscopy and transmission electron microscopy has been used to further prove biotagging. Preliminary results showing glucose sensing with chitosan capped ZnS Mn NPs has been shown. In the last part some initial results related to DNA capping on ZnS NPs surface and their enzyme sensing applications has been presented.

6.1 PVP (0.1, 1.5%) capped Mn (0.1%) doped ZnS nanoparticles

6.1.1 Brief Introduction related to tunable white light emission

The optical, electronic and chemical properties, as well as synthesis methods of nanostructured materials are of great interest in both basic and applied research [1-5]. Blends of organic polymers and colloidal semiconductor quantum dots (QDs) have an application as light emitting diodes (LEDs), ultrasensitive radiation detection and solar cells [6-14]. CdSe and CdTe are well known II-VI semiconductors, which show tunable emission with change in particle size [6-8]. However, the intrinsic toxicity of Cd and Se ions creates hindrances for its potential use as tunable biosensors. Doped ZnS nanoparticles (NPs) have been extensively investigated because of their tunable emission property with variation in doping concentration or change in dopant ions [3-4].

To obtain white light, all the three primary colors (red, green, and blue) have to be produced simultaneously. White light solid state lighting (SSL) LEDs are expected to reduce worldwide electricity consumption by ~ 50% and total consumption of electricity by more than 10% [15]. Subsequently, different methods have been reported to generate white light. White organic light emitting diodes (WOLEDs) are one of the most important species for white light generation [16–18]. Wang *et al.* [19, 20] first reported the single polymer with simultaneous blue, green, and red emission for white electroluminescence. Another important white light source is SSL based on the inorganic phosphor. These methods possess multiple advantages such as simple synthesis, high yield, good stability, and does not disturb the chromaticity. Different structures of white light emitting SS-LEDs that have been reported so far include multi chip white light LEDs, monolithic white light LEDs and color-conversion white light LEDs based on phosphor coatings [21]. Many strategies have been reported to realize white emission in organic LEDs.

These include blending emissive polymers with different emission colors [22], doping with phosphorescent complexes or fluorescent dyes into a small molecule or polymer host [23, 24], multiple component emissive layers containing an appropriate ratio of red, green, and blue (RGB) phosphorescent[25] or fluorescent dopants [26].

Semiconductor nanocrystals (NCs) have many potential applications in the fields of electro-optical devices [27–29], photovoltaic cells [30, 31], sensors [32, 33], and biological labeling [34] because of their interesting size-dependent properties and unique optical and electronic features. Combining semiconductor QDs with organic materials creates functional materials with optical and electronic properties not observed in any of the source materials [12]. The mechanism of charge separation and coupling between Frenkel and Wannier exciton in organic- inorganic hybrid systems have been discussed for polymer capped QDs [11-14] and efficient energy transfer from conjugated polymers to colloidal QDs [4, 12] is also reported. Their emission properties can be easily tuned by changing the particle size and surface state structure or by doping with suitable ions. White light emission from semiconductor NCs has also been reported. In this direction, Nag *et al* [35] reported white light from the Mn doped CdS nanocrystals of efficiency around 2%, whereas Demir *et al.* [36] observed white light emission from CdS/ZnS core/shell quantum dots. Sun *et al.* [37] prepared nanocomposites emitting pure white light by incorporating different sizes of CdTe NCs into a carbazole-containing positively charged polymer. The Eu doped ZnO nanoparticles are also found suitable for white light generation [18, 19]. It is also reported that by doping transition metal ions or rare-earth elements into ZnS NCs, the luminescence region can extend to the full UV–visible band. Bhargava *et al.* [9, 38] first reported the preparation and photoluminescence (PL) properties of ZnS: Mn NCs. Thereafter, Mn^{2+} doped ZnS NCs became a favorable

phosphor, contributing to the characteristic luminescence properties in orange region for potential applications in displays, sensors, and lasers [39–46]. In Mn^{2+} doped systems usually orange emission around 590 nm resulting from $^4T_1$–$^6A_1$ transition of the Mn^{2+} impurity excited by energy transfer from the ZnS host is observed. If we can supply a blue and/or green emission in this system, then white light emission may be carried out. Based on this Mn^{2+} doped CdS [47] and ZnS [48, 49] NCs with white light emission have been successfully prepared by the combination of the orange emission of the $^4T_1$–$^6A_1$ transition of Mn^{2+} impurity and the blue emission and/or green emission of the surface defect state of NCs. However, in all reports mentioned above many samples of different particle sizes (CdSe, CdTe etc.) or with different dopants (ZnS: Mn, ZnS: Cu, CdS: Mn, ZnO: Eu etc.) or different doping concentrations (ZnS: Mn (0.1-5%) are required to achieve tunable color [3, 4, 9, 10, 11]. Despite the promise of these systems, so far, no study has been reported on tunable emission in visible region including white light in a single sample which at nanoscale can be functionalized for biosensing applications.

Here, we report white light emission from the PVP capped Mn^{2+} doped ZnS nanoparticles synthesized by an easy and facile colloidal route. We have investigated the role of optimum capping concentration for enhanced and tunable luminescence properties as structural properties do not vary a lot with change in capping concentration. Efficient energy transfer from capping polymer PVP to sulphur vacancies (trap states) of the host ZnS and from ZnS to dopant Mn^{2+} is reported for single sample at variable excitation energies. Furthermore, by varying excitation wavelength in single hybrid organic-inorganic sample tunable emission is observed in nearly all visible region which according to earlier reports needs many samples [3-10]. To our knowledge, no report has

been found on tuning emission color from blue to orange (including white) in a single sample. The origin of white luminescence was studied by steady-state spectroscopy and further confirmed by calculating its CIE color coordinates, which show tunable emission, including white color in single sample. The study gives an idea of how the emission from trap states of the host can be combined with emission from the dopant Mn^{2+} ions that extend towards longer wavelength to impart bright and efficient white light (along with blue and orange in the same sample), potentially useful for sensing applications.

6.1.2 Experimental

6.1.2.1 Materials

In the present study, raw materials used for preparing the samples were zinc acetate ($Zn(CH_3COO)_2.2H_2O$) (99.99%, Sigma Aldrich), sodium sulphide nonahydrate (99.99%, Sigma Aldrich), Poly Vinyl Pyrrolidone (PVP, 99.99%, Sigma Aldrich), Manganese acetate ($Mn(CH_3COO)_2.2H_2O$, 99.99%, Sigma Aldrich), double distilled water. All these materials were used without any further purification.

6.1.2.2 Synthesis of PVP capped Mn doped ZnS nanocrystals

PVP (0.1-2.0%) capped and Mn doped ZnS NPs were synthesized by chemical precipitation method as mentioned in experimental section and chapter 5.1. In the first step 40mL homogenous solutions of 0.5M zinc acetate and 0.5M sodium sulphide were prepared in distilled water separately by stirring them for half an hour. Also (0.1, 1.5 at. wt. %) solutions of PVP used in present investigation were prepared in 40mL distilled water separately. For the synthesis of PVP (0.1, 1.5%) capped ZnS: Mn NPs, 0.1% manganese acetate was added to zinc acetate solution prior to addition of PVP solutions. The further procedure followed for the synthesis remains same as discussed before in

chapter 3, 5.1. The solution was stirred for 8 h at room temperature. The capping agent PVP was used for avoiding the particle agglomeration and passivating surface defects. The solution containing particles (PVP capped doped NPs) were then centrifuged at 4000 rpm for 5 minutes. The precipitated particles were filtered using Whatman 40 filter paper. To remove the last traces of adhered impurities, the particles were washed several times using double distilled water. The washed particles were dried in vacuum oven at 60ºC for 24 hours.

6.1.3 XRD Studies

Structural and morphological studies are performed with XRD, HRTEM and ED to verify NC's size and phase. Figure 6.1 shows X-ray diffraction pattern of Mn (0.1%) doped PVP (0.1, 1.5%) capped ZnS NPs. Intensities of the three most important peaks of ZnS namely (111), (220) and (311) reflections corresponding to 2θ values 28.51º, 48.0º and 56.56º is observed in the XRD pattern which match well with those of the β-ZnS (cubic) reported in the ICDD powder diffraction files (File. No.05-0566). Broadening of the XRD peaks indicates the formation of ZnS NC's. No secondary phase(s) are present in the ZnS: Mn NP's. The nanocrystals size was estimated from Scherer formula [50]. The average crystallite size estimated from three planes are 3.90, 3.44nm for PVP (0.1, 1.5%) capped ZnS: Mn NC's respectively.

6.1.4 TEM Studies

Figure 6.2 (a, b) shows the HRTEM image and ED pattern of PVP (1.5%) capped ZnS NC's. It shows particles of uniform size about 4.0-5.0nm. Figure 6.2 (b) shows SAED pattern of same sample which shows a set of rings instead of spots due to random orientation of crystallites. The ED pattern shows three rings that correspond to (111), (220) and (311) planes of the cubic phase of ZnS and are well agreed with the results obtained from XRD.

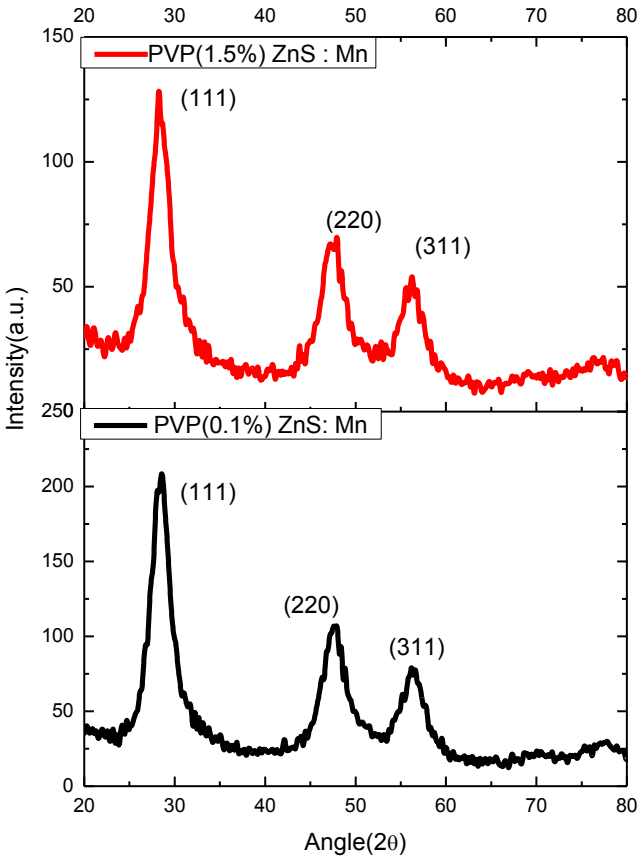

Figure 6.1 XRD pattern of PVP (0.1, 1.5%) capped ZnS: Mn NPs

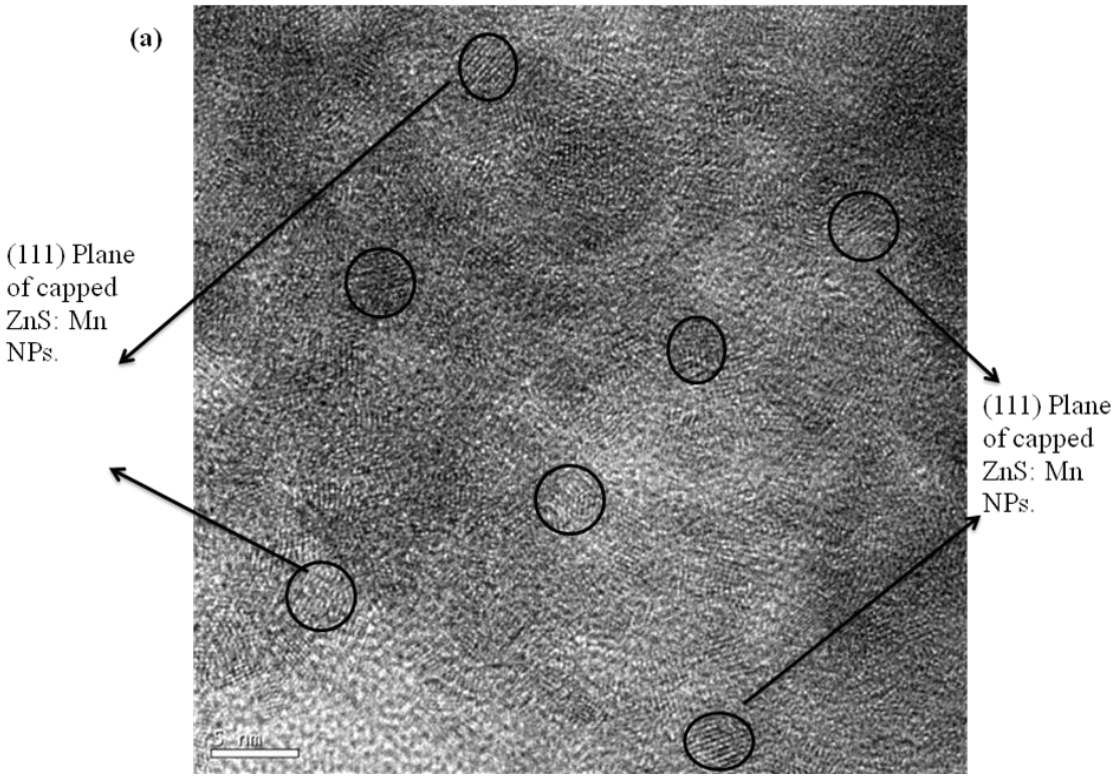

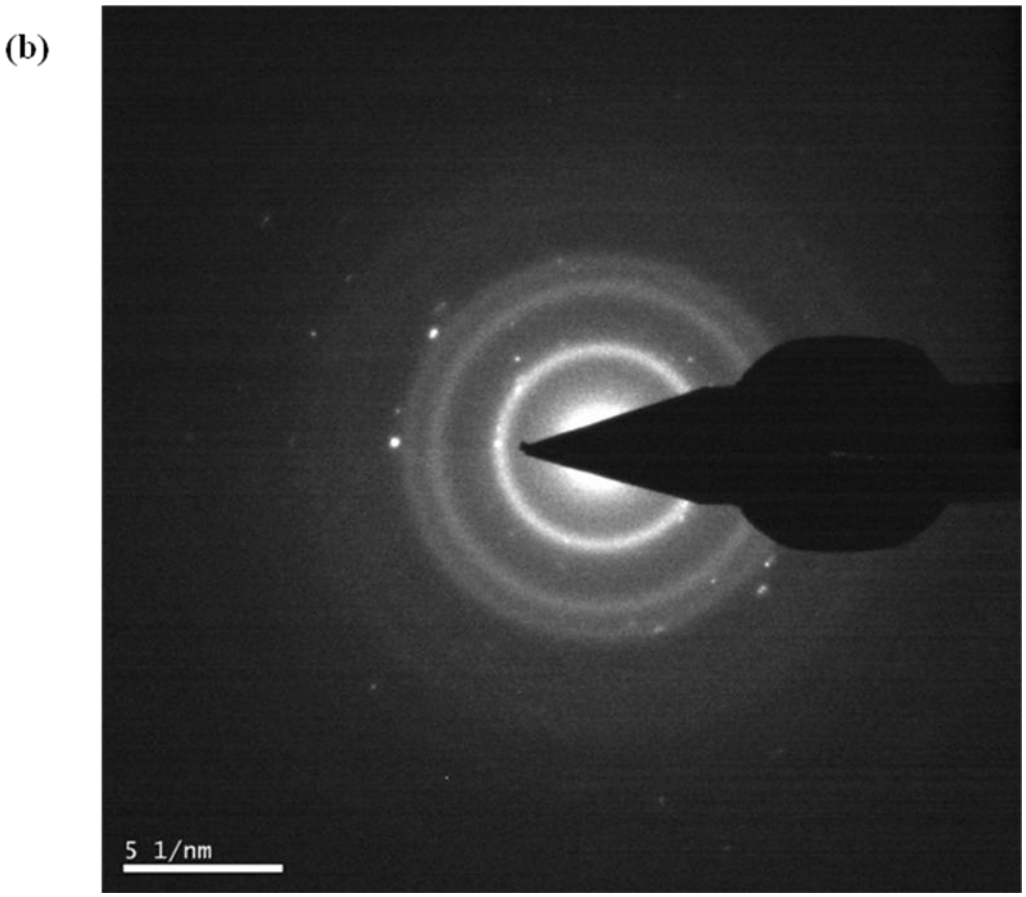

Figure 6.2 (a) HRTEM micrograph (scale bar- 5nm), (b) SAED of PVP(1.5%) capped ZnS:Mn NPs

6.1.5 UV-Visible Studies

After confirming single phase for ZnS nanoparticles, UV-Visible studies were performed to observe absorption spectra of synthesized nanomaterials. Figure 6.3 (a) shows UV-Visible absorption spectra of PVP (0.1%) capped Mn (0.1%) doped ZnS NPs. It shows absorption shoulder at 317nm along with absorption edge at 340nm. The band gap for 0.1% PVP capped ZnS:Mn NPs were determined by extrapolating the straight line portion of the $(\alpha h\nu)^{1/n}$ versus $h\nu$ graphs to the $h\nu$ [51] axis as shown in inset of Figure 6.3 (a). From the plots we find three slopes which correspond to energies 3.54, 4.02, 5.09eV. Out of these absorption energies 4.02eV can represent band gap of ZnS NPs because 3.54eV is less and 5.09eV is very high than bulk ZnS (3.6eV). Existence of three slopes instead of single slope show some modification in absorption energy of ZnS energy levels

with PVP capping. Further, Figure 6.3(b) shows UV-Visible absorption spectra of PVP (1.5%) capped Mn (0.1%) doped ZnS NC's. It is observed that the dominant absorption in UV region is caused by fundamental band- to- band absorption near 317nm. For observing possible influence of PVP molecules adsorbed on the surface of ZnS: Mn NC's, band gap of NC's is obtained by extrapolating the straight line portion of the $(\alpha hv)^{1/n}$ versus hv graphs to the hv axis as shown in inset of Figure 6.3 (b). Interestingly it shows clear multiple slopes for absorption energies of 3.71eV, 4.11eV and 4.71eV respectively. As explained above 4.11eV absorption energy corresponds to band gap of ZnS and absorption in higher and lower energies (4.71, 3.71eV) than band gap corresponds to absorption in molecular energy states of PVP. Existence of PVP and hence its molecular energy levels along with host ZnS was discussed previously in FTIR and excitation studies (PLE) (chapter-5.1).

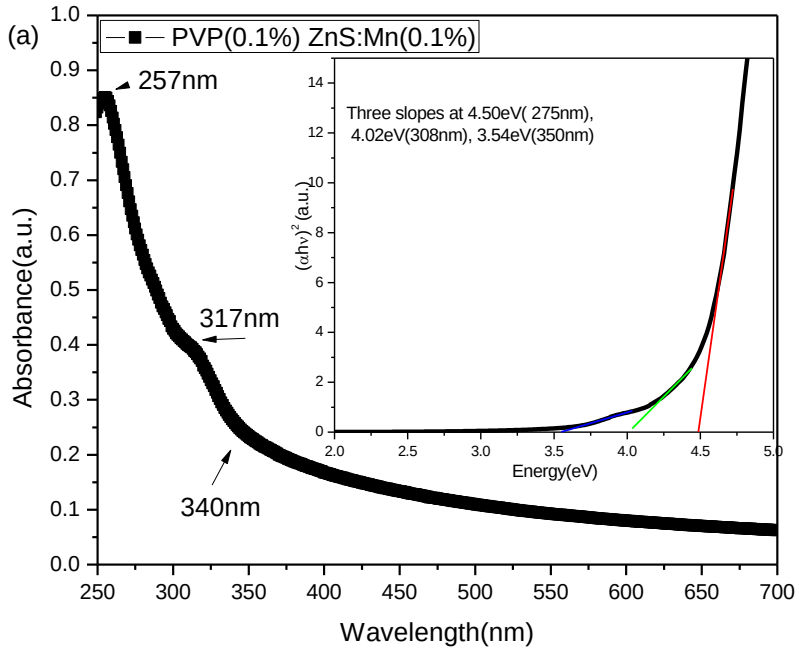

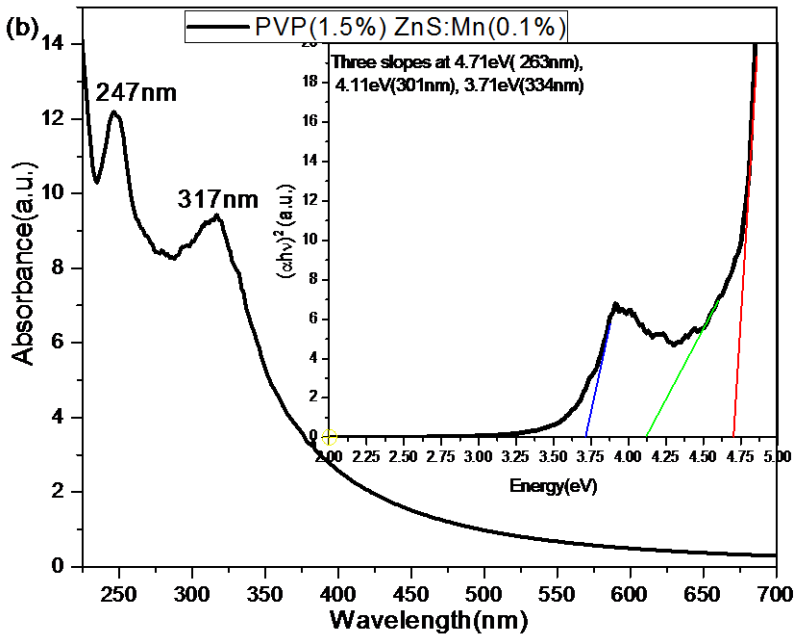

Figure 6.3 (a) UV- Visible absorption spectra of PVP (0.1%) capped, (c) PVP (1.5%) capped ZnS:Mn NPs (Inset of Figure 6.3(b, c) shows calculated band gap of respective samples).

6.1.6 Photoluminescence Studies

Figure 6.4 and Figure 6.5 shows steady state room temperature photoluminescence spectroscopy results of all synthesized samples. Figure 6.4 shows excitation spectra of PVP (1.5%) capped Mn doped NPs for different possible emission sites. The reason for showing PLE spectra for only 1.5% PVP capped ZnS Mn NC's is due to high PL intensity for this sample in comparison to other synthesized samples which is discussed earlier in chapter 5.1. Mn doped ZnS NPs gives orange emission at 590nm due to Mn d states and around 400-450nm due to trap states of host ZnS NPs [9, 48-49]. Based on this in excitation studies of synthesized doped and capped NC's emission wavelength used is 590nm, 423nm respectively. In excitation spectra of PVP capped NC's, broad excitonic peak around 350nm is observed for 590nm emission which

suggests dopant related emission in capped NC's which is arising from excitation in host ZnS (as 350nm excitation is near 340nm for bulk ZnS). Also for 423nm emission in same sample excitation spectra is broadened having multiple excitation peaks instead of single excitonic peak. Maximum intensity peak is observed at 235nm with small peaks at 275nm and 304nm respectively. After observing difference in excitation spectra for different emission sites in capped NC's we have also studied excitation spectra of only PVP for 423nm emission (Figure 6.4b). This spectra is also shown earlier in section 5.1. Interestingly it shows weak excitonic peaks at 258nm, 286nm and 321nm respectively. Along with excitation peak, gaussian distribution of all present peaks is shown. This clearly suggests only PVP has multiple energy levels having multiple absorptions at 235, 258, 286, 321 and 333nm respectively. This has been already discussed in chapter 5.1 for undoped PVP capped ZnS NC's. It shows introduction of new excitonic peaks (235, 275nm) in PVP (1.5%) capped ZnS:Mn NPs for 423nm emission which is due to PVP molecular energy states. The variation in PLE peak from 325 to 235nm and 275nm for variation in emission site from 590 to 423nm respectively is observed. Similar results were also reported by Manzoor et al. [4] where they have observed similar shift of excitation peak with change in PVP concentration for 590nm emission (dopant related). But here we have observed this change in excitation peak for different possible emission sites (423, 590nm) in single sample. Previously in chapter 5.1, we have observed same shift in PLE peak from 325 to 275 and 235nm. But there it was observed for change in emission wavelength from 461 to 423nm whereas for doped and capped samples it is observed for change in emission site from 590nm to 423nm. As reported earlier by Manzoor et al. [4] and discussed in previous chapter 5.1 that 235nm and 275nm excitations is due to chemisorbed PVP molecular energy levels and 325nm excitation is

due to band to band transitions of host ZnS (bulk ZnS excitation is 340nm) so, it can be proposed that 590nm emission is due to 350nm excitation which is band to band excitation in ZnS. Furthermore, 423nm emission can be due to 235nm and 275nm excitations of surface adsorbed PVP. As 235 and 275nm excitations are due to excitation in PVP molecular energy states so there could be transfer of energy from adsorbed PVP to trap states of host ZnS for 423nm emission. This interaction causes alteration of tautomeric form of surface adsorbed organic molecules due to change in effective charge on N and C=O. These excitation peaks at 235, 258 nm arise from enol-tautomer of pyrrolidone whereas 275 and 286, 321 nm are from the keto form of pyrrolidone moiety [4]. This new mode of transfer in PLE and whole energy transfer mechanism is explained in detail in PL studies.

Previously (chapter 5.1) emission spectra of PVP capped ZnS NPs shows maximum PL intensity which comes for 1.5% concentration of PVP. Emission peak is observed at 418nm and 453nm for PVP (0.1-1.5%) capped ZnS NPs. As 1.5% PVP capped NC's show maximum PL intensity so for further PL studies with capping and doping both this concentration of PVP is selected.

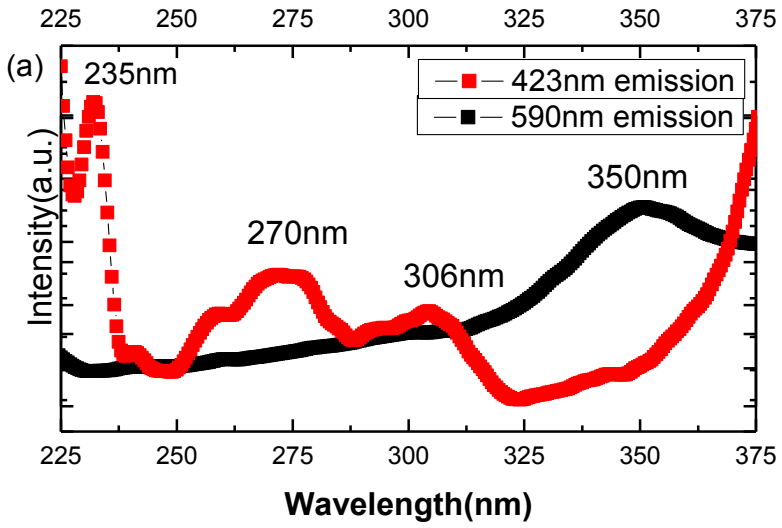

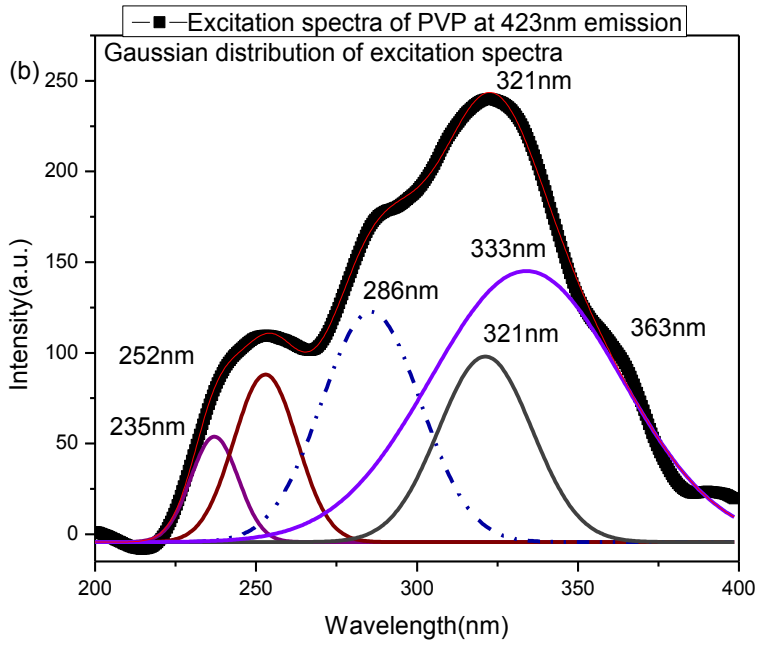

Figure 6.4 (a) Excitation spectra of PVP (1.5%) capped ZnS: Mn NPs for different emissions, (b) excitation spectra of only PVP.

Figure 6.5 shows PL spectra of PVP (1.5%) capped Mn (0.1%) doped ZnS NPs at three excitation wavelengths observed in excitation spectra (Figure 6.4). At 235 nm excitation we observe strong emission peak at 423nm along with weak peaks at 483nm and 590nm. As discussed previously (section-5.1), 423nm peak is due to sulphur vacancies acting as trap states in band gap of host ZnS and 590nm band is characteristic emission of Mn^{2+} ion, which can be attributed to $^4T_1$- $^6A_1$ transition [11, 18, 19]. Weak peak at 483nm arises due to zinc vacancies as discussed in chapter 5.1 earlier. From Figure 6.5, for 235nm excitation, $I_{423/590}$ ratio comes out to be 2.74. It shows, this sample emits blue color instead of orange (which is expected from Mn doped ZnS). Figure 6.6 (I) shows digital picture of this sample excited by UV lamp at high energy (low wavelength).This shows intense blue emission at this excitation. Corresponding Commission Internationale de I' Eclaerage (CIE) color coordinates for this same sample at 235nm excitation as shown in Figure 6.7 are (0.26, 0.23) suggesting blue emission. For

change in excitation wavelength from 235nm to 275nm emission intensity of all peaks centered at 423nm, 483nm and 590nm decreased. But if we see carefully $I_{423/590}$ ratio comes out to be nearly one (1.28), which suggests at this excitation energy emission contribution from 423nm (blue) and 590nm (orange) colors in same sample is equal. Along with this, considerable peak intensity is also observed from 483nm (green) peak having $I_{423/483} = 1.48$. For clear observation this PL spectra in Figure 6.5 has been shown separately as magnified view. Corresponding to 275nm excitation wavelength CIE color coordinates were calculated as (0.32, 0.28) and are shown in Figure 6.7. These color coordinates are found to be very close to ideal Commission Internationale de I' Eclaerage (CIE) chromaticity coordinates for pure white light (0.33, 0.33). It is important to mention here that peak position is not shifted here but their emission intensities are changed with shift in excitation energy from 235nm to 275nm respectively resulting in shift of emission color from blue to white in same NC sample. For 325nm excitation in same sample we observe further decrease in intensity for 423nm emission and increase in 590nm intensity as compared to emission spectra for 235 and 275nm excitations. $I_{458/590}$ for 325nm excitation wavelength comes out to be 0.701 showing orange color dominant emission. Figure 6.6 (II) shows orange color emitting NC's excited with UV lamp having lower excitation energy. The corresponding CIE color coordinates comes out to be (0.35, 0.29). So, CIE color coordinates (Figure 6.7) for corresponding emission spectra (Figure 6.5) are shifted from (0.26, 0.23) to (0.32, 0.28) and (0.35, 0.29) for single sample with shift in excitation wavelength from 235 to 275 and 325nm respectively. This clearly shows by changing excitation energy in this hybrid PVP (1.5%) capped Mn doped ZnS NC's sample we can manipulate the relative emission intensities of blue light and orange light. This results in a tunable color output in visible region (including warm white) for a single

sample. It is important to note that this kind of tunable emission is also reported for ZnS: Mn NPs having different concentrations of Mn [3]. Secondly this is achieved by doping different transition metal ions (Mn, Cu, Eu etc.) in host ZnS or varying particle size of same sample [4, 10]. But here we report same tunable emission but in single sample instead of many samples.

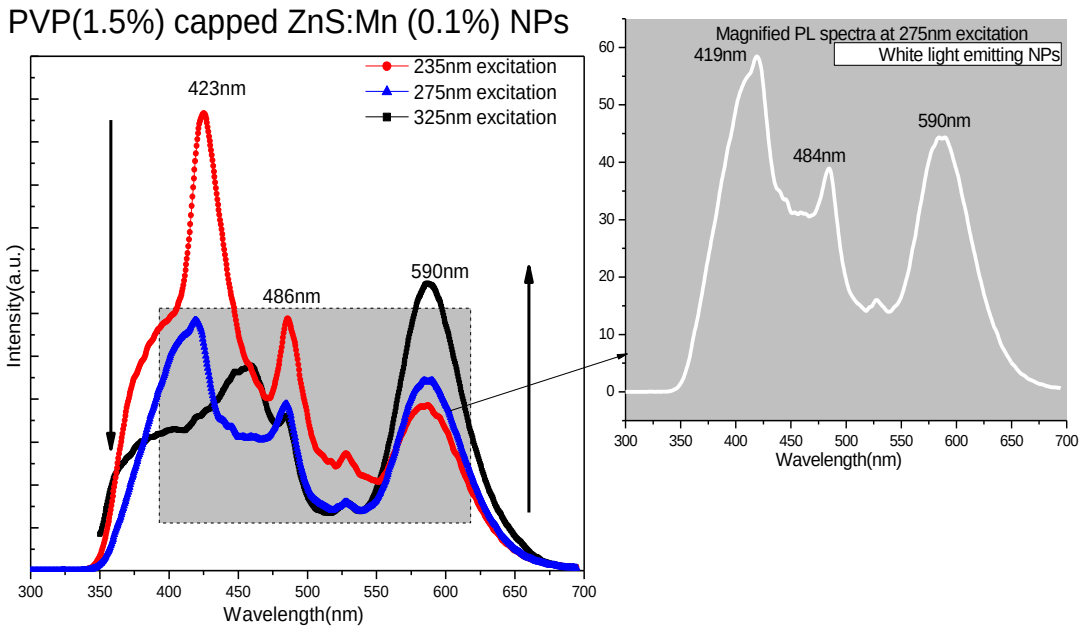

Figure 6.5 Emission spectra of PVP (1.5%) capped ZnS:Mn NPs at different excitations (inset showing magnified PL spectra having white light emission for same sample at 275nm excitation).

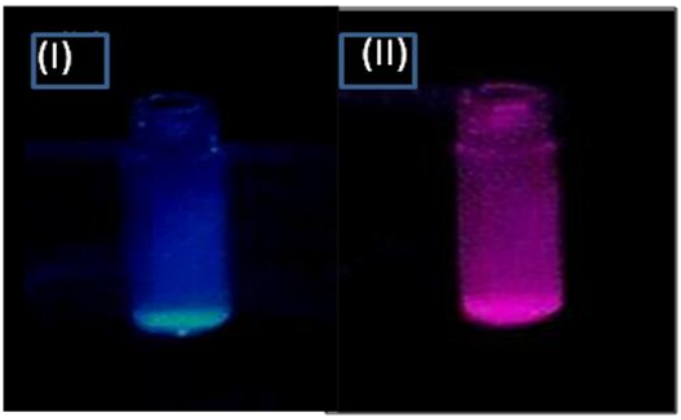

Figure 6.6 Digital images of PVP (1.5%) capped ZnS:Mn (0.1%) NP's under UV lamp (i) having low excitation energy, (ii) having high excitation energy.

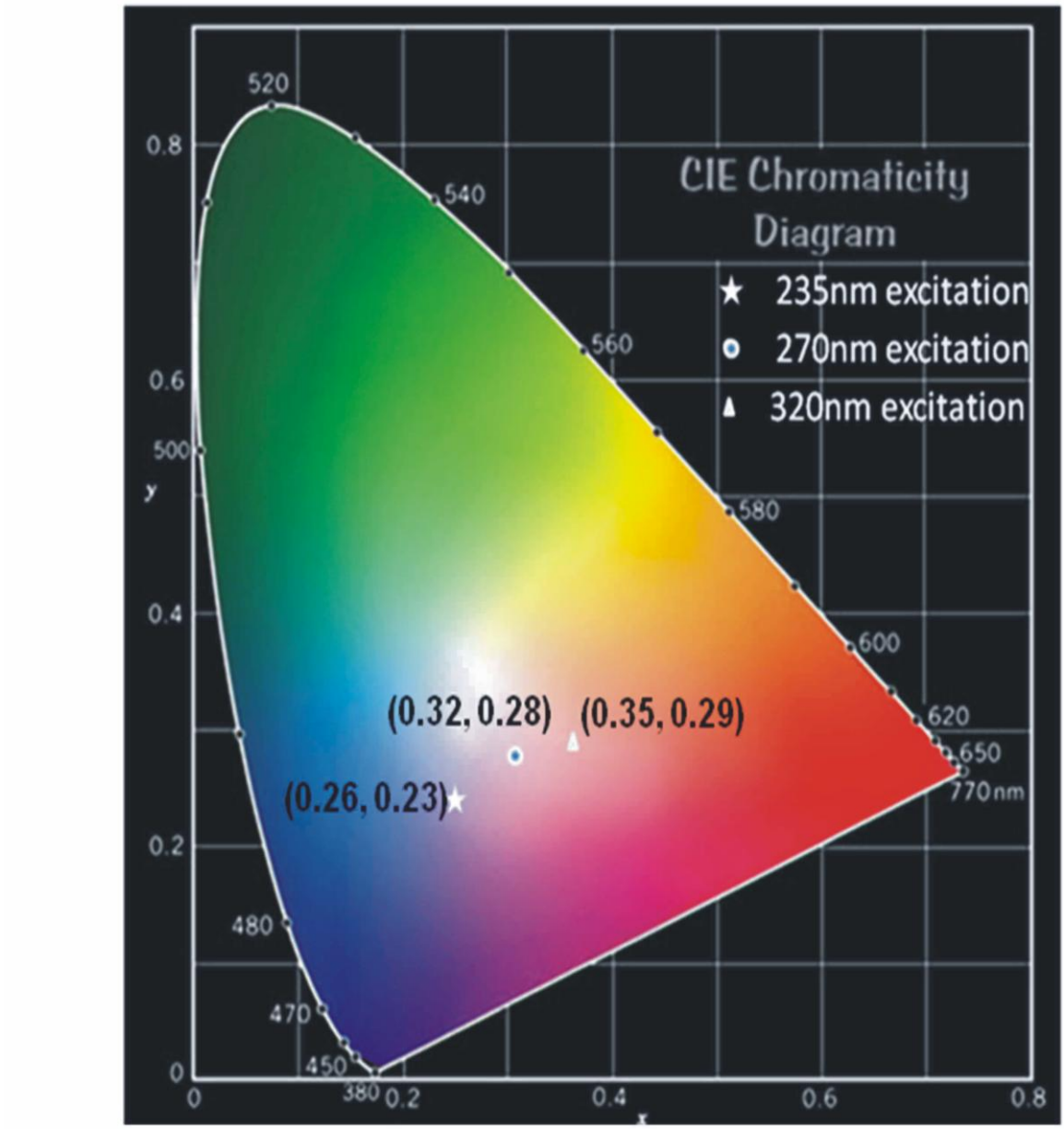

Figure 6.7 CIE color coordinates of PVP (1.5%) ZnS: Mn (0.1%) sample at three different excitation wavelengths.

This variation in present case can be explained by energy transfer mechanism (Figure 6.8 a, b, c) for three different excitations. Emission peaks having high intensity are represented by solid lines and with low intensity are represented by dotted lines in all cases. According to which PL spectra for 325nm excitation (Figure 6.5) are somewhat similar to earlier reported work which shows broad 420nm band along with highly intense

590nm peak [3, 9]. But emission results are interestingly different for same sample at 235nm excitation which shows enhancement in 423nm band and quenching of 590nm emission band. Also for 275nm excitation, blue (423nm) and orange (590nm) emissions having same intensity is observed simultaneously. Along with it relatively small peak at 486nm is also observed. The coexistence of three broad emissions results in the white light directly under suitable excitation wavelength (275nm). Thus combining emissions of vacancies and dopant ions may provide a novel strategy to obtain white light and tunable luminescence in single sample instead of many samples used previously. This shows that same sample at excitation in higher energy (235nm and 275nm instead of 325nm) can emit blue or white color instead of orange, which according to our knowledge is not reported so far. So, three different emission colors (in visible region) are observed independently for same sample at three different excitations.

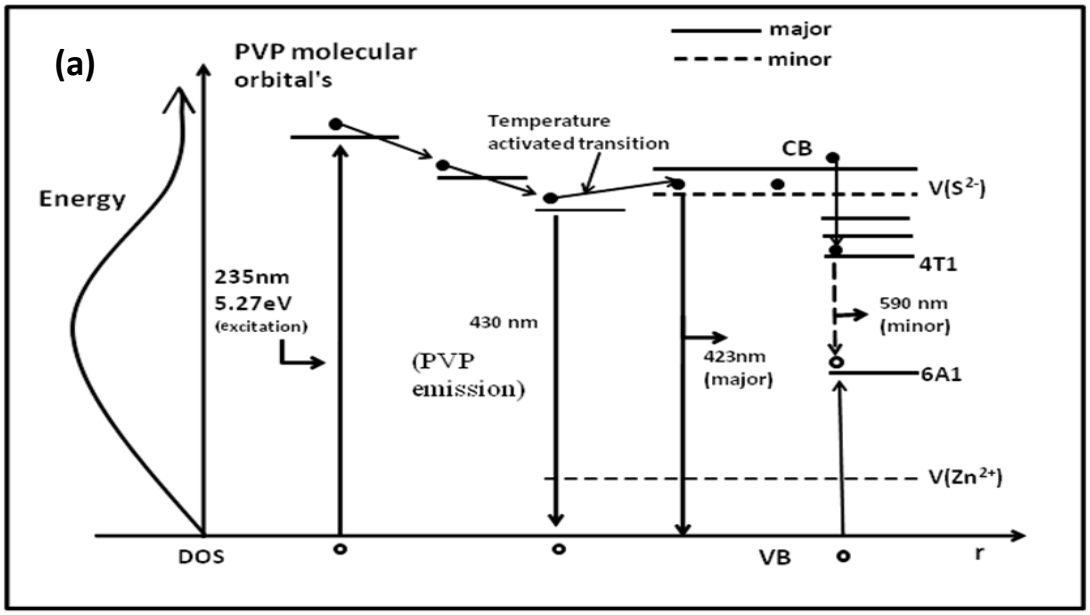

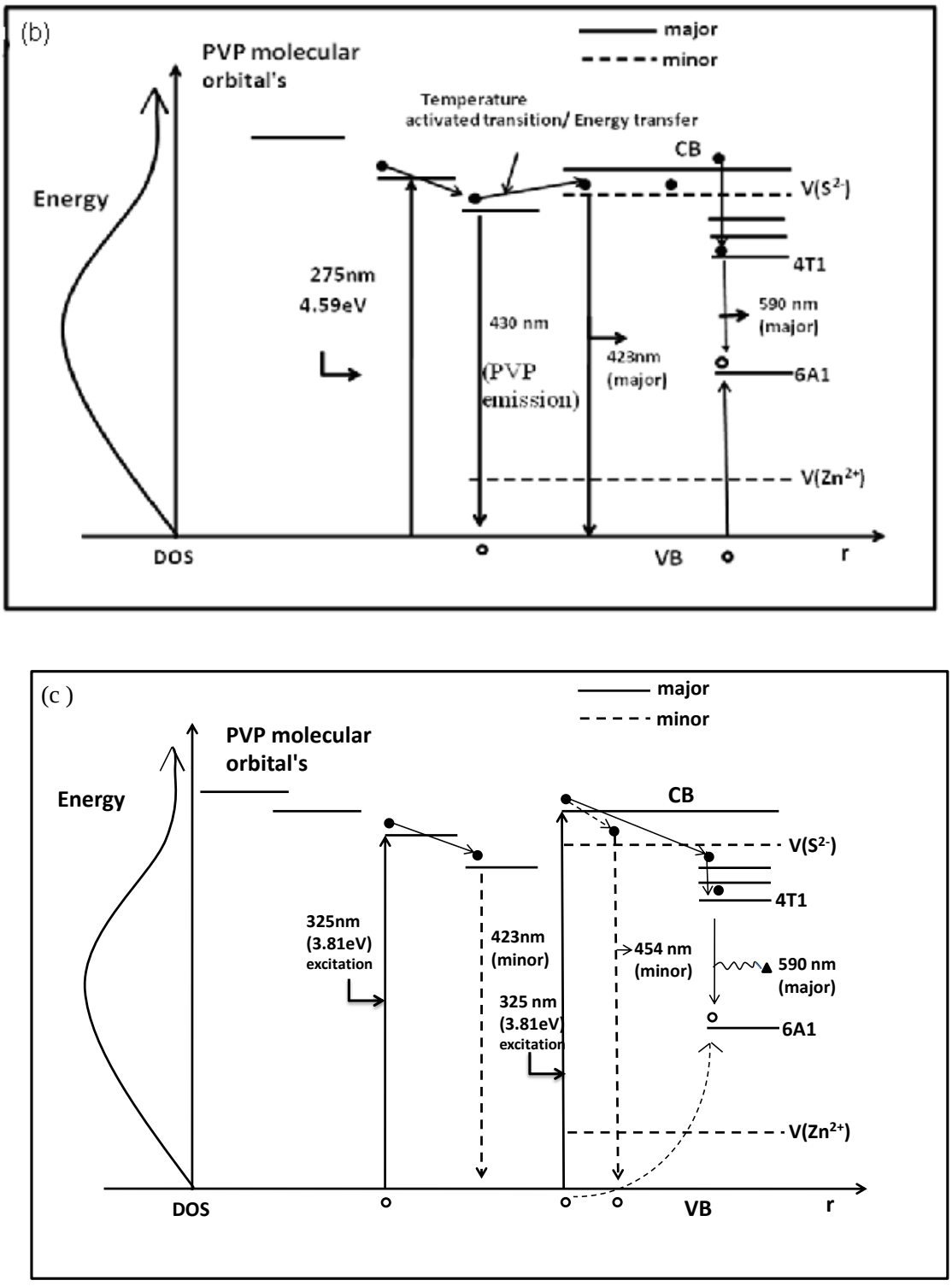

Figure 6.8 Energy transfer mechanism for PVP capped ZnS: Mn NPs at (a) 235nm excitation (b) 275nm excitation, (c) 325nm excitation (solid lines represent major transitions whereas dotted lines represent minor transitions).

This new type of tunable emission can be explained by two mechanisms, Foster energy transfer and convolution of emission from PVP and trap states around 423nm. Since, energy transfer behavior is dependent on spatial distance between donor and acceptor states. Foster theory [13, 52] suggests that Foster radii are determined by the oscillator strength of optical transitions and spectral overlap between donor emissions (380-430nm) and acceptor absorptions (300-350nm) as shown in Figure 6.9. As explained in case of undoped PVP capped ZnS NPs (chapter 5.1) pure PVP gives emission around 410nm when excited by 235 or 275nm radiation. Using 275nm excitation wavelength a broad fluorescence spectrum (380-430nm) with peak centered at 410nm was observed for pure PVP (Figure 6.9). Since the emission spectrum of PVP was observed to overlap with the absorption band of QDs, the fluorescence resonance energy transfer (FRET) should be taken into account for explaining excitation induced tunable emission in our case. In our case energy transfer is taking place from inhomogeneous energy levels of polymer PVP to the defect states efficiently (Exc.235nm→Emission 423nm). As more trap states lie at surface of ZnS because surface to volume ratio is more in nano regime so this provides less spatial distance from polymer to vacancies (acting as traps) in comparison to polymer and dopant (Mn) ions. It is represented by energy transfer mechanism (Figure 6.8a) where due to more spatial distance, energy transfer is very less from capping layers to d levels of Mn^{2+} and due to less spatial distance between trap states and capping layers, energy transfer is maximum which is supported by our PL results as shown in Figure 6.5 . Second possibility exists in case of overlapping of emission spectra of pure PVP (which is broad and centered on 410nm) with emission spectra of NPs due to sulphur vacancy (which is also broad and centered around 423nm [8, 16]). This results high emission intensity for 423nm in comparison to 590nm emission at 235nm excitation for same sample. As the created exciton relaxes to energetically lower energy states which is

biased by high spatial distance from polymer to Mn^{2+} states i.e. why exciton energy has not been transferred from trap states to dopant states although dopant site has less excited state life time in comparison to defect emission which is reported earlier [11, 52-55]. But for 325 nm excitation (band to band excitation in host ZnS) orange emission (590nm) is prominent and blue (423nm) and green (483nm) emissions are quenched. Instead of this a relatively small broad band at 453nm is observed. Since Mn^{2+} d levels lie inside the host ZnS at a subsitutional site so coupling with host ZnS is more pronounced which has already been reported [52-55]. Photoluminescence characteristics of Mn^{2+} doped ZnS nanocrystals exhibit different spectra which depend upon the nature of occupancy of Mn^{2+} ions [54, 55]. In our results we have observed a peak at 590nm which according to literature reports indicate that Mn^{2+} is occupying interstial site inside ZnS [52-55]. Therefore proposed mechanism (Figure 6.8) explains our results, which shows that there is strong coupling between ZnS host and Mn^{2+}, as it occupies interstitial site inside ZnS NPs. Also there is strong coupling between polymer and trap states as both are present on the surface of ZnS. Hence energy transfer takes place from polymer to defect states (resulting blue and white emission), and host ZnS to dopant Mn (resulting orange emission).

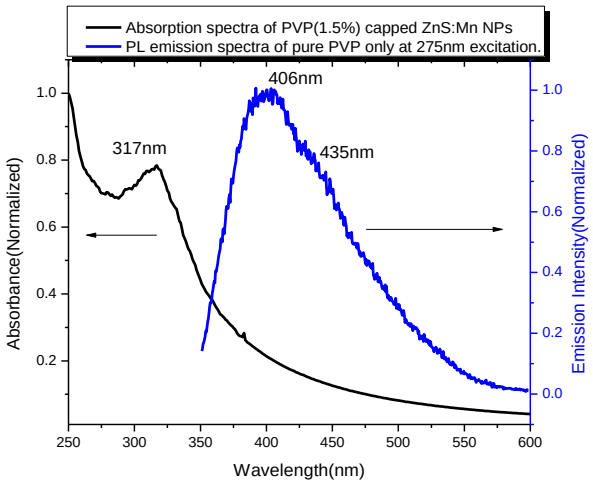

Figure 6.9 FRET mechanism with absorption spectra of PVP capped ZnS Mn NPs (acceptor) and PL spectra of pure PVP (donor).

6.2 Chitosan capped Mn doped ZnS nanoparticles

6.2.1 Brief introduction

Often organic polymers are used to stabilize the NPs and also terminate growth [56]. Here organic polymer is not only stabilizing the NPs but may result charge generation, charge transfer and charge separation at the interface between polymers and NPs [56, 57]. Here in this part of chapter we have used three different concentration of chitosan (0.01, 0.1, 1.0 at. %) (CH) for synthesis of ZnS: Mn^{2+} (0.1at. %) NPs. Tunable emission from blue to green and green to yellow orange is achieved by changing excitation wavelength for the same sample. Also increase in chitosan concentration from 0.01 to 1.0 at. % tenfold rise in PL intensity along with tunable emission property in same sample is obtained. Optimized concentration of capping polymer has been used by studying PL characteristics of chitosan (0.1, 0.5, 1.0, 1.5 and 2.0%) capped undoped ZnS NPs (previously discussed in Chapter 5.2). Based on results showing high PL emission intensity in 1.0% capped sample, this capping concentration is used for further tunable emission and sensing studies. Also fluorescence resonance energy transfer (FRET) mechanism is used to explain this new type of tunable emission in single sample. This work illustrate coupling between Frenkel exciton in organic polymers with Wannier exciton in inorganic semiconductors which has been observed for the present nanophosphors and is used for sensing different concentrations of glucose. Also tunable emissions from 400nm to 587nm have been reported for same sample. Moreover, chitosan capped ZnS: Mn NPs are found to be biocompatible with all above mentioned properties. The color modulation is demonstrated by attaching staphylococcus (SAU) bacteria which exhibits different colors with variation in wavelength.

6.2.2 Reagents and Synthesis

High purity research grade chemicals purchased from Sigma Aldrich were used. Chitosan, a natural biopolymer was also purchased from Sigma Aldrich. Chitosan capped and manganese doped ZnS NPs were synthesized by chemical precipitation method as described earlier in chapter 5.2. Chitosan is hydrophilic, nontoxic, biocompatible and biodegradable polymer. In the first step 40mL homogenous solutions of 0.5M zinc acetate, 0.5M sodium sulphide and 0.1 at. % manganese acetate was prepared separately in distilled water by stirring them for half an hour. Also solution of different concentration of capping agent (chitosan) used in present investigation was prepared in 40mL solution of 1.0% acetic acid in distilled water separately. Chitosan is insoluble in water and strong acids but is soluble in dilute acids, as amine group is protanated to NH_3^+. Here we have used 1.0% acetic acid solution in distilled water to dissolve chitosan. For the synthesis of capped ZnS:Mn NPs, 40mL solution of zinc acetate and manganese acetate were mixed in a beaker and stirred for 15 minutes. Then to this reaction mixture 40mL solution of capping agent was added slowly. The solution was stirred for half an hour at room temperature. 40mL solution of 0.5M sodium sulphide was added drop wise in this reaction mixture. Soon after the addition of sodium sulphide the precipitation phenomenon occurs and concentration of precipitates increases as addition was increased. The stirring was done for half an hour. The solution containing ZnS particles were then centrifuged at 4000 rpm for 5 minutes. The precipitated particles were filtered using Whatman 40 filter paper. To remove the last traces of adhered impurities and excess chitosan in capped ZnS: Mn^{2+}, the particles were washed several times using double distilled water and 0.1 % acetic acid solution for 48 hours. The washed particles were dried in vacuum oven at 60ºC for 24 hours.

For comparison of PL intensity and tunable emission property ZnS: Mn^{2+} (0.1at.%) NPs were synthesized with three different concentrations of chitosan (0.01, 0.1, 1.0 at.%).

6.2.3 XRD Studies

Figure 6.10 shows X-ray diffraction pattern of Mn (0.1%) doped, CH (0.01, 0.1, and 1.0%) capped ZnS NPs. It shows three broad peaks corresponding to the (111), (220) and (311) planes of FCC ZnS structure. It is to be noted that, the peaks observed in the XRD pattern match well with those of the β-ZnS (cubic) reported in the JCPDS powder diffraction file No. 80-0020. Broadening of the XRD peaks indicates the formation of ZnS NC's. No secondary phase(s) are present in the ZnS: Mn^{2+} NP's. The average crystallite size using Scherer's formula is estimated from three planes is 2.15, 2.13 and 2.01nm respectively for CH (0.01, 0.1, 1.0 at. %) capped ZnS: Mn^{2+} NC's.

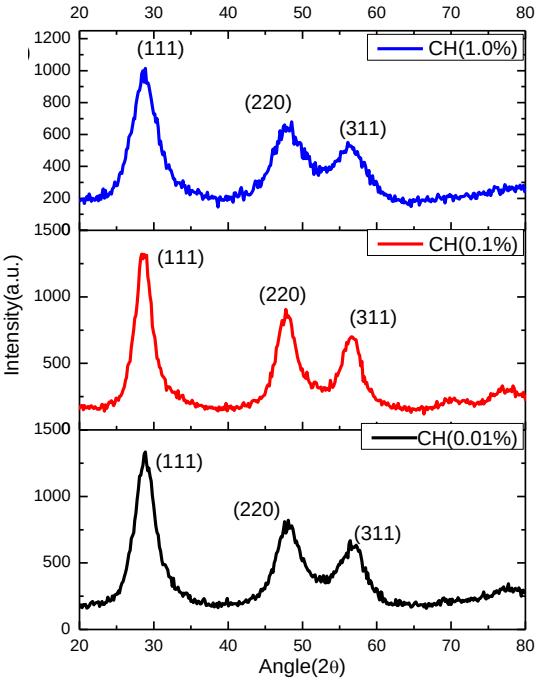

Figure 6.10 XRD pattern of CH (0.01-1.0%) capped ZnS:Mn NPs.

6.2.4 TEM Studies

Figure 6.11 (a) shows TEM micrograph of 0.1% capped ZnS NPs showing spherical crystallites of average size 3.0nm. TEM micrograph of CH (1.0%) capped NPs are shown in Figure 6.11(b), which shows spherical crystallites having mean size ~3.0-4.0 nm. Figure 6.11 (c) shows HRTEM micrograph of CH (1.0 at. %) capped NPs. It shows an abundance of nearly spherical crystallites, which also have a mean particle size of 3.0 nm. HRTEM picture shows presence of (111) plane. Figure 6.12 shows EDAX pattern of CH (1.0%) capped NPs showing presence of zinc, sulphur and little oxygen and carbon due to polymer.

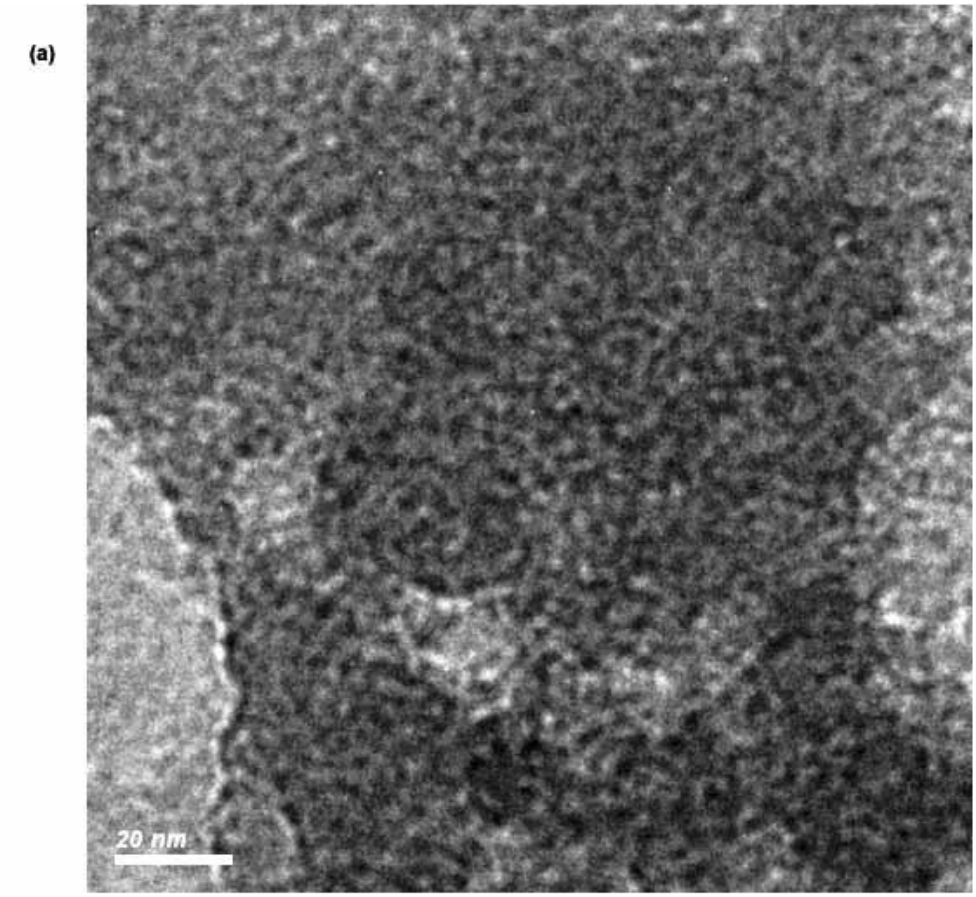

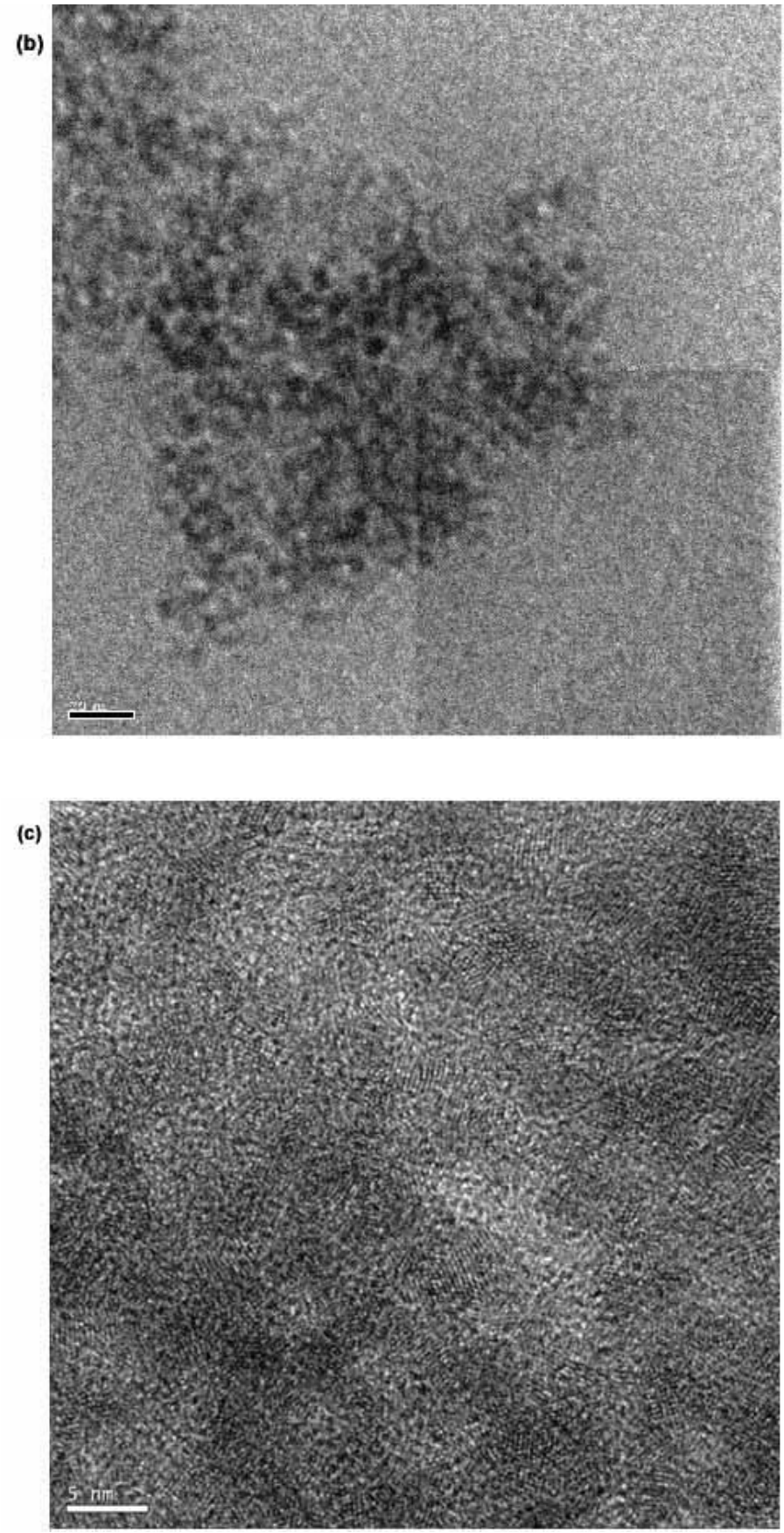

Figure 6.11 (a) TEM micrograph of CH(0.1%) capped, (b) CH (1.0%) capped (c) HRTEM of CH (1.0%) capped ZnS:Mn(0.1%) NPs

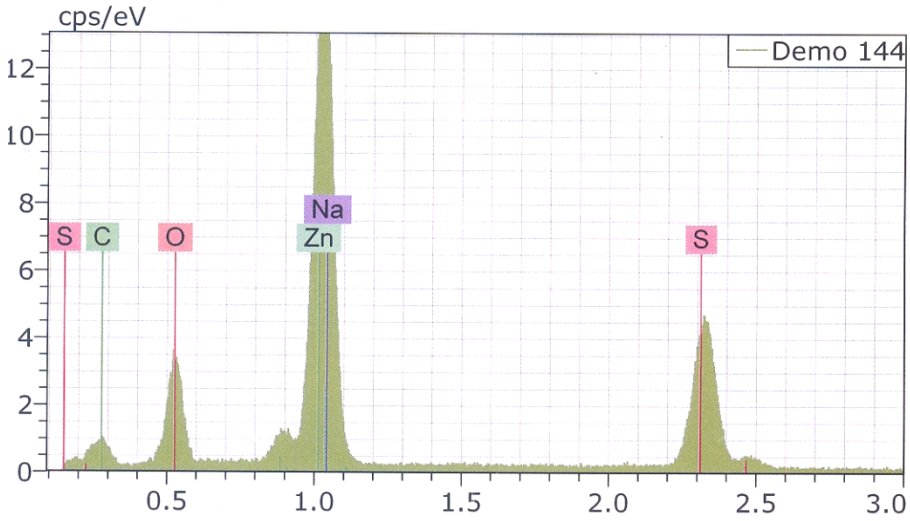

Figure 6.12 EDAX spectra of CH (1.0 %) capped ZnS: Mn NPs

6.2.5 UV-Visible Absorption Studies

The optical absorption spectra of the CH capped and Mn doped ZnS NPs are shown in Figure 6.13(a). The absorption spectrum for CH (0.01, 0.1, and 1.0%) capped NP's shows absorption shoulder at 325nm, 325nm and 311nm respectively. Again using the Manifacier model [51], the absorption coefficients (α) were calculated in the region of strong absorption. The exact values of the band gap were determined by extrapolating the straight line portion of the $(\alpha h\nu)^{1/n}$ versus $h\nu$ graphs to the $h\nu$ axis as shown in Figure 6.13 (b). From the plots the values of band gap were obtained as 4.65eV, 4.73eV and 4.82eV for CH (0.01, 0.1 and 1.0 at. %) capped ZnS: Mn^{2+} NPs respectively. The band gap values were found to increase due to reduced particle size showing strong quantum confinement effects which is higher than the bulk value 340nm of ZnS having band gap of 3.6 eV.

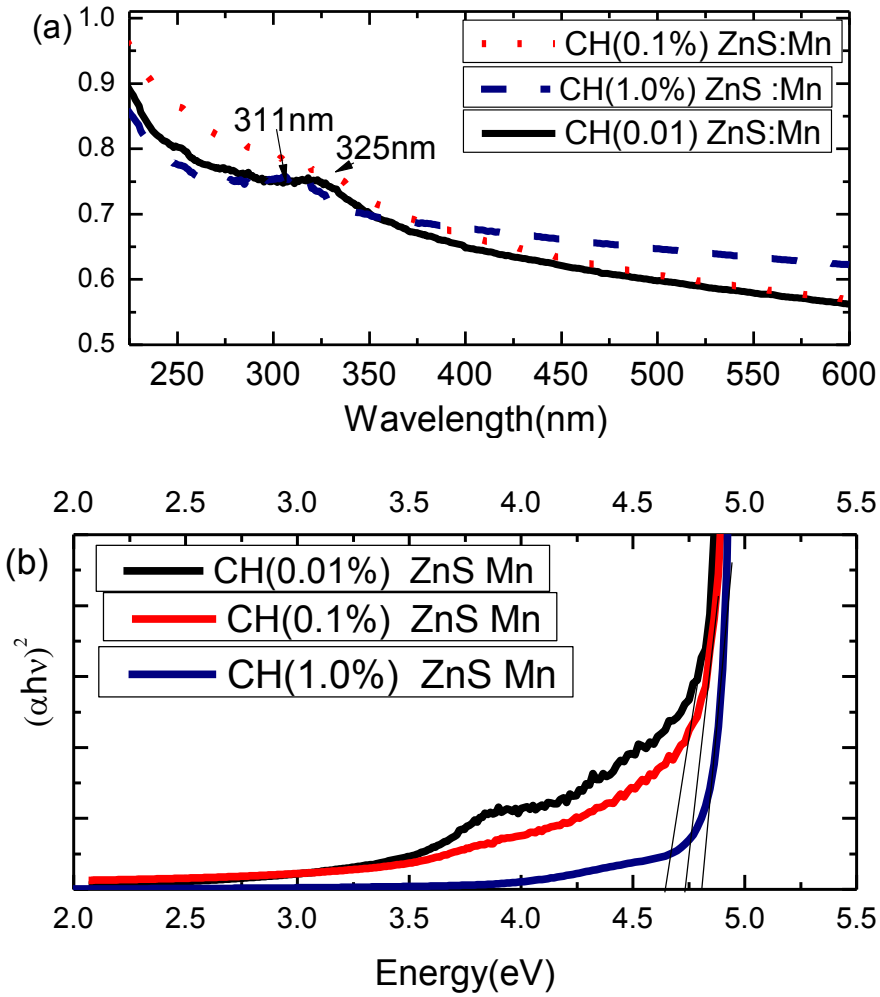

Figure 6.13 (a) Absorbance spectra, (b) estimated band gap by $(\alpha h\nu)^2$ Vs hν plot for CH capped ZnS: Mn NPs.

6.2.6 Photoluminescence Studies

It is discussed previously in chapter 5.2 that out of all concentrations of chitosan (0.1-2.0%), 1.0% chitosan is showing high emission intensity. Since enhanced emission intensity with tunable emission in visible region is important for NPs to be used as biolabels and luminescent material. 1.0% CH capped ZnS: Mn NPs have been compared for their luminescence characteristics with CH (0.01, 0.1%) capped Mn doped NPs.

Figure 6.14(a) shows excitation spectra of CH (1.0%) capped ZnS: Mn^{2+} NC's for two possible emissions (400, 590nm). For emission in range of 400nm, excitation spectra is broadened in comparison to undoped CH (1.0%) ZnS NPs (chapter 5.2) showing

highest excitonic peak at 280nm along with weak peaks at 305nm, 330nm respectively. This broadening can be attributed to more energy states present in doped and capped sample in comparison to undoped and capped sample. Further for Mn dopant related emission (590nm), PLE spectra red shifts from 284nm to 298nm and 318nm is observed. This shows that in doped sample there are two possible emission sites. As excitonic peak around 284nm is observed for undoped samples also so it can be responsible for 410nm emission due to trap states and 350-400nm emission is due to chitosan (discussed later). Also excitonic peak around 298-330nm results for 590nm emission so dopant related peak around 590nm can be due to band to band excitations in ZnS. This indicates that emission spectra would be dependent on excitation wavelength. In order to explain further these dual excitonic peaks for same sample in excitation spectra, emission spectra were recorded for all doped samples at two different excitation wavelengths (284, 325nm).

Figure 6.14 (b, c) shows a comparison study of PL spectra of these ZnS: Mn^{2+} NP's at two different excitations (284, 325nm). The spectra were recorded at an emission filter at 290 and 350nm for corresponding excitation wavelength of 284 and 325nm. Figure 6.14 (b) shows PL spectra of chitosan capped ZnS: Mn NPs at 284nm excitation wavelength showing emission at 400nm in all the samples. This emission corresponds to the self activated blue emission near band edge emission which is due to radiative transition from the sulphur vacancies (V_s) to valence [54-62] and adsorbed chitosan on host ZnS surface (discussed later). Emission at 587 nm is due to $^4T_1$ - $^6A_1$ transitions in dopant Mn^{2+} energy levels which is already discussed in previous section (6.1) [4, 38]. As shown in Fig 6.14 (b, c) an increase in integrated PL emission intensity is observed with increase in capping concentrations from 0.01-0.1 -1.0 at. % for both excitations. This rise in PL intensity for 1.0% CH capped sample is also studied for undoped CH (0.1-2.0%)

ZnS NPs and is discussed above by presence of chitosan emission. So, for further study we have used CH (1.0%) capped sample only (as was concluded in chapter 5.2).

It is observed in Figure 6.14 (b) that for excitation wavelength of 284nm, emission spectrum is broad having two peaks at 400nm and 587nm. Emission intensity of 400nm peak is higher than 587nm peak which is calculated and presented in Table 6.2. Apart from symmetrical peak around 587nm due to Mn in all samples, additional small peak around 571nm arises in this case which can be due to excitation by doublet of 284nm. Although we have used proper filters in all samples as discussed earlier. However, at 325nm excitation, emission corresponding to 400nm is quenched partially and 590nm is enhanced for the same sample (Figure 6.14 c). This shows single sample (CH 1.0 at. % ZnS: Mn^{2+}) is emitting two different colors at different excitations.
It is clear that CH (1.0%) capped sample is having maximum integrated emission over full emission range. But relative contribution of 400 and 587nm emissions is not clear in combined PL graph. So, in order to compare $I_{\mathbf{blue/orange}}$, all spectra have been shown independently and compared with uncapped ZnS:Mn emissions also at same excitations.

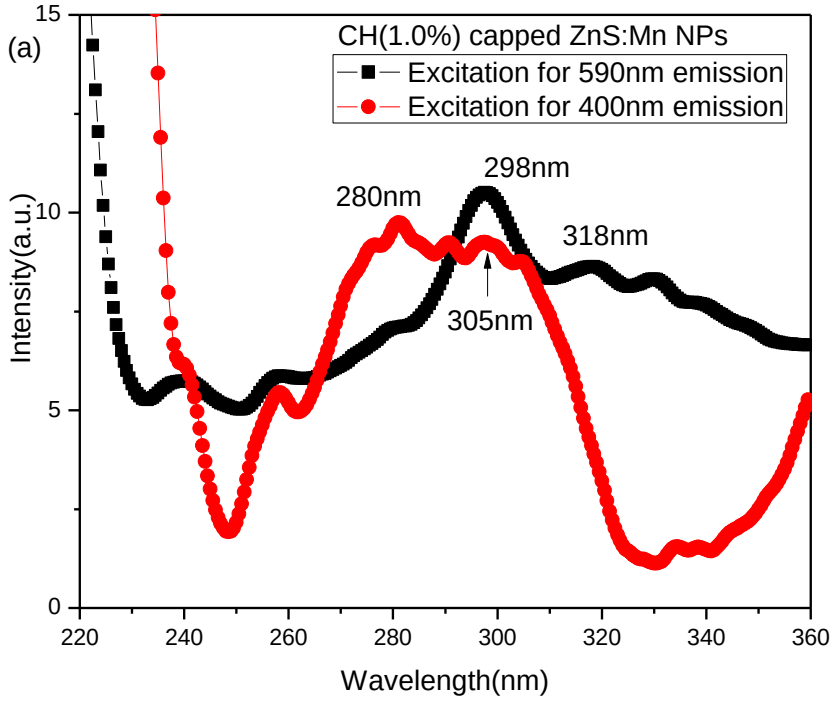
(a)
CH(1.0%) capped ZnS:Mn NPs
Excitation for 590nm emission
Excitation for 400nm emission
280nm
298nm
318nm
305nm
Intensity(a.u.)
Wavelength(nm)
0
5
10
15
220
240
260
280
300
320
340
360

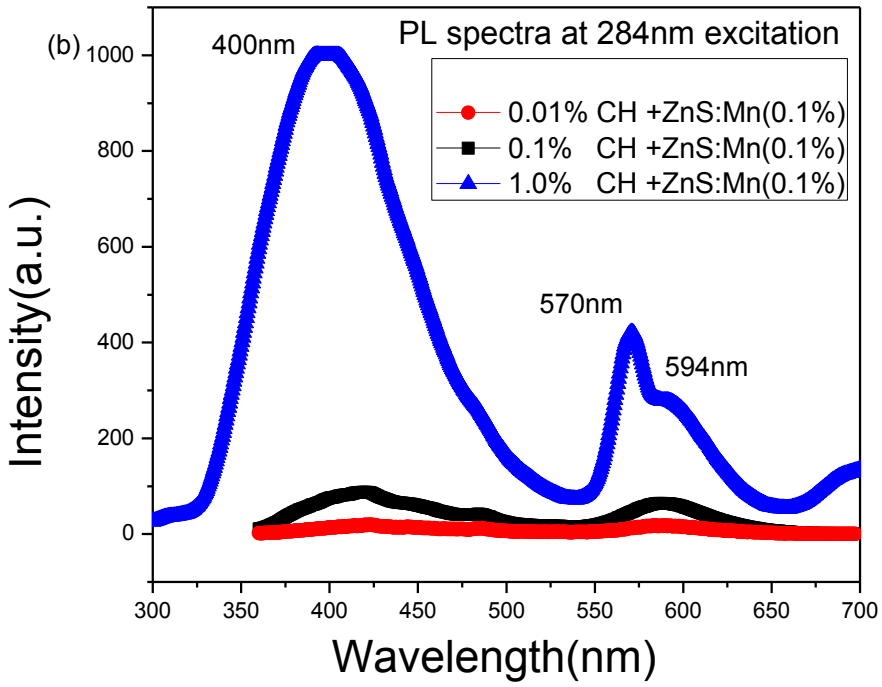
(b)
PL spectra at 284nm excitation
400nm
570nm
594nm
0.01% CH +ZnS:Mn(0.1%)
0.1% CH +ZnS:Mn(0.1%)
1.0% CH +ZnS:Mn(0.1%)
Intensity(a.u.)
Wavelength(nm)
0
200
400
600
800
1000
300
350
400
450
500
550
600
650
700

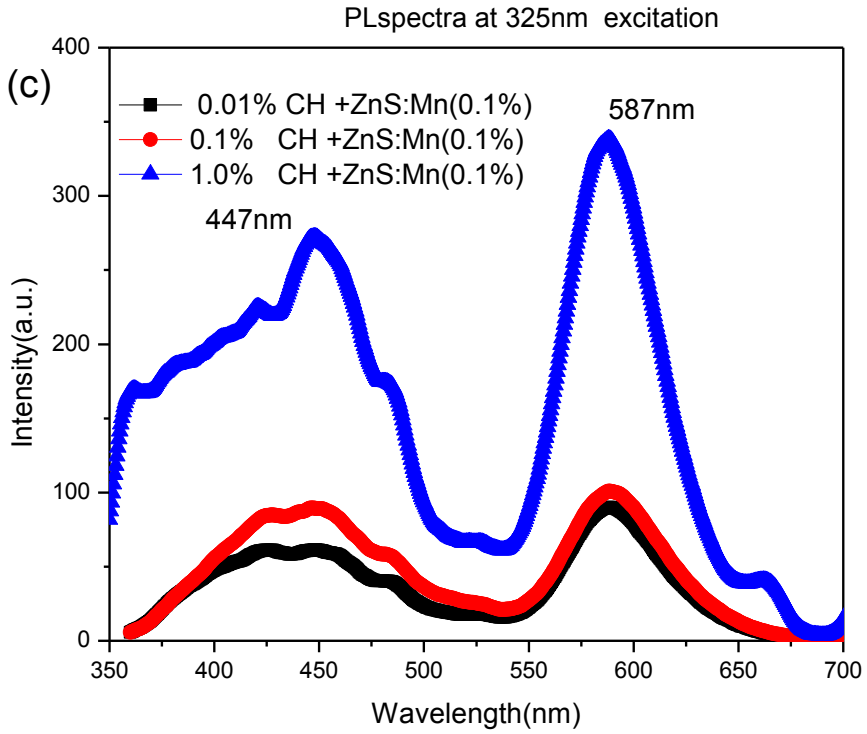

Figure 6.14 (a) Excitation spectra of CH capped ZnS Mn NPs. (b, c) PL spectra of chitosan (CH) capped ZnS: Mn at different excitation wavelengths. (Excitation wavelength and sample specifications are written as an inset for each case).

Figure 6.15(a-f) shows PL spectra of samples prepared in concentrations of 0.01, 0.1and 1.0% chitosan and compared with uncapped ZnS: Mn NPs at two different excitations (280, 320nm). In emission spectra it is observed that emission peaks at 421 and 481nm are having high intensity in comparison to 590nm, if excitation wavelength is 280nm or 320nm for uncapped ZnS: Mn NPs (Figure 6.15(a, b)). The absence of emission peak at 590nm (dopant related) suggests unsuccessful doping in uncapped ZnS NPs. The whole mechanism for the presence of dopant ions inside matrix of host ZnS or on its surface is discussed later on.

Fig 6.15(c-h) shows PL spectra of chitosan capped ZnS: Mn NPs at 280 and 320nm excitation. PL spectra of uncapped ZnS:Mn NPs shows high emission intensity at 421 and 486 nm for 280 and 320nm excitations whereas Fig 6.15(c, e) shows chitosan

(0.01 and 0.1%) capped ZnS : Mn NPs have high emission intensity at 421 and 486nm for 280nm excitation wavelength only. However, if excitation wavelength is changed from 280nm to 320nm then there is a strong emission at 590nm for capped samples. Figure 6.15(g) shows that CH (1.0%) capped ZnS: Mn NPs gives high emission intensity at 400nm for 280nm excitation. In comparison to CH (0.01, 0.1%) capped samples where 423 and 486nm emissions are dominant at this excitation here broad emission at 400nm is observed. The relative contribution of blue emission in comparison to orange emission is calculated and shown in Table 6.2 which shows $I_{400/587}$ is 3.59 for CH(1.0%) capped sample which is very higher than CH(0.01, 0.1%) capped samples having $I_{400/587}$ values 1.11 and 1.35 respectively. This shows that for CH (1.0%) capped NPs blue/orange emission along with high integrated emission is also quite high in comparison to CH (0.01, 0.1%) capped ones. Figure 6.15(h) shows PL spectra of CH (1.0%) capped ZnS: Mn NPs at 325nm excitation. It shows relatively high 590nm orange emission in comparison to 400nm blue emission. As shown in Table 6.2, $I_{400/590}$ for 325nm excitation are 0.66, 0.85 and 0.79 respectively for CH (0.01-1.0%) capped samples. This shows 0.1 and 1.0% samples exhibits high orange luminescence in comparison to 0.01% capped samples. The peak at 590nm corresponds to $^4T_1$ - $^6A_1$ transitions of Mn^{2+} [4, 62-63]. This emission peak was not observed in uncapped samples at both excitations (280, 320nm). Also the peak at 590 nm was not intense for capped samples if excitation wavelength is of higher energy (280nm). For capped samples if excitation wavelength is 280nm then emission peak at 421 and 486nm is enhanced and 590nm emission is quenched. However, at 320nm excitation, emission corresponding to 421 and 486 nm is quenched and 590nm emission is enhanced for the same sample. In case of CH (0.01, 0.1 at %) capped ZnS: Mn^{2+} NP's two emission colors (blue-green and orange) were obtained at 280 and 320nm

respectively. For CH(1.0%) capped sample instead of blue green highly intense violet-blue and orange color is emitted by changing excitation wavelength from 280nm to 325 nm.

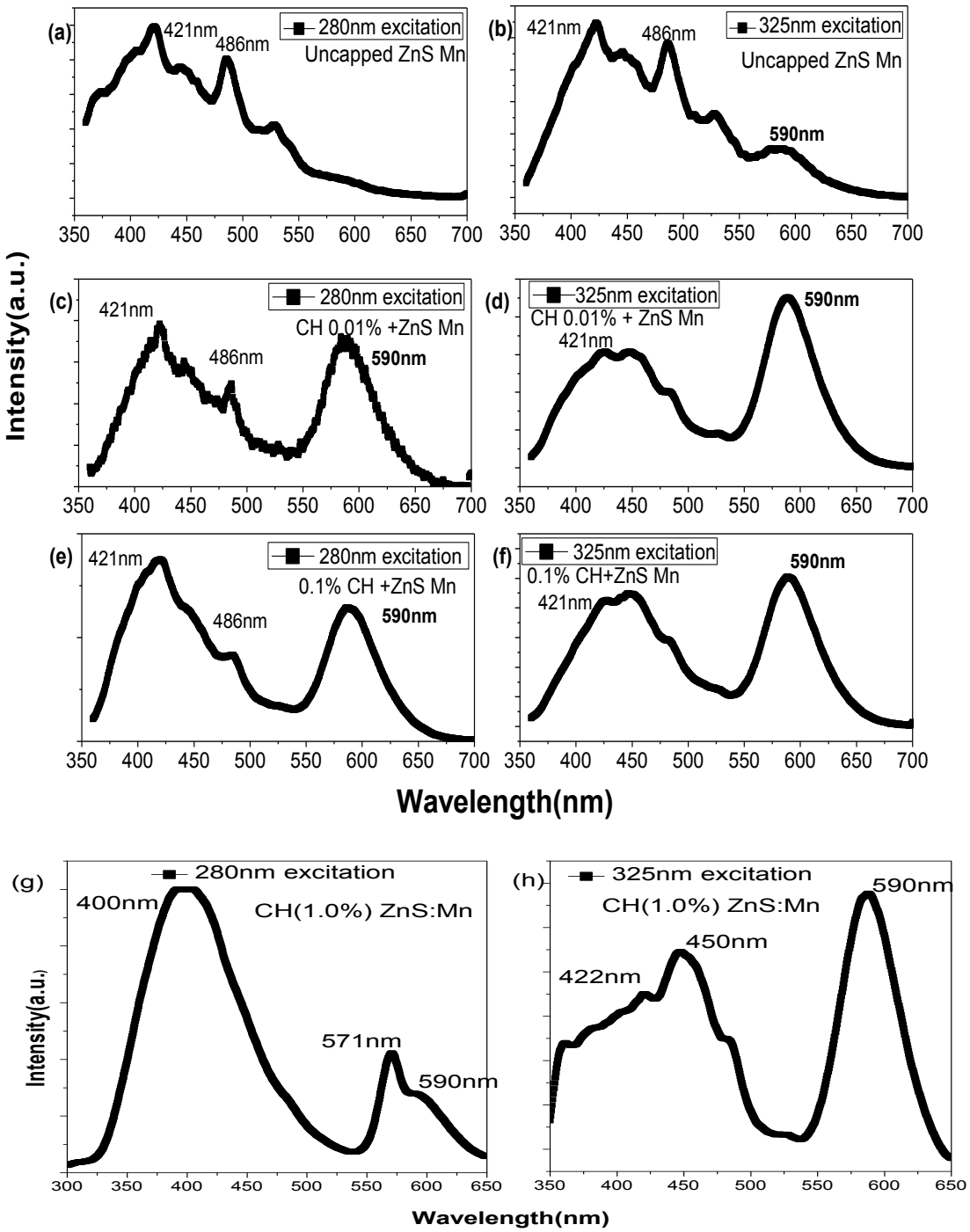

Figure 6.15 (a-h) PL spectra of uncapped and chitosan (CH) capped ZnS: Mn at different excitation wavelengths (excitation wavelength and sample specifications are written as a inset for each case).

So, for CH (1.0%) capped NPs broad peak centered at 400nm (for 284nm excitation) due to sulphur vacancies and adsorbed chitosan (discussed later) exhibiting tenfold rise in emission intensity in comparison to CH (0.01, 0.1%) synthesized samples (Figure 6.14b, c). This can be due to more concentration (1.0% than 0.01, 0.1%) of chitosan having broad 350-450nm emission overlaps with 423nm emission of trap states in ZnS giving strong violet blue emission instead of weak blue- green emission for CH(0.01, 0.1%) capped ZnS: Mn NPs at same excitation. Also for 325nm excitation, dopant (Mn^{2+}) related emission peak at 587nm is greatly enhanced (four fold) than CH (0.01, 0.1%) capped NPs. Also in previous section of this chapter we have studied chitosan (0.1, 0.5, 1.0, 1.5, 2.0%) capped ZnS NPs. Maximum PL intensity is observed in 1.0% capped NPs which is also used as basis for doped samples for subsequent study.

Figure 6.16(a, b) shows Gaussian distribution of emission spectra for CH (0.1% and 1.0%) capped ZnS: Mn NPs at 280nm excitation. CH (0.1%) capped sample shows five emission peaks corresponding to this excitation. From these peaks 421 and 447nm emission peaks have high emission intensity in comparison to 522 and 587nm peak. CH (1.0%) capped sample shows intense 400nm peak along with 571 and small 590nm emission. This shows that with increase in capping concentration from 0.1-1.0% relative contribution of 400nm emission as compared to 590nm emission increases. Further in Figure 6.16(c, d) excitation wavelength used is 325nm and Gaussian distribution is showing five peaks again. But in both cases 590nm emission peak is enhanced and 421 and 486nm peak is suppressed which is also shown previously in Figure 6.15. Since with increase in capping concentration of chitosan from 0.1 to 1.0% at 280nm excitation highly intense 400nm peak appears in comparison to 423 and 486nm emission peaks. So for understanding the possible influence of chitosan on PL intensity of doped QDs, the

fluorescence of chitosan was investigated. Using 284nm excitation wavelength a broad fluorescence spectrum (300-500nm) with peak centered at 364nm was observed for pure chitosan (Figure 6.17a). Since the emission spectrum of chitosan was observed to overlap with the absorption band of QDs, the fluorescence resonance energy transfer (FRET) should be taken into account to explain excitation induced tunable emission in our case. The enhancement in fluorescence of QDs with increase in concentration of chitosan (0.01 to 1.0at. wt. %) was more pronounced for 400nm emission in comparison to 587nm emission. This can be explained by two mechanisms. First effective FRET is taking place (from adsorbed chitosan to ZnS) in case of 400nm emission as compared to 587nm emission. This is because the absorption spectra of QDs (around300-350nm) is overlapping to some extend with emission spectra of chitosan (300-500nm) causing enhancement of emission at 400nm instead of 590nm (Figure 6.17a). Second possibility exists in case of overlapping of emission spectra of pure chitosan (which is broad and centered around 364nm) with emission spectra due to sulphur vacancy (which is also broad and centered around 420nm) [4, 11, 62]. It is shown by shaded portion in Figure 6.17a.

As per published work [52-55] if Mn^{2+} ions are substituted outside the ZnS crystal then emission peak at 350nm appear instead of 430 and 590nm. Since this type of behavior is not observed in our case (Figure 6.14c) so, it can be concluded that Mn^{2+} ions are doped at interstial sites, inside of host ZnS NPs. According to Foster theory [13] energy transfer is dependent on spatial distance between donor and acceptor. In all the samples sulphur vacancies exist at the surface giving rise to Zn dangling bonds which forms shallow donor levels. As these dangling bonds are lying at surface of quantum dots so there can be strong coupling between defect states and capping polymer. The distance between adsorbed chitosan and interstitially existing Mn^{2+} ions is more as compared to

sulphur vacancy (zinc dangling bonds) which is existing at surface. Because of this the effective energy transfer (based on Foster theory) would take place from chitosan molecular energy levels to defect states which get further enhanced with increase in concentration of chitosan (0.01 to 1.0%) on surface (Figure 6.14b, c).

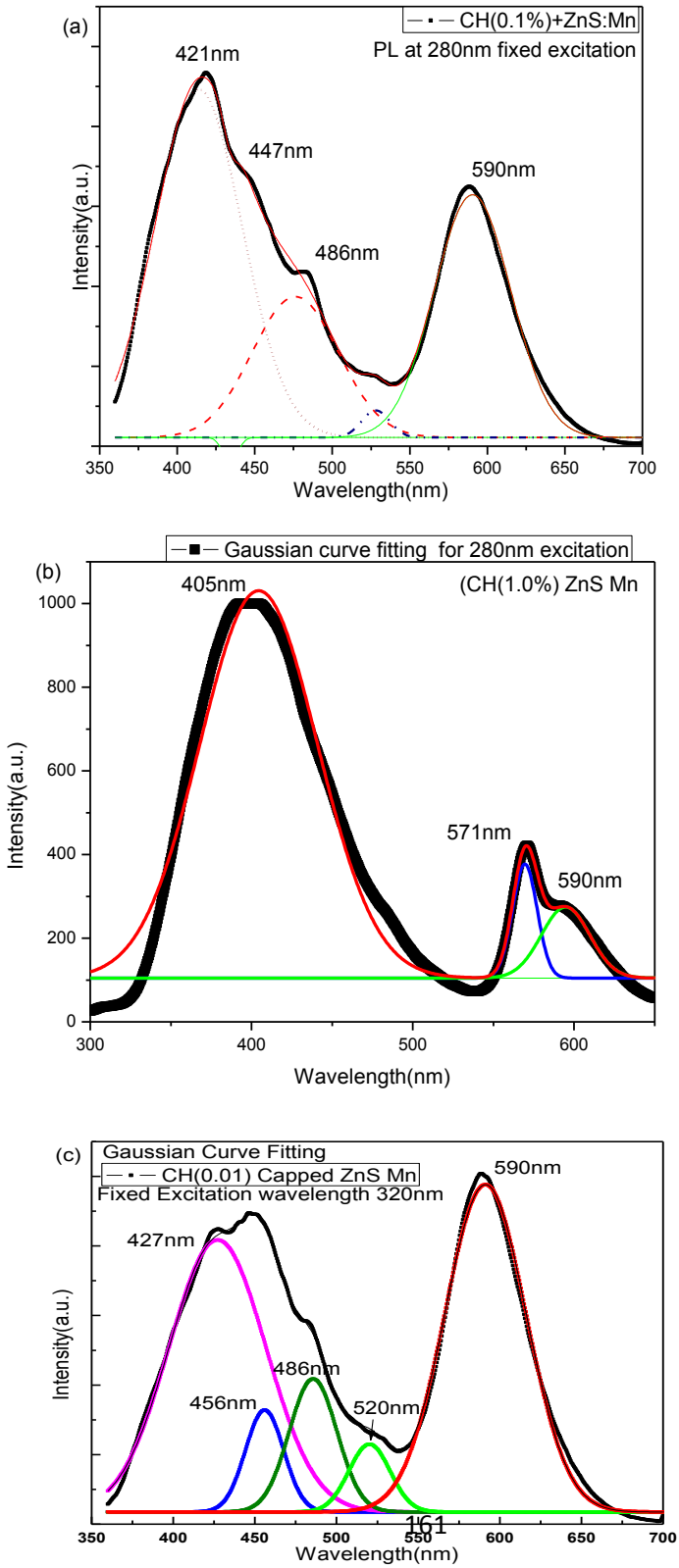

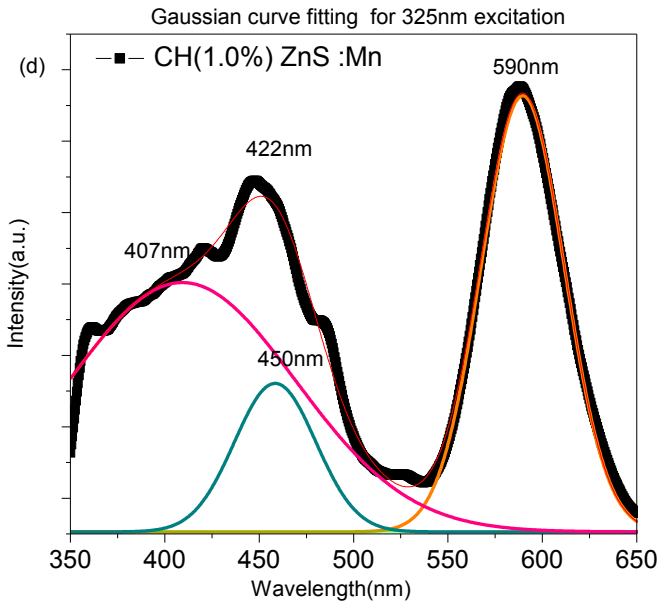

Figure 6.16 Tunable PL spectra with Gaussian Curve Fittings for CH (0.1, 1.0%) capped ZnS:Mn^{2+} (a, b) at fixed excitation wavelength 280 nm, (c, d) At fixed excitation wavelength 325nm.

Kong et al. [63] have also studied the effect of distance between acceptor and donor on optical properties of composite semiconducting polymer films. They have shown that energy transfer efficiencies calculated from time resolved PL spectra are consistent which was calculated from emission spectra of donor with and without acceptor. The energy transfer efficiency from adsorbed chitosan to host ZnS and chitosan to dopant Mn can be calculated from emission occurring from donor (chitosan) in the absence and presence of acceptor (ZnS:Mn QDs), which can be written in the following form:

$$\Phi_T = 1 - \frac{\int_0^\infty I_D(\lambda)d\lambda}{\int_0^\infty I_D^0(\lambda)d\lambda} \qquad (1)$$

where, $I_D^0(\lambda)\,d\lambda$ and $I_D(\lambda)\,d\lambda$ are the PL intensities of chitosan without ZnS: Mn and with ZnS:Mn, respectively, at the emission wavelength of λ (nm). It can be calculated from PL spectra of pure chitosan without ZnS:Mn and with ZnS:Mn in Figure 6.17 (a) that energy transfer efficiency from chitosan to ZnS :Mn for 284nm excitation is 55.8%.

Also following the same procedure energy transfer efficiency from chitosan to dopants for 325nm excitation comes out to be 40.0% which is less than for 284nm excitation. These studies suggest that if molecular energy levels of chitosan are excited then emission is obtained from defect states of ZnS and not from dopant sites (Figure 6.17b). Figure 6.17 (c) shows second case for same capped sample where dopant related emission (587nm) is enhanced and defect related emission (~400nm) is partially quenched, when excitation wavelength is 325nm i.e. near conduction band of ZnS. Figure 6.17 (b, c) shows energy transfer mechanism for two possible emissions (400nm, 587nm) corresponding to 284nm and 325nm excitations in single sample respectively.

So, we have optimized capping concentration for achieving high emission intensity and at the same time dual emission is achieved at this concentration in same sample. As shown in Figure 6.14 (c) we have also observed broad emission peak at 450nm along with 587nm, which corresponds to sulphur vacancy related emission. But for (1.0 at. %) CH capped ZnS:Mn^{2+} NP's 587nm emission peak is sharp and slightly higher in intensity than 450nm peak although concentration of Mn^{2+} is same in all samples. This shows better coupling of sp states of ZnS with $3d^5$ levels of Mn^{2+} instead of defect states of ZnS NPs. Bhargava et al. [38] reported that in Mn^{2+} doped ZnS NP's, very strong hybridization occurs between the sp levels of zinc and d levels of Mn^{2+} ions which results in crystal field splitting of Mn^{2+} levels in between the bands of host material. Subsequent transfer of excited electrons from CB to Mn^{2+} levels and further transition between $^4T_1$ - $^6A_1$ leads the emission of orange color. Secondly at 325nm excitation wavelength, energy states of adsorbed polymer are not excited which otherwise could have given emission at 400nm.

The emission observed in our case is different than reported previously [4, 10-11] because we are getting energy transfer in two different ways. In the first case energy transfer takes place from molecular energy levels of capping agent to defect states where dopant related emission is partially quenched, which according to earlier reports is enhanced [4]. In second case for same sample at different excitation wavelength energy transfer takes place from ZnS band states to Mn^{2+} d levels giving orange emission as shown in Figure 6.14 and defect related emission is partially quenched.

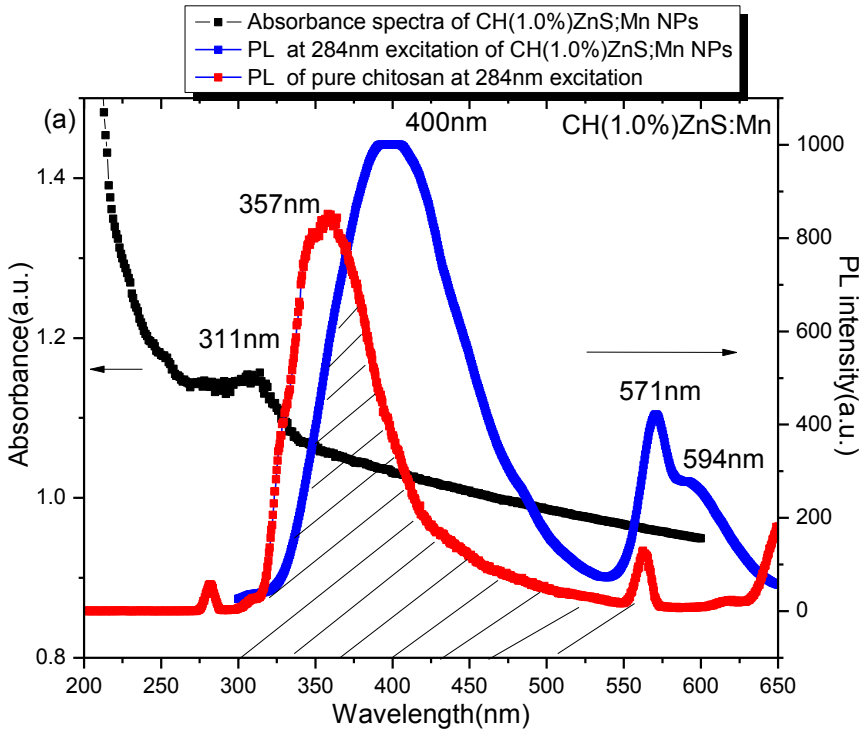

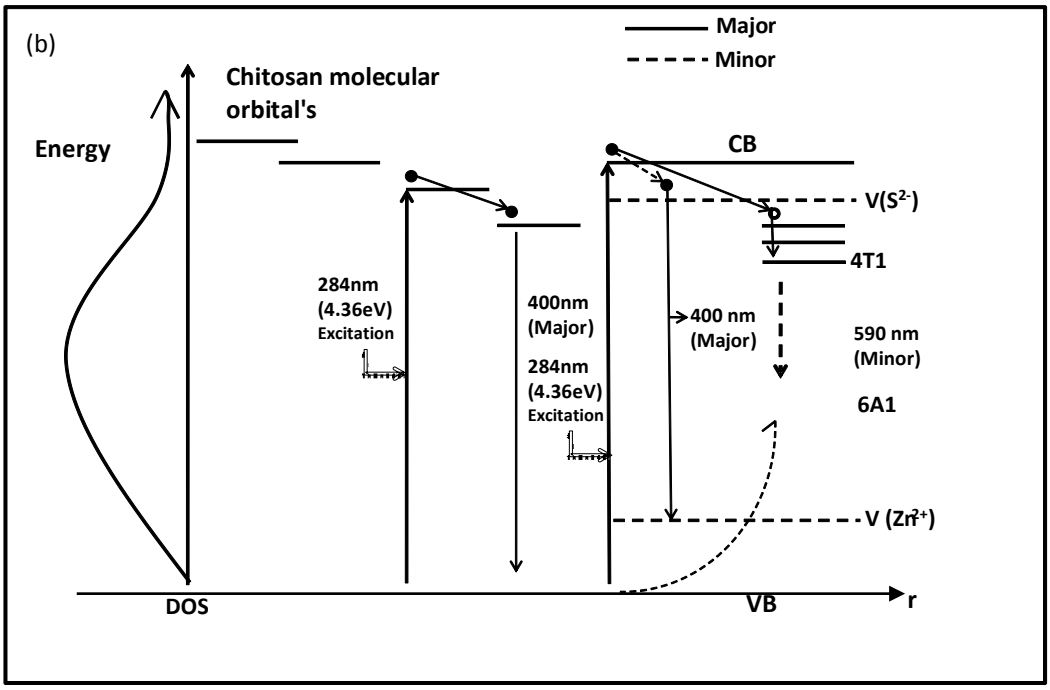

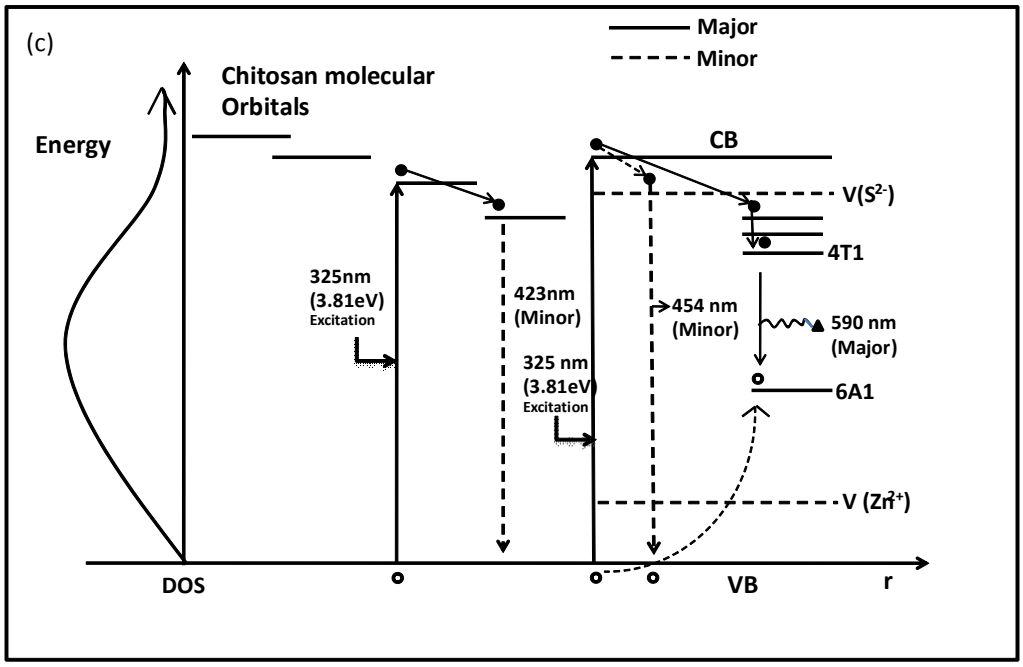

Figure 6.17 (a) FRET mechanism with absorption and PL spectra (b) Energy transfer mechanism for CH capped ZnS: Mn NPs at 284nm excitation (c) Energy transfer mechanism for CH capped ZnS: Mn NPs at 325nm excitation.

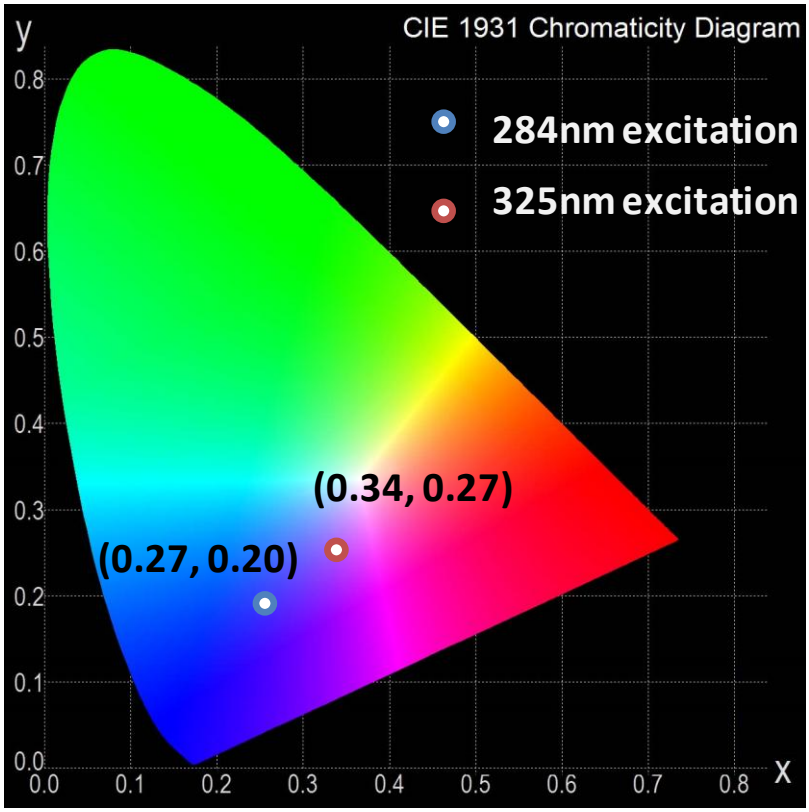

Figure 6.18 Showing CIE color coordinates of CH (1.0%) capped ZnS:Mn NPs at two different excitation wavelengths.

Table 6.2 shows $I_{400/587}$ (violet-blue/orange) ratio for all doped and capped samples. For CH (1.0%) capped ZnS:Mn sample it comes out to be 3.59, which shows, this sample emits intense violet-blue color instead of orange (expected for Mn doped ZnS) at 284nm excitation. Corresponding Commission Internationale de I' Eclaerage (CIE) color coordinates for this same sample at 284nm excitation as shown in Table 6.2 and Figure 6.18 are (0.273, 0.200) suggesting violet-blue emission. $I_{458/587}$ (blue/orange) for 325nm excitation wavelength comes out to be 0.79 (less than one) showing orange color dominant emissions (Table 6.2). There corresponding CIE color coordinates comes out to be (0.344, 0.275) and are shown in Figure 6.18 and Table 6.2. So, CIE color coordinates corresponding to emission spectra (Figure 6.15g, h) are shifted from (0.273, 0.200) to (0.344, 0.275) for single sample with shift in excitation wavelength. This clearly

shows that by changing excitation energy in this hybrid CH (1.0%) capped Mn doped ZnS NC's sample we can manipulate the relative emission intensities of blue light and orange light. This results in a tunable color output in visible region for a single sample. It is important to note that this kind of tunable emission is also reported for ZnS: Mn NPs having different concentrations of Mn [61]. Secondly this is achieved by doping different transition metal ions (Mn, Cu, Eu etc.) in host ZnS or varying particle size of same sample[4, 10]. But here we report same tunable emission but in single sample instead of many samples. It is important to mention here that peak position is not shifted here but their emission intensities are changed with shift in excitation energy from 284nm to 325nm respectively resulting in shift of emission color from blue to orange in same NC sample.

6.2.7. Biotagging Studies

Figure 6.19 (a, b) shows initial experimental demonstrations of attachment of capped ZnS: Mn quantum dots with staphylococcus aueurs (SAU) bacteria.

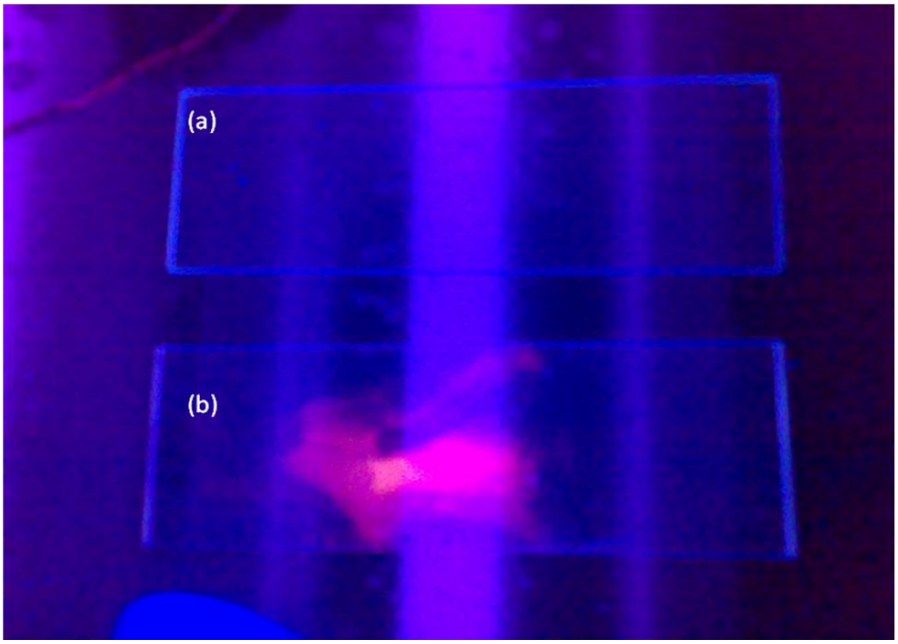

Figure 6.19 UV illumination of slides (a) control bacteria without ZnS:Mn (b) fixed with bacteria (SAU) and sprinkled chitosan capped ZnS:Mn NPs.

Synthesized capped ZnS: Mn QDs were sprinkled on slides fixed with SAU and then washed with double distilled water for few minutes to see the attachment of QDs with cell walls. Figure 6.19 (a) shows control slide fixed with bacteria which shows no considerable color. But Figure 6.19(b) shows orange red color which takes the shape of the fixed bacteria. This experiment performed after rigorous washing of sprinkled powder samples on SAU fixed slides shows no decrease of color. This suggests binding of capping agent chitosan on cell walls of bacteria. In order to prove further this tunable emission in single sample and biocompatibility microstructures under fluorescent microscope were recorded which is shown in Figure 6.20. For confirmation of attachment of bacteria to chitosan capped ZnS:Mn we checked the attachment with fluorescent microscope operating in both visible and UV region. In order to see the attachment of these synthesized QDs with bacteria SAU, the slides of SAU were sprinkled with chitosan (0.1%) capped Mn^{2+} doped ZnS QDs. After washing these slides with distilled water several times we observed it under fluorescent microscope with different excitations as shown in Figure 6.20. It shows biotagging of chitosan capped ZnS: Mn NPs. Here SAU fixed slides sprinkled with ZnS: Mn QDs gives no color because excitation wavelength is not in the range of excitation. In Figure 6.20(b) the slide is showing orange red color which shows attachment of ZnS: Mn QDs with SAU. PL spectra of chitosan capped ZnS: Mn shows orange emission color with 320nm excitation, so in Figure 6.20(b), emission is due to Mn dopant sites. In Figure 6.20(c) we have captured image at some other place of the slide and changed UV filter of higher energy with different one so we get green color, which shows that, same sample is emitting different colors with change in excitation wavelength as we have explained above in PL studies.

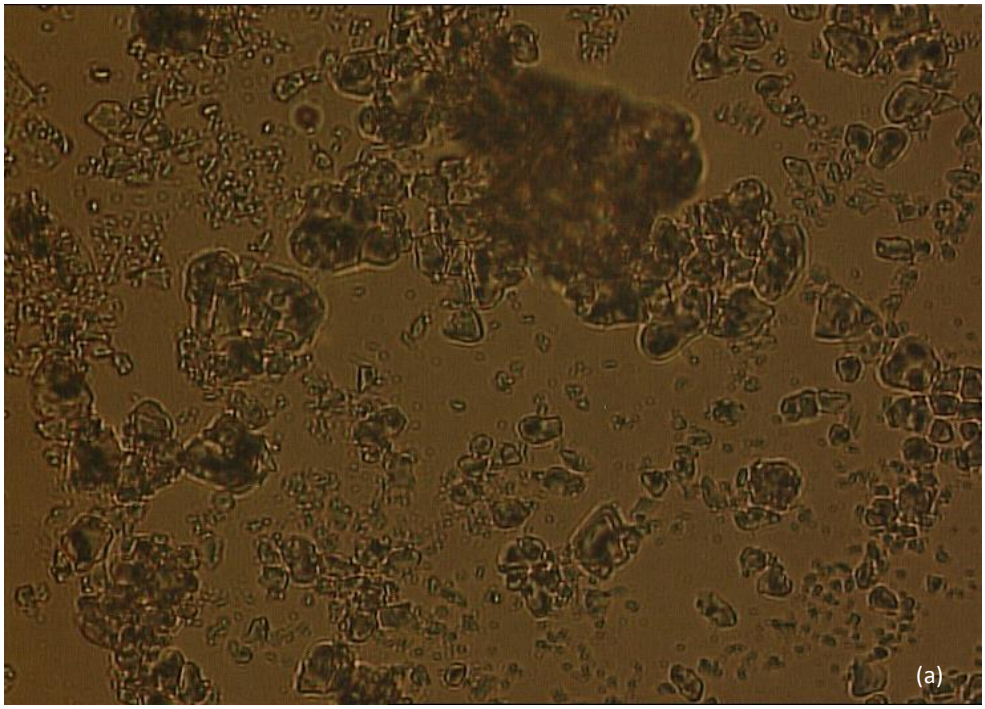
(a)

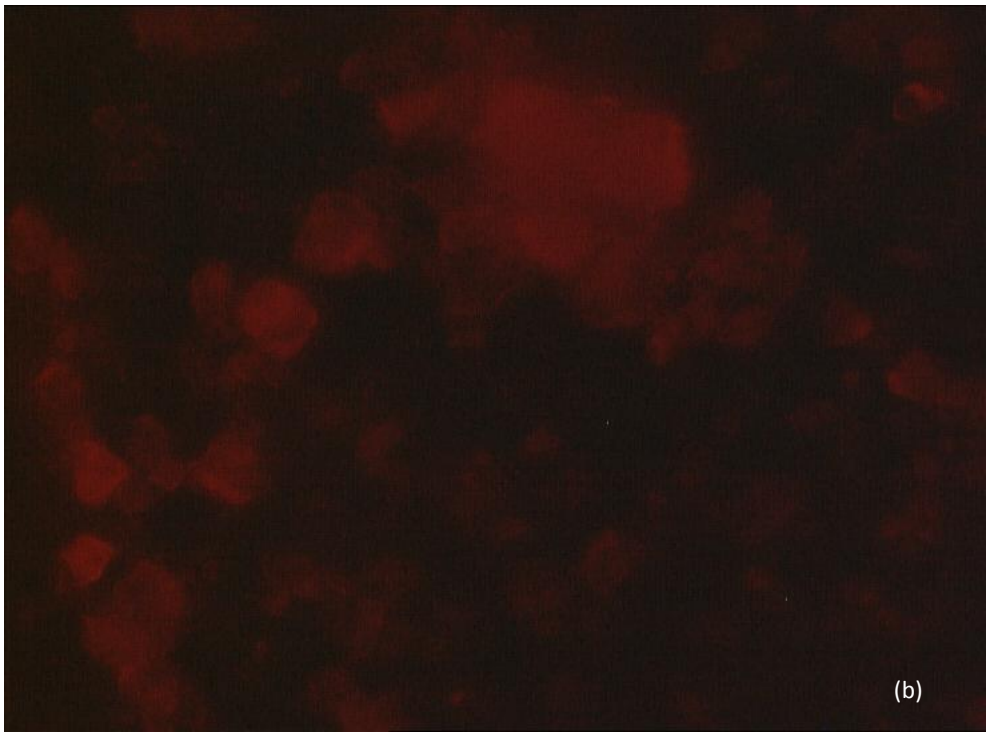
(b)

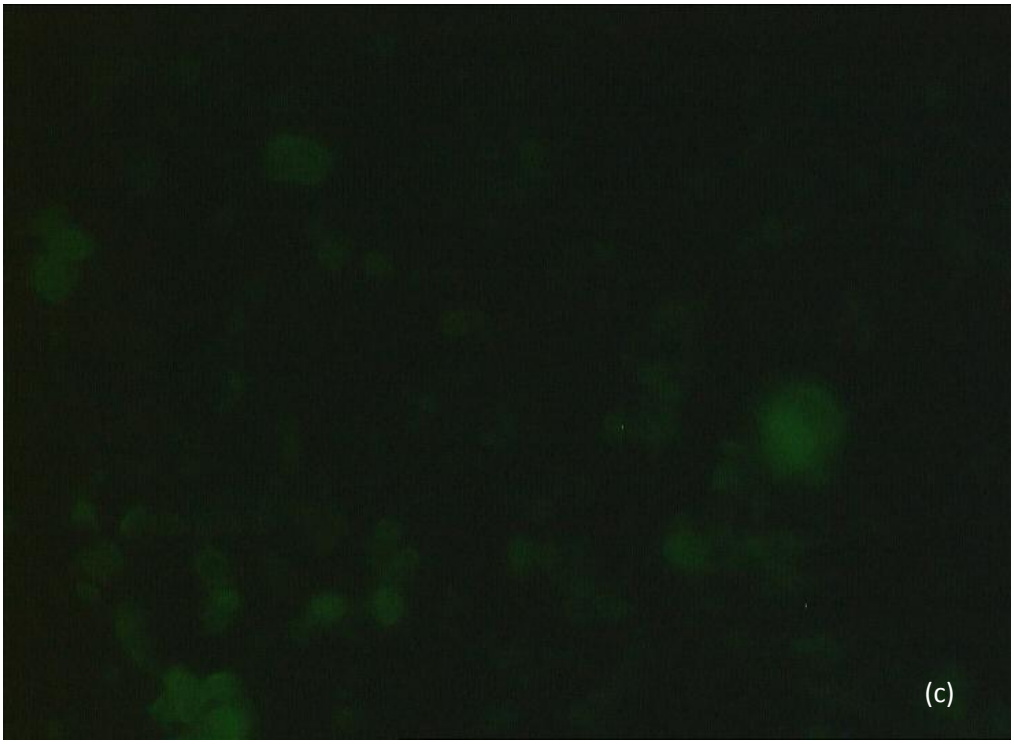

Figure 6.20 Fluorescent image of S. auerus bacteria attached with ZnS: Mn QDs (a) without any UV light (b) with UV excitation (c) with different excitation in UV.

Figure 6.21(a, b, c) shows TEM micrographs of control SAU bacteria, bacteria tagged with uncapped and chitosan capped ZnS Mn NPs. As shown in fluroscent micrograph images SAU bacteria appear circular having grapes like shape. Uncapped ZnS Mn NPs appears to be tagged on cell walls of bacteria whereas chitosan capped NPs appears to be tagged on cell walls as well as present in between SAU bacteria. It appears that chitosan is penetrating cell walls and making easy path for capped ZnS : Mn NPs to go inside SAU bacteria. Detailed biological studies related to toxicological studies is out of scope of this thesis. But this single hybrid organic-inorganic sample showing tunable emission in various visible regions with biotagging properties can be very useful in future biosensing applications.

(a)

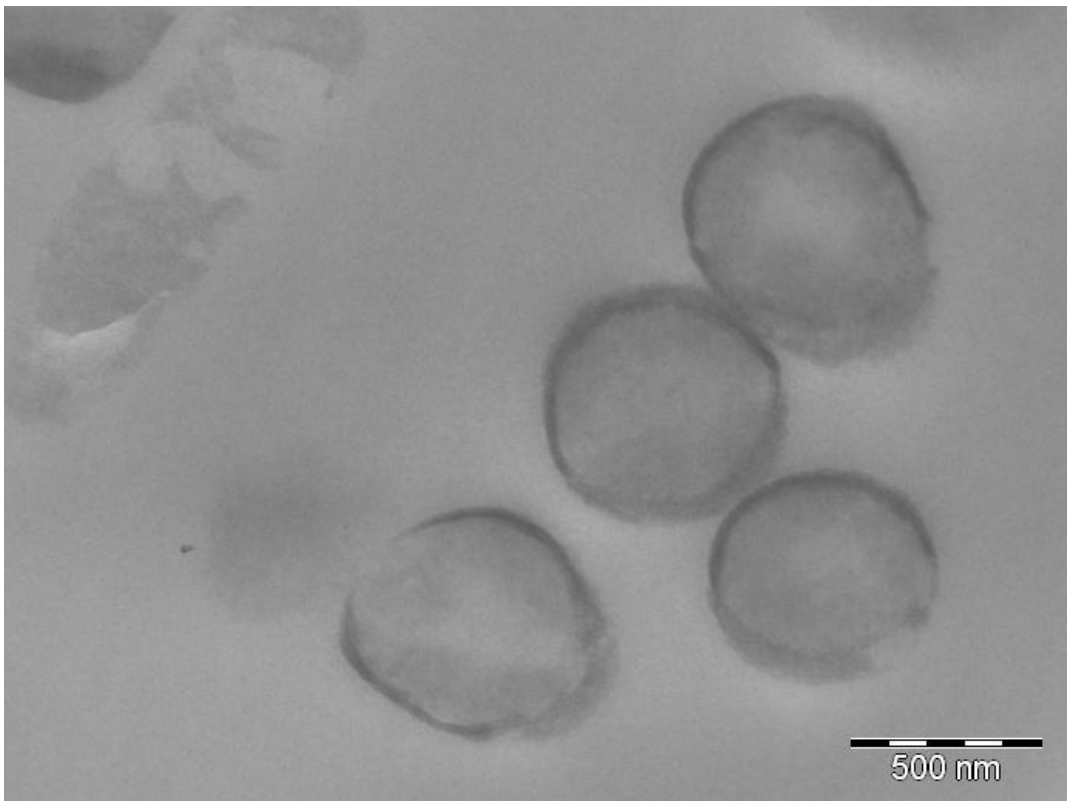
500 nm

(b)

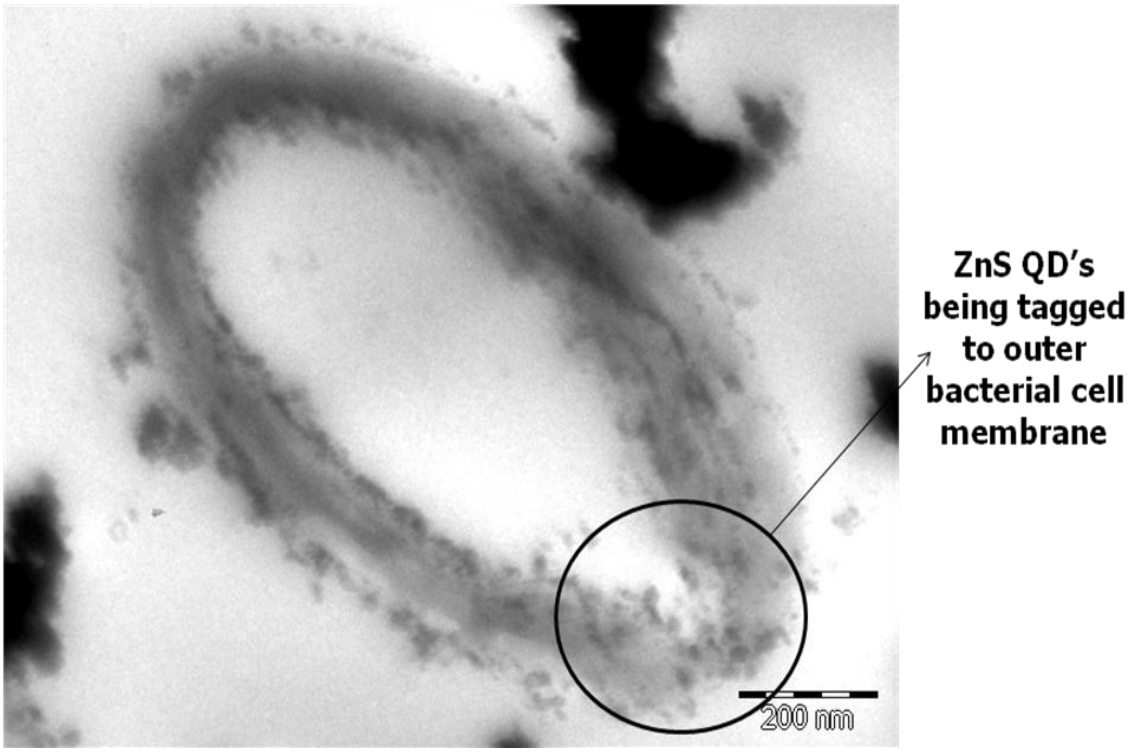
ZnS QD's being tagged to outer bacterial cell membrane
200 nm

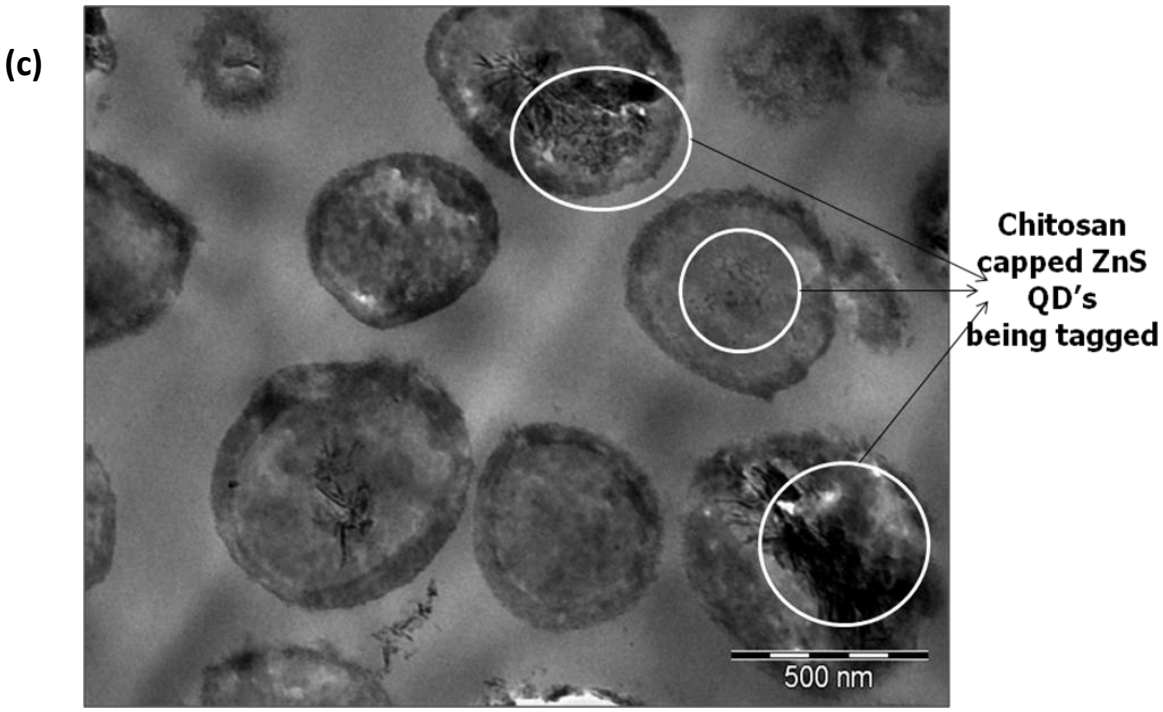

Figure 6.21 TEM images of (a) control S. auerus bacteria, (b) S. auerus bacteria attached with ZnS: Mn QDs, (c) S. auerus bacteria attached with CH capped ZnS: Mn QDs

6.2.8. Glucose Sensing

As glucose level in blood is usually used as a clinical indicator of diabetes, so rapid and accurate determination of glucose in human blood and urine is essential in the diagnosis of diabetes, which is affecting about 150 million people in the world [64]. Based on the enzyme-catalyzed oxidation mechanism glucose oxidase (GOD) has been widely used for optical and electrochemical determination of glucose. Also phosphorescence based detection for blood glucose is reported by tagging ZnS: Mn^{2+} with enzyme GOD [64]. But here we have used biocompatible polymer chitosan for functionalizing ZnS: Mn^{2+} core for sensing of glucose-D. So, tunable emission property is greatly enhanced with more specific emission color w.r.t. fixed excitation. Since these synthesized CH (1.0 at. %) capped NPs (single sample) are emitting two colors. So in the present study it is used for sensing of glucose. In this study, chitosan was used as surfactant to control the nanocrystal growth and to stabilize the nanocrystals against

aggregation. In addition, chitosan was also used to render the nanocrystals water soluble and provide functional chemical groups for further attachment of glucose. For glucose sensing five sets of 0.02 gm of ZnS: Mn^{2+} @ chitosan particles dispersed in 5 mL of Mili-Q water were made. First one is labeled as control. In other four sets 2.5µL, 5µL, 7.5 µL and 10µL of 0.5M glucose-D solution was added and used for further studies. As mentioned above in experimental section five sets were made for sensing studies of glucose with capped NP's. Though our PL studies exhibit multicolor emission from single sample but sample exhibiting high PL intensity (CH-1.0% capped NPs) has been selected for possible application in glucose-D sensing. Solution of glucose doesnot shows any considerable emission in the studied emission range (400-600nm) of CH capped ZnS: Mn^{2+} NPs. Figure 6.22 (a, b) shows PL intensity response of CH (1.0at. %) capped ZnS: Mn^{2+} at 284 and 325nm excitation with different concentration (0-10µL) of glucose–D. Quenching of PL intensity of NP's was observed with increasing glucose concentration from 0-10 µL. This quenching of PL peak for 284nm excitation is more pronounced than for 325nm excitation as shown in Fig 6.22 (a, b). This can be due to attachment of glucose with surface defects and adsorbed chitosan which will affect its luminescence peak at 400nm. The emission at 400nm for capped ZnS: Mn^{2+} NPs is due to surface defects and 587nm is due to Mn^{2+}. Also Mn^{2+} ions are incorporated inside the host ZnS at interstitial sites so interaction of Mn^{2+} with glucose is less probabilistic than with surface adsorbed chitosan and excess Zn^{2+} ions. So there is non- uniform quenching of PL intensity due to dopant related emission (587nm). It indicates that variation in PL intensity with concentration of surface adsorbed glucose is more at 284nm excitation having 400nm emission. When glucose is added there is change in surface of capped ZnS NPs. This is due to interactions between glucose and surface polymer (chitosan) which are shown in Figure 6.22c. These interactions may be due to: formation of hydrogen

bond between N of chitosan and H of glucose, formation of hydrogen bond between O of chitosan and H of glucose, formation of O-glycosidic linkage between glucose and chitosan and formation of N-glycosidic linkage between glucose and chitosan. Further research on the detailed mechanism of glucose sensing with CH capped NPs is being carried out.

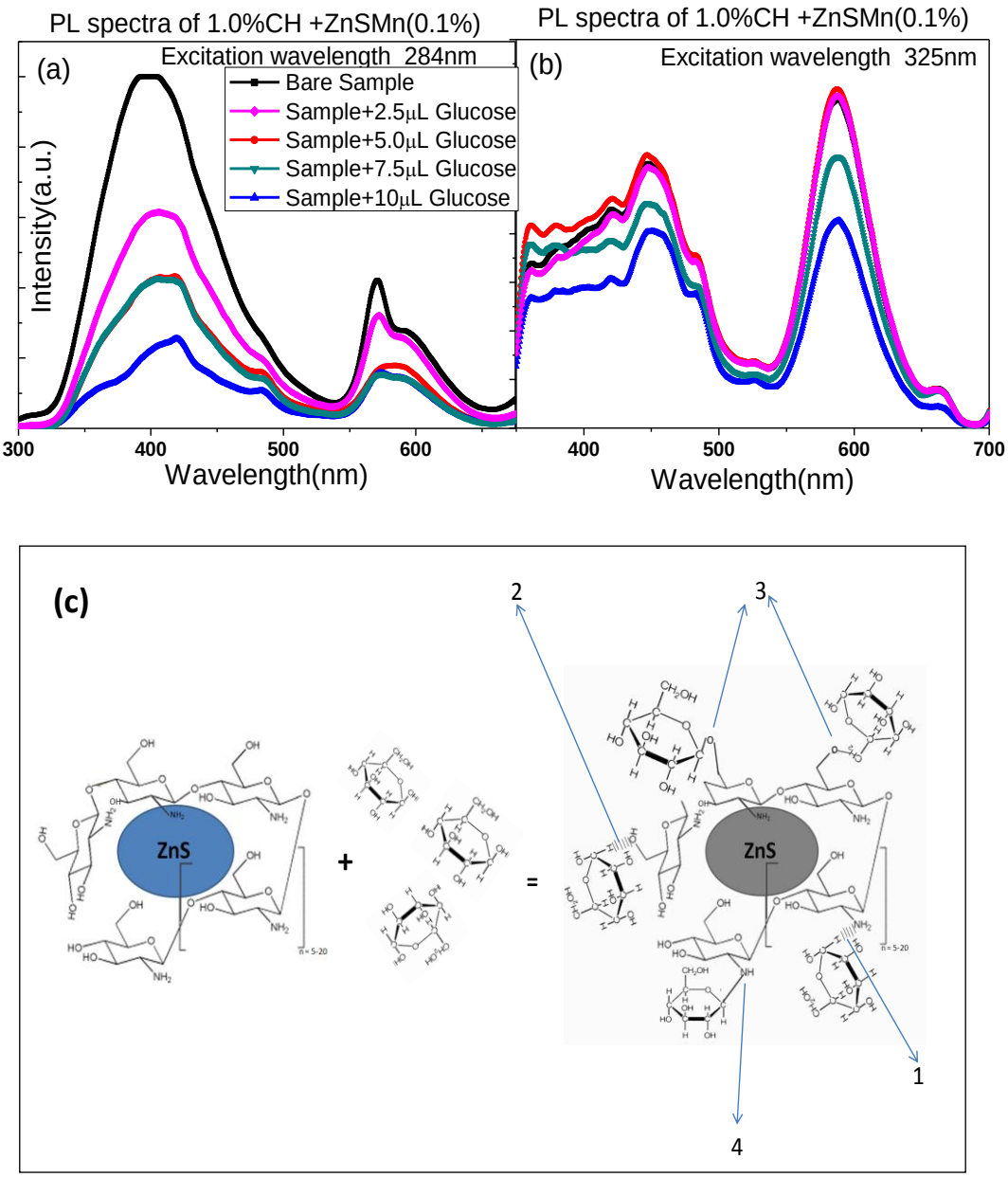

Figure 6.22 (a, b) Glucose detection by change in PL intensity of Chitosan capped ZnS Mn NPs at 284nm and 327nm excitation, (c) Sensing mechanism of glucose D with chitosan capped ZnS:Mn^{2+} NP's

Table 6.1 Showing particle size variation of all CH capped Mn doped ZnS NPs with absorption and photoluminescence results

Sample	Particle Size(nm)		Absorption wavelength (nm)	Excitation wavelength (nm)	Excitation wavelength (nm)	Band gap(eV)		Emission wavelength(nm)	
	XRD	TEM	UV-Vis. Spectra	410nm emission	590nm emission	UV-Vis.	PLE	284nm PLE	325nm PLE
CH (0.01%) ZnS: Mn (0.1%) NPs	2.15	3-4	325	281*	344*	4.65	-	400, 483	447, 587
CH (0.1%) ZnS: Mn(0.1%) NPs	2.13	3-4	325	284*	298, 340*	4.73	-	400, 487	447, 587
CH (1.0%) ZnS: Mn(0.1%) NPs	2.01	3-4	311	284	298, 318, 325	4.82	4.36	400, 587(weak)	447, 587

Table 6.2 Showing relative emission intensities of blue and orange color along with CIE coordinates.

Sample	$I_{400/587}$ (blue/orange)		CIE coordinates		Color O/P	
	For 284nm PLE	For 325nm PLE	For 284nm PLE	For 327nm PLE	For 284nm PLE	For 325nm PLE
CH (0.01%) ZnS: Mn (0.1%) NPs	1.11	0.66	-	-	green	Orange
CH (0.1%) ZnS: Mn(0.1%) NPs	1.35	0.85	-	-	green	Orange
CH (1.0%) ZnS: Mn(0.1%) NPs	3.59	0.79	(0.273, 0.20)	(0.344, 0.275)	Violet-Blue	Orange

* Data is not shown in Figures.

Spaces left vacant shows data not collected, not possible or not applicable.

6.3 DNA capped ZnS nanoparticles for enzyme sensing application

6.3.1 Brief introduction of DNA capping

Colloidal semiconductor nanomaterials exhibit color modulation which can be useful for various optoelectronic and biolabelling applications. Previous studies on CdSe and CdTe have shown tunable color modulation by varying the size of nanomaterials but toxicity of cadmium has created doubt for its end applications as biosensor [5, 8, 58, 65]. Biomolecules possess several unique fundamental features that make them very attractive for the construction of nanoassemblies [66-67]. One of such promising biomolecule is DNA. DNA has high physicochemical stability and mechanical rigidity and can be used as efficient linker or spacer molecules for guiding the nanoparticles assembly. Among the nanoparticle-biomolecule based hybrid materials, Semiconductor nanoparticles-DNA conjugates are of particular interest. Semiconductor nanoparticles (NPs) have much higher quantum efficiency for fluorescence as compared to their bulk counterparts. Surface charges as well as presence of capping molecules can modify the fluorescence emission of NPs. Surface functionalized NPs can be attached to larger particles or modified so as to suite a particular environment or application. It was further found that in contrast to fluorophores, fluorescence due to NPs is much more photo-stable. NPs can also be used to detect proteins or DNA [34, 65]. Semiconductor nanoparticles-DNA conjugates can be used as building blocks for preparing nano, meso and macroscopic architectures with well defined structures. The DNA functionalized nanoparticles can be used for ultra-sensitive and highly specific biological and biomedical detections. DNA have been used in generating novel nanostructure materials [66-71] and in templating the growth of nanocircuitry [72-73].

Willner et al. [74] employed complementary oligonucleotides to synthesize two types of CdS NPs and targeted them towards DNA attached to a solid substrate. It was shown that fluorescence intensity due to CdS NPs at 550 nm increased due to layer by layer aggregation of CdS NPs. Murphy group [6, 75] has shown that even DNA structure could be probed by its adsorption on CdS NPs. Their group reported that fluorescence at 480 and 600 nm in their Cd^{2+} rich CdS NPs (4 nm) get quenched rapidly in presence of 'kinked' DNA as compared to 'straight' or 'bent' DNA [8-9]. Also Kulkarni et al. [76] have reported protein detection with DNA capped CdS NPs. In all the previously reported work detection of proteins with DNA capped CdS NPs and functionalization with DNA has been done. But due to toxic effects of Cd^{2+} ions we have used ZnS as fluorescent materials and DNA as a capping agent. Here we have used DNA itself in synthesis of ZnS NPs (referred to as ZnS @ DNA) to control their size. While synthesizing such novel ZnS NPs, we also made some interesting observations, which will be presented here. Further we find that ZnS @ DNA particles may be useful as DNA interacting enzyme detectors.

6.3.2 Experimental Methods

6.3.2.1 Extraction of Plasmid DNA

E.coli cells were grown in Luria-Bertani Agar/Broth; the temperature for growth was 37^{o}C. Plasmid DNA used in present study as capping agent was extracted by Alkali lysis method. Log phase bacterial cells were centrifuged at 10,000 rpm for 5 min. Pellets were resuspended in 200µL of lysozyme solution (5 mg in 25 mM Tris, 50 mM glucose, 10 mM EDTA) and incubated for 30 min at 37^{o}C. After addition of 400 µL of 0.2 M NaOH-1.0% sodium dodecyl sulfate, the lysates were incubated on ice for 5 min. Subsequently, 300 µL of potassium acetate (pH 5.2, 5 M) was added and mixed carefully. The mixture was kept in ice bath for another 15 min. before centrifugation at 13, 000 rpm

for 20 min. The nucleic acid was redissolved in 1 mM ethylene diamine tetra-acetic acid (EDTA) and 10 mM Tris-HCl (pH 7.5) for digestion with *RNase A*. The lysate was then extracted with 900 µL phenol/chloroform followed by a chloroform extraction. DNA was precipitated with 0.7 volume of isopropanol and kept at –20^{o}C for 1 h. The pellet obtained after centrifugation for 30 min was washed with 70% ethanol.

6.3.2.2 Synthesis of DNA capped ZnS NPs

For this study chemicals of analytical grade were purchased from Sigma Aldrich. Zinc sulphide (ZnS) NPs were synthesized by chemical precipitation. 0.01M (20 mL) zinc acetate in ethanol solution (medium) was poured in reaction flask. Solution was stirred continuously for 2 h by magnetic stirrer. Now Plasmid DNA (Deoxyribonucleic Acid) having average size of 3550 base pair (bp) was added. This mixture was allowed to stir for another 1 h. Then to this reaction mixture sodium sulphide (0.01M) was added drop wise. Stirring was further continued for another 2 h. The crystal growth was further prevented by keeping the reaction flask in ultrasonic bath system. The ultasonication was continued for 10 h. The resulting white precipitate was centrifuged at 4000 rpm for 5 minutes and washed thrice with alcohol. This precipitate was subsequently washed continuously with hot Mili Q water (75^{0}C) for half hour to remove unbound polymer (DNA) and non reacted zinc and sulphide ions. White precipitate hence obtained was dried at 60^{0}C in vacuum oven for 8 hours. Hence DNA @ ZnS particles were synthesized. For further characterizations and studies particles were kept in cold (2-8^{0}C) to avoid further crystal growth.

6.3.3 XRD Studies

The XRD pattern of synthesized DNA capped ZnS NPs along with bulk ZnS powder is shown in Figure 6.23. It shows three broad peaks corresponding to the (111), (220) and (311) planes of FCC ZnS structure. It is to be noted that, the peaks observed in

the XRD pattern match well with those of the β-ZnS (cubic) reported in the ICDD Powder Diffraction files (File. No.77-2100). Broadening of the XRD peaks indicates the formation of ZnS NC's. The average crystallite size estimated from three planes by Scherer's formula [50] is 4-5nm for DNA capped ZnS NPs.

6.3.4 TEM Studies

Figure 6.24 shows the TEM micrograph of DNA capped NPs. It shows an abundance of nearly spherical crystallites, which have a mean particle size of 6.0-8.0nm having dark contrast in micrograph assembled on surface of plasmid DNA which is used as a capping agent. Figure 6.24 shows the magnified TEM micrograph of ZnS NPs assembled along plasmid DNA. It should be noted that a distribution of circular nanostructure shapes are formed by this process, reflecting the conformational diversity of the plasmid DNA as it adsorbs on the solid substrate. Additional experiments are now underway focusing on: (a) directing the DNA more exclusively toward a relaxed, open circular geometry, and, (b) acquiring a better understanding of the DNA-substrate interaction(s).

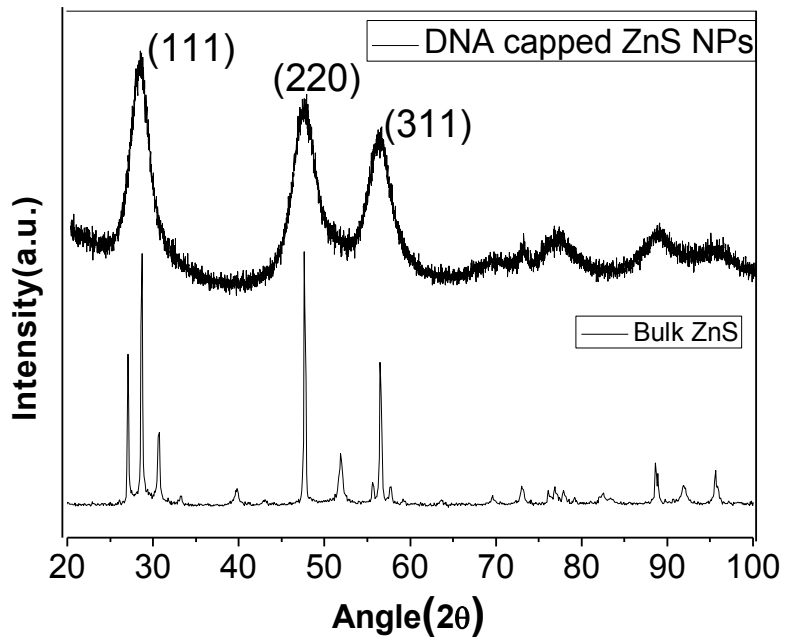

Figure 6.23 (a) XRD pattern of DNA capped ZnS nanoparticles with bulk ZnS powder.

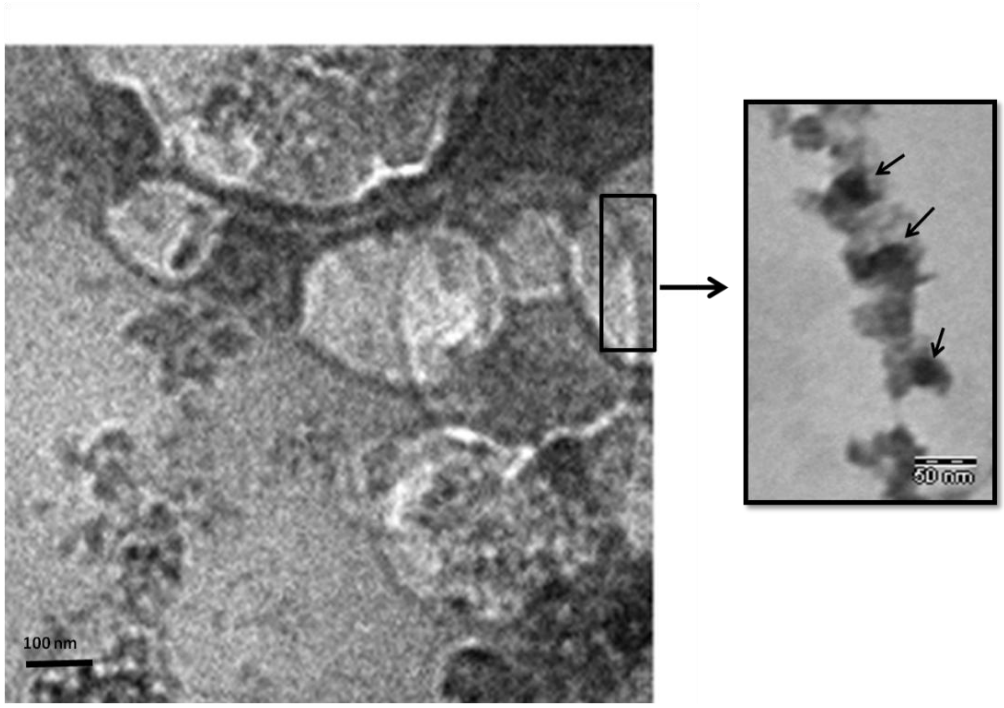

Figure 6.24 TEM of DNA capped ZnS nanoparticles (selected area TEM micrograph showing ZnS NPs assembled along plasmid DNA)

6.3.5 FTIR Studies

In order to examine whether DNA capped ZnS NP's have really been formed or not, FTIR studies of the samples were performed. Figure 6.25 illustrates typical spectrum of DNA capped ZnS NPs. For the sake of comparison a spectrum of DNA and uncapped ZnS NPs has also been plotted in the same diagram. Table-6.3 represents the FTIR spectra data showing the position of different groups of pure DNA along with some observed position in our experiment for uncapped ZnS and DNA capped ZnS NPs. The sharp peaks in all samples at 2358cm^{-1} is due to carbon which is instrumental error which is confirmed one. The weak peaks at 612cm^{-1} in uncapped ZnS NPs and DNA capped ZnS NPs are assigned to the ZnS band (i.e., corresponding to sulphides). Bands around 1200 and 1100 cm^{-1} are due to the characteristic frequency of inorganic ions. These modes indicate the presence of resonance interaction between vibrational modes of sulphide ions in the crystal. In FTIR spectra of DNA, a broad and medium band in the

800-666 cm^{-1} region results from out of plane N-H wagging. For DNA capped ZnS NPs this N-H wagging is also observed at same place confirming interaction of DNA with ZnS NPs. Moreover, this N-H band is not observed in uncapped ZnS NPs.

For capped ZnS NPs the N–H vibration at 3250 cm^{-1} was not clearly observed, although a shoulder at a lower frequency was observed indicating a change in hydrogen bonding. These characteristic frequencies (3,128 cm^{-1} and 3,032 cm^{-1}) for the peptide bond are not significantly affected by coupling with QD's surface. It is suggested that the vibrations are quenched or shielded by the ZnS NPs and the energy is transferred to the internal modes of the nanoparticles. One of the reasons may be that the molecules which are attached to the NPs on the side of IR source are getting absorbed and the vibrational energy is not transmitted to the detector, whereas the molecules on the other side of the NPs are getting transmitted but vibrational energy is not sufficient to be detected. C-H stretching occurs in the region of 3000-2840cm^{-1} in DNA capped ZnS NPs.

Medium band near 1250cm^{-1} in DNA and DNA capped ZnS NPs is due to C-N streching coupled with adjacents bonds in the molecule. Also the peaks at 1,252 and 1,209 cm^{-1} due to –C–N stretching are suppressed and significantly shifted to 1,212 and 1,067 cm^{-1} in the presence of ZnS NPs. O-H symmetric streching vibrations around 3400cm^{-1} appears in all samples. Sharp peak around 1667-1640cm^{-1} region in DNA and DNA capped ZnS NPs is due to streching vibrations of C=C which further confirms presence of DNA on ZnS NPs. The sholder around 1000-820 cm^{-1} in DNA is due to presence of P-O-P which converts into sharp peak at 850cm^{-1} in DNA capped ZnS NPs. Also, presence of P-O-CH_2 in DNA is confirmed by moderate peaks around 1640-1620cm^{-1} and strong peak at 1020-750cm^{-1} in FTIR spectra of DNA. P=O in DNA is showing its charactersitc peak in the range of 1220-1200cm^{-1} which is clearly observed in

DNA capped ZnS NPs. This modification in peaks of DNA in DNA capped NPs is due to attachment of zinc ions and hence ZnS on negative charge of $P=O^-$ and $P-O^-$ which results some deviation in 1200-500cm^{-1} range for DNA capped ZnS NPs in comparison to only DNA. Further removal of characterstic emission (to be discussed in PL studies later) of zinc defects explains attachment of $P=O^-$ and $P-O^-$ with excess zinc ions. Based on TEM and FTIR results proposed mechanism of assembly of ZnS NPs on plasmid DNA acting like templete is shown in Figure 6.26.

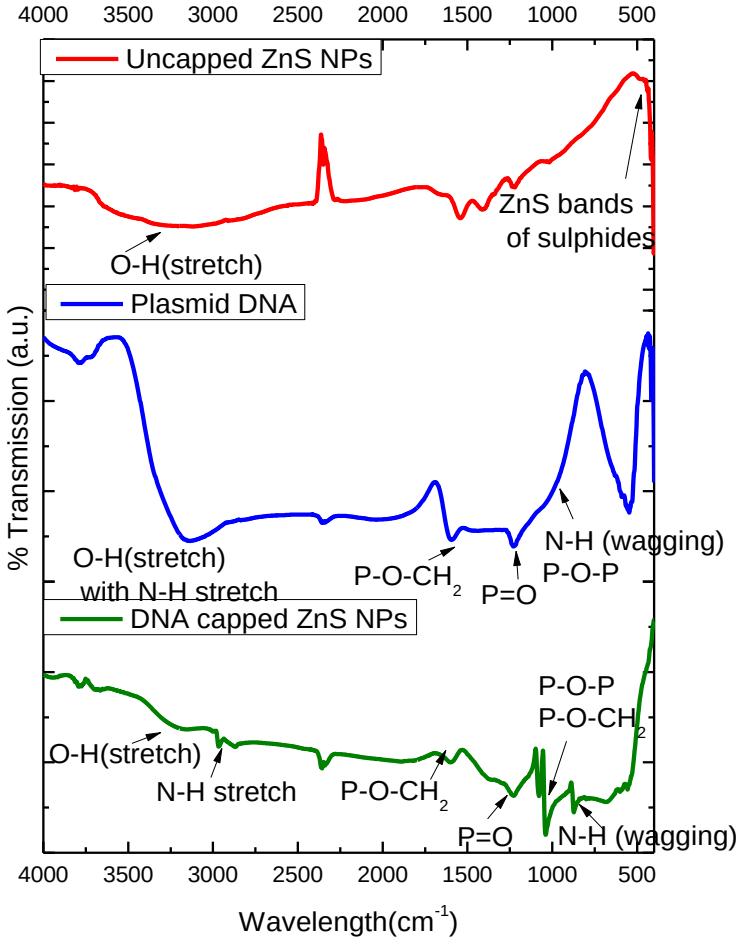

Figure 6.25 FTIR spectra of DNA and DNA capped ZnS NPs.

Table 6.3 Various peak assignments for DNA, DNA capped ZnS and Uncapped ZnS NPs

Peak assignment	Frequency(cm^{-1})		
	DNA	**ZnS + DNA**	**ZnS**
N-H (wagging), N-H stretching	800-666, 3250	800-666, 3128, 3032	-
C-H (stretch)	3000-2840	3000-2840	-
C-N(stretch)	1250	1250	-
O-H(stretch)	3400	3400	3400
C=C (stretch)	1667-1640	1667-1640	-
P-O-P	1000-820	850	-
P-O-CH_2	1640-1620 1020-750	1640-1620, 850	-
P=O	1220-1200	1220-1200	-

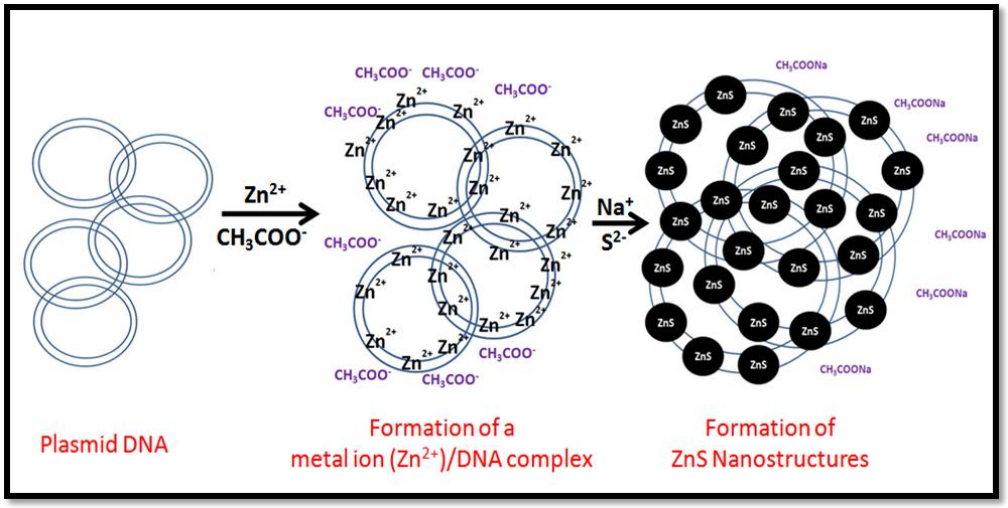

Figure 6.26 Proposed mechanism for growth of ZnS NPs on surface of plasmid DNA which behaves as template.

6.3.6 UV-Visible Studies

Figure 6.27 shows UV-Visible spectra of DNA capped ZnS NPs which shows absorption at 329nm along with weak shoulder at 265nm.This weak shoulder at 265nm is due to DNA present on surface of ZnS NPs. This also confirms presence of DNA with

ZnS NPs. Using the Manifacier model, the absorption coefficients (α) were calculated in the region of strong absorption [51]. The exact values of the band gap were determined by extrapolating the straight line portion of the $(\alpha hv)^{1/n}$ versus hv graphs to the hv axis as shown in Figure 6.27 (inset). From the plots the correct values of band gap was obtained as 3.86eV for DNA capped ZnS NPs. The band gap values were found to increase due to reduced particle size showing strong quantum confinement effects which is higher than the bulk value 3.6 eV.

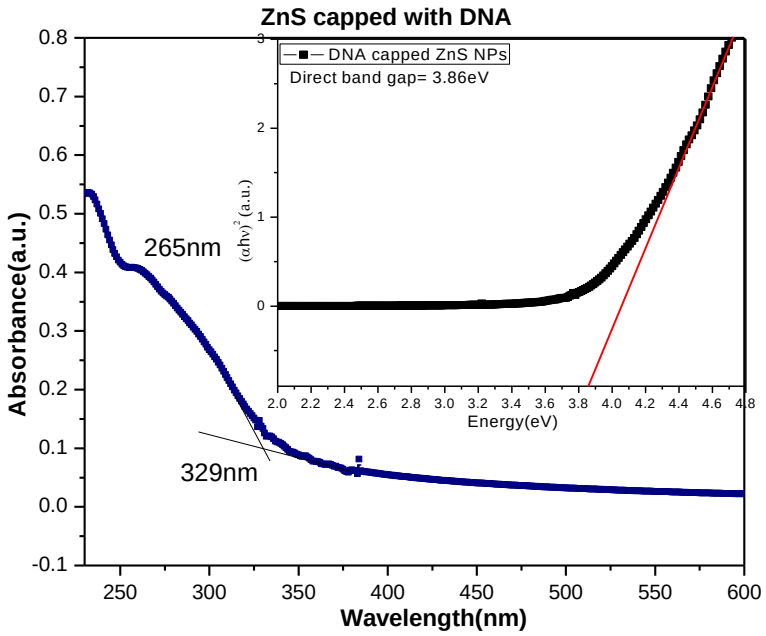

Figure 6.27 Absorption spectra of DNA capped ZnS nanoparticles

6.3.7 Photoluminescence Studies

Figure 6.28 shows PL spectra of DNA capped ZnS NPs along with PL spectra of enzyme functionalized DNA capped ZnS NPs. PL spectra is recorded at fixed excitation wavelength of 265nm. Broad peak around 400nm is observed for all the samples. Yanagida et al. [77] have observed longer wavelength defect luminescence at about 420nm in addition to the band gap luminescence in ZnS NPs. It is well reported and

discussed in previous chapters that emission due to sulphur vacancies is around 420 nm [51, 42]. However, with excess sulphur these vacancies are filled so there is quenching effect in emission of 420nm [42]. But at low concentration of sulphide ions during precipitation of ZnS, energy levels of large number of sulphur vacancies (Vs) are formed which lies just below the conduction band. These vacancies are doubly ionized donor centers. Sulphur vacancies act as electron traps whereas zinc vacancies, excess sulphur, excess zinc act as hole traps which lie just above valence band [42]. Also impurity centers if added can act as hole traps. Due to this, electron hole recombination at the acceptor centers will lead to sulphur vacancy related multiple emissions in case of undoped ZnS NPs. Emission peak at 402nm in all samples can be due to emission from sulphur vacancy to valence band. The increase in intensity of this peak around 402nm in comparison to other peaks at 438nm and 461nm can be assigned for the role of capping agents. First DNA molecules are adsorbed on surface of ZnS by making bonds with excess zinc or sulphur which are acting as defects. These exhibit two types of intensity variation. First a decrease in emission intensity at 438 and 461nm is observed which is mainly due to transfer of electron from trap states to zinc defect states**.** Also as shown in FTIR spectra that ZnS has interacted with DNA so effective capping in these cases has passivated the unreacted zinc ions which are normally responsible for emission at 438nm and 460nm region. Also it is discussed above that excess zinc of ZnS has interacted with $P{=}O^-$ and $P{-}O^-$ which results elimination of its characterstic emission. Secondly in our samples excess sulphur is not taken, so probability of sulphur vacancies is more. It is well reported by Manzoor et al. [4, 10] that excited state life time of 420nm emission is less in comparison to other transitions so this can also be the reason of increased emission intensity of peak at 402nm in all the samples in comparison to other peaks (438, 461nm).

TEM studies also suggests DNA is acting like template for growth of ZnS nanoparticles on its surface. When these synthesised NPs assembled on DNA interact with enzyme (pepsin) there is decrease in PL intensity of ZnS NPs. With further increase in concentration of enzyme (pepsin) decrease in emission intensity of DNA capped ZnS NPs is observed. It is observed with increase in concentration of pepsin upto 10µL there is considerable decrease in PL of ZnS NPs but with further increase in concentration of enzyme (pepsin) to 15 µL there is again rise in PL intensity along with small blue shift in peak from 400 to 379nm. These studies suggest PL sensing is very sensitive to concentration of enzyme (pepsin) which further suggest enzyme sensing (by quenching of PL peal intensity) is accurate up to 10 µL which can be further studied with more number of samples with concentrations taken in small steps. This would enable us to find exact concentration in between 10-15 µL upto which decrease in PL intensity is sensing the presence of enzymes with increasing concentrations. Further experiments on detailed mechanism of quenching of PL intensity of DNA capped ZnS in presence of pepsin is required for its potential use in sensing applications. Figure 6.29 shows proposed mechanism for interaction of pepsin with DNA template assisted ZnS NPs.

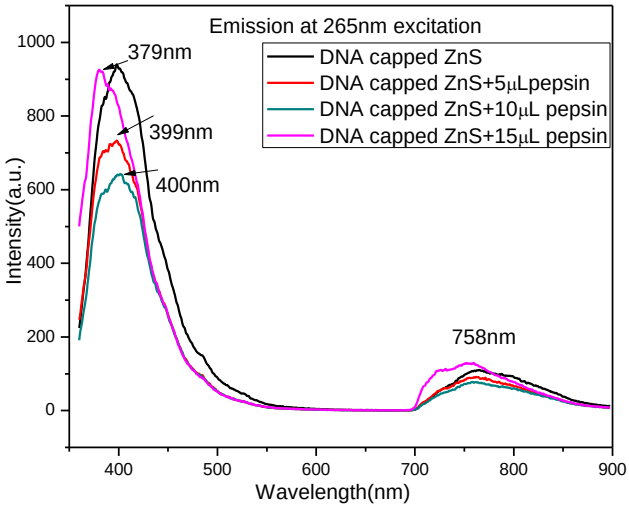

Figure 6.28 PL spectra of DNA capped ZnS NPs with various enzyme concentrations. (Excitation wavelength and sample specifications are written as inset for each case).

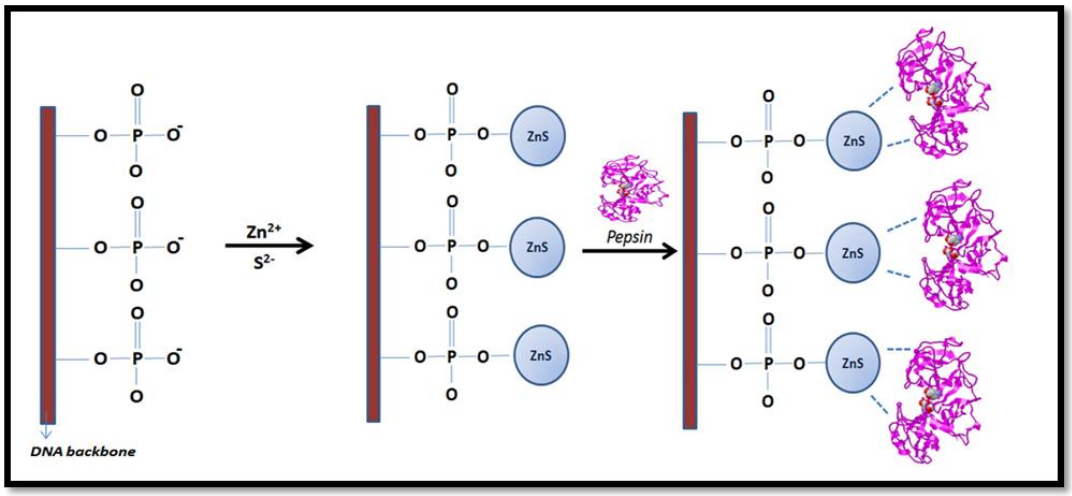

Figure 6.29 Proposed mechanism for interaction of pepsin with DNA template assisted ZnS NPs.

6.3.8 Refrences

[1] J.-H. Choy, E.-S. Jang, J.-H. Won, J.-H. Chung, D.-J. Jang and Y.-W. Kim, *Adv. Mater*., **15**, 1911 (2003).

[2] D. H. Lee, S. J. Kim, S. Y. Heo and D.-J. Jang, *Appl. Phys. Lett*., **87**, 233103 (2005).

[3] Z. Quan, D. Yang, C. Li, D. Kong, P. Yang, Z. Cheng and *J. Lin,Langmuir*. **25**, 10259 (2009).

[4] K. Manzoor , S. R. Vadera , N. Kumar and T. R. N. Kutty, *Solid State Communications*. **129**, 469 (2004).

[5] D. Denzier, M. Olschewski and K Sattler, *J. Appl. Phys*, **84**, 5 (1998).

[6] C. B. Murray, D. J. Norris and M. G. Bawendi, *J. Am. Chem. Soc.* **115**, 8706 (1993).

[7] J. E. B. Katari, V. L. Colvin and A. P. Alivisatos, *J. Phys. Chem*. **98**, 4109 (1994).

[8] N. Murase, K. Hirata, T. Yazawa and T. Kushida, *J. Phys. Chem. B.* **103**, 754 (1999).

[9] R.N. Bhargava, *J. Lumnin*. **70**, 85 (1996).

[10] K. Manzoor, S. R. Vadera a, N. Kumar and T. R. N. Kutty, *Mater. Chem and Phys*. **82**, 507 (2003).

[11] J.F. Suyver, S.F. Wuister, J.J. Kelly and A. Meijerink, *Nano Lett*. **1**, 429 (2000).

[12] Wei Chen, Alan G. Joly, Jan-Olle Malm, Jan-Olov Bovin, Shaopeng Wang , *J. Phys. Chem. B*, **107**, 6544 (2003).

[13] Stoferle Thilo, Scherf Ullrich and R. F. Mahrt, *Nano Lett*. **9**, 453 (2009).

[14] D. Qi, M. Fischbein, M. Drndic and S. Selmic, *Appl. Phys. Lett*. **86**, 93103 (2005).

[15] S. Gao, H. Zhang, R. Deng, X. Wang, D. Sun and G. Zheng, *Appl. Phys. Lett*. **89**, 123125(2006).

[16] J. Huang, G. Li, E. Wu, Q. Xu and Y. Yang, *Adv. Mater*. **18**, 114 (2006).

[17] D. Gupta and M. K. Deepak, *Opt. Mater*. **28**, 295 (2006).

[18] A. Misra, P. Kumar, M. N. Kamalasanan and S. Chandra, *Semicond. Sci. Technol*. **21**, R35 (2006).

[19] G. Tu, Q. Zhou, Y. Cheng, L. Wang, D. Ma,X. Jing and F. Wang, *Appl. Phys Lett*. **85**, 2172 (2004).

[20] J. Liu, Q. G. Zhou, Y. X. Cheng, Y. H. Geng, L. X. Wang, D. G. Ma, X. B. Jing and F. S. Wang, *Adv. Mater*. **17**, 2974 (2005).

[21] S. Nizamoglu, T. Ozel, E. Sari and H. V. Demir, *Nanotechnology*. **18**, 065709 (2007).

[22] J. Zou, J. Liu, H. Wu, W. Yang, J. Peng and Y. Cao, *Org. Electron*.**10**,843 (2009).

[23] H. B. Wu, J. H. Zou, F. Liu,A. Mikhailovsky,G. C. Bazan ,W. Yang and Y. Cao, *Adv. Mater*. **20**, 696 (2008).

[24] Y. Zhang, F. Huang, Y. Chi and A. K-Y Jen, *Adv. Mater*. **20**, 1565 (2008).

[25] Y.H. Xu, J. B. Peng, Y. Q. Mo, Q. Hou and Y. Cao, *Appl. Phys. Lett*. **86**,163502 (2005).

[26] Q. L. Niu, Y. H. Xu and J. B. Peng *J. Lumin*. **126**, 531(2007).

[27] S. Coe, W. K. Woo, M. Bawendi and V. Bulovic, *Nature*, **420**,800 (2002).

[28] H. S. Jang, H. Yang, S. W. Kim, J. Y. Han, S. G. Lee and D. Y. Jeon, *Adv. Mater*. **20**, 2696 (2008).

[29] A. Rizzo, M. Mazzeo, M. Palumbo, G. Lerario, S. D'Amone, R. Cingolani and G. Gigli, *Adv. Mater*. **20**,1886 (2008).

[30] W. U. Huynh, J. J. Dittmer and A. P. Alivisatos, *Science*, **295**, 2425 (2008).

[31] P. Brown and P. V. Kamat, *J. Am. Chem. Soc*., **130**, 8890 (2008).

[32] L. Medintz, A. R. Clapp, H. Mattoussi, E. R. Goldman, B. Fisher and J. M. Mauro, *Nat. Mater*. **2**, 630 (2003).

[33] S. Pathak, S. K. Choi, N. Arnheim and M. E. Thompson, *J. Am. Chem. Soc*. **123**, 4103 (2001).

[34] C. W. Chan Warren and S. Nie, *Science*, **281**, 2016 (1998).

[35] A. Nag and D. D. Sarma, *J. Phys. Chem. C*, **111**, 13641 (2007).

[36] H .V. Demir, S. Nizamoglu, E. Mutlugun, T. Ozel , S. Sapra , N. Gaponik and A. Eychmuller, *Nanotechnology* ,**19**, 335203 (2008).

[37] Haizhu Sun, Junhu Zhang, Ye Tian, Yang Ning, Hao Zhang, Jie Ju, Delong Li, Shidong Xiang, Bai Yang, *Chem. Phys. Chem*. **7**, 2492 (2006).

[38] R. N. Bhagava, D. Gallagher, X. Hong and A. Nurmikko, *Phys. Rev. Lett*. **72**, 416 (1994).

[39] K. E. Waldrip, J. S. I I I Lewis, Q. Zhai, M. R. Davidson,P. H. Holloway and S. S. Sun, *Appl. Phys. Lett.* **76**, 1276 (2000).

[40] F. Parsapour, D. F. Kelley, S. Craft and J. P. Wilcoxon, *J. Chem. Phys*. **104**, 4978 (1996).

[41] A. D. Dinsmore, D. S. Hsu, S. B. Qadri, J. O. Cross,T. A. Kennedy, H. F. Gray and B. R. Ratna, *J. Appl. Phys*. **88**, 4985 (2000).

[42] J. F. Suyver , S. F. Wuister,J. J. Kelly and A. Meijerink, *Nano Lett*. **1**, 429 (2001).

[43] P. H. Borse, D. Srinivas, R. F. Shinde, S. K. Date, W. Vogel and S. K. Kulkarni, *Phys. Rev. B.* **60**, 8659 (1999).

[44] S. Sapra, A. Prakash, A. Ghangrekar, N. Periasamy and D. D. Sarma, *J. Phys. Chem. B.* **109**, 1663 (2005).

[45] C. Graf, A. Hofmann, T. Ackermann, C. Boeglin, R. Viswanatha, X. G. Peng, A. F. Rodr´ıguez, F. Nolting and E. R¨uhl, *Adv.Funct. Mater*. **19**, 1 (2009).

[46] Y. He, H. Wang and X. Yan, *Anal. Chem*. **80**, 3832 (2008).

[47] A. Nag and D. D. Sarma , *J. Phys. Chem. C* , **111**, 13641 (2007).

[48] S. Kar and S. Biswas , *J. Phys. Chem*. C, **112**, 11144 (2008).

[49] Z. Quan, D. Yang ,C. Li, D. Kong, P. Yang, Z. Cheng and J. Lin, *Langmuir*, **25**, 10259 (2009).

[50] B.D. Cullity, Elements of X-Ray Diffraction, second ed., Addison-Wesley publishing, Massachusetts, **2003.**

[51] J.I. Pankove, Optical Processes in Semiconductors (Prentice-Hall, Englewood Cliffs, NJ) (1971).

[52] YQ. Li, A. Rizzo, M. Mazzeo, *J. Appl. Phys*. 97, 113501 (2005).

[53] S. C. Erwin, L. Zu, M. I. Haftel, A. L. Efros, T. A. Kennedy and D.J. Norris, *Nature*. **436**, 9194 (2005).

[54] K. Sooklal, B. S. Cullum, S. M. Angel and J. Murphy,J. Phys. Chem.,**100**,4551 (1996).

[55] M. R. Kim, J. H. Chung and D. J. Jang, Phys. Chem. Chem. Phys. **,** 11**, 1003 (2009)**

[56] W. Chen, A. G. Joly, J.-O. Malm, J.-O. Bovin and S. Wang, J. Phys. Chem. B, **107**, 6544-6551 (2003)

[57] H. Wei, H. Sun, H. Zhang, C. Gao and B. Yang, Nano Res, **3**, 496–505 (2010)

[58] *Zewei* Quan, Dongmei Yang, Chunxia Li, Deyan Kong, Piaoping Yang, *Langmuir* **25**, 10259 (2009).

[59] Dae-Ryong Jung, Jongmin Kim and Byungwoo Park, *Appl. Phys. Lett*. **96**, 211908 (2010).

[60] M. Sharma, S. Kumar, and O. P. Pandey, *J Nanopart. Res*. **12 (7)**, 2655 (2010).

[61] R. Sarkar, C. S. Tiwary, P. Kumbhakar, S. Basu and A K. Mitra, *Physica E*. **40**, 3115 (2008).

[62] M. Sharma, S. Singh, O.P Pandey, *J. Appl. Phys*. **107**, 104319 (2010).

[63] F. Kong et al. J. Lumni, doi: 10. 1016/j.jlumin.2010.12.009 (2010).

[64] Wu P. He Yu. Wang, He-Fang and Yan Xiu-Ping. *Anal. Chem*. **82**, 1427 (2010).

[65] F. Caruso. *Adv. Mater*. **13 (1)**, 11 (2001.).

[66] E. Katz, I. Willner, *Angew. Chem. Int. Edit.* ***43***, 6042 (2004).

[67] Niemeyer, C. M. *Angew. Chem. Int. Edit.* ***40***, 4128 (2001).

[68] C. A. Mirkin, R. L. Letsinger, R. C. Mucic, J. J. Storhoff, *Nature.* ***382*** , 607 (1996).

[69] C. M. Niemeyer, W. Burger, J. Peplies, *Angew. Chem. Int. Edit.* **1998**, *37*, 2265-2268.

[70] A. P. Alivisatos, *Science.* ***271***, 933 (1996).

[71] A. M. Cassell, W. A. Scrivens, J. M. Tour, *Angew. Chem. Int. Ed.* **1998**, *37*, 1528-1531.

[72] E. Braun, Y. Eichen, U. Sivan, Ben-Yoseph, G. *Nature*, ***391***, 775 (1998).

[73] K. Keren, Krueger, R. Gilad, G. Ben-Yoseph, U. Sivan, E. Braun, *Science*, ***297***, 72 (2002).

[74] I. Willner, F. Patolsky, A. Lichtenstein, Anal. *Sci*. **17**, 351 (2001).

[75] R. Mahtab, J.P. Rogers, C.P. Singleton, C.J Murphy, *J. Am. Chem. Soc*. **118,** 7028 (1996).

[76] S.K. Kulkarni A.S. Ethiraj, S. Kharrazi, D.N. Deobagkar and D.D. Deobagkar

, *Biosensors and Bioelectronics*. **21**, 95 (2005).

[77] S. Yanagida , Y. Ishimaru, Y. Miyake, T. Shiragami, C. Pac, K. Hashimoto, T. Sakata, *J. Phys. Chem.*, **93**, 2576 (1989).

CHAPTER 7

CONCLUSIONS AND FUTURE SCOPE

Overview

The present chapter summarizes the results of various experiments described in previous chapters. At the end the suggestions for future work on the basis of results obtained in the work is given.

7.1 Conclusions

In the present work emphasis is on synthesis and characterizations of ZnS NPs with and without capping agents. Capped ZnS NPs shows better stability, uniform size distribution, decrease in particle size, blue shift of absorption edge and enhanced PL intensities than corresponding uncapped ZnS NPs synthesized under similar conditions. Optical (UV-Visible absorption and photoluminescence spectroscopy) and morphological (XRD, TEM, SAED, EDX etc.) studies of synthesized uncapped and capped ZnS NPs with various capping agents (PVP, Chitosan, Mercaptoethanol, Thioglycerol, SHMP etc.) having different concentrations (0.1, 0.5, 1.0, 1.5, 2.0%) have been done. The effect of different capping agents on optical and morphological properties of ZnS NPs gives information about tuning emission color characteristics at nano regime with variation in capping amount and capping agents. XRD and TEM studies show ZnS NPs synthesized by chemical precipitation route are in nano regime. With variation in capping agents and their amount large change in particle size is not observed for all studied series. But optical properties from UV-Visible absorption studies and photoluminescence studies have shown variation in band gap and emission characteristics even with small variation in capping agents of different nature. Earlier in literature reports it is reported that with variation in particle size and due to quantum confinement effect emission color can be tuned in visible region. Here in this case emission color characteristics are shifted with variation in capping amount. It is generally observed for all capping agents that emission color of ZnS shifts from 360 to 460nm region i.e from UV to blue region with increase in capping concentration. This is because of passivation of interstitial sulphur and its vacancy by increase in concentration of adsorbed capping molecules. But in case of SHMP capped ZnS NPs shifting of emission peak from

blue to UV has been observed which is opposite of other studied series as mentioned above. It has been explained by quantum confinement effect as done earlier by many groups. The ZnS NPs synthesized by chemical precipitation method gives broad emission spectra consisting of four well reported emission multiples viz. 392, 430, 461 and 484nm respectively. In order to enhance and eliminate one emission out of all mentioned above different capping polymers with different concentrations were used. Integrated emission intensity for all the series has been compared. With increase in capping concentration of particular capping agent we find increase in PL intensity and passivation property but it is found that after some specified concentration of particular capping polymer all properties start to degrade. It is observed that this particular capping concentration is different for different polymers. It can be concluded that optical properties are very sensitive to nature and amount of capping polymer. Also depending on required emission color, capping amount and its nature can be changed. But it is reported in literature that optical properties can be tuned with small variation in amount of precursors, annealing temperatures and time of annealing for ZnS NPs. But in all cases particle size and crystal structure also changes as it is sensitive to these. So by varying capping agents and their amount optical properties can be tuned without changing their morphology.

Apart from this it is earlier reported that many samples are needed with controlled synthesis procedures to obtain tunable emission properties. Also in our case discussed above for capped NPs many samples with different capping concentrations are needed for tuning emission color. In order to decrease number of samples for achieving tunable emission color two capping agents were selected from all studied series and a new kind of tunable emission is observed and explained which is excitation induced. Out of all studied series PVP (0.1-

2.0%) capped ZnS and chitosan (0.1-2.0%) capped ZnS NPs shows a new kind of tunable emission which is excitation induced. Earlier for tunable emission samples of different particle sizes or samples with different dopants were required. But in our case single sample has been observed to emit two or three colors. The reason for this new type of tunable emission is explained by FRET mechanism. In the first studied series of PVP capped ZnS NPs we have observed white light emission from the PVP capped Mn^{2+} doped ZnS NPs synthesized by an easy and facile colloidal route. We have investigated the role of optimum capping concentration for enhanced and tunable luminescence properties as structural properties do not vary a lot with change in capping concentration. Efficient energy transfer from capping polymer PVP to sulphur vacancies (trap states) of the host ZnS and from ZnS to dopant Mn^{2+} is reported for single sample at variable excitation energies. Furthermore, by varying excitation wavelength in single hybrid organic- inorganic sample tunable emission is observed in nearly all visible regions (423-590nm) which according to earlier reports needs many samples. To the best of our knowledge, no report has been found on tuning emission color from blue to orange (including white) in a single sample. The origin of white luminescence was studied by steady-state spectroscopy and further confirmed by calculating its CIE color coordinates, which show tunable emission, including white color in single sample. CIE color coordinates shows shifting from (0.26, 0.23) to (0.32, 0.28) and (0.35, 0.29) with variation in excitation energy showing tunable color characteristics in single sample. The study gives an idea of how the emission from trap states of the host can be combined with emission from the dopant Mn^{2+} ions that extend towards longer wavelength to impart bright and efficient white light (along with blue and orange in the same sample), potentially useful for sensing applications.

For the second selected series (CH capped ZnS NPs) we have also synthesized samples by doping Mn ions in CH capped ZnS NPs. The sample showing high PL intensity from above mentioned series has been selected for doping studies. As mentioned above also by doping we can tune emission color but in this case single sample has given color from dopant ions and host semiconductor ZnS NPs. This has been achieved by changing excitation wavelengths from high UV to low UV which has been explained by studying PL characteristics of pure chitosan that shows emission characteristics of their own around 400nm which is responsible for enhancement of blue color when excited in energy levels of CH. Secondly for band to band excitation orange emission is observed and blue color of pure chitosan and trap states is quenched partially. So we have shown a shift in PL emission spectra from orange to blue in chitosan capped Mn-ZnS sample. Our studies suggest that different colors in visible range can be observed in a single organic-inorganic hybrid sample with change in excitation wavelength. Earlier it is reported that only PL intensity varies if excitation wavelength is changed. But here we have shown multicolor emission in single sample with enhanced PL intensity. Energy transfer mechanism from donor (chitosan) to acceptor states (ZnS) based on resonance energy transfer has been discussed in detail. CIE color coordinates shows shifting from (0.273, 0.200) to (0.34, 0.275) with variation in excitation energy showing tunable color characteristics in single sample.

Biotagging of SAU bacteria with uncapped and chitosan capped NPs have been compared and shown by fluorescent microscopy and TEM microscopy. Uncapped NPs appear to be tagged on surface whereas chitosan capped NPs penetrate inside cell walls. Also fluorescent microscopy results shows that same sample exhibits green and orange color when excited at different energies. These synthesized NPs have also shown preliminary results

showing glucose sensing with biocompatible chitosan capped manganese doped ZnS NP's and compared their results for two possible emission (400, 587nm) sites of same sample. Our introductory results of capping ZnS NPs with DNA and their enzyme sensing studies has been presented in the last part of results and discussions. It has been shown that DNA itself is used in synthesis of ZnS NPs (referred to as ZnS @ DNA) to control their size. While synthesizing such novel ZnS NPs, we also made some interesting observations regarding passivation of defect states of ZnS with negative charge of $P=O^-$ and $P-O^-$ in DNA. Plasmid DNA is behaving as a template for the growth of ZnS nanostructures. Proposed mechanism for growth of ZnS NPs on surface of plasmid DNA which behaves as template has been given. Further we find that ZnS @ DNA particles may be useful as DNA interacting enzyme detectors and mechanism for interaction of pepsin with DNA template assisted ZnS NPs has been given.

7.2 Scope for further work

Since some of work related to excitation induced tunable emission in single sample, biotagging studies of same samples with surface adsorbed polymer CH (which is responsible for steric stabilization and tunable emission also) is in early stage so further studies on same series with variation of solvent medium and effect of pH on all above mentioned properties can be done. Doping of other cation like Cu ions along with Mn in host ZnS NPs with CH and PVP as capping agents can be studied. This can help to improve white light emission from these NPs at variable excitations because Cu doping can provide required green color along with existing blue and orange. Also other polymers should be reviewed which can passivate the NP surface and at the same time have their own emission spectrum. This will

elaborate the studies of tunable emission from organic – inorganic semiconductor NPs for tunable emission applications. At last DNA capping on ZnS NPs surface which is at early stage is behaving like template growth on plasmid DNA can be studied in detail because semiconductor NPs-DNA conjugates can be used as building blocks for preparing nano, meso and macroscopic architectures with well defined structures and can be used for ultra-sensitive and highly specific biological and biomedical detections.